

AD-A262 008

2



WL-TR-92-4068

ADVANCED NDE TECHNOLOGY PROGRAM

DTIC
ELECTE
MAR 22 1993
S C D



Ames Laboratory
Iowa State University
Ames, Iowa 50011

AUG 1992

FINAL REPORT FOR 10/11/90 - 09/30/91

APPROVED FOR PUBLIC RELEASE; DISTRIBUTION IS UNLIMITED.

MATERIALS DIRECTORATE
WRIGHT LABORATORY
AIR FORCE MATERIAL COMMAND
WRIGHT PATTERSON AFB, OH 45433-6533

93-05855




98-9 19 030

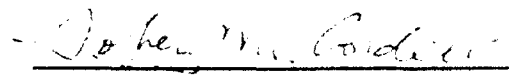
NOTICE

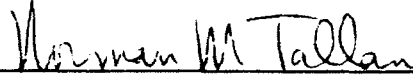
When Government drawings, specifications, or other data are used for any purpose other than in connection with a definitely Government-related procurement, the United States Government incurs no responsibility or any obligation whatsoever. The fact that the government may have formulated or in any way supplied the said drawings, specifications, or other data, is not to be regarded by implication, or otherwise in any manner construed, as licensing the holder, or any other person or corporation; or as conveying any rights or permission to manufacture, use, or sell any patented invention that may in any way be related thereto.

This report is releasable to the National Technical Information Service (NTIS). At NTIS, it will be available to the general public, including foreign nations.

This technical report has been reviewed and is approved for publication.


PRAMODE K. BHAGAT
Nondestructive Evaluation Branch
Metals and Ceramics Division


TOBEY M. CORDELL
Chief
Nondestructive Evaluation Branch
Metals and Ceramics Division


NORMAN M. TALLAN, SES-04, Chief
Metals and Ceramics Division
Materials Directorate

If your address has changed, if you wish to be removed from our mailing list, or if the addressee is no longer employed by your organization please notify WL/MLLP, WPAFB, OH 45433-6533 to help us maintain a current mailing list.

Copies of this report should not be returned unless return is required by security considerations, contractual obligations, or notice on a specific document.

REPORT DOCUMENTATION PAGE			Form Approved OMB No. 0704-0188	
<small>1. Report number, 2. Report title, 3. Report type, 4. Report status, 5. Report number, 6. Report title, 7. Report type, 8. Report status, 9. Report number, 10. Report title, 11. Report type, 12. Report status, 13. Report number, 14. Report title, 15. Report type, 16. Report status, 17. Report number, 18. Report title, 19. Report type, 20. Report status, 21. Report number, 22. Report title, 23. Report type, 24. Report status, 25. Report number, 26. Report title, 27. Report type, 28. Report status, 29. Report number, 30. Report title, 31. Report type, 32. Report status, 33. Report number, 34. Report title, 35. Report type, 36. Report status, 37. Report number, 38. Report title, 39. Report type, 40. Report status, 41. Report number, 42. Report title, 43. Report type, 44. Report status, 45. Report number, 46. Report title, 47. Report type, 48. Report status, 49. Report number, 50. Report title, 51. Report type, 52. Report status, 53. Report number, 54. Report title, 55. Report type, 56. Report status, 57. Report number, 58. Report title, 59. Report type, 60. Report status, 61. Report number, 62. Report title, 63. Report type, 64. Report status, 65. Report number, 66. Report title, 67. Report type, 68. Report status, 69. Report number, 70. Report title, 71. Report type, 72. Report status, 73. Report number, 74. Report title, 75. Report type, 76. Report status, 77. Report number, 78. Report title, 79. Report type, 80. Report status, 81. Report number, 82. Report title, 83. Report type, 84. Report status, 85. Report number, 86. Report title, 87. Report type, 88. Report status, 89. Report number, 90. Report title, 91. Report type, 92. Report status, 93. Report number, 94. Report title, 95. Report type, 96. Report status, 97. Report number, 98. Report title, 99. Report type, 100. Report status</small>				
1. AGENCY USE ONLY (Leave blank)		2. REPORT DATE AUG 1992	3. REPORT TYPE AND DATES COVERED FINAL 10/11/90--09/30/91	
4. TITLE AND SUBTITLE ADVANCED NDE TECHNOLOGY PROGRAM			5. FUNDING NUMBERS C FY1457-91-N-5014 PE 62102 PR 2418 TA 06 WU 06	
6. AUTHOR(s) D.O. Thompson				
7. PERFORMING ORGANIZATION NAME(S) AND ADDRESS(ES) Ames Laboratory Iowa State University Ames, Iowa 50011			8. PERFORMING ORGANIZATION REPORT NUMBER	
9. SPONSORING / MONITORING AGENCY NAME(S) AND ADDRESS(ES) MATERIALS DIRECTORATE WRIGHT LABORATORY AIR FORCE SYSTEMS COMMAND WRIGHT PATTERSON AFB OH 45433-6533 WL/MLLP, Attn: BHAGAT 513-2559799			10. SPONSORING / MONITORING AGENCY REPORT NUMBER WL-TR-92-4068	
11. SUPPLEMENTARY NOTES				
12a. DISTRIBUTION / AVAILABILITY STATEMENT APPROVED FOR PUBLIC RELEASE; DISTRIBUTION IS UNLIMITED.			12b. DISTRIBUTION CODE	
13. ABSTRACT (Maximum 200 words) This document contains the final reports of the various projects included in the Advanced NDE Technology Program at the Ames Laboratory (DOE), Iowa State University. The technologies covered include Thermal wave methods, Image enhancement, Laser based ultrasonics, Detection of brittle phase in Ti alloys, Adhesive bond characterization, and eddy current methods.				
14. SUBJECT TERMS Nondestructive evaluation, Thermal wave, Laser generated ultrasound, image enhancement, adhesive bond, eddy current			15. NUMBER OF PAGES 152	
			16. PRICE CODE	
17. SECURITY CLASSIFICATION OF REPORT UNCLASSIFIED	18. SECURITY CLASSIFICATION OF THIS PAGE UNCLASSIFIED	19. SECURITY CLASSIFICATION OF ABSTRACT UNCLASSIFIED	20. LIMITATION OF ABSTRACT UL	

TABLE OF CONTENTS

	Page
IR Thermal Wave Tomographic Studies of Structural Composites R. L. Thomas (Wayne State University).....	1
Application of Time-Resolved Infrared Radiometry (TRIR) to Identify Structural Damage in Composite Materials J. C. Murphy (Johns Hopkins University).....	11
Limited Data Computed Tomography Using <i>A Priori</i> Data R. Roberts (Ames Laboratory and Center for NDE).....	30
Laser-Based Ultrasonics Robert C. Addision, Jr. (Rockwell International Science Center).....	44
Detection of Hard Alpha Inclusions in Titanium Jet Engine Materials J. H. Rose (Ames Laboratory and Center for NDE).....	57
Ultrasonic Detectability of Small Flaws in Advanced Engine Alloys R. B. Thompson and F. J. Margetan (Ames Laboratory and Center for NDE).....	72
Spectroscopic Evaluation of Adhesive Bonds: Linear and Nonlinear Analysis J. D. Achenbach (Northwestern University).....	95
Spectroscopic Evaluation of Adhesive Bonds: Linear and Nonlinear Methods Laszlo Adler (Ohio State University).....	110
Nondestructive Evaluation Method for Assessment of Environmental Degradation of Adhesive Joints S. I. Rokhlin (Ohio State University).....	123
Eddy Current Characterization of Composites R. E. Beissner (Southwest Research Institute).....	135
Advanced Technology Program-Properties and Materials Characterization Ward D. Rummel (Martin Marietta).....	146

Preface

This document contains the final reports of the various projects included in the Advanced Technology Program at the Ames Laboratory and the Center for NDE, Iowa State University, for FY91. Because it is the first annual report of its kind for this program, each of the project reports has been prepared to provide the reader with a limited summary of appropriate background information (both general and project specific) as well as technical details of the FY91 work. For the past several years, this information has been published in various Proceedings of the Review of Progress in Quantitative NDE, Vols. 1-10, (Plenum Press, New York) and other archival journals including the Journal of NDE, Research in NDE, and the Journal of Applied Physics. Although it is expected that the investigators will continue to use these vehicles for broad dissemination of their results, it is clear that this report will provide a more easily accessible and focussed view of work done specifically in this program. It is also hoped that the report will contribute significantly to the technology transfer process by providing a coherent trail of technology development in the various projects.

Since this is a first annual report, it is worthwhile to review briefly the research philosophy that has been followed in this program for several years, namely, the "research window" philosophy. By its name, it is evident that the philosophy is oriented toward research opportunities that are applications oriented. In this program, some "window" choices have been quite narrow, while others have been broader. In all cases, the approach that has been taken is to develop the science base needed to provide solutions to the applications problem. Thus, the end point of a project in this program is the provision of the scientific/engineering knowledge needed to solve the problem, but not necessarily the provision of prototypic instrumentation or other deliverables that represent the final solution. The latter step has been traditionally viewed as the next step in the technology transfer chain. It should be noted that the science based knowledge needed to solve a window problem does not imply the need to learn everything about the problem, but only enough to permit technology transfer to occur. This research philosophy has been remarkably successful over the years; using it, this program has become recognized by many as the leading research program in quantitative NDE in the U.S., possibly in the world, and has generated a broad spectrum of new results available for transfer as well as a new community of NDE researchers and practitioners.

Projects that have been pursued in FY91 described in this report address a variety of "windows." These "windows" are summarized below together with brief research highlights. As will be noted in the reports, emphasis has always been placed in this program upon the parallel development of theory and experiment; in some cases, this joint development is pursued as two related tasks in parallel whereas in other cases they have, and are, being pursued serially. Details of the work and references are given in the main body of the report.

- **Thermal Wave Studies**

Two projects that are focussed upon both the development and application of these powerful techniques are reported. In one of these, "IR Thermal Wave Tomographic Studies of Structural Composites" (R. Thomas et al., Wayne State University) emphasis is placed upon the development of tomographic methods for the production of thermal images in composite materials suitable for large scale inspections. This has been a very successful project in which the first tomographic images of defects in composites are reported. Technology transfer has also been effective in that a system

was built and assembled for a major AF program under separate funding using technology developed in this (and some other) research programs. Further, it is likely that this system will be the element of commercialization in the near future. The second project, "Application of Rapid-Scan Time-Resolved Infrared Radiometry to Identify Impact Damage in Composite Materials" (J. Murphy, et. al, Johns Hopkins University) has been highly successful with a materials characterization window. Accomplishments this year include the demonstration of quantitative characterization of defects in composites, (despite anisotropy in heat flow characteristics), as well as the theoretical development of a model to quantitatively take this anisotropy into account. Another highlight of the work includes the characterization of impact damage in multilayer composites in which it is shown that both depth and extent characterization can be obtained.

- **Image Enhancement**

Work in this project (R. Roberts et al., Ames Laboratory and Center for NDE) is aimed at the development of techniques to enhance computed tomographic images of flaws and dimensional abnormalities in cases in which only limited data are available due to any one of several reasons. A target of the work is the development of a reconstruction algorithm for missing data that also includes the CAD drawing of a component as one of the possible sources of additional data. A highlight of this year's work includes the incorporation of the CAD drawing component geometry and composition information into the algorithm constructed last year. This advance obviously provides many attendant benefits in the limited angle reconstruction feature. Experimental verification of the algorithms was also initiated together with their adaptation for execution on a state-of-the-art massively parallel computer.

- **Laser Based Ultrasonics**

Significant progress has been made in this project towards developing a capability to rapidly scan and characterize defect structures in complex composite geometries and material. Specifically, it has been demonstrated (R. Addison et. al, Rockwell International Science Center) that rapid scanning via angular beam deflection on complex composite parts is feasible. Further, it was shown that sufficiently high ultrasonic amplitudes can be generated and maintained for scanning purposes while remaining comfortably below the material damage threshold. Although emphasis has been placed upon composites in this work, broad application potentials of the technology are obvious, including composite cure control, corrosion detection, and others in remote and hostile environments.

- **Quantitative Feature Characterization--Detection of Brittle Phases in Ti Alloys**

Two tasks have been pursued this year in this very difficult project with significant results. Jointly, the two tasks are focussed upon the engineering development of a quantitative ultrasonic approach for the detection of the hard alpha phase in commercial titanium engine alloys. This is a difficult problem because of the expected small difference in acoustic impedance between the oxygen/nitrogen stabilized hard α phase and acceptable material. The engineering approach that is being taken, laying the foundation for the later development of a quantifiable ultrasonic system, uses a variety of both previously and currently generated NDE modeling tools (materials and techniques). Highlights of FY91 theoretical work (J. Rose, Ames Laboratory and Center for NDE) includes both the validation of a new theory of

backscattering from titanium microstructures, an essential contribution for both understanding the detection process and in estimating worst case signal/noise ratios, and its extension to commercial multi-phase commercial materials. In a companion experimental/analytic task, (R. B. Thompson, F. Margetan, Ames Laboratory and Center for NDE) a number of highlights occurred including the quantitative determination of the effects of nitrogen/oxygen upon the elastic constants (and therefore the acoustic impedance) of alpha titanium, the definition of and measurement of a new material property (figure of merit, FOM) essential to detectability calculations, the determination of the variability of FOM in commercial, 2-phase alloys, and performance of calculations for hard α detectability using these new concepts.

- **Characterization of Adhesive Bonds**

Work in this project is aimed at the development of NDE techniques (ultrasonic) that can be used to characterize strength degradation in adhesively bonded joints. Three tasks were pursued in FY91. The first of these, a theoretical task (J. Achenbach et al., Northwestern University), is designed to provide theoretical analysis and interpretation of the two related experimental tasks (see below). A significant theoretical highlight included the characterization of the adhesive bond's nonlinear stress-strain response. Another included the investigation of viscous phenomena in pre-stressed adhesive bonds and their effects/limitations upon the experimental results. In an experimental task it was shown (L. Adler et al., Ohio State University) that non-linear ultrasonic measurements could be used to enhance the detection of strength degradation in a joint. This work also highlighted a technique to detect "kissing" bonds (contacting adhesive-adherend but no bond) using an acoustic guided wave technique. Finally, it was shown (S. Rohklin, Ohio State University) that a new ultrasonic technique produced results that suggest it may become possible to predict the remaining safe lifetime of an environmentally degraded adhesive joint.

- **Eddy Current Characterization of Metal Matrix Composites**

This project is aimed at the development of eddy current techniques as a NDE process control procedure that can be used to characterize metal matrix composites in the manufacturing environment. In this work (R. Beissner, Southwest Research Institute) effort was focussed upon the principal impediment to eddy current characterization of composites, i.e., the highly anisotropic nature of composites. A number of highlights were achieved including the completion of a theory of eddy currents in biaxial conductors, the development of a theory for the conductivity tensor for arbitrary arrangement of parallel fibers, and initial experimental verification of the models. The completion of the theory work for this complex material system must be regarded as a milestone of significance with possible broad applications.

Finally, it should be noted that this program has always been, and remains, a highly leveraged research program. In most instances, the investigators have been encouraged to view their projects as "seed" tasks and to augment their research activities in this program with additional research projects from other sources. Thus, more information on the research projects described herein may be contained in other references. Probably the most concentrated source of this related information is in Proceedings of the Review of Progress in Quantitative Nondestructive Evaluation referred to in the first paragraph of this Preface.

The continuing support of this program is gratefully acknowledged.

IR THERMAL WAVE TOMOGRAPHIC STUDIES OF STRUCTURAL COMPOSITES

R. L. Thomas, L. D. Favro, P. K. Kuo
Wayne State University

Executive Summary

The primary objective of this project has been to implement the new technique of IR thermal wave tomography in real time, and to study its utility for NDE of structural composite materials. A second objective was to develop an NDE technique which, in addition to being wide-area, contactless and rapid, can provide both flaw shape and depth information. It was also our objective to develop a technique which would provide an image in which each subsurface defect would be displayed simultaneously with its maximum possible contrast, regardless of its depth.

The following is a summary of our accomplishments under this project:

- Assembled three independent Thermal Wave IR Video Imaging Systems, each capable of carrying out real-time thermal wave tomography. Two of the systems are MacII/Perceptics systems, the third is our original Sun 3/160 C/DataCube System. Also part of the assembly are three sets of xenon flash lamp pulsed heat sources. Two of the sets contain 8 flash units each, the third contains 4 flash units. Each individual flash unit produces a 2 msec duration, 6.4 kJ energy, pulse, under the control of the computer hardware and software developed at Wayne State.
- Demonstrated the feasibility of carrying out thermal wave tomography by implementing a (slow) post-processing version which utilized a large data set, stored as a sequence of images on a hard disk.
- Developed and implemented the real-time image processing techniques in which: 1) thermal wave "echo" images are obtained field-by-field [two interlaced video fields constitute one video frames, where the frame rate is 30Hz] as they are transmitted from the IR 600, 2) the time at which the echo returns is obtained for each pixel and stored in one image buffer, and 3) the magnitude (peak contrast) of the same echo is also determined for each pixel and stored in a second image buffer. This is done "on the fly", currently at a maximum processing rate of 10 Hz. The resulting two image buffers constitute our thermal wave tomogram, and maximum contrast images, respectively.
- Tested our Real-Time Thermal Wave Tomographic Imaging capability, first on flat-bottomed hole test specimens, then on several graphite-reinforced composite test panels which contained subsurface impact damage. The results conclusively demonstrate the viability of our technique and compare favorably with the results of ultrasonic C-scan imaging.
- Developed successful numerical deconvolution methods, based on an inverse Born approximation analytical model, and aimed at deducing the subsurface defect geometry from the time-dependent thermal wave images at the heated sample surface.

Accession For	
NTIS	CRA&I <input checked="" type="checkbox"/>
DTIC	TAB <input type="checkbox"/>
Unannounced	<input type="checkbox"/>
Justification	
By	
Distribution /	
Availability Codes	
Dist	Avail and/or Special
A-1	

Background

A. General

This investigation was intended primarily to address the problem of obtaining rapid depth mapping of planar subsurface defects in structural aerospace materials. The technique employed was that of infrared (IR) Thermal Wave Imaging. The detailed results of this investigation will appear in the archival series: Review of Progress in Quantitative Nondestructive Evaluation, [1] as well as in the Springer Series in Optical Sciences, [2] and the Proceedings of the 14th International Congress on Acoustics. [3] The only prior attempt to implement this particular type of Tomographic IR Video Imaging took place as the result of a collaboration between the authors of this report and Prof. Vladimir Vavilov from Tomsk. Together, we attempted to carry out a post-processing version of Tomography, an account of which has subsequently been published elsewhere. [4] In the course of our investigation, we recognized that the image processing technique could be quite useful as an extension of, and addition to the synchronous thermal wave IR imaging techniques under development in our laboratories (see Sec. B., below). It was also evident that the technique should be implemented in real time for its to be truly useful for NDE applications.

We also addressed another previously unsolved problem in thermal wave imaging during these investigations. This latter problem is the difficulty of obtaining reliable size and shape information from thermal wave images. The difficulty arises from the dispersive nature of thermal wave propagation, which in turn leads to severe blurring of the images with time (or depth). We therefore developed numerical deconvolution methods for "deblurring" of thermal wave echo images so as to obtain quantitative information on the shapes and sizes of subsurface defects. [5-7]

B. Project

This project is a logical extension of previous research under the Air Force QNDE program. A summary of previous research by the authors under the Air Force QNDE Program is in preparation as part of a separate Report under this project, entitled "Thermal Wave IR Video Imaging for Wide-Area NDE Applications." [8] The latter report will contain a more detailed description and set of references to related work found in the literature. To summarize briefly, we devoted our research efforts in previous years to the development of time-domain versions of our IR thermal wave imaging techniques. In a parallel activity, we have been assessing the feasibility of applying thermal wave IR methods for several NDE problems of importance to the Air Force. The conclusions of our efforts in prior years have been that the technique shows considerable promise, in that it has the potential for rapid and contactless evaluation of wide areas of aerospace structures. Also, the technique has the potential for providing images which are readily interpretable, and can provide quantitative, as well as qualitative information regarding the subsurface defects which are imaged. Although the technique is especially useful for shallow defects, we have also demonstrated a capability for imaging structures which are 6mm or more beneath the surface. [3] A seemingly troublesome feature for the technique is the fact that deeper defects are imaged with progressively greater thermal "blurring". However, as we have just begun to demonstrate in FY91, [5-7] and propose to explore in greater detail in FY92, it is possible to apply numerical deconvolution algorithms for successful thermal wave image "deblurring" and the resulting acquisition of quantitative size and shape information. Another, more detailed, review of these techniques is currently under preparation. [9]

Among the highlights of our accomplishments in previous years on thermal wave imaging projects under this program are the successful "box-car" thermal wave IR video imaging of coating delaminations and inter-ply delaminations caused by impact damage in structural polymer composite materials. The instrumentation and software development has progressed steadily during the course of these projects, as has the development of

appropriate pulsed heat sources and the validation of the technique on flat-bottomed hole specimens fabricated from materials having a very wide range of thermal properties (metals to plastics).

Objective and Scope

The objective of this project has been to implement the new technique of IR thermal wave tomography in real time, and to study its utility for NDE of structural composite materials. An NDE technique which, in addition to being wide-area, contactless and rapid, can provide both flaw shape and depth information. It was also our objective to develop a technique which would provide an image in which each subsurface defect would be displayed simultaneously with its maximum possible contrast, regardless of its depth.

The application for the project involves the development of a prototype system which would find use in QNDE programs of interest to the Air Force. For example, the F-22 Advanced Tactical Fighter Program makes extensive use of structural composite materials, and a need exists for rapid and reliable NDE, both as a process control monitor with rapid "feedback" and for a damage assessment monitor with potential field applications. Tomographic capability enhances the usefulness of such a prototype imaging method at fixed gate times for obtaining images of subsurface coating defects, delaminations in composites, etc.

Approach

Under the current project, our approach has been to develop and carry out feasibility testing of a real-time tomographic imaging technique which can display thermal wave propagation times, pixel-by-pixel, as a pseudocolor image (the thermal wave tomogram). The hardware and software development was to be implemented on two systems under development in our laboratory, one our original Sun 3/160 C/DataCube System, the other a newer MacII/Perceptics system, two copies of which are owned by our laboratory. The latter system is also intended to serve as a possible "Beta test site" for technology transfer activity. In addition to the instrumentation development and feasibility experimentation, we are also pursuing theoretical studies and development of numerical deconvolution algorithms which place the technique on a sounder interpretive basis.

Technical Progress

A. Tomography

Technical progress on this project has been summarized in the literature. [1-3] As noted in these papers, Vavilov et al. [4] have recently described a technique for making tomographic thermal wave images. Their method involves recording a succession of thermal wave images after a flash-heating pulse, followed by a numerical pixel-by-pixel search of the images for the time at which the reflected thermal waves from subsurface features have their peak amplitudes. Since the peak time is related to the depth of the scatterer, this information enables one to separate the image into time (or depth) slices. The result is a thermal wave tomogram. Since their process involves post-processing and a search through a large number of stored images, it is memory-intensive, and is difficult to accomplish in real time. In this project, we have developed a thermal wave tomographic method which accomplishes the same result, but does so with real-time techniques which avoid the storage of a large number of images, and produces the tomogram without post-processing.

The tomographic method we have developed [1-3] is based on wide area pulse heating (e.g. by flashlamps) of the sample's surface. Experimental curves showing the time dependence of the surface temperature of a fabricated test specimen, following such pulse heating, are shown in Fig. 1. These curves result from temperature measurements over several subsurface flat bottom holes at different depths in the (polymer) test specimen, and are plotted together with a curve of the temperature at a point above a featureless region of the same sample. It can be seen that, after the flash occurs, the surface temperature in all regions rises very rapidly to a peak which is essentially independent of spatial position. This is followed by a more or less exponential decay, with the rate of decay varying both in time, and from point to point on the surface. This can be explained in the following way. A typical cooling curve corresponding to some point on the surface can be thought of as being comprised of two components. One component is simply that which would occur if the

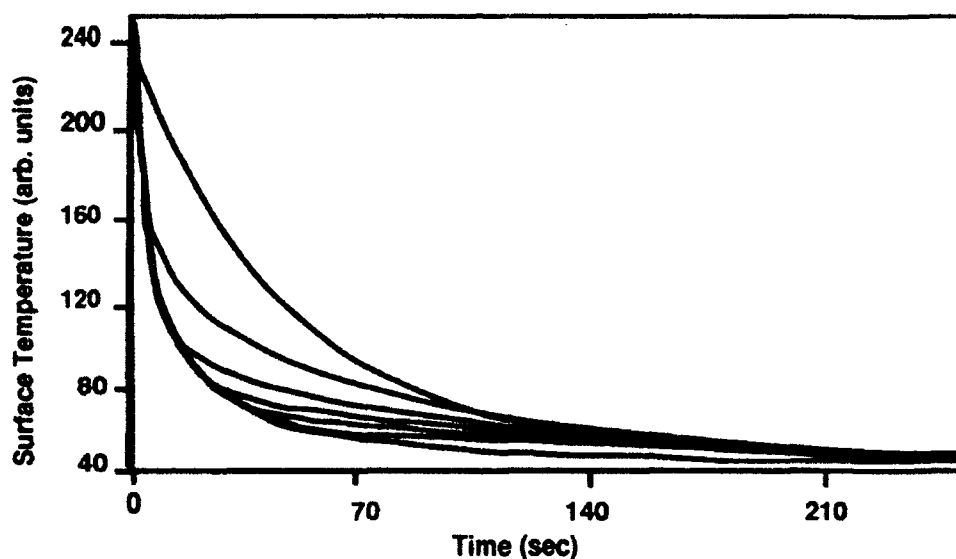


Figure 1 Heating and cooling curves over six, 19 mm diameter, subsurface flat bottom holes at different depths in a plastic sample. The reference (lowest) curve corresponds to a region away from the holes. The remaining curves correspond to regions directly above the holes, ranging in subsurface depths 1.1mm (top curve), 1.86mm (2nd from top), 2.6mm (3rd), 3.4mm (4th), 4.1mm (5th), and 4.9mm (6th).

material underneath that region contained no thermal wave scatterers. The other component results from the thermal wave reflected from any such scatterer (the thermal wave "echo"). This reflected thermal wave slows the rate of cooling. It can be seen from Fig. 1 that there are varying cooling rates over different regions, as expected on the basis of the description above. As mentioned above, the curve with the fastest cooling rate corresponds to the featureless region beneath which there are no subsurface scatterers. In our tomographic method we make use of this curve as a reference and subtract this reference from the time dependence of every pixel of the image as it is generated. The resulting thermal wave echo curves (expanded in scale) are shown in Fig. 2 for the six selected regions corresponding to the cooling curves of Fig. 1. Although the thermal wave echoes are broadened because of the diffusive nature of the heat propagation (see Fig. 2), they are seen to vary both in height and in temporal position, with the echoes corresponding to the deeper holes being lower and later in arrival time. In our real-time method, we carry out a pixel-by-pixel determination of the magnitudes and arrival times of these thermal wave echoes. This is accomplished by smoothing the curves to avoid spurious peaks caused by noise in the signal, followed by a determination of the peak of the smoothed curve. The resulting 512 x 480 collection of peak times is stored as a pseudo-image in a buffer of the real-time processor. Thus, when the heating and cooling cycle is completed, a map of thermal wave echo arrival times (the real-time tomogram) is stored in one image buffer. In addition, a second image buffer contains a pixel-by-pixel map of the peak amplitude of the thermal wave echo at its corresponding arrival time (the "peak contrast" image). Currently, we have the ability to produce the tomographic and peak contrast images simultaneously with a single heating flash, and with post-heating sampling rates up to 10 Hz.

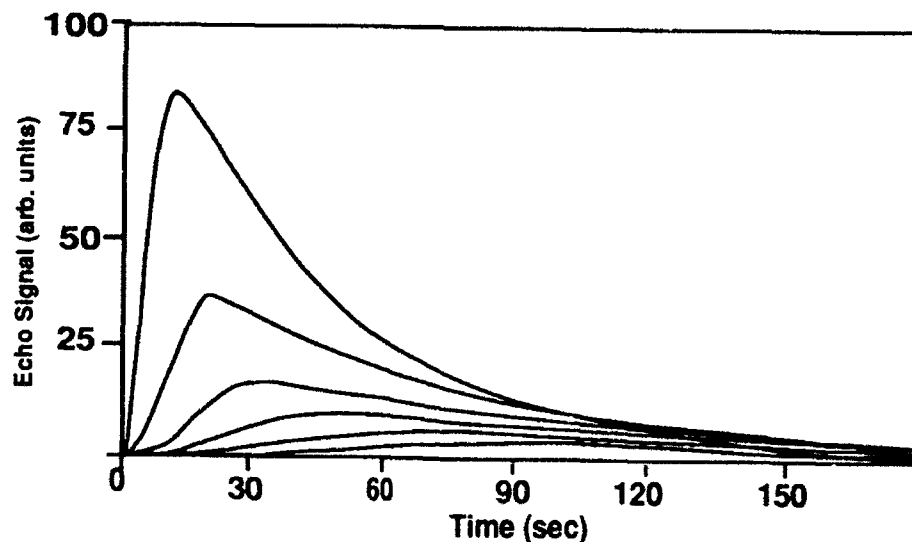


Figure 2 Thermal wave echo curves (expanded in scale) for the reference curve subtracted from the six curves above the subsurface holes of Fig. 1. The order of depths is the same as for the six top curves of Fig. 1.



Figure 3 Thermal wave tomogram of a sample of graphite-epoxy material with impact damage. White indicates longer time (greater depth), black shorter time (lesser depth). [1]

In Fig. 3 we show a tomogram of a graphite-epoxy sample which had been subjected to an impact which caused damage which extends from directly under the point of impact out to the edges of the sample in the horizontal direction. The sample was viewed from the side opposite the impact [1]. The tomogram is displayed with a gray-scale color map for which black represents short time and white represents long time. Figure 3 shows that the damage near the edges (e.g. the large white region in the middle of the right edge) is further from the surface than the damage under the impact site (e.g. the gray elliptically shaped region in the center, surrounded by the black [shallow] elliptical region). In addition, there are other areas of the sample which indicate reflections from immediate depths (various levels of gray) which may indicate porosity or incomplete bonding of the plies. Figure 4 is a peak contrast image of the sample shown in Fig. 3. [1] This image shows each pixel of the image as it appeared when its contrast was maximum. The greatest contrast (white) corresponds to the shallowest defects (compare with Fig. 3), as expected for heat diffusion.

Figure 5 shows a series of time-slice images derived from the tomogram of Fig. 3, showing only those features (as white) whose contrast peaks at the times shown beneath each image. [1] At the shortest time (230 ms) following the heating pulse, the features show the pattern of the near-surface fibers, along with a shallow region of delamination surrounding the central feature. At 460 ms, these shallow features begin to fade, and a slightly deeper region of delamination appears beneath the central feature. Next (700 ms), these central features all fade away, and a delamination near the left horizontal edge appears. Finally (1640 ms, 1870 ms, 2100 ms), only the deep delamination near the right edge is seen.

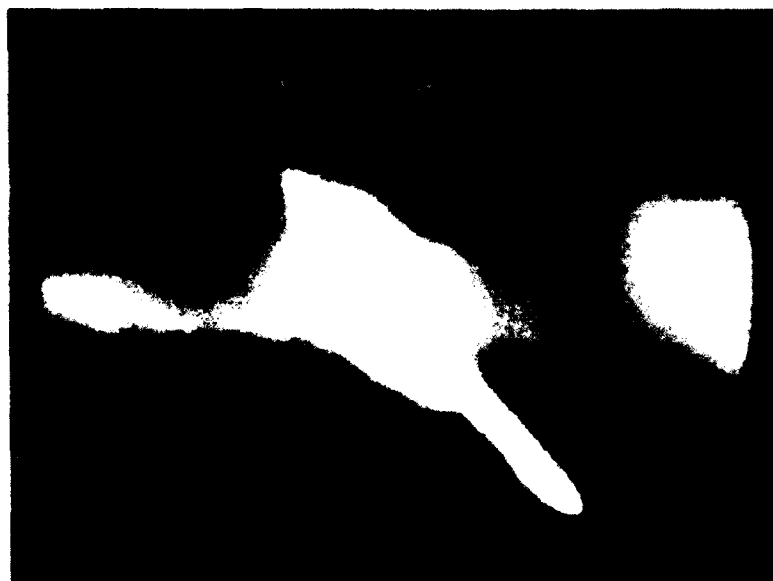
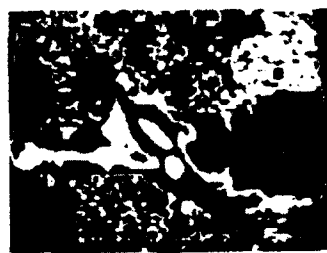


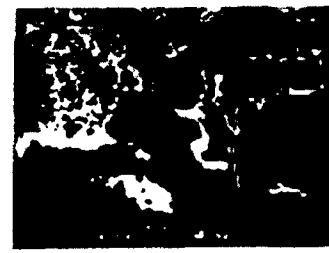
Figure 4 Peak contrast image of the impact damage sample shown in Fig. 3. White indicates greater contrast, black lesser contrast. [1]



230 ms



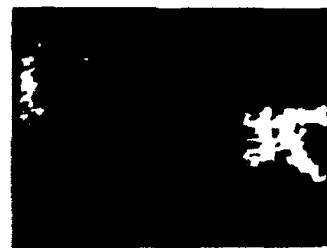
460 ms



700 ms



1640 ms



1870 ms



2100 ms

Figure 5 Time-slice images derived from the tomogram of Fig. 3, showing only those features (as white) whose contrast peaks at the times shown beneath each image. [1]

Several other examples of thermal wave tomographic imaging of impact damage in structural polymer composites are presented elsewhere. [1-3] Among them are examples of conically shaped damage and spiral damage in our tomograms. In one case, [3] the damage correlates extremely well with (much slower) ultrasonic C-scan imaging previously carried out on the same specimen.

B. Deconvolution of Thermal Wave Images

One criticism that has been directed at thermal wave imaging is that the resolution of the images is not as good as that of high-quality ultrasonic images. The origin of this criticism is the blurring of thermal wave images which occurs as a result of the lateral diffusion of heat while the waves are propagating back to the surface. Ultrasonic images are much less susceptible to such problems because, for many purposes, ultrasound can be regarded as propagating in straight lines. Crowther, et al. [5-7] have recently demonstrated a technique for removing the blurring of thermal wave images by means of a simple numerical algorithm based on inverse scattering theory. The algorithm at present is applicable only to planar scatterers, but this covers a very important class of defects of practical interest, namely delaminations and disbands in laminated composites and adhesively bonded structures.

As is the case with any inverse scattering calculation, an absolute prerequisite for inversion of thermal wave images is an accurate direct scattering model. The inversions developed at Wayne State were obtained through the use of the Born approximation, with appropriate modifications to take account of the strong thermal wave scattering which occurs at delaminations and disbands. A detailed derivation of this model will be published elsewhere. [10] Its essential feature is that the theoretical expression for a thermal wave echo signal in an image can be written as a convolution of two, two-dimensional functions. The first of these describes the propagation of a thermal wave pulse down to the scatterer, the scattering, and the subsequent propagation of the echo back to the surface of the sample. Although it describes more than just the propagation of the pulse from the scatterer to the detector, it serves as a mathematical analog of the "point-spread function" used in optics and ultrasonics. The second function in the convolution is just the function which describes the two-dimensional shape of the scatterer. The result is an equation of the form,

$$\Delta T(x, y, t) = \iint dx' dy' g(x - x', y - y', t) f(x', y')$$

Here $\Delta T(x, y, t)$ represents the echo (or equivalently, contrast) signals, comprising the image as a function of time; $g(x, y, t)$ is the "heat-spread function", and $f(x, y)$ represents the shape of the scatterer. The exact form of $g(x, y, t)$ depends on the approximations used in the model. The inverse scattering calculation is begun by performing a two-dimensional spatial Fast Fourier Transform (FFT) on the experimental echo image, represented above by $\Delta T(x, y, t)$. The same procedure is then applied to the appropriate expression for $g(x, y, t)$ at a value of t corresponding to the time delay at which the image was obtained. In principle, then, one simply has to divide the first of these FFT's by the second, and do an inverse FFT on the result to obtain the desired shape function $f(x, y)$. However, the experimental image represented by ΔT is not arbitrarily accurate, because it contains both digital and thermal noise. The effect of this noise is to obscure the shape of the scatterer in the image of the inverted FFT. Fortunately, both kinds of noise tend to appear only in relatively high spatial frequencies, and these frequencies can be removed by applying any of a variety of low-pass filters to the FFT of the experimental data. When this is done, the result of the division and the inverse transformation is an image

of the shape function $f(x, y)$ with only a slight rounding of the corners due to the loss of high-frequency information. We have published several examples of applying this series of algorithms to deblur thermal wave images, [5-7] and the preliminary results are good. The complete numerical calculation takes about one minute on a MacIntosh IIfx. It would take considerably less time if the FFT of the heat-spread function $g(x, y, t)$ were calculated and stored prior to the processing of the experimental image. This latter idea is among those being considered for implementation in FY92, as described below.

Summary

We have demonstrated a real-time thermal wave IR tomographic method which shows promise for defect depth determinations. The technique has been illustrated by forming tomographic images of impact damage in polymer composite test specimens, which together with the complementary peak contrast images, permits more rapid and quantitative characterization of subsurface damage zones in these materials. We have also developed analytical expressions and numerical deconvolution algorithms for carrying out a strategy for "deblurring" thermal wave images to obtain reliable shape and size information to complement the depth information obtained through our real-time thermal wave tomography. These techniques have shown considerable promise, and the initial studies carried out in FY 91 form the basis for our planned work in FY 92.

Plans for Next Year

Our proposed work will extend the above described concepts for use in the detection and analysis of defects in anisotropic materials. We will consider both thermal anisotropy and multiple scattering, and extend our capability to obtain correct size and shape information for subsurface defects in fiber-reinforced polymer composite materials of interest to aerospace applications. Numerical algorithms will be developed to invert experimental IR thermal wave images of defects in such composite materials. The results will be tested on both simulated and actual damage-induced defects in composite test panels. The research will be closely coordinated with at least one end user, by means of a recently established Beta Test Site for the WSU Instrumentation, located at Lockheed Aeronautical Systems Company in Marietta, GA (LASC-GA). As results from the proposed research become available, they will be transferred to our collaborators in the Advanced Materials Development Center at LASC-GA for evaluation as improved techniques for evaluating composite materials related to the Advanced Tactical Fighter Program. Results will also be available to other relevant programs identified through the QNDE Program and Wright Patterson AFB. For example, we have recently begun an interaction with the C/KC-135 Disassembly and Hidden Corrosion Project, being coordinated by the Oklahoma City Air Logistics Center, and it is possible that the results may find an application for detection and evaluation of corroded metal structures in the aging military fleet.

References

1. L. D. Favro, H. J. Jin, Y. X. Wang, T. Ahmed, X. Wang, P. K. Kuo, and R. L. Thomas, in Review of Progress in Quantitative NDE (Plenum Press, NY, 1992), Vol 11 (in press).
2. L. D. Favro, H. J. Jin, P. K. Kuo, R. L. Thomas, and Y. X. Wang, "Real-Time Thermal Wave Tomography," 7th International Topical Meeting on Photoacoustic and Photothermal Phenomena, Doorwerth, The Netherlands, August 26-30, 1991, Proc. to be published in the Springer Series in Optical Sciences: "Photoacoustic and Photothermal Phenomena."

3. R. L. Thomas, L. D. Favro, H. J. Jin, P. K. Kuo, and Y. X. Wang, "Pulse-Echo Thermal Wave Tomography," Proc. 14th International Congress on Acoustics, Beijing, 1992 (to be published).
4. V. Vavilov, T. Ahmed, H. J. Jin, R. L. Thomas, and L. D. Favro, Sov. J. NDT 12 (1990).
5. D. J. Crowther, L. D. Favro, P. K. Kuo and R. L. Thomas, "Analytic Calculations and Numerical Simulations of Box-Car Thermal Wave Images of Planar Subsurface Scatterers," in Review of Progress in Quantitative NDE, (Plenum Press, N.Y. 1992), Vol. 11 (in press).
6. D. J. Crowther, L. D. Favro, P. K. Kuo and R. L. Thomas, "Inversion of Pulsed Thermal Wave Images for Recovery of the Shape of the Object," 7th International Topical Meeting on Photoacoustic and Photothermal Phenomena, Doorwerth, The Netherlands, August 26-30, 1991, Proc. to be published in the Springer Series in Optical Sciences: "Photoacoustic and Photothermal Phenomena."
7. L. D. Favro, D. J. Crowther, P. K. Kuo and R. L. Thomas, "Inversion of Pulsed Thermal Wave Images for Defect Sizing and Shape Recovery," SPIE Proceedings, Thermosense XIV, 22-24 April 1992, Orlando, Vol. 1682 (1992), pp. 178-181.
8. R. L. Thomas, L. D. Favro, and P. K. Kuo, to appear in Vol. II: [Nondestructive Evaluation] of the Series, Progress in Photothermal and Photoacoustic Science and Technology, Andreas Mandelis, Editor, Elsevier Science Publishing Company, Inc., New York (submitted for publication).
9. "Thermal Wave IR Video Imaging for Wide-Area NDE Applications," separate supplementary report on this research project, in preparation.
10. D. J. Crowther, L. D. Favro, P. K. Kuo and R. L. Thomas, in preparation.

APPLICATION OF TIME-RESOLVED INFRARED RADIOMETRY (TRIR) TO IDENTIFY STRUCTURAL DAMAGE IN COMPOSITE MATERIALS

J. W. MacLachlan Spicer, L. C. Aamodt, and J. C. Murphy
Applied Physics Laboratory
The Johns Hopkins University
Laurel, Maryland 20723-6099

Executive Summary

Composite materials play an increasingly important role as advanced structural materials. However, they also present new challenges in assessing their fitness for service since the complex combination of fiber and matrix which provides the basis for enhanced properties also makes inspection difficult. A topic of special concern is impact damage which can cause internal damage within the impacted part with little or no surface damage. This issue is a focus of our study.

This year's work focussed on the application of time-resolved infrared radiometry (TRIR) for characterization of various types of structural damage in composites. Emphasis was placed on the extension of the TRIR technique to include the effects of (a.) lateral heat transport in composites and (b.) the interplay between normal and lateral heat flow. The objective of this extension was to determine the ability of these thermal methods to image subsurface defects and to assess their threat to the integrity of the structure. The approach was both experimental and analytical in keeping with our goal of developing quantitative NDE methods which can provide numerical criteria for success not merely qualitative information. The experimental program included examination of real defects in test specimens prepared from multilayer carbon-carbon composite materials and studies of multilayer graphite epoxy specimens which were subjected to impact from fast projectiles. In the first set of specimens the initial defects studied were blind holes monitored from the reverse (no hole) side of the specimen. TRIR temperature time experiments were made and showed that these defects could be located and their depth determined with good accuracy. This work established that quantitative TRIR measurements could be made on non-homogeneous specimens such as composites where significant lateral heat flow was present. The presence of significant lateral heat flow was demonstrated in these experiments and a refined analysis is in progress to determine its extent and characteristics.

The second set of composite specimens were multilayer hybrid composites formed using more than ten interior layers of graphite/epoxy covered with a surface layer formed from E-glass/epoxy. These samples were impacted with relatively high energy projectiles and experienced substantial damage both at the point of impact and in regions well removed from the impact site. The nature of the damage was thought to be partial delamination of adjacent layers of the specimen, fiber breakage and fiber-matrix disbonding. Conventional one-dimensional TRIR measurements confirmed a number of these assumptions and located and assessed damaged regions even when there was no surface evidence of damage. An example of this class of measurements is the detection of delamination at the interface between the E-glass/epoxy layer and the interior graphite/epoxy at locations far from the impact site. The basis of identification of site of this disbond was the deviation of the TRIR temperature-root time curve from a straight line. This deviation occurred at the thermal transit time of the E-glass/epoxy layer alone as determined by independent experiments. Damage in the graphite/epoxy core was also seen and its location and depth determined by other features of the temperature-root time curves. Some of the image features may be due to fiber breakage in the graphite-epoxy core.

Localized application of heat to the specimen was used to enhance heat flow in the plane of the specimen (lateral heat flow) in order to investigate the ability of such methods to improve the lateral spatial resolution of subsurface impact damage. Experiments on these complex specimens confirmed that patterned heat sources enhance the lateral image resolution in some cases. However, the nature of the internal damage in these composite specimens was too complicated to model in the initial studies hence there was no reliable basis for making quantitative comparisons of experiment and theory. As a result a simpler specimen geometry was developed and studied both experimentally and theoretically comparing the effectiveness of Gaussian and line heating sources for the detection of vertical defects as described in the body of text. The experiments monitored the surface temperature of a thermally homogeneous specimen as a function of distance from a well-defined vertical boundary which was selected to simulate an open crack. The visibility of the vertical defect was studied as a function of time and of source-detector separation with good agreement obtained between experiment and theory. This work provides the basis for analysis of more complex samples such as the graphite/epoxy composite. Some of that work is in progress.

In summary, experimental and theoretical work has shown:

- TRIR can be applied to composite materials and to their defect structures.
- TRIR measurements can assess impact damage in composites via lateral and normal heat flow.
- Applications include assessment of impact damage in airframes and wings.

Background

A. General

The internal and surface temperatures of a heated specimen are determined by its thermal properties, its internal structure, its environment and geometry, and by the characteristics of the heating source. These dependencies have been exploited in a family of measurement and analysis methods based on photothermal phenomena to determine materials properties of selected specimens and to locate and characterize certain types of defects. These techniques can also be used to measure bond integrity in structured or composite material, and to determine the thickness of coatings applied to substrates. From a broad applications viewpoint, thermal methods based on use of laser or other optical heating and infrared detection are significant since they are noncontacting, can work at large standoff distances and are nondestructive when used in an appropriate manner. This means that their applications to problems of Air Force interest are broad and can include assessment of materials and structures in service and also aid in improved fabrication when used for control of a manufacturing process.

Photothermal measurements can be made in either the frequency or time domain. Frequency domain measurements use a periodically modulated heat source and measure the modulated sample temperature at a particular frequency. For opaque samples the depth to which this modulated heat can penetrate the specimen (and hence locate defects) is determined by the modulation frequency and by the thermal diffusivity of the material. As the frequency increases, or the sample becomes more thermally insulating, this depth becomes smaller. Consequently location of deep flaws in a sample requires use of low modulating frequencies. This requirement introduces some experimental difficulties since the signal to noise ratio decreases with decreasing frequency due to convection, changes in ambient temperature and other environmentally related drifts. Also long times are required. Consequently these techniques are of limited value when very low frequencies are required.

Time domain techniques use a pulsed source with a known temporal profile to heat the sample and then measures the sample temperature as a function of time either during heating or after heating has ended. In principle, the maximum depth at which flaws or other thermal feature can be located by these techniques is limited only by the observation time with deeper features requiring longer observation times. In practice, other factors limit these measurements. One limitation is the peak specimen temperature change which must exceed the noise threshold of the detection system. This implies either use of short pulse, high fluence sources with correspondingly high peak specimen temperatures or longer pulse, lower fluence sources whose of total energy is roughly equal to the short pulse example. A second major limiting factor is lateral (transverse) heat flow. If a heating beam of finite area is used, heat flow is not only into the sample (normal heat flow), but also parallel to the sample surface (transverse or lateral heat flow) away from the heated volume. Lateral heat flow reduces the amount of heat flowing into the sample and eventually limits the depth of penetration of heat flowing normal to the specimen surface. This reduces the visibility of subsurface features. Studying the effect of lateral heat flow on the visibility of buried defects in complex materials has been one objective of this year's work.

Time-resolved infrared radiometry (TRIR) is a time-domain, long pulse technique which was developed at the Applied Physics Laboratory initially to study flaws in poorly conducting specimens which required very low modulation frequencies when measured in the frequency domain. Since its initial development, it has been used on a variety of samples of different types. This method, which uses infrared detection, is non-contacting, can operate at large standoff distances from the sample and can use a variety of heating sources and heating patterns. As practiced at this time, TRIR technique is a quantitative NDE

technique which differs from some other thermographic techniques in being able to measure thermal transit times, sample diffusivity, and the thermal mismatch between layers in coated and structured materials quantitatively [6]. In addition, it has a "self-calibrating" feature which permits effects of sample emissivity to be extracted from data acquired on the region of the sample of interest during the course of the actual measurement. This feature, which is unique to the TRIR method, is clearly important in applications to real materials and structures where emissivity can vary widely between samples and across the surface of individual samples.

Prior to the work described in this report, we had shown that this technique was an effective method for quantitatively detecting coating thickness variations and for characterizing the degree of coating disbonding [1,2]. In 1991 we extended the TRIR technique to composite systems based upon the results of a multilayer model [3]. This work also included an investigation of lateral heat flow, where we have shown that three-dimensional thermal diffusion, and, more specifically lateral heat flow in the plane of the specimen surface, can provide improved visualization and quantification of the location of defects and their characteristics.

The TRIR technique differs from other pulsed thermography techniques in that the surface temperature of the specimen is monitored as a function of time during the application of a step heating pulse. One advantage of this technique, in contrast with techniques using an instantaneous heating pulse, is that the peak temperature excursion is low and potential damage to the specimen is minimized. A second advantage is that the time varying temperature change of specimen produced by heating can be maintained at a high level throughout the measurement process. The temperature does not fall to values which are difficult to measure quantitatively later in the measurement process. This is especially important when searching for deep lying flaws. Full-field images can be obtained with temporal resolution much faster than video frame rates.

TRIR measurements can result in TRIR X-Y images and TRIR time-traces of the temperature response of individual regions of the sample. A TRIR X-Y image reveals spatial variations in the temperature of the sample surface obtained at different time intervals following the onset of the heating pulse. These images reveal the general pattern of heat flow and indicate, qualitatively, the presence of normal and lateral heat flow. TRIR time-traces monitor the temperature-time history at individual, selected points on the sample surface. An analysis of this temperature-time history provides a quantitative measure of thermal transit times and the thermal mismatch between components in a composite sample. This analysis also determines the depth of defects and the thermal resistance of the defect. The TRIR method differs from other time varying thermographic methods in that it provides full information about surface features in a single measurement.

In a planar sample, the surface temperature increases linearly with the square root of time until either lateral heat flow begins to draw heat away from the area under the heating source or the presence of a defect (or change in thermal properties) is sensed by heat flow deep in the sample. Because of this, TRIR time-traces are always plotted versus the square root of time. Any deviation from a straight line indicates the presence of a defect, a change in thermal properties at some depth in the sample, or the presence of lateral heat flow. These effects can be distinguished experimentally and modeled theoretically.

Figure 1 shows the types of information that can be obtained from a TRIR time-trace. Curves A and B show the temperature response obtained when a thermally insulating defect is located at a certain depth in a thermally conductive specimen. The surface temperature rises linearly with the square root of time until the thermal transit time to the defect is reached. This time is given by $0.38 L^2/\alpha$ where L is the depth of the defect and α is the specimen thermal diffusivity [1]. Following the thermal transit time, the slope of the curve

increases due to the presence of the thermally-insulating defect-the temperature of the shallow defect rises earlier than that of the deeper defect. Should the subsurface structure be more thermally conductive than the specimen, the response the slope of the curve decreases at the thermal transit time as shown in curve D.

The TRIR technique can be applied to multilayered samples as indicated by Curve E where the presence of a thermally insulating layer is detected beneath another insulating layer and a thermally conductive layer. The capability for multilayer analysis is heavily dependent on the relative thermal properties of the different layers [3].

The final curves in Figure 1 show the role of heating beam geometry in determining the TRIR response. When the heating source is broad relative to specimen thickness or the depth of a defect, a one-dimensional model is applicable and lateral heat flow is absent. When narrow-beam (or any spatially non-uniform) heating source is used, a three-dimensional model is required and lateral heat flow is present, but its magnitude differs at different points in the specimen. Curves G and H show the response for broad and narrow beam heating.

It is possible to accentuate lateral heat flow relative to normal heat flow by varying the size or shape of the heating source. It is also possible to obtain information about the lateral thermal diffusivity and normal diffusivity in a single measurement. The presence of vertical defects can be detected through their influence on lateral heat flow. Studying this has been one objective of this year's work. Preliminary results indicates that shaping the spatial pattern of the heating source will prove to be a valuable technique for locating and describing vertical defects.

B. Project

A unifying aspect of this program is the development of photothermal techniques and their application to materials systems of Air Force interest. One component of this work has been the identification and development of appropriate photothermal methods for the Air Force environment. This has included TRIR methods in general as a class of rapid-scan thermal NDE techniques. In addition specific Air Force applications have been addressed including turbine blade coating integrity for a range of coating types and more recently damage in advanced composites.

This year's work is described in the next section of this report. In this section a review of prior work is presented to provide an appropriate background.

The initial photothermal imaging and characterization was carried out on coated specimens of NiAl coatings on high temperature metal substrates using optical beam deflection, thermoelastic detection and single point IR detection methods. The IR detection investigation included studying the fast-time response of NiAl coatings to pulsed laser heating on a submicrosecond time scale. This work showed temporal response for these coatings which had a fractal character consistent with the structure of the coatings themselves. Optical beam deflection images of surface and subsurface features of the coated surface were obtained with spatial resolution at the 3 micrometer scale. This work indicated the complex structure of the coatings and suggested that some of the failure mechanisms could be connected with small sized compositional variations of the coating.

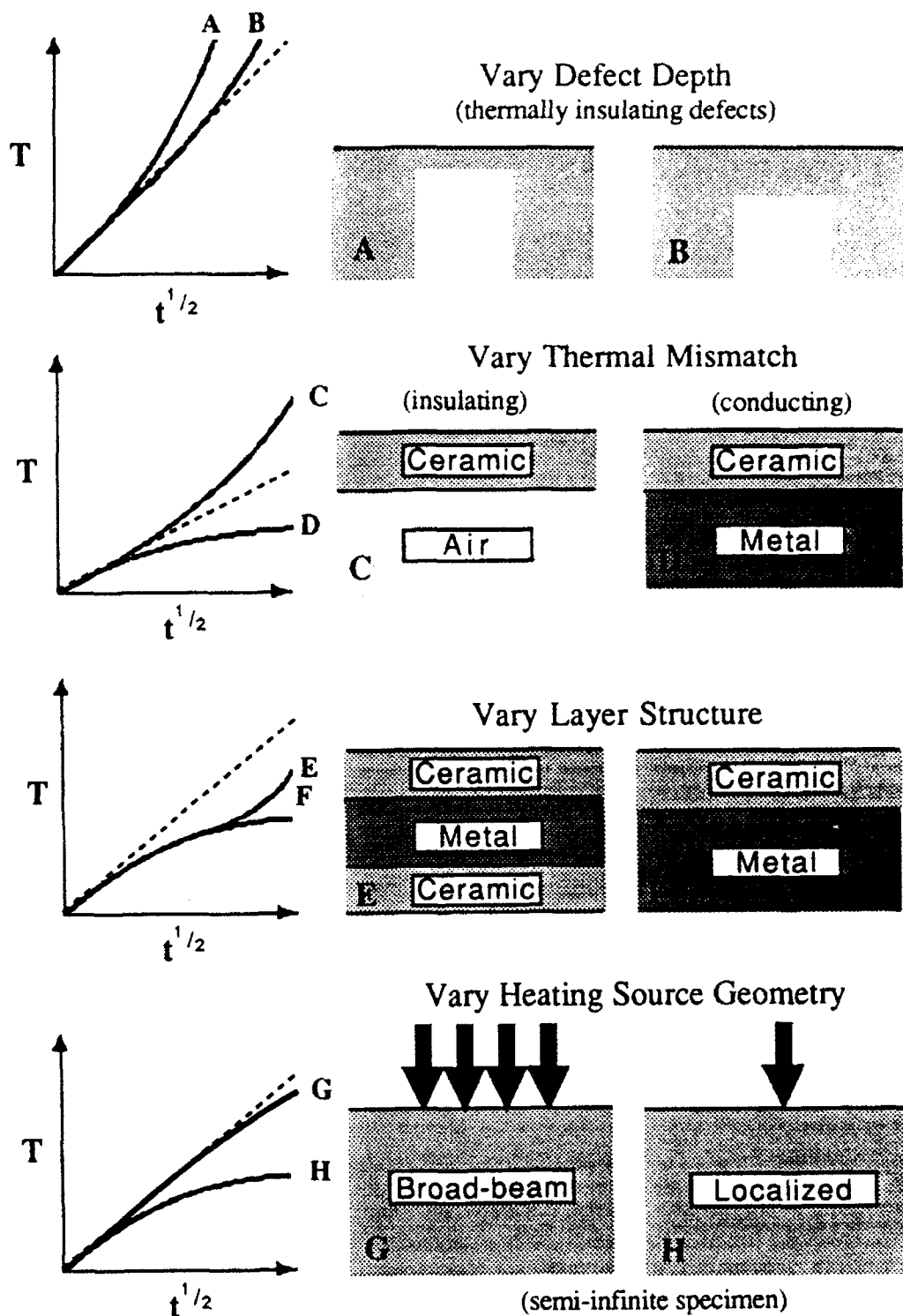


Figure 1 Summary of typical TRIR T_s - $t^{1/2}$ linescans obtained for a series of specimen configurations and experimental situations.

Coating thickness was measured thermally and compared with profilometer measurements of the coated surface. All three analytical tools were shown to provide complementary but consistent information about these samples.

Based on this initial work the TRIR technique was developed as a non-contacting, noninvasive tool for monitoring large areas. In its initial form the method was based on a one-dimensional analysis of heat flow through a single layer, a configuration which was appropriate for study of subsurface defects. It was of special value in poorly conducting materials where measurements in the frequency domain required such low frequencies that noise was a problem. After evaluation of alternative heating sequences, step function heating was selected as the preferred mode of heating for TRIR measurements with very successful results. The single layer, one-dimensional heat flow model was experimentally confirmed in a succession of experiments on plates with and without buried defects for boundary conditions that included thermally insulating and thermally conducting regions on either side of the specimen [3]. These measurements also involved the development of considerable instrumentation to collect and store experimental data.

The experiments and analysis were extended to engineering samples including zirconia barrier coatings on a superalloy substrate. These results showed that the thermal transit times through individual layers in the sample could be measured and that the results were in agreement with the theoretical transit times, the known coating thicknesses and the sample diffusivities. These results agreed with a finite element analysis that showed details of heat flow through the sample.

"Real" specimens (in contrast to fabricated specimens) were tested including turbine blades. Experiments showed the presence of poor diffusion bonding in certain areas. These measurements also imaged the subsurface structure of the blade. Finite element calculations were used to determine the temperature-time development that might be expected for specimens of varying composition and geometry including a thermally thick ceramic coating, a bonded ceramic coating, and a disbonded ceramic coating. These results were used to evaluate experimental results obtained on bonded and disbonded areas of specific samples. These experiments showed that the TRIR technique was a simple and reliable method of studying coatings. It allowed coating thicknesses to be measured, disbonded areas to be detected, and the relative conductivity of coating and substrate to be determined. Measurements could be made routinely and rapidly [1,9].

In a TRIR measurement the temperature of a small area on the sample can be followed by the IR detector as a function of time (time-temperature). The area used varies depending on the spatial profile of the source. Initially uniform heating was used. Successive traces obtained using a sequence of source pulses can be combined to give an X-Y image of the temperature at a particular time after application of the pulse heating. These images were of great value in locating defective areas in test specimens and determining their depth and thermal characteristics. Instrumentation was developed to obtain these X-Y images.

The measurements and analysis were extended to multilayered samples and to nonuniform heating sources where lateral heat flow was present. A multilayer theory was developed for one dimensional heat flow [3], and the single layer model was extended to include non-uniform and narrow-beam heating. Concurrently single layer samples were studied experimentally on a range of test specimens to determine the visibility of flaws when a simple one-dimensional thermal model was inadequate. One set of experiments performed with a Macor/aluminum test specimen with known subsurface defects showed that TRIR could locate and size these defects even when non-uniform heating was used. The experiments including the temperature-time curves were in good agreement with theoretical predictions. A ceramic-superalloy-ceramic specimen was also tested. Again the

results confirmed the theoretical predictions of the multilayer model. Although multilayer specimens still present a number of technical difficulties in analysis, the theory provides a straight-forward method for approaching this analysis.

Coating disbonding was studied using specimens of thermal barrier coating on a superalloy substrate. The data showed a range of temperature-time responses at different points in the disbonded area suggesting various degrees of disbonding. This illustrated the ability of TRIR methods to distinguish different degrees of disbonding. To provide a theoretical basis for these conclusions, a series of theoretical curves were calculated using the multilayer theory. Air gaps of different thicknesses were used to represent disbands of different degrees. These results from the equivalent air-gap model were compared with experimental results on a TBC/superalloy sample. All of the qualitative features of the experimental temperature-response curves were correctly identified. An interesting result is that in both theory and experiment air gaps as small as 0.1 micrometers produced measurable changes in the temperature response. The TBC/superalloy specimen was subjected to destructive analysis. This analysis showed that the spatial variation of the amount of coating-substrate separation seen in the micrograph was well correlated with the results obtained from the TRIR temperature-time curves. However, there was a systematic difference between the measured and calculated values obtained for the separation distances. This may indicate that the air gap model does not represent the spatial varying bonding expected for failure at a real interface. This important issue deserves further study.

The work described above provided a basis for this year's work. First, the successful application of the multilayer model showed that the TRIR technique should be applicable to composite and structured materials. Secondly, a study of lateral heat flow was necessary to exploit shaped heating sources in TRIR measurements so as to enhance the method's ability to detect subsurface vertical cracks.

Objective and Scope

Composite materials have become increasingly important in engineering structures. Their usefulness is dependent upon the integrity of the composite structure which can be damaged by improper fabrication, by impact (producing partial or complete disbonding of composite layers, broken fibers, etc.), and by deterioration with age, wear, and other causes. Accordingly it is important to be able to ascertain the type of damage that a structure may have sustained and the extent of this damage. In addition to determining the integrity of a particular structure, such tests can provide information about the efficacy of fabrication techniques, the development of new materials useful in composites, and improved design of composite structures. An inspection system that could rapidly supply quantitative image information could be used both to monitor structural components in an "aging aircraft fleet," and to aid the design and construction of new aircraft.

The importance of composite and structured materials and the previous successful use of the TRIR technique in studying coatings and multilayer materials strongly suggested that TRIR could be used to study this class of materials. A full development of the capabilities of TRIR in study of composites will require a level of effort well beyond the resources available under this program. Hence, the tasks projected for 1991 are only a beginning. Several specific objectives were selected for the initial work. These were:

- to study impact damage experimentally in a representative composite sample in order to determine if technique could identify and characterize this damage.
- to extend the multilayer theory upon which TRIR measurements are based to composite and structured materials which contain thermal structure within each layer. The initial goal was to model planar specimens containing repetitive thermal structures.

- to develop finite element or finite difference programs to study composite systems, that are too complicated to be studied analytically.
- to study the effects of lateral heat flow on TRIR measurements and to use this information to increase the ability to locate and characterize vertical defects in complex specimens.

This last objective was related to results that indicated that modifying the spatial pattern of the heating source could allow TRIR measurements to enhance the spatial resolution of the method via competition between normal and lateral heat flow. This could help the ability to characterize composites.

Given the resources available under this contract, the following specific activities were conducted under the four objectives:

- study impact damages in a specimen consisting of E-glass/epoxy face plates surrounding a graphite/epoxy core--damage having been caused by a projectile fired through the specimen.
- restructure the multilayer model to apply to planar samples with repetitive thermal structures and adapt this formulation for comparison with experimental results.
- develop a desk-top finite element program for studying heat flow in moderately complicated thermal configurations of interest in analysis of composite specimens.
- study lateral heat flow using line and point heating sources as examples of more general class of shaped heating sources and to evaluate how changes in source geometry modifies and ability of TRIR to detect vertical cracks.

In all of this work, theoretical development and experimental work was closely coupled.

Approach

Our work with composite systems has had two thrusts--(1) to model heat flow in composite materials and (2) to use this model to extend the TRIR technique to test composite systems. Models have been developed in a progression from a one-dimensional, single layer model to more complex models which reflect features of composite materials. For the more complicated cases, finite difference and finite element models were developed to permit evaluation. An effort was made to keep this procedure from becoming a purely numerical exercise where important features of the results would be lost by doing some analytical studies in parallel. To assist the experimental work, some theoretically derived rules of thumb were developed and characteristic parameters identified. A semi-analytic approach has been used wherever possible to avoid the nonintuitive results sometimes obtained when a purely numerical approach is used. An effort was made to simplify the computational procedures so that they could be carried out rapidly.

Modeling had a two fold purpose, i.e., to provide a basis for interpreting experimental data and to suggest additional experimental modifications that might be of value. The latter involved investigating different heating and detection patterns and determining the results to be expected from them. Experimental work also followed a progression through more complicated systems. Since the original TRIR technique is based on one-dimensional theory and uses broad beam heating, the first work on composite materials used this approach. It was extended by using localized heating sources, which required the use of a three dimensional analysis including lateral heat flow.

Both fabricated and engineering specimens were used in the experiments. Fabricated specimens allowed specific features of the sample response to be correlated with theory. Throughout the project theoretical analysis and modeling has paralleled experimental work providing it with calculated thermal properties and an estimate of characteristic parameters.

Technical Progress

A. Experimental Studies on "Real" Composite Systems

A series of experimental studies was performed in the first two quarters of this program on simple and hybrid composite systems. Artificial defects drilled to different depths in a carbon/carbon composite have been detected and distinguished based on defect depth. Figure 2(a) shows a sketch of this specimen and indicates the region scanned by TRIR and the locations of 4 reference points for sound material (A) and over defects of increasing depth (B, C and D). Figure 2(b) shows the TRIR $T_s - t^{1/2}$ linescans for these

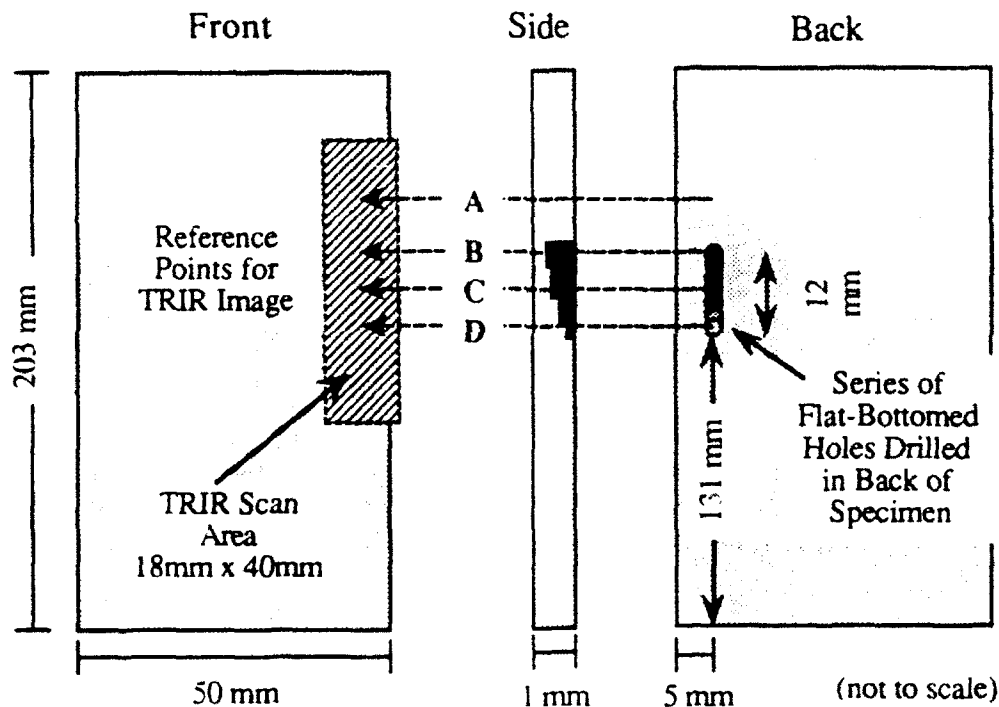


Figure 2(a) Diagram of carbon/carbon composite specimen with flat-bottomed holes drilled from the back face. The TRIR scan region on the front face is shown.

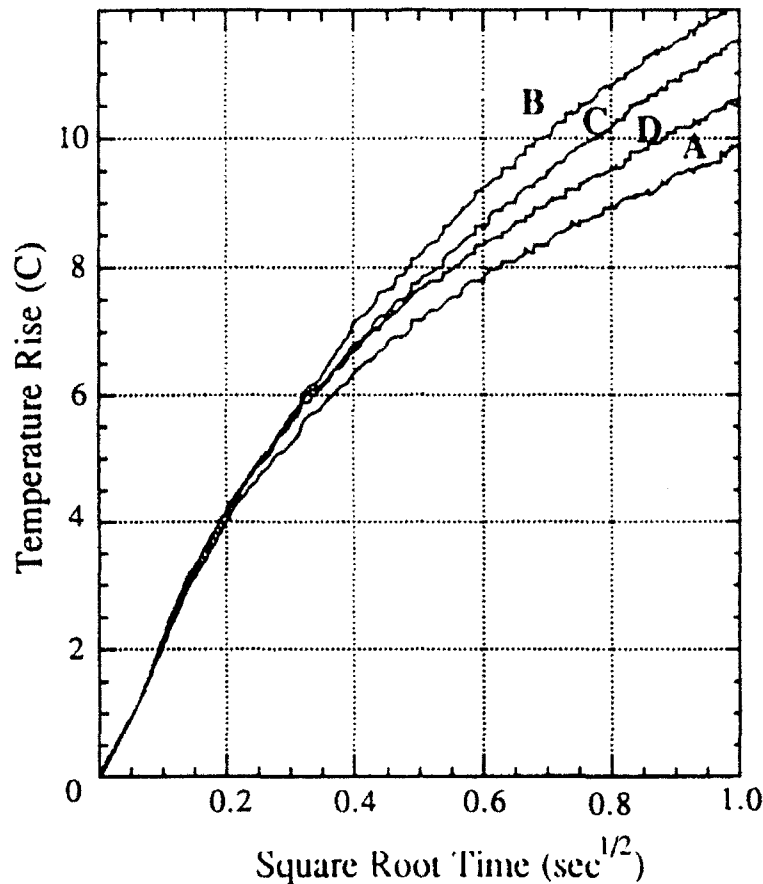


Figure 2(b) TRIR $T_s-t^{1/2}$ linescans for the locations marked on the figure of the carbon/carbon composite specimen shown in Fig. 2(a).

locations for a line heating source with a pulse duration of 1 second. Note the largest temperature excursion occurs over the shallowest hole (Location B) with smaller excursions for deeper holes until the response of intact material (Location A) is obtained. These results illustrate the ability of the TRIR technique to measure differences in the thickness of a sample. In Fig. 2 as the hole becomes shallower, the sample thickness decreases and the corresponding temporal line scan deviates more from linescan A (where no hole had been drilled). A practical application of this capability of the TRIR technique is testing the uniformity of a composite layer. For materials with homogeneous thermal properties, the accuracy of thickness measurements is approximately 2% [1].

Subsurface delamination produced by impact damage has also been imaged in a hybrid composite. A diagram of this specimen is given in Fig. 3(a) and a series of TRIR $T_s-t^{1/2}$ linescans is shown in Fig. 3(b) for different locations on the composite. Note that all the curves agree with one another up to about 0.3 sec^{1/2}. This is the expected thermal transit time for the E-glass/epoxy layer. At this time the data for Location A which is well-removed from the damaged area in the specimen shows a slope decrease as is expected for a well-bonded region of the specimen. The curves for the other locations where damage has occurred all show a slope increase at this location indicating that delamination occurred at this depth. The shape of these curves does vary, however, and at present we interpret this as resulting from different degrees of delamination of the E-glass/epoxy layer from the graphite-epoxy layup. The use of localized heating methods and lateral heat flow for improved resolution of defects has also been demonstrated by comparing images obtained

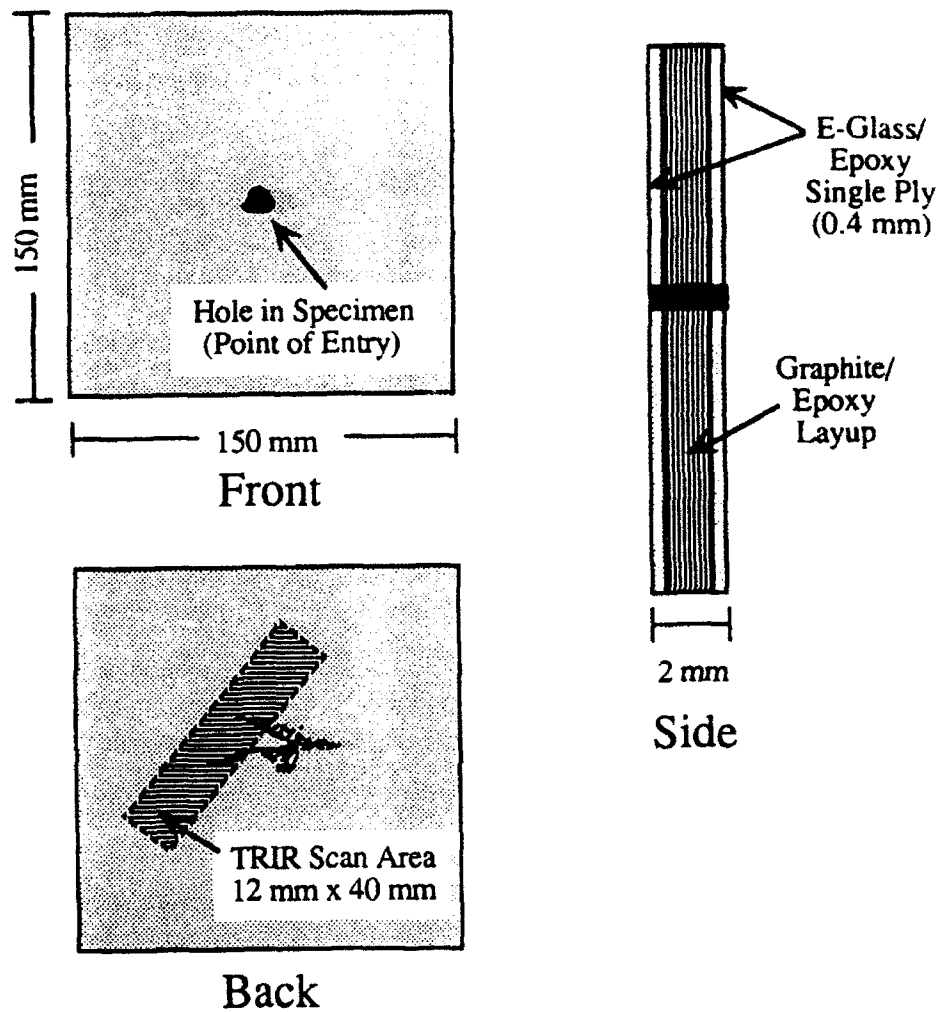


Figure 3(a) Diagram of hybrid composite specimen subjected to impact testing showing TRIR scan region on the back face.

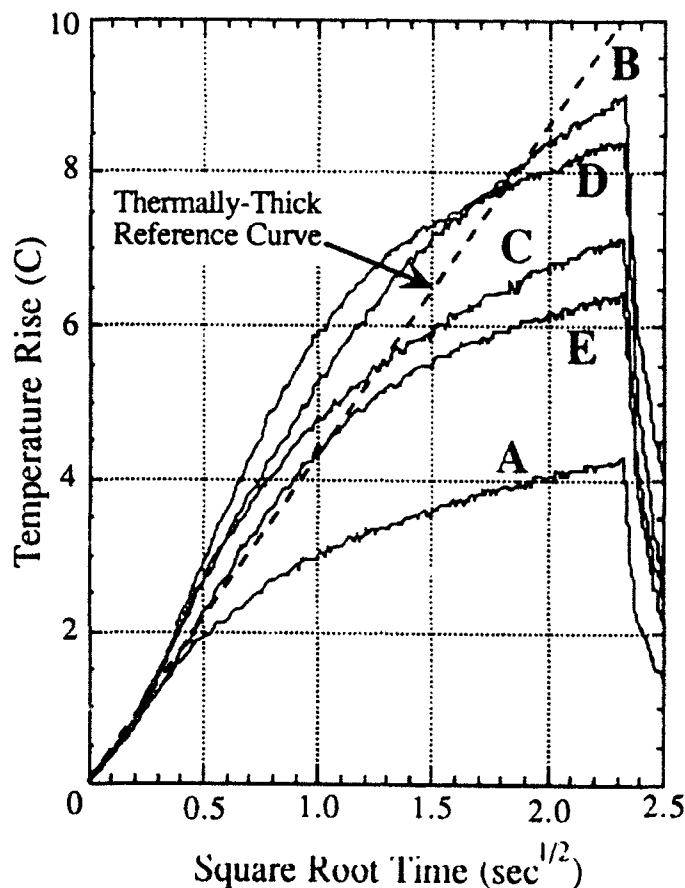


Figure 3(b) TRIR $T_s-t^{1/2}$ linescans for different locations marked on the back face of hybrid composite shown in Fig. 3(a).k

with area heating methods with those obtained with a line heating source.

B. Finite Element Model for Heat Flow in Composite Structures

Analytical solutions obtained from modeling have the advantage that they clearly portray the factors producing the resulting heat flow pattern. They are limited, however, by the degree of complication that can be introduced in the model and still obtain a solution. More complicated structures including composite materials with defects must, of necessity, be studied using finite element or finite difference calculations. In addition to the statistical nature of these measurements, which are not always easy to analyze, such studies for composite materials have other difficulties. In order to properly model the repetitive nature of the sample, a large number of nodes are required, placing heavy demands upon the available memory and computation time. Model creation time is also a factor. Ideally a finite difference or finite element program is desired that can easily be set up and easily modified to allow a quick comparison of competing models to be made.

Two finite difference programs using the iterative approach were developed during the second and third quarters of 1991. Both programs were three dimensional and were constructed to allow rapid entry of repeated structures within the node pattern. A processing procedure was devised that conserves the amount of memory needed for each substructure thus allowing a larger number of nodes to be included in the model which are needed to study composite materials. Provisions were made to use various heating patterns and to introduce a variety of defects of several standard shapes. In particular, delta-function

heating, gaussian heating and uniform heating could be accommodated, as well as a moving heating source. Each of these heating patterns could be designated as producing surface or exponential heating. The display allowed the viewing of various planes in the sample as well as monitoring the temperature at particular points as a function of time. Use of these programs allowed a quick check for accuracy of intuitive feelings regarding heat flow in a moderately complicated configuration.

C. Lateral Heat Flow - Modelling and Experiment

When the studies of the hybrid composite systems described above indicated that lateral heat flow plays an important role in the resolution of detection of subsurface damage, some simpler laboratory experiments were conducted with an idealized specimen during the last quarter of 1991. This provided a means for more clearly determining the effect of instrumental and physical parameters on the thermal measurements. The sample is shown in Fig. 4 and consisted of a large block of Macor in which the edge of the block was considered to represent a well defined vertical defect.

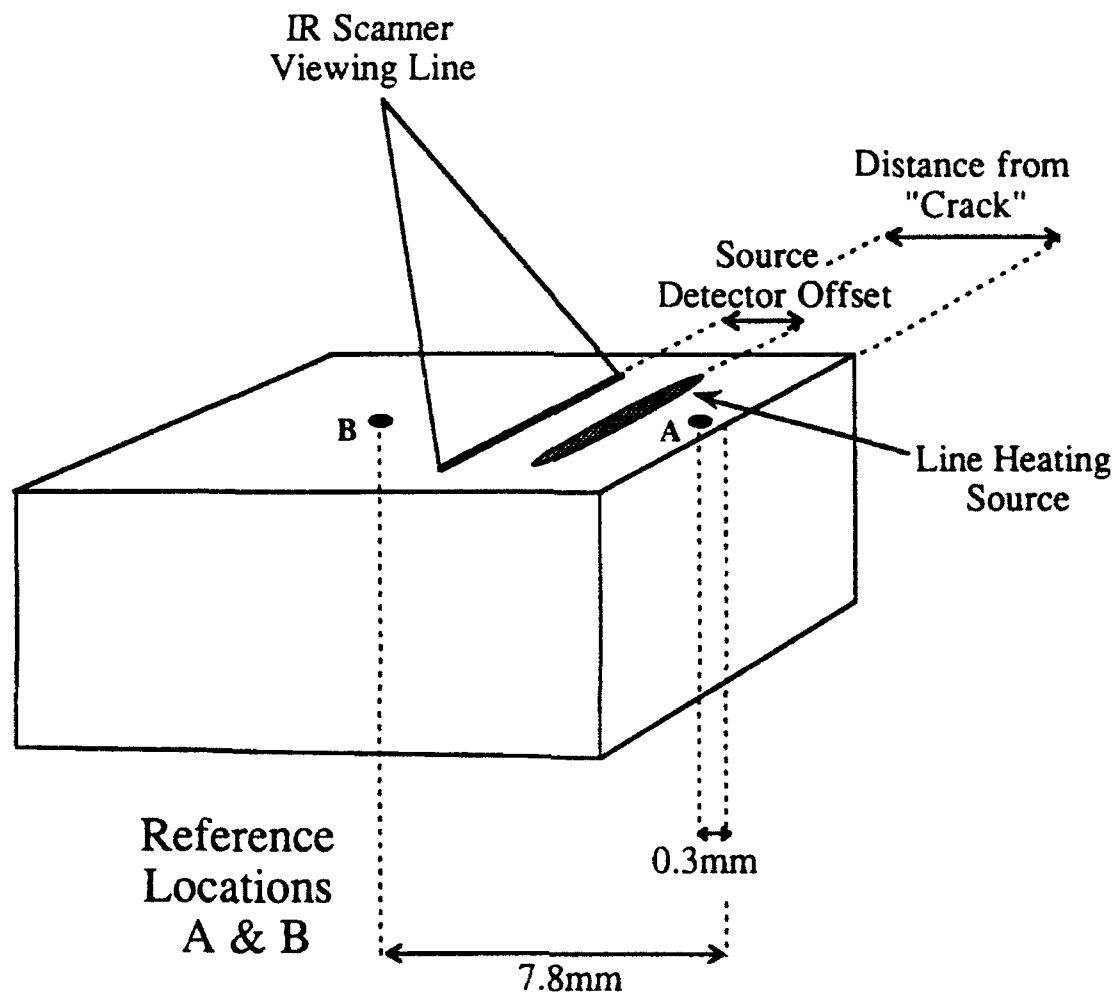


Figure 4 Schematic diagram of specimen used for source-detector offset experiments.

The simplified conditions of this experiment allowed the development of a model that accurately described the real situation for a relatively non-heat conducting gas such as air. This same model also provided a good initial approximation for other lateral defects, especially those that block most of the lateral heat flow. The model was evaluated for heat sources that were small compared with the separation between the heat source and thermal detector, but the model was more general and could accommodate any heating pattern. It assumed a planar sample and was developed by inserting a continuum of instantaneous and localized heat sources in such a manner that duplicated the experimental heating source. A variety of boundary conditions could then be matched by inserting image heat charges defined in terms of the well known method of images, as needed. Experimental conditions allowed the assumption of a thick plate, but results could equally as well be obtained for a thin plate.

An expression for the specimen surface temperature as a function of source-detector separation, S , and distance, L , from a vertical defect for heating with an infinitely narrow line source is as follows:

$$T(L, S, t) = -\frac{H_0}{4\pi\kappa} \left[E_i\left(\frac{S^2}{4\alpha t}\right) + E_i\left(-\frac{(S+2L)^2}{4\alpha t}\right) \right]$$

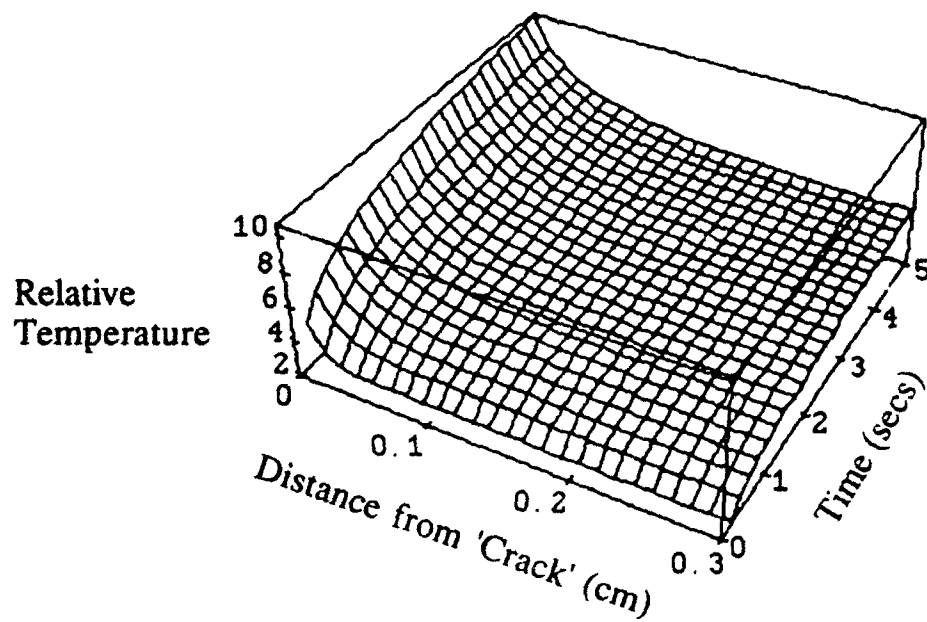
where α is the thermal diffusivity, κ is the thermal conductivity, and E_i is the Exponential-integral function. Figure 5(a) shows this expression plotted in three-dimensional form as a function of both distance from the crack, L , and time after turn on of the heating pulse for values of source-detector separation of 0.2 mm and 2.0 mm. Note that the development of surface temperature with time is quite different for these two source-detector distances showing concave downward and upward curvative, respectively, at small times. Also note the significant increase in surface temperature as the distance from the crack is decreased.

Experimental validation of these results was performed by measuring the time-development of the surface temperature for a series of source-detector offsets at a number of positions with respect to the crack. Some of these results are shown in Fig. 5(b) which gives the temperature-time response for Location A adjacent to the crack (solid curve) and Location B well-removed from the crack (dashed curve) for source-detector separations of 0, 0.8, 1.4 and 2.0 mm. Note that the difference between the responses for Location A and B is not large for an offset of 0 but increases as the offset increases. This result is summarized in the following table. The contrast ratio is defined as the temperature at 1 sec for Location A divided by the temperature at 1 sec for Location B and provides a measure of the relative visibility of the 'crack' for different offsets.

Offset (mm)	Temperature at 1 sec Location A	Temperature at 1 sec Location B	Contrast Ratio
0	5.8	5.4	1.07
0.8	5.5	4.2	1.31
1.4	2.8	1.8	1.56
2.0	1.6	1.0	1.6

Note that although the magnitude of the temperature rise decreases as the offset is increased, the contrast ratio increases. This illustrates the advantage of using a line heating source and a detection line that are not collinear for detecting vertical defects. Choice of a source-detector separation that is too large will however produce temperature rises which are too small to be accurately measured.

A. Source-Detector Separation = 0.2 mm



B. Source-Detector Separation = 2.0 mm

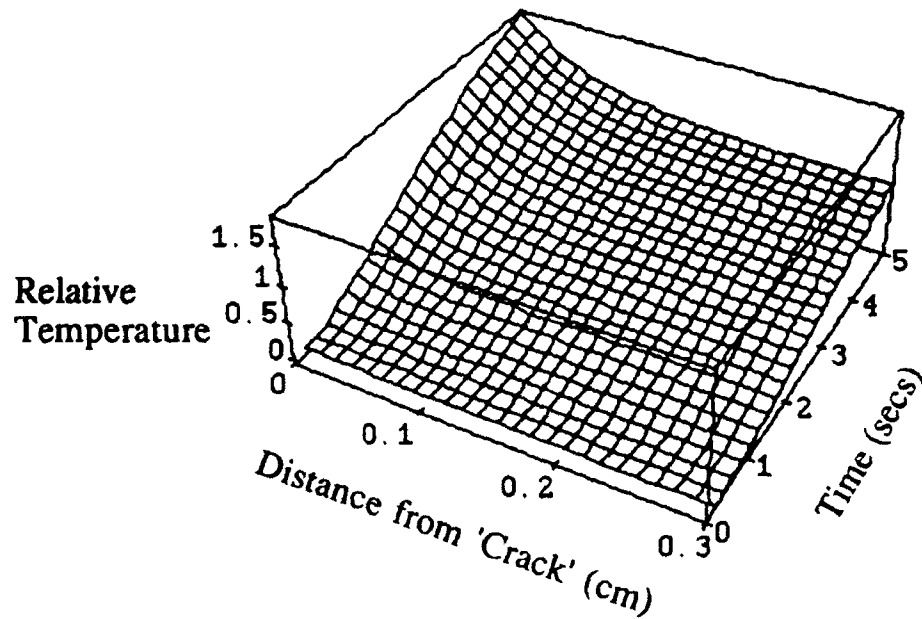


Figure 5(a) Analytical results for detection of vertical crack by lateral heat flow.

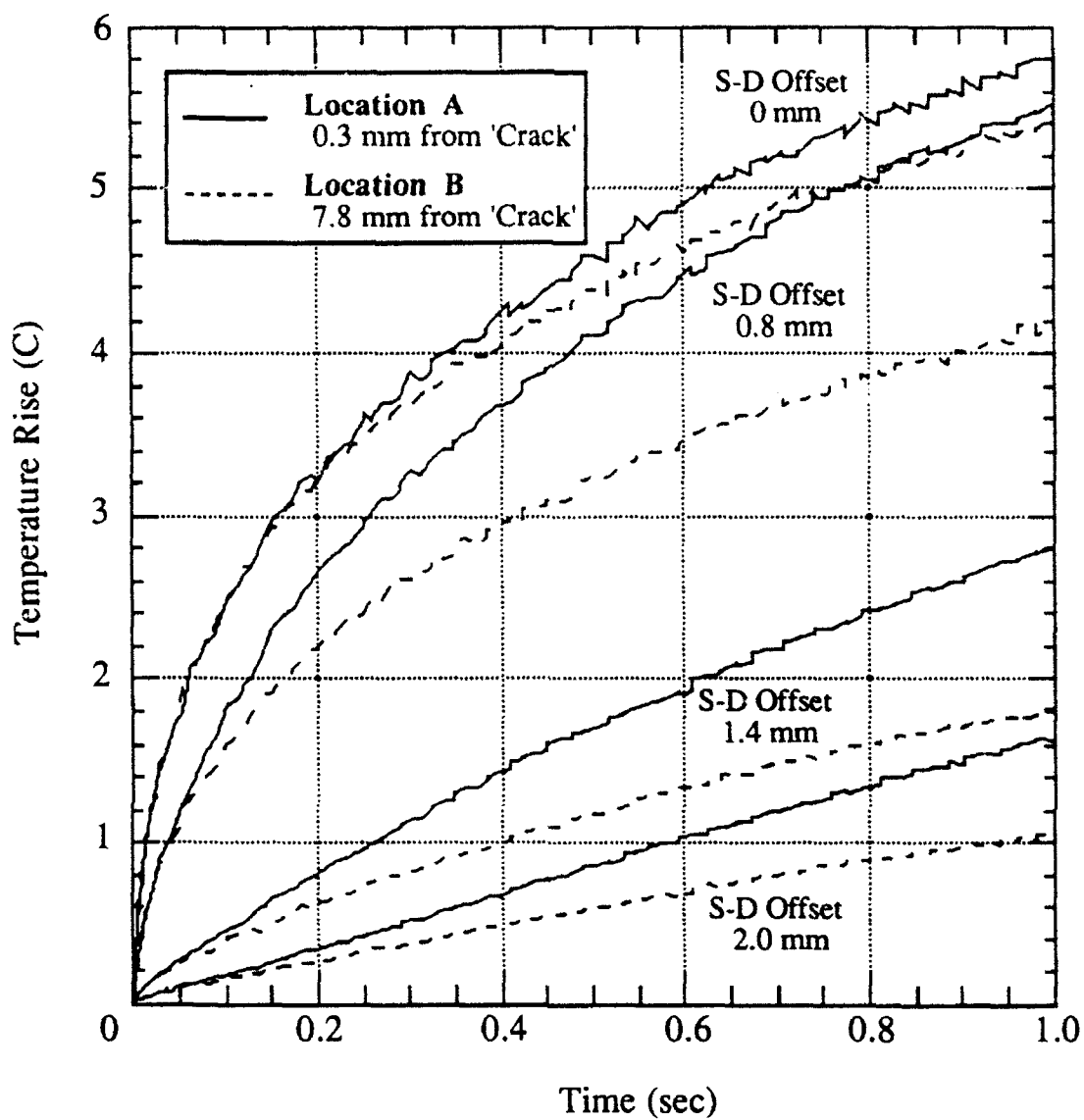


Figure 5(b) Experimental TRIR temperature vs time curves for a series of source detector offsets for Location A near the sample edge ('crack') and Location B which is well-removed from the edge.

Summary

The thermal NDE methods using infrared detection and based on the TRIR method of analysis have been shown to be able to detect and quantify defects in structured and composite materials. Experiments using spatially controlled deposition of heat have also shown the importance of lateral heat flow and has demonstrated that shaping the heating source affects image contrast in TRIR images. This enhances TRIR's ability to locate and characterize vertical defects.

There is excellent agreement between the experimental measurements in composites and the multilayer model that has been developed. These results point toward further refinements in the TRIR technique that can make it capable of more detailed analysis of defects and bond integrity

At this stage in its development, the TRIR method can be used to measure thermal properties in a material, determine thermal transit times for heat flow through layers, locate defects including the disbonding between layers in a composite or structured specimen, image disbonded areas, provide a quantitative measure of the integrity of bonds, and determine the thickness and bond integrity of coatings.

Plans for Next Year

This particular project will not be continuing in 1992. A new project entitled "Thermal Wave Studies of Airframe Corrosion" will be started and its objective is to investigate the application of thermal wave imaging techniques to detection and characterization of hidden corrosion on airframe structures.

References

1. "Coating Thickness Determination Using Time Dependent Surface Temperature Measurements," Review of Progress in Quantitative Non-Destructive Evaluation, D. O. Thompson and D. E. Chimenti, eds. (Plenum Press, New York), Vol. 6A, pp. 277-284, March 1987.
2. "Nondestructive Characterization of Coatings in Metal Alloys," by J. C. Murphy, G. C. Wetzel, Jr., and L. C. Aamodt, Review of Progress in Quantitative Nondestructive Evaluation, D. O. Thompson and D. E. Chimenti, eds., Vol. 5A (Plenum Press, New York), pp. 759-766, March 1987.
3. "Thermal Imaging Barrier Coatings on Refractory Substrates," by J. C. Murphy, J. W. Maclachlan, and L. C. Aamodt, Review of Progress in Quantitative Nondestructive Evaluation, D. O. Thompson and D. E. Chimenti, eds., Vol. 7A (Plenum Press, New York), pp. 245-252, March 1988.
4. "Thermal Wave Imaging: Detection of Subsurface Features in Opaque Solids," by J. C. Murphy, J. W. Maclachlan, and L. C. Aamodt, "Scanning Microscopy Techniques and Applications," E. Teague, ed., Proc. SPIR 897, pp. 135-141 (1988).
5. "Time Resolved Infrared Radiometric Imaging of Coatings," by J. W. Maclachlan Spicer, J. C. Murphy, and L. C. Aamodt, Review of Progress in Quantitative Nondestructive Evaluation, D. O. Thompson and D. E. Chimenti, eds., Vol. 8A (Plenum Press, New York) pp. 1297-1304.
6. "Measurement of Coating Physical Properties and Detection of Coating Disbonds by Time-Resolved Infrared Radiometry," J. Nondestructive Evaluation, Vol. 8, pp. 107-120 (1989).
7. "Characterization of Ceramic Coatings by Advanced Nondestructive Evaluation Methods," J. W. Maclachlan, J. C. Murphy, and L. C. Aamodt, Proc. Ceram. Eng. Sci., Vol. 9, pp. 1181-1188 (1989).

8. "The Effect of Transverse Heat Flow and the Use of Characteristic Times in Studying Multilayered Coatings in the Time Domain," Photoacoustics and Photothermal Phenomena II, J. C. Murphy, J. W. Maclachlan Spicer, L. C. Aamodt, and B. S. H. Royce, eds., Springer-Verlag (Berlin-Heidelberg), Vol. 62, pp. 59-63 (1989).
9. "Analysis of Characteristic Thermal Transit Times for Time-Resolved Infrared Radiometry Studies of Multilayered Coatings," L. C. Aamodt, J. W. Maclachlan Spicer, and J. C. Murphy, J. Appl. Phys., 68, pp. 6087-6098 (1990).

LIMITED DATA COMPUTED TOMOGRAPHY USING *A PRIORI* DATA

R. A. Roberts
Center for NDE
Iowa State University

Executive Summary

This task is aimed at the development of improved limited angle computed tomography (CT) reconstruction techniques for NDE of structural components. This is an important problem in inspections where angular access to a structural component is limited due to, say, a physical obstruction. A related limited data problem is likewise encountered when inspecting high aspect ratio components for which X-ray penetration is not practical in the long dimension. Considerable effort has been directed towards related problems in medical CT applications. However, the NDE CT application has attributes (as explained below) not found in the medical problem, which, if exploited properly, could significantly improve the quality of limited data reconstructions beyond that provided by medical application algorithms. The objective of this work is to develop limited data CT algorithms which compensate for the missing data through the exploitation of the *a priori* known attributes of a structural component.

The *a priori* known attributes of a structural component might be in the form of an explicit specification, such as a CAD drawing of the intended geometry and composition of a component, or the information may be of a more implicit nature, such as knowledge of the class of flaws (cracks, dimensional abnormalities, density gradients etc.) to be detected. The objective of this project is to develop means to incorporate both explicit and implicit *a priori* data into the reconstruction process. Work to date has targeted the problem of reconstructing compact flaws, such as cracks and dimensional abnormalities. Specifically, the project is aimed at developing an algorithm which i.) incorporates CAD geometry and composition information such that the reconstruction is as "close" to the CAD drawing as possible, and ii.) discrepancies between the CAD information and the reconstruction are as compact as possible.

Primary focus in calendar year 1991 was the incorporation of CAD drawing component geometry and composition information into the limited angle CT reconstruction procedure. This task utilizes the "support minimization" concept developed in the initial year of the project (FY90) to spatially register the *a priori* information, and to reconstruct any flaws (cracks, etc.) as compactly as is permitted by the available experimental data. Specific accomplishments include:

- Development of limited data CT algorithms to:
 - i) variationally register *a priori* data
 - ii) reconstruct data by minimizing support of difference between *a priori* and measured data
 - iii) smooth images while maintaining complete consistency with measured data
- Verification of algorithms through application to experimental data sets

Background

A. General

The project addresses the problem of computed tomographic (CT) image reconstruction when the available data is insufficient for an acceptable reconstruction. Such situations commonly arise in NDE applications where angular access to a component is limited, such as the inspection of panel-like structures (e.g. wings). Data can also be limited when inspecting high aspect ratio structures due to excessive X-ray attenuation in the long direction of the component. Similar problems are encountered in medical applications of X-ray CT. However, limited data CT of structural materials is a potentially more tractable problem than the medical counterpart due to the lesser complexity of the structures involved. As an example, NDE applications often require the detection of isolated cracks in an otherwise homogeneous material. In this case, the homogeneity of the material presents an extremely powerful symmetry to be exploited which is absent in medical applications. Likewise, the compactness of the defect is a potentially powerful attribute to be exploited. Furthermore, in many structural applications, complete geometric and compositional information of the defect-free component are available, often in the form of a CAD drawing. Due to this wealth of additional information available in the NDE application, it is conceivable that significant improvements in the reconstruction of limited data are attainable beyond what is provided by current medically-based approaches to the problem.

Attempts previous to this project have been made to utilize *a priori* component geometry information in the reconstruction process. In this previous work, missing projections are replaced by synthetic projections calculated from a CAD drawing of the component. Two significant problems are associated with this approach. Firstly, utilizing explicit *a priori* geometric and compositional information requires the registration of the *a priori* data with the available measured data. This problem proved quite formidable due to the extreme sensitivity of reconstruction artifacts to data misalignment. Secondly, the *a priori* data contains no information regarding unknown defects, so that even with perfect *a priori* data alignment, any flaws present will still reconstruct poorly. Thus approaches are needed which incorporate more abstract forms of *a priori* information, such as flaw compactness or material homogeneity. Previous efforts in limited data CT utilizing *a priori* component geometry information are described in references [1-3]. Less effort has been directed towards exploitation of more abstract forms of *a priori* data. An approach similar in intent to that reported in this document is the work by Tam [4] which constructs a convex hull to limit the support of the reconstructed object. However, the work reported here seeks not to impose an *a priori* specified convex hull, but rather to determine the hull of smallest area (or volume in 3-D) possible, as will be seen in the technical discussion below.

B. Project

Efforts in the first year of the project (FY90) addressed the problem of incorporating more abstract forms of *a priori* information into the reconstruction. A scheme for optimizing functional measures of image attributes was devised. In this approach, abstract notions of image attributes such as "smoothness" and "compactness" are quantified by operating on the reconstructed image with an appropriate functional, and this functional is optimized such that the reconstructed image remains *completely* consistent with the measured data. Using this approach, the problem is transformed into one of determining i) what image attributes is the reconstruction known *a priori* to possess, ii) which of these are the most significant, i.e., will yield the most image improvement when optimized, and iii) what are effective functional measures of the identified attributes? Experimentation in the first year of work identified the *compactness* of a reconstructed object to be an extremely significant attribute when reconstructing structural objects and/or isolated flaws such as cracks or inclusions. An algorithm was developed which measures and minimizes the area

occupied by the reconstructed object, i.e., the algorithm minimizes the *support* of the object. The applicability of the concept of support minimization to the reconstruction of various classes of objects was examined, as reported in ref. [5]. There it is demonstrated how the principle of support minimization can be applied to effectively reconstruct compact, high contrast objects using an extremely limited amount of data. The effectiveness of the algorithm in reconstructing a flaw-like object is demonstrated using 90 degrees out of the 180 degrees of projection data required for a "complete" data reconstruction. The applicability to complex geometry objects (turbine blade) is demonstrated. In addition to the limited angle problem, examples of application to attenuation-limited data are also shown. A quantitative comparison is made of the reconstruction of a "seeded" inclusion in a turbine blade using both complete data and severely attenuation-limited data, which demonstrates the power of support minimization in reconstructing this class of objects. At the conclusion of the first year's effort, a tool had been devised to compensate for missing data when reconstructing compact isolated flaws for which explicit geometric *a priori* information is unavailable. At that juncture, the project was poised to incorporate this capability into an algorithm which also utilizes explicit component geometry and composition information, such as CAD files.

Objective and Scope

This project has focused on a specific class of problems, namely, the imaging of compact isolated defects (e.g. cracks, inclusions, and dimensional abnormalities) in a monolithic material structural component. This is perhaps the most generic of NDE problems, and is likely the most solvable from a limited data CT point of view. In addition to explicit geometry and compositional information, this problem allow *a priori* solution constraints to be drawn from properties such as i) discontinuity in material properties at the component boundaries, ii) component material homogeneity, and iii) the compactness of defects. In contrast, the algorithms being developed in this project are not intentionally targeting problems such as the detection of slight gradients in material density. Results have emerged, however, which show promise in addressing such problems, and could form the basis of future initiatives.

The primary objective of this year's work was the development of a reconstruction algorithm which incorporates explicit component geometry and compositional data, and combines this capability with the support minimization concept developed in the previous year's work for the reconstruction of flaws for which no explicit geometry information is available.

The scope of work includes i) the conception of new principles and approaches, ii) implementation and testing of these new principles and approaches in a synthetic data environment, and iii) the assessment of resulting algorithm performance and further refinement using experimental CT data. An intended outcome of this activity is the transfer of the techniques developed at ISU to others working in the area of limited data CT, both at Air Force NDE facilities and elsewhere. This could be in the form of the transfer of software. However, because our new-generation software is quite machine specific, it is more likely that the transfer will take place through an interaction in which data sets provided by interested parties are studied using our algorithms, and if the results are deemed worthwhile, the interested parties would develop their own algorithms based on, and perhaps improving upon, our models.

Approach

In initial work, it was determined that an algorithm based on a variational functional optimization would be most appropriate for this project. In this approach, a functional measure of solution properties is optimized variationally so as to determine the solution consistent with the measured data which best optimizes the specified functional. Although potentially slower and more computationally intensive than other approaches, this approach generally assures convergence to a solution (although perhaps not the desired solution) even in the case of highly nonlinear functional operators. This allows efforts to be concentrated on higher-level conceptual issues, such as what behavior the optimized norm should display, as opposed to procedural issues such as how to arrange a non-linear iteration for convergence. Means of accelerating the performance of an otherwise effective reconstruction algorithm was not viewed as a primary focus of the preliminary research.

The most significant advance resulting from this work to date was the development in the first year of an approach which seeks to minimize the area occupied by the reconstructed image. This principle of "support minimization" yields reconstructions superior to maximum entropy and minimum l_2 norm methods when applied to structural components considered in this report. This fact indicates that object compactness is a very significant attribute, which, fortunately, most structural objects possess (i.e., structural elements generally do not diffuse gradually into their surroundings).

A novel approach has been implemented in the incorporation of explicit geometric and compositional *a priori* data into the reconstruction procedure. Earlier attempts at manual data registration (in this project and in the work of others) demonstrated the sensitivity of reconstruction artifacts on small misalignments of the data, thus indicating the need for a more sophisticated approach. A variational technique for data alignment was implemented which optimizes six registration variables (x-y translation, rotation, x-y scaling, pixel intensity scaling and mean pixel intensity). The variational data alignment is performed by minimizing the difference between the *a priori* object and the reconstructed object (which, of course, is not initially available). An algorithm was developed which performs this variational alignment simultaneously with the image reconstruction. The chosen measure of the alignment was not the integrated squared error, but rather the *minimal support of the difference* between the reconstruction and the *a priori* data. The use of the minimal support alignment has proven effective in the cases examined. The result of the procedure is that differences between the *a priori* data and the reconstruction are made as compact as possible. Thus compact flaws such as cracks, inclusions, and dimensional errors are reconstructed very well as seen in the results presented in this report.

The approach adopted for experimental algorithm verification is to remove projection data from an experimental data set which otherwise yields acceptable reconstructions. Algorithm performance is then judged by comparison of the limited data reconstructions with reconstruction of the complete data set. Experimental data sets are obtained using the microfocus radiography facilities at CNDE/ISU, and from other off-site sources.

Technical Progress

This discussion will be limited to measurements represented by Radon projections, such as projection radiography, although the concepts can in principle be applied to, say, measurements modeled by diffracting wavefields. Consideration is restricted to two dimensions, in which case the inverse mapping can be written

$$\mu(r, \phi) = \int_0^\pi d\theta \int_{-\infty}^{\infty} h(r \cos(\theta - \phi) - u) m(\theta, u) du \quad (1)$$

where, in an X-ray measurement, $\mu(r, \phi)$ is the attenuation coefficient, $m(\theta, u)$ represents the measured projection data and $h(s)$ is a filter function whose Fourier transform $\hat{h}(k)$ approximates $|k|$. In the examples of this paper, data are assumed to be collected on an equi-spaced rectangular grid over the $\theta - u$ measurement plane (i.e. parallel beam tomography). The discretized implementation of eq. (1) used in this work is a standard convolutional back projection algorithm employing a small amount of Gaussian filtering. The discretized algorithm is represented as a linear mapping by

$$\mu_{ij} = \sum_l e_{ijl} m_l \quad (2)$$

where i, j refer to discrete measurement points and image points in the $\theta - u$ and $r - \phi$ planes, respectively. It is assumed that the density of the measurement point spacing in the $\theta - u$ plane is sufficient to yield an acceptable reconstruction when accurate projection data is available at all discrete measurement points. For the present purposes, a limited data set is defined as one for which data at some of the discrete measurement points are unknown, or "missing." These data are denoted m_k^m . The reconstruction problem in this case is clearly under-determined, since random values assigned to the m_k^m will produce a reconstructed image which is completely consistent with the available data. The problem is therefore to determine a set m_k^m which yields an image most consistent with *a priori* information of the reconstructed image. Stated in the abstract, assume a functional exists $F(\mu)$ which measures image attributes for which there are *a priori* information, such that the minimum of $F(\mu)$ represents closest compliance with the *a priori* information. It could be argued that the desired reconstruction is the one which optimizes this functional, i.e. the desired reconstruction is the solution to

$$\partial F(\mu) / \partial m_k^m = 0 \quad (3)$$

The objective of the present research is to determine such functionals F appropriate for applications of interest to nondestructive evaluation.

The functionals examined in this work are operators which can be expressed in the form

$$F = \int P(\mu(x)) dx \quad (4)$$

where $P(\mu(x))$ is a scalar quantity determined by

$$P(\mu(x)) = L_x(\mu(x)) \quad (5)$$

where $L_x(\mu)$ is a differential operator. Hence P represents the measure of a local image property, whereas F represents the global sum of these measures.

The development of primary importance in this work is the implementation of a functional $F(\mu)$ which measures the *support* of the reconstructed image. The motivation for this development was the repeated empirical observation that, when non-zero projection values m_j are set to zero within some arbitrary region of the $\theta - u$ plane, the resulting reconstructed image displays an increase in the number of non-zero valued pixels, i.e., the non-zero support of the image increases. This observation suggested that an effective limited data reconstruction scheme might be one which minimizes a measure of the

non-zero support of the image. The practical implementation of this notion requires not the measure of non-zero support, but rather the measure of support above some prescribed noise level ϵ . Hence the *penalty* $P(\mu)$ should be one which approximates the behavior

$$P(\mu) = 1, \quad |\mu(x)| > \epsilon \quad (6)$$

$$P(\mu) = 0, \quad |\mu(x)| < \epsilon$$

More generally, the penalty function should be essentially zero for $\mu(x) < \epsilon$ and should asymptotically approach a constant value for $\mu \rightarrow \text{infinity}$, i.e., the penalty function should be *bounded*. Clearly, such a penalty function will result in a functional F which is non-linear in μ .

The system of equations represented by eq. (3) will therefore be non-linear in the m_k^m . In the work presented here, a conjugate gradient algorithm is used to solve this non-linear system, hence it is important that the penalty function have the additional property of

$$P'(\mu) > 0, \mu > 0 \quad (7)$$

$$P'(\mu) < 0, \mu < 0$$

so as to avoid local minima or plateaus in the gradient search. The function chosen to approximate eq. (6) is

$$P(\mu) = (1 + (\epsilon/|\mu|)^\eta)^{-1}, \eta, \epsilon > 0. \quad (8)$$

Equation (8) approaches eq. (6) as $\eta \rightarrow \text{infinity}$, and also satisfies eq. (7). In practice, it is desirable to set η small (say $\eta = 2$) at the initiation of the iteration, so as to provide a larger gradient at large μ (i.e., P' not too small). This will accelerate convergence to an approximate result. At the later stages of the optimization, η can be increased (say $\eta = 6$) to improve the support minimization.

Other measures of image properties are often desired. In examples which follow, a measure of image negativity is imposed by the following modification of eq. (8)

$$P(\mu) = (1 + (\epsilon/\mu)^\eta)^{-1}, \mu \geq 0 \quad (9)$$

$$P(\mu) = \mu^2, \mu < 0$$

Equation (9) applies a quadratic penalty to negative pixel values. Note that a negative pixel value is not always non-physical. For example, if *a priori* information of a component has been subtracted from a data set, then a void within the component will have a negative attenuation in the difference image. Thus eq. (9) is not applied universally, but rather only in cases where a negative pixel indicates the generation of energy.

In examples which follow, it will be seen that the minimal support penalty allows considerable freedom in the specification of pixel values which are well above the support threshold ϵ , i.e., once the pixel value is significantly above the threshold value, the actual value of that pixel is of little consequence to the overall measured support. For this reason,

additional penalty functions can be applied which operate only on pixel values well over the support threshold, thereby having negligible effect on the total measured support. A simple penalty function of this type which enforces a maximum pixel value is obtained by the following modification of eq. (9)

$$\begin{aligned}
 P(\mu) &= (\mu - \mu_0)^2 + (1 + (\epsilon/\mu_0)^\eta)^{-1}, \mu > \mu_0 \\
 P(\mu) &= (1 + (\epsilon/\mu)^\eta)^{-1}, \mu_0 \geq \mu \geq 0 \\
 P(\mu) &= \mu^2, \mu < 0
 \end{aligned} \tag{10}$$

This penalty will discourage pixels above the threshold μ_0 . A second type of penalty applied to pixel values well above the support threshold provides a measure of image smoothness through the use of second derivative information. This is accomplished by adding the following operator to either Eqs. (8, 9, or 10)

$$\begin{aligned}
 Q &= M(\mu) [H(\partial_x^2 \mu)(\partial_x^2 \mu)^2 + H(\partial_y^2 \mu)(\partial_y^2 \mu)^2] \\
 M(\mu) &= (1 + (\epsilon/(\mu - \mu_c))^\eta)^{-1}, \mu \geq \mu_c \\
 M(\mu) &= 0, \mu < \mu_c \\
 H(s) &= 0, s < 0 \\
 H(s) &= 1, s > 0
 \end{aligned} \tag{11}$$

The factor $M(\mu)$ "turns on" the operator Q when μ exceeds a threshold μ_c which is set appreciably larger than the noise threshold η , say at 50% of the maximum image value. The operator Q equals zero when the second derivatives of the image are both zero or less. The operator is seen to take on non-zero values when $\mu > \mu_c$ and either $\mu_{,xx} > 0$ or $\mu_{,yy} > 0$. This operator allows image line profiles to rise sharply, level off, and fall sharply without penalty, but will penalize any oscillations occurring above the threshold μ_c . Thus, this penalty is, more accurately, a measure of "concavity" rather than smoothness. The observed effect of this constraint, however, is to smooth the image, and is therefore referred to as such. The relative strength of this penalty is controlled by the constant factor γ .

In addition to the functional measures applied to the reconstructed image, an additional penalty is available which penalizes negative values of interpolated projection data m_k^m

$$W = \beta \sum_k H(-m_k^m)(m_k^m)^2 \tag{12}$$

As with Equation (9), Equation (12) is applied in those cases where negative projection values would indicate the generation of energy by the object. The relative strength of this penalty is controlled by the parameter β .

Comparisons will be made with reconstructions obtained using the maximum entropy functional, obtained through the use of the penalty function

$$P(\mu) = \mu \ln |\mu/\mu_*| \tag{13}$$

The parameter μ_0 controls the width of the negative excursion of the penalty curve [5]. This penalty is seen to be unbounded as $\mu \rightarrow \text{infinity}$.

The limited data inversion technique will now be demonstrated using synthetic and experimental data. Results showing the behavior of the various penalty functions are presented using limited projection data derived from the simple half-moon object shown in Figure 1. The image of Figure 1a displays the reconstruction of a synthetic "complete" data set consisting of 101 translational points and projections at 5 degree intervals. For purposes of demonstration, half the projections (covering 90 out of 180 degrees) were set equal to zero. The resulting reconstruction is shown in Figure 1b to be poor. The negative projection penalty was incorporated in Figures 1-3.

The result of the functional optimization using the penalty function of Equation (9) is shown in Figure 2a. A threshold $\epsilon = 0.5\mu_{\text{max}}$ was used, where μ_{max} is the maximum value of the complete data reconstructed image of Figure 1a, and $\eta = 4$. The use of the minimal support minimization has essentially recovered the shape of the object. However, the image remains quite non-uniform, and the maximum pixel magnitude exceeds that of Figure 1a by 37% (maximum pixel magnitudes are 0.767 and 1.06 in Figs. 1a and 2a respectively). This is due to the relative insensitivity of the image support to the large-valued pixels. We are essentially free to optimize separate measures over the large-amplitude pixels. As an example of this, the penalty function of Equation (10) which employs a maximum amplitude threshold, was applied in conjunction with the smoothness operator of Equation (11). During the optimization, the threshold μ_0 was initially set at a very large number, then was incrementally decreased at the conclusion of each of repeated intermediate optimizations. The decreasing amplitude constraint was observed to decrease the maximum amplitude of the resulting image, but was seen to have negligible effect on the image support as long as μ_0

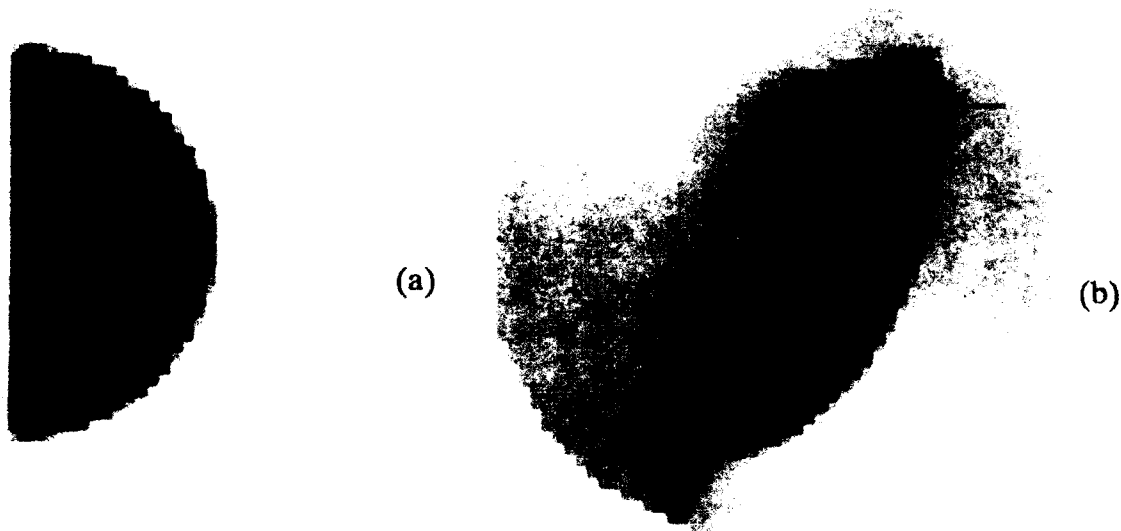


Figure 1 Simple geometry reconstructed from a.) complete and b.) incomplete projection sets.

was above the maximum pixel intensity of Figure 1a, μ_{max} . However, once the threshold fell below μ_{max} , the support of the image began to severely distort. Results are compared in Figures 2b, c for $\mu_{max} = 0.8$, and 0.2, resulting in maximum pixel magnitudes of 0.806 and 0.737, respectively. Figure 2b is a nearly correct reconstruction, whereas Figure 2c is quite erroneous. In Figure 2b, no pixel exceeds μ_0 , whereas in Figure 2c a large percentage of the pixels exceeds μ_0 . This implies that the available data requires pixel values above the threshold in Figures 2c but not in Figure 2b, which in turn indicates a measure of the information content of the available data. The success of the algorithm applied in Figure 2b is due to the fact that the penalty assigned to large amplitude pixels is more sensitive to local smoothness than absolute pixel magnitude.

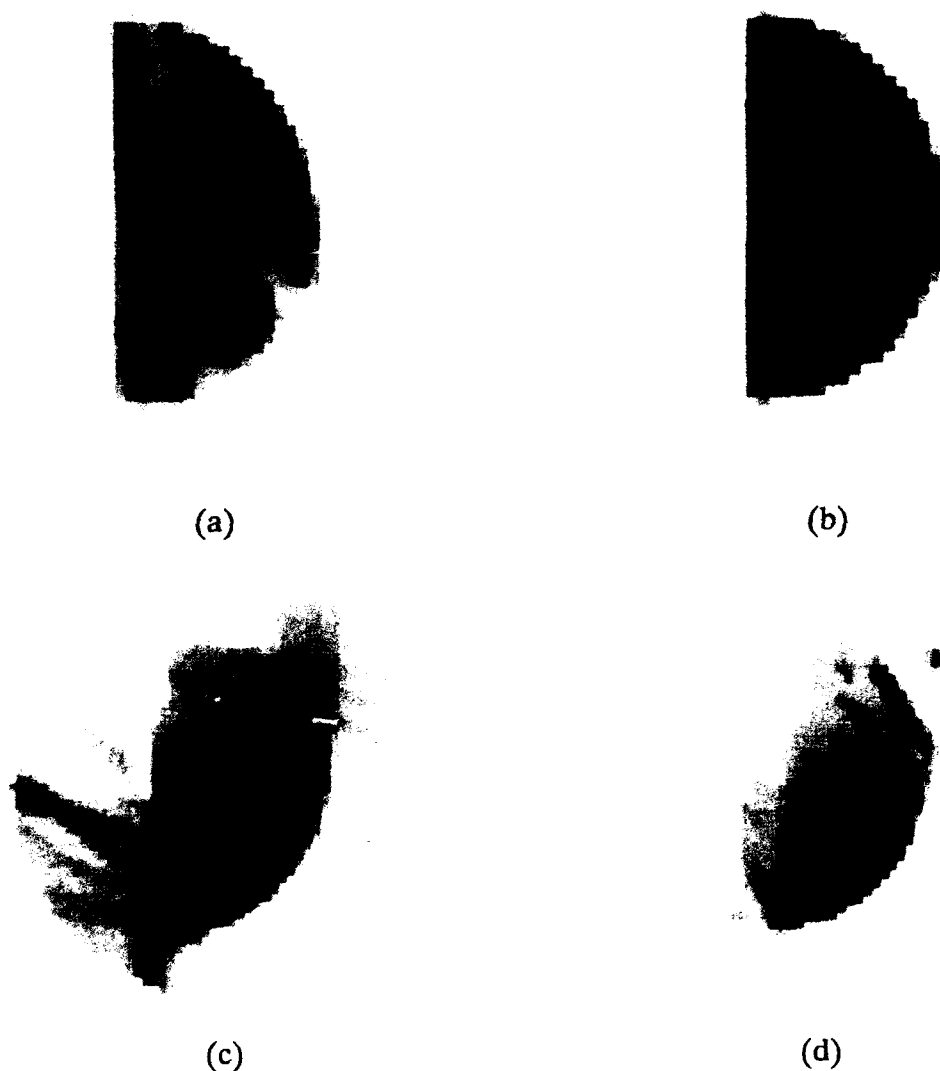


Figure 2 Application of support minimization a.) alone, b.), c.) with smoothing and maximum amplitude penalty at b.) .8, c.) .2, d.) maximum entropy penalty.

Note that, when $\mu_0 = 0.2$, Figure 2c, the penalty function is nearly quadratic, i.e., the reconstruction is essentially a minimum $(L_2)^2$ -norm reconstruction. The penalty function in this case is unbounded with a monotonically increasing slope. Numerical experimentation performed to date suggests that any penalty function displaying this qualitative behavior will yield similar results. As an example, a reconstruction using the maximum entropy penalty function of Eq. (13) with $\mu_s = 0.5 \mu_{\max}$ (i.e. $\mu_s = \epsilon$) is shown in Figure 2d. Note the similarity between Figures 2c and d. Both penalty functions are sacrificing the uniformity of the image and compactness of the image boundary so as to reduce the number of pixels in the largest range of magnitude.

It is important to stress the fact that all the images of Figures 1 and 2 are completely consistent with the available data; there is no grounds to prefer any one of the images over the others based on agreement with the available projection data. Our preference must be based on other objective and subjective measures, such as close agreement with a component CAD drawing.

The functional optimization technique is next applied to experimental data. The object examined is the metal band attaching the eraser to the end of a wood pencil. Mono-energetic projection data was obtained at 2 degree intervals using 101 translational points. The complete data reconstruction of this set is shown in Figure 3a. An incomplete data set was fabricated by removing a third of the projections (60 out of 180 degrees). Reconstruction of the incomplete data set is shown in Figure 3b. The reconstruction obtained through the application of the penalty function of Eq. (9) with $\eta = 6$ and $\epsilon = 0.17 \mu_{\max}$ is shown in Figure 3c.

The primary problem encountered in the incorporation of *a priori* geometry and material information in a reconstruction algorithm is the registration of the data with the measured data both spatially and in magnitude. Six variables are identified as controlling the registration x-y translation (r_0, ω_0 in polar coordinates), rotation (θ_0), spatial magnification (S_0), mean intensity (brightness) (I_0), and intensity magnification (contrast) (A_0). The approach to data registration taken in this work is to treat these six registration variables as additional unknowns to be optimized. An algorithm was developed which fits the projections of the *a priori* data to the measured data projections. A projection set $D(\theta, u)$ is defined as the difference between the measured projections $m(\theta, u)$ (including the missing projection data) and the projection of the registered *a priori* data $m_0(\theta, u)$

$$D(\theta, u) = I_0 + A_0 m_0(\theta - \theta_0, (u - c)S_0 + c_0 + r_0 \cos(\theta - \omega_0)) - m(\theta, u) \quad (14)$$

where c and c_0 are the centers of rotation of the measured and *a priori* projection sets, respectively, on the translation u axis. The reconstruction proceeds by applying the variational methods demonstrated in the previous discussion to the difference projection $D(\theta, u)$. However, the solution vector includes the six registration variables in addition to the discrete missing data points $m_k m$. Numerical difficulties arose in the initial implementation of this scheme due to potential orders of magnitude differences in the sensitivity of the optimized functional to the registration variables compared to the missing projection data. A normalization process was implemented in the algorithm which, when sensing numerical problems, automatically rescales the registration variables to produce approximately uniform sensitivity to all variables. This modification resulted in a robust algorithm which has thus far proven free from local minima traps.

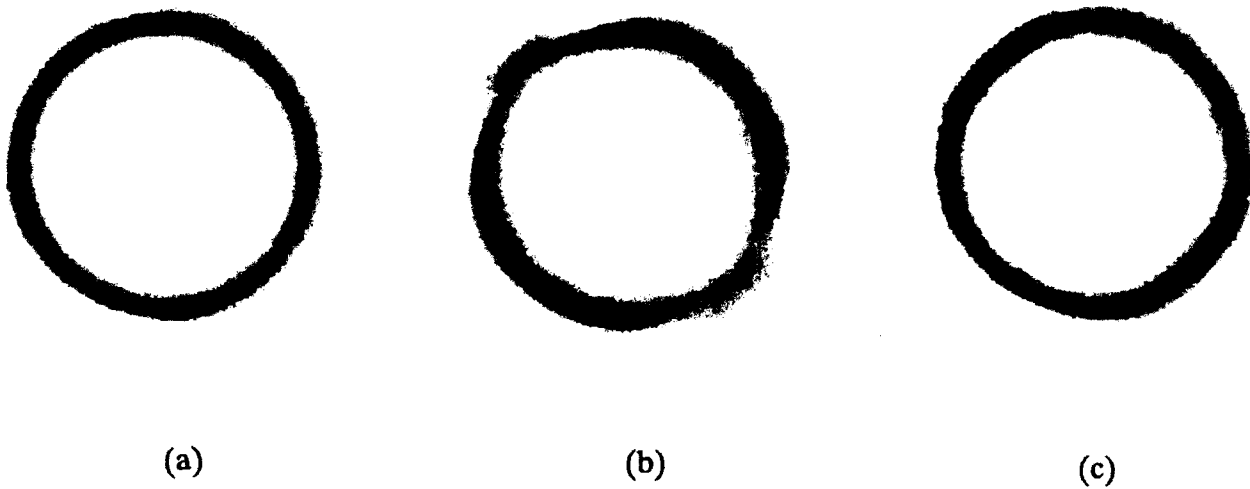


Figure 3 Application to experimental data. a.) complete data set, b.) incomplete data set, c.) incomplete data set with minimal support reconstruction.

The registration algorithm is demonstrated using a synthetic projection set derived from a turbine blade CAD drawing. The data set consists of projections at 5 degree intervals using 201 translational points, shown reconstructed in Figure 4. This data set represents the unregistered *a priori* data. An "experimental" data set was constructed by removing every other translational point, rotating the image 90 degrees, then seeding the data with an additional hole in the blunt end of the blade to simulate an "unknown" flaw. The reconstruction of this "experimental" data set is shown in Figure 5a. An incomplete data set was then formed by removing half the data (90 out of 180 degrees), resulting in the reconstruction shown in Figure 5b.

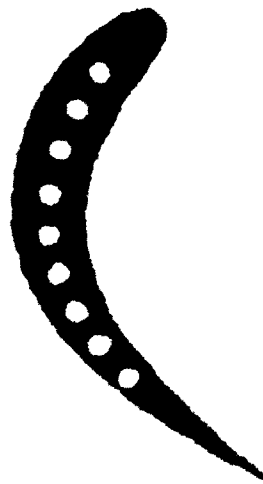


Figure 4 Reconstruction of *a priori* turbine blade data.

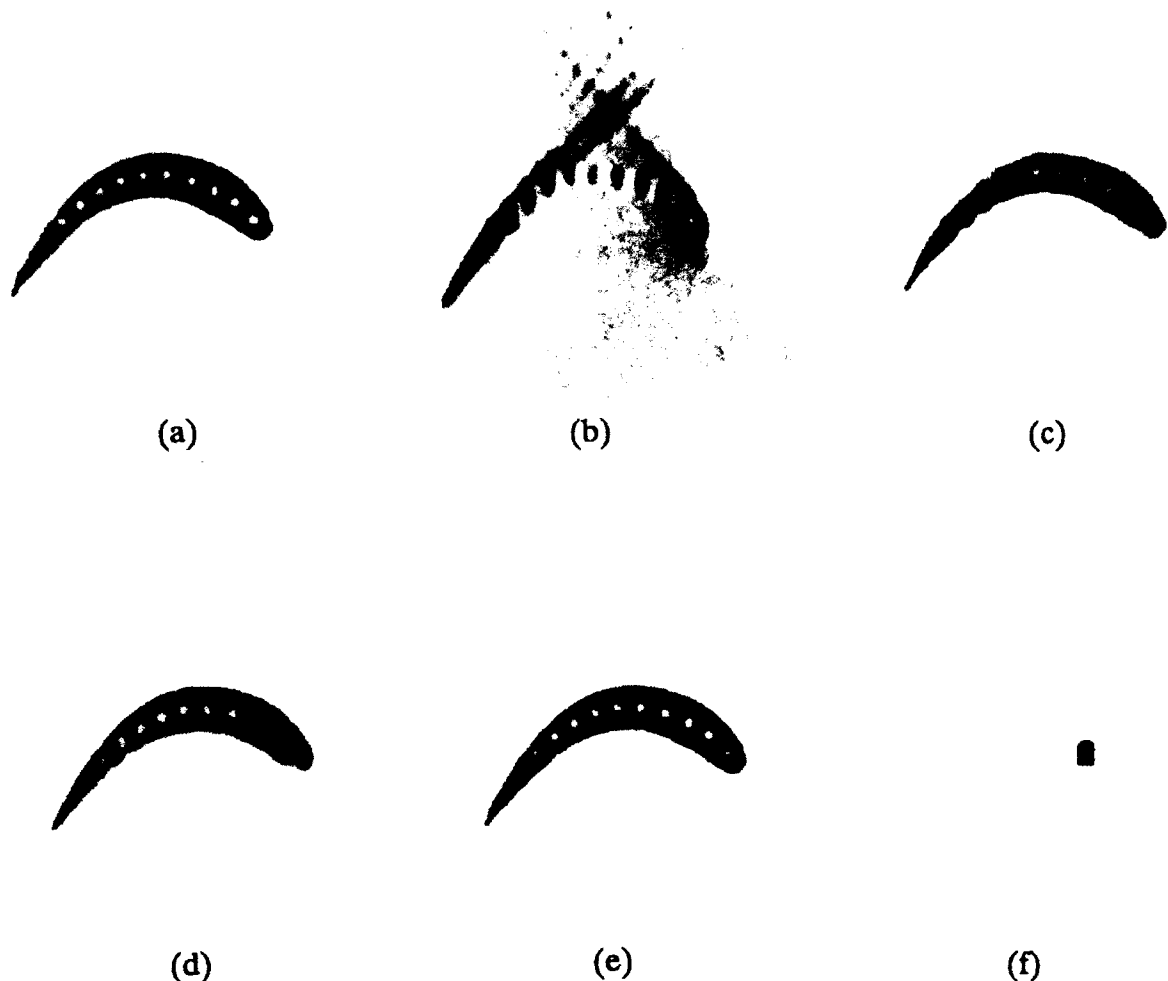


Figure 5 "Experimental" data set seeded with flaw. a.) complete data, b.) incomplete data, c.) minimal support reconstruction, d.) quadratic registration of *a priori* data, e.) minimal support reconstruction with *a priori* data, f.) image of penalty function of e.)

The reconstruction was initiated by applying the variational reconstruction algorithm to the incomplete data set alone (i.e., the *a priori* data was not used) using Eq. (9) with $\eta = 4$, $\epsilon = .05\mu_{\max}$ and Eq. (12) resulting in Figure 5c. The reconstruction has improved significantly, but the holes in the thin portion of the blade are not sharply defined. Next, the registration algorithm is applied to the difference projection, Eq. (14), using Eq. (8). The penalty on negative valued pixels is not imposed on the difference image. To initiate the registration, a quadratic fit was performed (i.e. least integrated squared error) by setting $\eta = 2$ and $\epsilon \gg \mu_{\max}$. This significantly accelerates the initial alignment of the *a priori* and measured data. Figure 5d shows the reconstruction of the "experimental" data at the conclusion of the initial registration. Finally, the threshold is lowered to $\epsilon = .05\mu_{\max}$, and $\eta = 4$. The algorithm then fine-tunes the data alignment, and adjusts the missing projection points so as to minimize the support of the difference image. The final reconstruction of the "experimental" data is shown in Fig. 5e. Comparison with Figure 5a indicates good

algorithm performance. A quantitative indication of agreement between Fig. 5a and e is provided by Fig. 5f, in which the penalty function $P(\mu(x))$ is displayed as an image. Note that the algorithm has reduced the support of the penalty function to a few pixels in the vicinity of the "unknown" flaw. Figure 5f suggests the use of the penalty function image as a means for flaw detection, since in the absence of a flaw, the penalty function would be uniformly zero.

Summary

In summary, a means of compensating for missing projection data in CT reconstruction has been developed based on the optimization of measures of image properties, and in particular on the minimization of a measure of the image support. Implementation of these concepts has taken the form of a variational algorithm which displays robust convergence properties. The behavior of the reconstruction algorithm has been related to the general qualitative shape of the penalty curve used in the optimization. A functional measure has been demonstrated which allows the simultaneous, and relatively independent, optimization of image support and image smoothness. A comparison to a conventional maximum entropy method demonstrated the superiority of the minimal support approach in the reconstruction of a compact, high-contrast object. A means for the variational registration of *a priori* data has been incorporated into the reconstruction process. The algorithm proceeds by minimizing the support of the difference between the reconstructed image and the *a priori* data, resulting in a reconstruction with unknown flaw data displayed in an optimally compact form. It is conceivable that such an algorithm could have particular utility in the area of dimensional analysis, due to the compact, high-contrast nature of the differences between the object and *a priori* data.

Plans for Next Year

In FY 92, the reconstruction procedure will be reformulated in a mode more amenable to the handling of large data sets. The existing algorithm is based on a filtered back projection reconstruction. In this algorithm, the missing projection data serve as the independent variables manipulated in the norm optimization. This approach has the advantage of requiring relatively few independent variables, hence array sizes manipulated in the conjugate gradient minimization can be handled in a workstation environment. The significant drawback of this approach is that the evaluation of the gradient vector is computationally intensive, requiring a separate back projection for the evaluation of each element of the gradient vector. As a consequence preliminary research has been restricted to array sizes of 200 by 200 pixels or smaller, so that calculations can be performed within an un-enhanced workstation environment. Alternatively, if the image pixels are designated as the independent variables, rather than the missing projection values, the calculation of the gradient vector is relatively trivial. The problem with this approach is, of course, that the gradient vector has N^2 elements in an N by N image reconstruction. Implementation of such an algorithm in a workstation environment is limited by memory requirements. However, because this later approach consists of a large number of relatively trivial calculations which can by-and-large be performed independently, it is ideally suited for a parallel computing environment. Therefore, a task to be performed in FY 92 will be to translate the existing algorithms to this later operational format for execution on a 16,384 process Maspar computer supported by the Ames Laboratory Scalable Computing Laboratory.

Emphasis in the upcoming planned final year of the project will be placed on application to existing problems for which high quality experimental x-ray CT data is available. The ideal situation for algorithm evaluation is a problem for which both complete projection data and complete *a priori* data are available. This allows the controlled removal of projection data, and the reconstruction of the complete data provides an effective

measure by which to gauge algorithm performance. Work to date has primarily utilized data obtained with the microfocus CT facilities at CNDE/ISU. These data were adequate for the preliminary development undertaken thus far, and data collected in-house will continue to be utilized. Future emphasis, however, will shift towards application to off-site problems. This will not only provide a greater variety of data for algorithm evaluation, but will also serve to inform other researchers of the algorithm capabilities. Data being generated by research groups also working on limited data CT reconstruction is obviously of particular interest. Efforts are currently underway to establish contacts for the exchange of data.

The new algorithm format currently under development is based solely on a forward projection model. This fact has potentially significant implications for future algorithm development, potentially beyond the upcoming year. Generally speaking, the exact modeling of a forward measurement process is relatively straight forward, whereas the inversion of the measurement process usually requires a number of simplifying approximations to yield a tractable calculation. Fortunately, the x-ray projection measurement process can be effectively approximated by a linear model, which forms the basis of back-projection tomography. There are, however, x-ray measurement phenomena which are not accurately modeled as linear, which can introduce potentially significant artifacts in the reconstruction. For example, measurements using a poly-chromatic x-ray source with an energy insensitive detector will display a non-linear relation between component thickness and photon count. Modeling this measurement with a linear model results in well-known beam hardening artifacts in back-projection tomography. Formulating a non-linear inversion formula for this process would be a formidable analytic task. However, the forward modeling of this phenomena is trivial. Thus implementing a beam hardening correction will be a simple task within the framework of the proposed next generation reconstruction algorithms. Other non-linear effects such as edge effects could likewise be treated in future work.

References

1. K. C. Tam and V. Perez-Mendez, "Principles of Tomographical Imaging with Limited Angle Input", *J. Opt. Soc. Am.* 71, 582 (1984).
2. K. C. Tam, J. W. Eberhard, and K. W. Mitchell, "Incomplete Data Image Reconstructions in Industrial X-Ray Tomography", in *Review of Progress in QNDE*, edited by D. O. Thompson and D. E. Chimenti (Plenum Press, New York, 1989), Vol. 8, pp. 407-414.
3. M. . Hsiao and J. W. Eberhard, "A Model-Based Reconstruction Method for Incomplete Projection Industrial Computed Tomography Imaging", in *Review of Progress in QNDE*, edited by D. O. Thompson and D. E. Chimenti (Plenum Press, New York, 1989), Vol. 9, pp. 415-422.
4. K. C. Tam, "The Application of Convex Hull in Industrial X-Ray Computed Tomography", in *Review of Progress in QNDE*, edited by D. O. Thompson and D. E. Chimenti (Plenum Press, New York, 1989), Vol. 8, pp. 389-397.
5. R. A. Roberts, "Limited Data Tomography Using a Minimal Support Constraint", in *Review of Progress in QNDE*, edited by D. O. Thompson and D. E. Chimenti (Plenum Press, New York, 1989), Vol. 10, pp. 435-442.
6. R. Narayan and R. Nityananda, "Maximum Entropy Image Restoration in Astronomy", *Annual Review of Astronomy and Astrophysics*, Vol. 24, edited by G. Burbidge, D. Layzer, and J. Phillips, Annual Reviews, Palo Alto, 1986 (127-170).

LASER-BASED ULTRASONICS

**R. Addison
Rockwell International**

Executive Summary

The objective of this program is to demonstrate the feasibility of using laser-based ultrasound technology for the rapid inspection of large area composite structures. This year we have investigated two key issues that affect the performance of such a laser-based ultrasonic system: the angular reflectivity of polymer composite materials, surface coatings, and surface textures; and the threshold for laser beam damage in these materials with and without surface coatings. The results of these investigations are critical inputs to the design and fabrication of a system that will angularly scan a laser beam over the surface of a structure. The angular reflectivity studies show the rate at which the reflected beam intensity decreases as the incident angle is increased. The damage threshold studies determine the ultimate limits for the generation and probe laser intensities and thereby ascertain if the signal-to-noise ratios will be adequate for an angular C-scan inspection technique. The results of these studies which are detailed in the report show that it is indeed feasible to angularly scan the laser beams over a structure while still maintaining an adequate signal-to-noise ratio. The major accomplishments for FY 91 are listed below:

- The angular reflectivity measurements have shown that rapid scanning via angular beam deflection, and also contoured part inspection, is feasible.
- Probe laser beam damage threshold measurements have indicated that signal-to-noise ratios can be increased in excess of 40 dB by using a high peak power, pulsed probe laser.
- Generation laser beam damage threshold measurements have shown that ultrasonic waves of sufficiently high amplitude may be generated with a laser pulse, while remaining comfortably below the material damage threshold.

Background

A. General

Laser generation and detection of ultrasound in solids has been investigated extensively over the past 20+ years. In general, a short duration pulse from a Q-switched laser is used to generate ultrasonic waves through thermoelastic, ablative or constrained surface mechanisms [1,2]. To complement the noncontact generation of ultrasound various laser systems have been developed to detect laser-generated acoustic waves [3,4].

When a laser is used to generate ultrasonic waves, bulk and surface ultrasonic waves are simultaneously generated. Since a substantial amount of the total ultrasonic energy is contained in the surface waves [5], they have been widely used for material characterization and for nondestructive inspection applications. Laser generated surface waves have been used to detect surface breaking cracks [6] and laser detection techniques have produced high accuracy surface wave velocity measurements [7,8]. Laser-based methods have also been used to make velocity measurements in materials at elevated temperatures of up to 1100°C [9-11].

Of the two requirements, laser-generation and laser-detection, the detection of ultrasound using lasers has proven to be the more difficult problem. Many optical techniques have been proposed for detecting ultrasound. Initial studies were based on a simple optical beam deflection or knife-edge technique [12]. Although simple to implement, the optical beam deflection technique has largely been superseded by interferometric techniques, because of their greater sensitivity. Numerous interferometer systems have been developed, each with their own relative advantages [3]. Typically the majority of interferometric techniques developed required specimen surfaces which had a mirror-like finish and angular alignment of the specimen was critical making it difficult to perform large area scans. However, the use of a time-delay or Mach-Zender interferometer [13,14] provided a method to interferometrically examine materials with rough surfaces. This technique was superseded by the spherical Fabry-Perot interferometer [15] which provides the advantages of the Mach-Zender interferometer plus a larger collection angle for diffusely reflected light. A third type of interferometer, which makes use of a phase-conjugating mirror, has also been shown to be applicable to rough surface inspection [16]. However, this technique is currently not capable of achieving sensitivities as high as that of the spherical Fabry-Perot interferometer.

To further improve the signal-to-noise ratio, various techniques have been investigated for obtaining larger signals from the generating laser. For instance, the directivity can be significantly changed by adding constraining or absorptive materials to the specimen's surface [17]. Changes in the directivity can also be obtained by increasing the incident laser power density until ablation of the surface occurs. The use of arrays of laser sources has also been investigated for directing or focusing the generated ultrasonic energy [18]. Other techniques use temporal or spatial modulation to concentrate more of the generated energy into a narrower bandwidth that better matches the detector's bandwidth [19-21].

The use of these techniques plus the advances in state-of-the-art laser technology have led to substantial improvements in system sensitivity. This has led to the use of laser-based systems for generating bulk longitudinal ultrasonic wave in materials and using them for the nondestructive inspection of large area structures.

Currently available automated inspection techniques for airframe structures that use piezoelectric transducers can only examine limited areas that have large radii of curvature. Manual techniques are used in areas with small radii of curvature. The use of existing techniques to inspect an entire airframe is both costly and time-consuming and frequently does not provide a permanent record of the inspection. To overcome these deficiencies, we have been developing an inspection system, which is referred to as laser-based ultrasonics, that uses laser-generation and laser-detection techniques. Since the inspection is performed with ultrasound, this method provides the advantages that are inherent to this inspection technique, namely; high resolution, depth resolution of defects and the capability to accurately characterize damage zones.

The inherent advantages of laser-based ultrasound, compared with other more traditional acoustic methods which often require the part to be immersed in a water tank, enables nearly 100 percent inspectability. The most significant features of laser-based ultrasound include:

- A noncontact and couplant-free ultrasonic generation which is also conformal to the part surface.
- A capability for inspection at oblique angles relative to the part surface.
- A capability for rapid inspection of corners, edges and radii.
- The potential to scan inside enclosed cavities, and
- Increased ultrasonic generation efficiency from typical surface coatings.

The use of laser-based ultrasound offers significant potential advantages that could translate into improved in-service inspection capability.

B. Project

This project has been focused on demonstrating the feasibility of using laser-based ultrasound technology for the rapid inspection of large area composite structures. Our initial work concentrated on the investigation of the principles underlying the optical generation and detection of ultrasonic waves in composite materials. [19,22,13] Using model test specimens, we sought to determine the best way to reliably generate and detect ultrasound. When this was successfully accomplished, we directed our activities toward automatic scanning techniques including mechanical raster scanning of flat panels through the laser beams and phased array techniques for electronic scanning of the ultrasonic beams. [18]

The optical detection technique that we have implemented has followed that first described by J.-P. Monchalin [15] where a spherical Fabry-Perot interferometer is used in conjunction with a probe laser. Other companies within the aerospace industry are also working on LBU. However, it is difficult to surmise their progress since these parties have not reported their work in the open literature.

During FY 90, a thorough study was made of the angular diffraction pattern of the longitudinal acoustic waves generated in graphite/epoxy composites with a pulsed laser. [18] Several significant results were obtained from this study. It was found that the angular diffraction pattern was substantially the same whether the surface of the composite was constrained or not. This result was contrary to the conventional wisdom that some sort of constraint such as tape, a peel ply or a light oil coating would have to be placed on the surface to enable longitudinal acoustic waves, of sufficiently large amplitude, to be generated in the material. A second finding was that there was no significant change in the angular diffraction pattern as the angle of incidence of the generating laser beam was varied from zero degrees to angles as large as 30 degrees. Although this result was not surprising it

demonstrates that as the optical spot from a laser conforms to the complex curvature or sloping surface of a composite part, the resulting longitudinal acoustic beam generated will propagate normal to the surface. Taken together these two results are very important to the successful use of this technology for the inspection of large area composite airframe structures. It means that the inspection can be done without any special preparation or modification of the composite surface. Further, the laser beam can be scanned over an air foil having a complex curvature and the acoustic beam will be generated normal to the surface allowing a complete inspection of the interior volume of the composite panel. These are key elements of a rapid scan NDE capability for use on aircraft in a depot environment.

These studies provided an adequate foundation for us to study the use of laser generated and detected signals to synthesize sector scanned phased arrays. We acquired longitudinal acoustic signals that had been generated with a pulsed laser at an array of 16 periodically spaced points, and similarly used our laser detection system to acquire longitudinal acoustic signals at an array of 16 periodically spaced points. For both configurations, we performed an off-line synthesis of a sector scanned phased array scanning over a 100 degree sector. The results [18] showed that array techniques work well in an isotropic material such as aluminum and for small vector angles can also be used in the anisotropic Gr/epoxy composite material. This ability to form arrays of acoustic transducers that conform to sloping or complex curved surfaces allows the laser generated and detected acoustic beams to be directed and focused as is now done with focused piezoelectric transducers. Further this method of array generation with its surface conforming capabilities offers a way to overcome a significant barrier to the widespread use of phased arrays in the NDE field. Heretofore to use a sector scanned array for NDE applications, it has been necessary to either have a flat, smooth entry surface onto which the face of the array could be bonded or to have an immersion system with its associated problems related to the strong refraction of the acoustic waves at the entry surface of the part. Now the rapid scan capabilities of phased arrays and their accompanying beam agility can be employed for NDE applications just as they are now widely used in the medical field.

Highlights of the accomplishments through FY 90 since the initiation of this program are given below.

- Characterization of laser-generated signals in materials with both constrained and unconstrained surfaces.
- Analysis and experimental characterization of operation of spherical Fabry-Perot interferometer.
- Testing of integrated LBU system using composite specimens.
- Operation of LBU system in automated C-scan mode with flat and curved test specimens (both composite and coated metal materials)
- Demonstration of feasibility of phased array operation-characterization of angular diffraction spectrum of thermoelastic source and synthesis of 16 element transmitting array and 16 element receiving array.

Objectives and Scope

The objective of this program is to demonstrate the feasibility of using an integrated source and detector for laser-based ultrasonic nondestructive inspection. The system will be designed with the intent of eventually applying the concept to the inspection of large-area composite airframe structures including the automated inspection of integrally stiffened and complexly curved composite structures. The concept resulting from this work will need to

be insensitive to environmental disturbances typically found in industrial and Air Force depot inspection areas. The concept must have sufficient sensitivity to detect flaws of interest without causing surface damage to the part under test.

The specific objectives for FY91 were to determine both the generation and probe laser beam damage thresholds in composite materials so that signal-to-noise can be maximized while remaining in a nondestructive regime. Furthermore, it was necessary to determine the changes in signal-to-noise ratio as the probe laser angle of incidence was changed from 0° to 45° . This was to simulate the conditions which would clearly arise if contoured parts were inspected or a rapid scanning system were developed based on angular beam deflection.

The scope of this program includes: 1.) improvements in the generation and detection efficiencies for LBU, 2.) the development of a scanning system to rapidly manipulate the generating and receiving laser beams. We envision a system that consists of generation and probe laser beams that are scanned over the surface of a composite airframe structure or the surface of an engine component. The generation laser would thermoelastically generate elastic waves in the part. These waves would propagate through the part and reflect from flaws such as delaminations, voids, inclusions, etc. The reflected echoes would propagate back to the entry surface where they would cause a displacement of that surface. This surface displacement would be detected using the probe laser in conjunction with an optical interferometric technique.

Approach

To fully realize the high-speed scanning capabilities of a same side laser-in/laser-out inspection system the laser beams must be deflected across the part surface, as depicted in Figure 1. In addition to rapid inspection, a need exists for inspecting curved and complexly shaped parts. In contrast to an LBU system configuration scanning flat parts with a normal angle of incidence, inspection of curved parts (or flat parts via angular deflection of the laser beams) dictates that the probe laser angle of incidence is variable, with the extent of the angular variation depending on part geometry. Generally, laser light incident on a rough

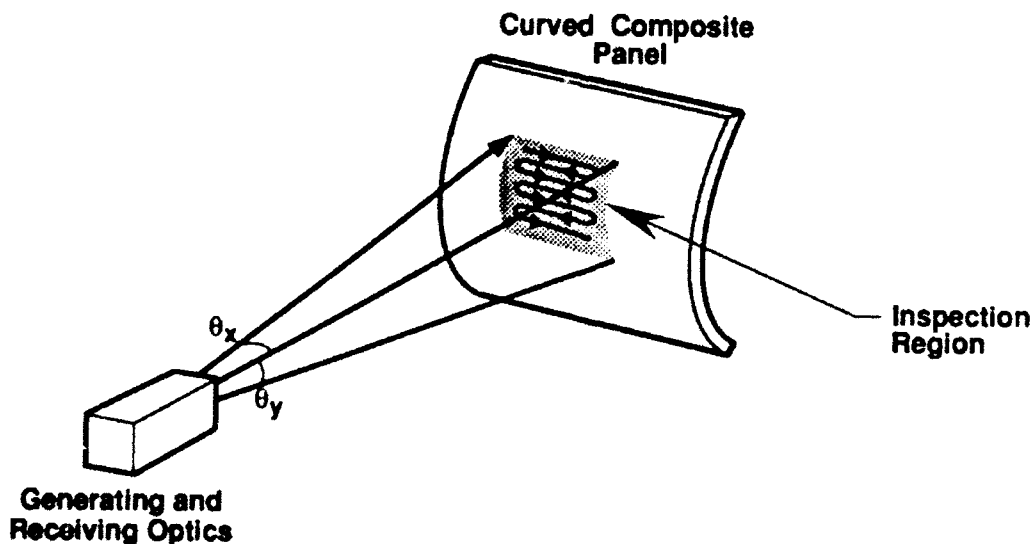


Figure 1 Concept for angular deflection of laser beams to provide rapid scanning of curved and complexly shaped parts.

surface will be scattered diffusely into a large solid angle with a large amplitude specular reflection superimposed along the angle of reflection. The relative distribution of the specularly and diffusely reflected wavefields is a function of surface texture. This results in an LBU system sensitivity variation that is directly dependent on the angular reflectivity properties of the material being inspected. To successfully implement rapid inspection of curved (or flat) components using an LBU scanning system which incorporates angularly deflected laser beams, the optical power backscattered from the part surface and received at the output photodetector of the spherical Fabry-Perot interferometer (SFPI) must be sufficient to permit detection of ultrasonic signals. To this end, the FY91 we have determined the extent of the changes in signal-to-noise ratio by measuring the amount of light reflected from the surface of various reinforced polymer composite parts, as the probe laser angle of incidence was varied. It is also important that the generation and probe laser powers be controlled so that a suitable compromise is reached for high inspection sensitivity while remaining below the thermal damage threshold for the composite materials. The damage thresholds were determined using microscopy techniques to characterize the level of surface damage as the generation and probe laser power densities were increased.

Technical Progress

To determine the extent of signal-to-noise ratio (SNR) variations when using the LBU system for inspection of contoured parts, angular reflectivity measurements were made for a number of specimens having different surface textures and coatings applied to the surface. The data were acquired using the experimental configuration shown in Figure 2, where the test part was rotated through an angle, ϕ , to emulate conditions arising from using an angularly scanned probe laser beam. The optical power retroreflected along the incident probe laser beam path and detected at the output of the SFPI was measured as a function of

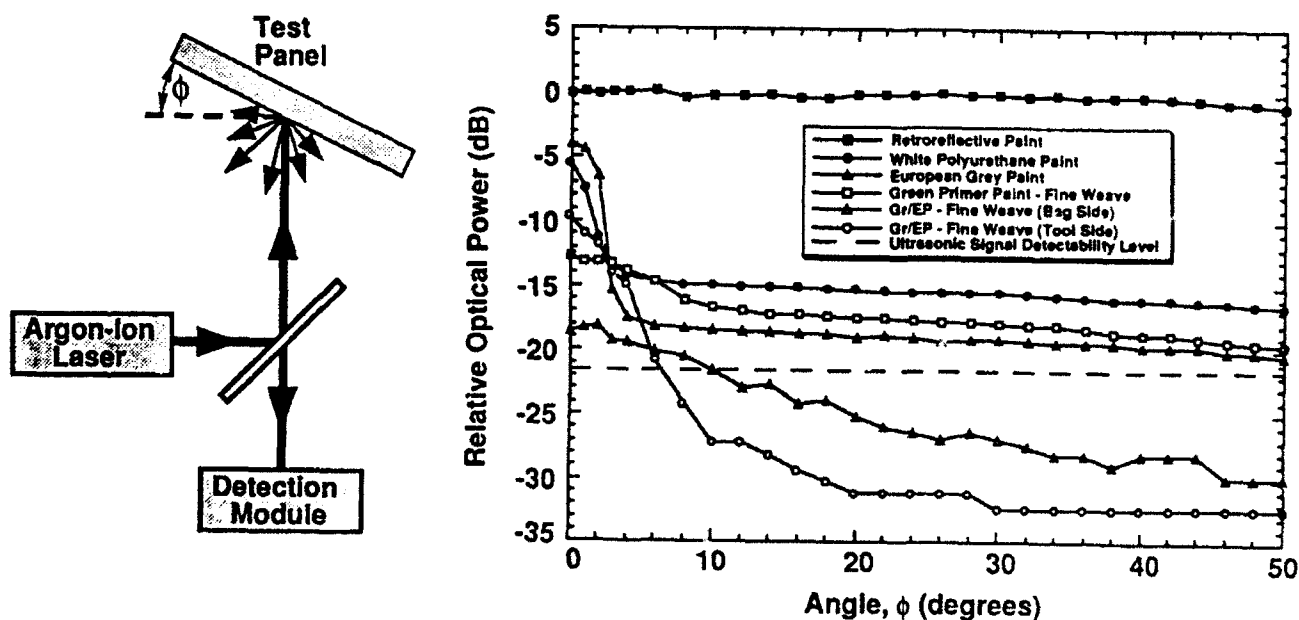


Figure 2 Left side-Experimental setup for measuring angular dependence of reflected optical power from test specimens. Right side-Results of measurements for six specimens having different surface coatings and textures.

probe laser angle of incidence. The data acquired from these studies, also shown in Figure 2, indicate that most materials tested exhibited a large amplitude on-axis specular reflection. Off-axis, the optical power received from the diffusely reflected component decreased at differing rates depending on the material surface condition. The dashed line in the graph represents the ultrasonic signal detectability level, defined as the optical power level at which the longitudinal wave was determined experimentally to be indistinguishable from noise, on a single shot basis. The first four materials listed, coated with different types of paint, exceeded the ultrasonic detectability threshold for probe laser angles of incidence in excess of 45° indicating that ultrasound may be detected, provided the ultrasonic attenuation of the material is not too great. For a graphite/epoxy composite panel coated with a white polyurethane paint, a reduction in received optical power of ~ 10 dB was measured as the angle of incidence was changed from 0 to 45° , corresponding to a decrease in ultrasonic amplitude of ~ 20 dB. A peelable retroreflective coating was developed which, optically, gave an approximately uniform response over the full angular range. Unfortunately, acoustically the coating was lossy and the reflectivity properties of the coating were susceptible to damage from the Nd:YAG laser pulses. However, this coating was useful for inspecting curved materials in which, with our present system SNR, ultrasonic detection was not possible over the full angular range.

A black graphite/epoxy material was also tested on the tool and bag sides. Neither side was modified in any way and the fabric texture was characterized as a fine-weave. The reflected optical power from either side decreased below the current LBU system threshold for ultrasound detectability at angles significantly less than 45° . The specular reflection was largest from the tool side but that also resulted in the greatest reduction in received optical power at off-axis angles. The responses measured with this specimen show that to obtain adequate sensitivity for inspection of uncoated black composite specimens, an increase in received optical power of 15 to 20 dB, corresponding to an increase in ultrasonic SNR of 30 to 40 dB, is required. This is feasible with current laser technology and will be discussed in more detail in a later section.

To complement the optical data of Figure 2, ultrasonic waveforms acquired from a graphite/epoxy panel (coated with white polyurethane paint) for probe laser angles of incidence of 0° and 45° are shown in Figure 3. As predicted by the angular reflectivity data, the ultrasonic amplitude was reduced by just over 20 dB when the incident angle changed from 0° to 45° . Note that for this specimen, the apparent noise evident in Figure 3 caused by acoustic reverberations within the material, has a much higher amplitude than the fundamental shot noise limit. These optical and ultrasonic results verify the applicability of using LBU for inspection of curved components, where the probe laser angle of incidence varies.

To generate ultrasound in the nondamaging thermoelastic regime, the LBU technique relies on a thermal expansion which takes place at the material surface [1]. Unlike conventional ultrasonic techniques, the efficiency of ultrasonic generation with a laser depends on the transduction properties of the material as well as the amount of laser energy deposited at the material surface. However, damage in composite materials occurs if the incident generation laser (or probe laser) peak power level exceeds the thermal damage threshold for the material. The laser damage studies have been separated into two regimes, characterized as cosmetic and structural damage. Cosmetic damage is defined as surface discoloration within the illuminated region, without any degradation of the material integrity. Structural damage is defined as partial or total removal of the epoxy layer, resulting in exposure of the underlying fiber matrix and possible fiber breakage. Thus a compromise must be made between improving the detectability of ultrasonic waves and remaining below the material damage threshold.

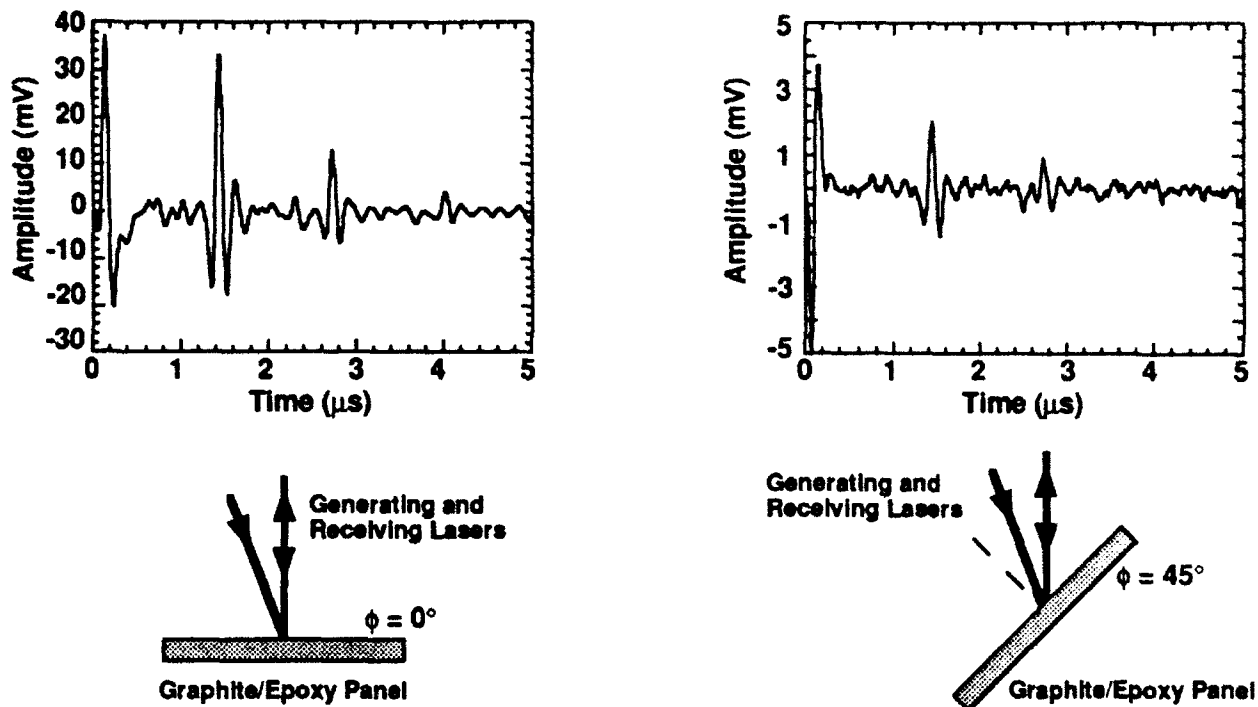
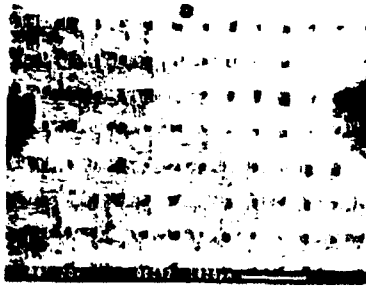


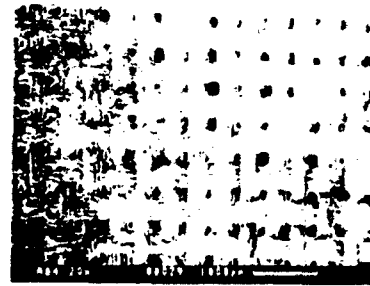
Figure 3 Experimentally acquired ultrasonic waveforms for probe laser angles of incidence of 0° and 45° .

One graphite/epoxy and three bismaleimide (BMI) composite materials have been irradiated with Q-switched Nd:YAG laser pulses of 15 ns duration (full-width-half-maximum) which is used in the LBU system for ultrasonic generation. For each material, 10 samples were irradiated with a single laser pulse with energies ranging from 17 mJ to 190 mJ and a laser beam diameter of 4 mm at the sample surface. While more sensitive analysis methods are certainly available, microscopy techniques were chosen for evaluation of the material surface condition after laser irradiation. Scanning electron micrographs (Figure 4) were made of the surface regions of four BMI composite specimens, which were irradiated with single laser pulses having energies of 17, 65, 96 and 132 mJ. Note that the weave pattern in the photographs is an impression in the resin that remained after a peelply layer was removed after manufacture. The results indicate that at 17 mJ, no visible damage to the composite surface had occurred. The black marks at the edges of the photograph are fiducial markers which were intentionally applied to the surface to delineate the region of illumination. As the laser energy was increased, at ~ 40 mJ a very faint surface discoloration of the resin appeared within the illuminated area. Increasing the laser energy to 65 mJ increased the visibility of the surface discoloration. As the laser energy was increased further, epoxy layer removal occurred exposing the underlying fibers. The threshold level for removal of the resin layer was determined to be ~ 65 mJ for graphite/epoxy and ~ 95 mJ for two of the BMI specimens. BMI was expected to have a significantly higher thermal damage threshold since it is designed for operation at higher temperatures. However, the third BMI specimen was damaged at the same level as the graphite/epoxy material indicating a large statistical variation present between materials of nominally identical composition. Further studies on composite materials indicated that the thresholds for both cosmetic and structural damage could be increased significantly with the application of white polyurethane paint to the material surface.

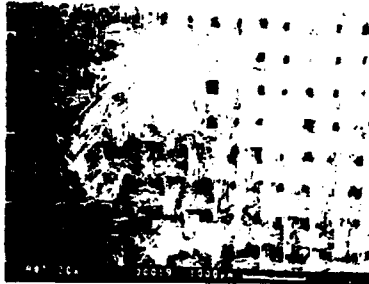
Laser Energy = 17 mJ



Laser Energy = 65 mJ



Laser Energy = 96 mJ



Laser Energy = 132 mJ

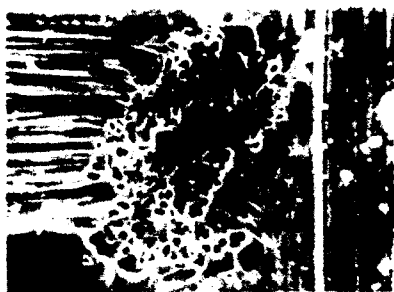


Figure 4 Scanning electron micrographs of four BMI composite specimens after each had been irradiated with a single (15 ns) laser pulse. The pulse energies were 17, 65, 96, and 132 mJ.

Similar investigations were also performed for the maximum probe laser intensity thresholds allowable for ultrasonic detection in composite materials. Both graphite/epoxy and BMI composite specimens were irradiated with 400 mW of laser power from the argon-ion laser used in the LBU system for ultrasonic detection. For each material the power density at the sample surface was increased by reducing the spot size and both bare and painted surfaces were irradiated. The threshold power density was determined to be $\sim 0.375 \text{ kW/cm}^2$ for an uncoated surface and $\sim 1.1 \text{ kW/cm}^2$ for a surface coated with white polyurethane paint. It appears that the reflective properties of the paint increased the usable power density by a factor of 3. It should be noted, however, that the threshold levels for damage were difficult to determine, since at that level no damage was visible. However, a technique was adopted whereby the reflected laser speckle pattern was observed during illumination. The speckle pattern would no longer be stationary if damage was occurring at the specimen surface.

Further studies examined the effect of spot sizes of $\sim 330, 215, 105$ and $25 \mu\text{m}$ with corresponding power densities of $0.48, 1.1, 4.6$ and 81 kW/cm^2 . After irradiation the samples (uncoated BMI and graphite/epoxy composites) were examined both with an optical microscope and a scanning electron microscope (SEM). Results from irradiation of a BMI composite specimen are shown in Figure 5. The results indicate that at sufficiently high power density levels, damage to the composite surface occurred. For power densities of 0.48 kW/cm^2 melting of the epoxy layer was initiated. As was found in the previous studies of generation laser damage thresholds, the graphite/epoxy had a slightly lower threshold than that of the BMI. Further increases in power density resulted in subsequent removal of the epoxy layer exposing the underlying fibers. For a power density of 4.6

Power Density = 0.48 kW/cm²



Power Density = 1.1 kW/cm²



30µm

Probe Laser Power = 400mW

Power Density = 4.6 kW/cm²



Power Density = 81 kW/cm²



Figure 5 Scanning electron micrographs of four BMI composite specimens after each had been irradiated with a cw laser beam. The intensities of the beams were 0.48, 1.1, 4.6, and 81 kW/cm².

kW/cm² the first five layers of fibers were cut through leaving a hole $\sim 40\text{ }\mu\text{m}$ in diameter. Interestingly, at power densities sufficiently high to drill through several layers of fibers, the damaged zone became elliptical with the major axis always lying in the fiber direction. It is thought that this is caused by significant heat conduction along the fiber length. Similar studies performed on the same specimens, this time coated with white polyurethane paint, resulted in visible damage occurring only for the $25\text{ }\mu\text{m}$ spot size (81 kW/cm²) case. As was the case for damage caused by the generation laser beam, at the probe laser power levels investigated in this study, the presence of the white polyurethane paint inhibited structural damage to the composite.

These results indicate that substantial increases in incident probe laser power may be realized before the damage threshold is reached, provided the spot size is also increased. For example, with a spot size of 5 mm, the CW power incident at the surface could be increased to $\sim 70\text{ W}$ resulting in a potential increase in received power of a factor of 150 or an increase in signal-to-noise ratio of 43 dB. The angular reflectivity measurements have shown that an increase in signal-to-noise ratio of ~ 30 to 40 dB was required to be able to inspect uncoated black composite surfaces with the probe laser incident at off-axis angles. Thus rapid inspection of composite parts by deflecting the generation and probe laser beams across the component surface using the LBU system appears to be feasible, providing the average power incident at the part surface can be increased. This is possible with current laser technology. Furthermore, it should be noted that the probe laser power can be increased significantly above the CW threshold level for damage if a pulsed probe laser is used, thereby reducing the duty cycle. A technique which we will implement is to use a long pulsed Nd:YAG laser for the probe laser. This laser will have a peak power output of

about 1 kW. However, since the laser is pulsed and will operate at a repetition rate of 100 Hz, the duty cycle is reduced to 0.6% assuming a pulse duration of 60 ms. The average power at the material surface is thus reduced to the order of 6W, which should be well within the damage threshold for the composite materials.

Summary

Angular reflectivity measurements were made on a number of reinforced polymer composite (RPC) materials, that had different surface textures and coatings applied to the surface. The data acquired has identified the relative distribution between diffusely reflected light and specularly reflected light in the different materials. These data allowed us to quantitatively determine the probe laser power required to exceed the detection threshold and detect ultrasonic waves with the laser-based ultrasound system at off-axis angles out to ± 45 degrees. For a black graphite/epoxy specimen (bag side) and a composite surface coated with white polyurethane paint the results indicated a reduction in ultrasonic SNR of ~ 20 dB when the probe laser beam angle of incidence was varied from 0 to $\pm 45^\circ$. However, to sensitively inspect the uncoated graphite/epoxy an increase in current SNR of ~ 40 dB is required. This increase is feasible with current laser technology.

Investigations of the maximum incident laser intensity thresholds allowable for ultrasonic generation in composite materials in the nondamaging thermoelastic regime were also performed in FY 91. No visible damage occurred in BMI composites or graphite/epoxy for laser pulse power densities ≤ 20 MW/cm² (40 mJ). Increasing the incident laser pulse power density above 20 MW/cm² (40 mJ) caused surface discoloration within the illuminated region. The threshold for removal of the resin layer was ≥ 35 MW/cm² (65 mJ) for one of the BMI specimens and a graphite/epoxy specimen. For the other BMI specimens the threshold for removal of the resin layer was ≥ 50 MW/cm² (> 90 mJ) indicating a 40% variation between materials of nominally identical composition. Most importantly, however, every C-scan obtained with the laser-based ultrasound system was acquired with incident power densities of < 8 MW/cm² (< 15 mJ). These results indicate a safety margin of at least a factor of 2 before cosmetic damage occurs and a factor of at least 4 before removal of the resin layer. Similarly, the threshold for material damage from the CW probe laser was found to be ~ 0.375 kW/cm² for an uncoated surface. The probe laser beam configuration typically used for C-scan inspection of composites with the LBU system results in a power density of ~ 0.05 kW/cm², indicating a safety margin of a factor of ~ 7 before melting of the resin layer begins for uncoated composite specimens. For illumination from both the generation and probe lasers, the material damage threshold can be increased significantly by applying white polyurethane paint, which is typically applied to components after manufacture.

The results of this years studies have confirmed that LBU can be used for inspection of contoured parts where the probe laser angle of incidence is nonzero. This is an important result indicating that it is feasible to achieve full high speed scanning potential of a same side laser-in/laser-out system by angularly deflecting the laser beams across the stationary part surface.

The laser-based ultrasound system that we have been developing at Rockwell has now been advanced to a stage where it is capable of producing high resolution C-scan images of reinforced polymer composite specimens. The system operates best on flat composite parts that have been coated with a paint layer. However, black uncoated composite parts have also been sensitively inspected from the tool side. The LBU system has also been used for inspection of a number of curved composite parts. However, the current system signal-to-noise ratio is limiting the advances that can be made toward realizing the goal of an in-field inspection system. In addition the current mode of inspection necessitates that the

part be mechanically translated in front of the laser beams, which is inherently slow. We will be making significant improvements in the system SNR over the next year by changing to a pulsed probe laser beam. Increases in speed of inspection will be achieved by using an angular beam deflection technique in conjunction with a generating laser that can be operated at repetition rates of up to 150 Hz.

Plans for Next Year

The present mode of C-scanning components with the LBU system is to mechanically transport the test specimen in front of the generation and detection laser beams. This approach, however, is inherently slow and would not meet sufficiently high scan rates to be acceptable for depot or field implementation. To fully realize the high speed scanning potential of a same side laser-in/laser-out inspection system it is necessary to deflect the laser beams across the part surface. It is the goal of this next years program to greatly increase the scanning and data acquisition rates. To implement these enhancements, we will make a number of modifications to the existing Rockwell laser-based ultrasound system.

It is anticipated that the scanning system will utilize a pair of galvanometers to which mirrors are attached for precise positioning of the generation and probe laser beams in a 2D plane (x-y axes). This proposed method of scanning will eliminate the need for transporting large parts through the laser beams.

The present LBU configuration uses a Nd:YAG laser ($\lambda = 1.064 \mu m$) for ultrasonic generation which is operated at a pulse repetition rate of 10 Hz. In order to increase the scanning rate we will investigate the operation of a CO₂ laser ($\lambda = 10.6 \mu m$) at pulse repetition rates of up to 150 Hz. With the angular deflection system implemented, and a repetition rate of about 20 Hz, substantially less than its full capability, we will be able to achieve a target scanning rate of 100 ft.²/hr. for a 0.5 inch x 0.5 inch pixel size. Operating the CO₂ laser at 100 Hz implies a scan rate as high as 625 ft.²/hr. for a 0.5 inch x 0.5 inch pixel size. To achieve a high scan rate it is also essential to be able to acquire data at a rate at least comparable to, or greater than, the laser repetition pulse rate. Thus, we will also investigate techniques for rapid data acquisition and storage.

Additionally, the laser pulse width from the CO₂ laser is of the order of 100 ns, compared with 10 ns for the Q-switched Nd:YAG laser system used currently. By using the longer pulse CO₂ laser, significantly more ultrasonic energy will be generated in the 1-10 MHz region of the spectrum, which is the frequency range most commonly used for reinforced polymer composite (RPC) material inspection. Concentration of the ultrasonic energy into a narrower spectral band could result in an increase in the system signal-to-noise ratio of about 20 dB. Thus we will also investigate the generation efficiencies of both CO₂ and Nd:YAG lasers. With this increase in generation efficiency, coupled with the results of the angular reflectivity analysis of last year, we expect to be able to demonstrate C-scanning capability using angularly deflected laser beams.

References

1. D. A. Hutchins, in "Physical Acoustics", edited by W. P. Mason and R. N. Thurston (Academic Press, New York, 1988), Vol. XVIII, p. 21.
2. C. B. Scruby, R. J. Dewhurst, D. A. Hutchins and S. B. Palmer, in "Research Techniques in Nondestructive Testing" edited by R. S. Sharpe (Academic Press, New York, 1982), Vol. V, pp. 281-327.
3. J. W. Wagner, in "Physical Acoustics", edited by W. P. Mason and R. N. Thurston (Academic Press, New York, 1990), Vol. XIX, p. 201.
4. J. -P. Monchalin, IEEE Trans. Ultrason. Ferroelec and Freq. Contr. UFFC-33 485 (1986).
5. L. R. F. Rose, Wave Motion 6 359 (1984).

6. J. A. Cooper, R. A. Crosbie, R. J. Dewhurst, A. D. W. McKie and S. B. Palmer, IEEE Trans. on Ultrason. Ferroelec. and Freq. Contr. UFFC-33, 462 (1986).
7. A. D. W. McKie, J. W. Wagner, J. B. Spicer and J. B. Deaton, Jr., in "Review of Progress in Quantitative Nondestructive Evaluation" Edited by D. O. Thompson and D. E. Chimenti, (Plenum Press, New York, 1990) Vol. 10A, pp. 531-538.
8. J. Huang and J. D. Achenbach, J. Acoust. Soc. Am. 90(3) 1269 (1991).
9. R. J. Dewhurst, C. Edwards, A. D. W. McKie and S. B. Palmer, J. Appl. Phys. 63(4) 1225 (1988).
10. J. -P. Monchalin, R. Heon, J. F. Bussier and B. Farahbakhsh, in "Nondestructive Characterization of Materials II" edited by J. F. Bussiere, J. -P. Monchalin, C. O. Ruud and R. E. Green, Jr. (Plenum Publishing Corporation, 1987), pp. 717-723.
11. H. N. G. Wadley, S. J. Norton, F. Mauer, B. Droney, Phil. Trans. Roy. Soc. Lond. A320 341 (1986).
12. R. Adler, A. Korpel and P. Desmare, IEEE Trans. on Son. and Ultrason. SU-15(3) 157 (1969).
13. L. M. Barker and R. E. Hollenbach, J. Appl. Phys. 43(11) 4669 (1972).
14. W. Kaule, in "Proceedings of the Eighth World Conference on Nondestructive Testing", paper 3J5 (1978).
15. J. -P. Monchalin, Appl. Phys. Lett. 47(1) 14 (1985).
16. M. Paul, B. Betz and W. Arnold, Appl. Phys. Lett. 50(22) 1569 (1987).
17. D. A. Hutchins, R. J. Dewhurst and S. B. Palmer, Ultrasonics 19 103 (1981).
18. R. C. Addison, Jr., H. A. Ryden and A. D. W. McKie, in "Review of Progress in Quantitative Nondestructive Evaluation" Edited by D. O. Thompson and D. E. Chimenti (Plenum Press, New York, 1991 Vol. 10A, pp. 485-492.
19. R. C. Addison, Jr., L. J. Graham, R. S. Linebarger and B. R. Tittmann, in "Review of Progress in Quantitative Nondestructive Evaluation" Edited by D. O. Thompson and D. E. Chimenti (Plenum Press, New York, 1988) Vol. 7A, pp. 585-594.
20. J. W. Wagner, A. D. W. McKie, J. B. Spicer and J. B. Deaton, Jr., J. Nondest. Eval. 9(4) 263 (1990).
21. A. J. A. Bruinsma and J.A. Vogel, Appl. Opt. 27 4690 (1988).
22. B. R. Tittman, R. S. Linebarger and R. C. Addison, Jr., in "Review of Progress in Quantitative Nondestructive Evaluation" Edited by D. O. Thompson and D. E. Chimenti (Plenum Press, New York, 1989) Vol. 8A, pp. 513-520.
23. B. R. Tittmann, R. S. Linebarger and R. C. Addison, Jr., in "Review of Progress in Quantitative Nondestructive Evaluation" Edited by D. O. Thompson and D. E. Chimenti (Plenum Press, New York, 1990) Vol. 9A, pp. 479-486.

DETECTION OF HARD ALPHA INCLUSIONS IN TITANIUM JET ENGINE MATERIALS

J. H. Rose
Center for NDE
Iowa State University

Executive Summary

Contamination by nitrogen and/or oxygen causes localized changes in titanium jet engine alloys that can lead to catastrophic failure. The contaminants cause localized regions of embrittled metal that can lead to cracking and failure. The embrittlement is due to the conversion of the alloy's microstructure from a typical alpha/beta mixture to an alpha phase that is both hard and brittle (hard alpha). Hard alpha may be present in the part's interior and exist in the absence of associated voids or cracks. The problem is to detect these low-contrast regions of altered microstructure nondestructively and in the bulk of the material prior to failure. The present project is the theory component of a pair of experimental/theoretical tasks to develop methods, primarily ultrasonic, to detect and characterize hard alpha inclusions. The experimental work is described in the task: "Detectability of small flaws in advanced engine alloys."

In this years work (FY91), we focused on validating the new theory of ultrasonic backscattering from microstructure. First, we reduced the theory to calculation, and then we compared it with backscatter measurements. Calculable expressions were established for single phase metals for orthorhombic symmetry or higher; this includes pure beta phase and pure alpha phase titanium. The theory was found to be in good agreement with experiment for the single phase materials. Efforts in the last half of this year are focused on those developments that are needed to reduce the theory to practice for multiphase commercial alloys.

The ability to predict ultrasonic backscatter from the microstructure has several potentially useful outcomes. First, we can predict changes in the ultrasonic signal due to regions of altered microstructure. This is important in the design of ultrasonic inspection methods for hard alpha. Second, since the results connect the acoustic noise to the microstructure, they may be useful in understanding the relative acoustic quietness of various titanium alloys. In summary, the results for FY91 are that we:

- Reduced the theory of backscattering to a calculable form for single-phase materials with cubic and hexagonal symmetry (generally orthorhombic symmetry).
- Found quantitative agreement between theory and experiment for the first time for polycrystalline metals.
- Extended the formal theory to multi-phase commercial materials such as jet engine alloys.
- Established the effects of surface finish on the backscattered signal under separate funding (CNDE/NSF).

Background

A. General

The project problem is to develop the quantitative theory needed to determine the ultrasonic backscatter from titanium alloys, and to develop techniques for inferring the properties of the microstructure of the metal from the backscatter signal. This theory is to be applied as far as practical to characterizing the change in the backscattered signal due to regions of hard alpha.

Applications range from the very specific to the rather general. First, the development of a method for reliably detecting hard alpha would reduce the possibility of catastrophic failures known to occur due to the presence of hard alpha. Second, the ability to model the backscatter of ultrasound from microstructure opens up additional possibilities. It may be of help in the design of acoustically quiet titanium alloys. The designers of new alloys generally control the microstructure of the new material by various metallurgical and thermo mechanical processes. If they have a model that allows them to estimate the ultrasonic scattering from the microstructure, they will be able to work toward those microstructures that are acoustically quiet. Finally, the entire body of work contributes substantially to the development of ultrasonic methods for the quantitative characterization of materials.

Previous work can be divided into two areas. These concern: first, hard alpha and second, the backscatter of ultrasound from metals and its use in material's characterization. We will discuss previous work on hard alpha first, and then work on ultrasonic backscatter.

There is, at present, no generally accepted method for the reliable detection of hard alpha inclusions in the interior of a part. Work has appeared concerning the problem of alpha-case, a hardened region of alpha phase material that occurs on the surface of a part that has been overheated. The techniques used to characterize this problem, eddy currents and chemical etching, do not appear to be relevant to the characterization of sub-surface inclusions. The effects of oxygen contamination in titanium alloys at the 0.1% level were studied as part of the Navy's program to develop welding techniques for titanium hulls for submarines [1]. This program included a number of studies using ultrasound and neutron activation. A set of well characterized alloy samples with varying degrees of oxygen contamination were produced. These samples were made available to experimental project (R.B. Thompson et al.). [2] Since the most important contaminant in hard alpha appears to nitrogen, this previous work is indirectly but usefully connected to the hard alpha problem.

The major difficulty in pursuing this work has been the absence of a generally agreed upon quantitative definition of "hard alpha." This phrase was used as a catch-all for a wide range of deleterious metallurgical modifications. Detailed information on the acoustic properties and microstructure are absent although a very substantial effort at obtaining this information is underway in the experimental component of this program and at the CNDE, which is attempting to produce well characterized samples with known hard alpha regions. Hence, the attempt to detect hard alpha suffers from the problem that the target is ambiguous. This remains a substantial problem to the present time.

In the absence of detailed information on the properties of hard alpha, we have worked at producing those models that will be necessary to understand the signal-to-noise of the inspection process when such information does become available. We have focused on the general problem of computing the ultrasonic backscatter given the microstructure of structural metals, in particular, titanium alloys. The ability to model the backscatter will

allow us to predict both the incoherent signal from hard alpha as well as the material (grain) noise generated by the surrounding normal alloy as soon as reasonable estimates for the hard alpha microstructure are available. We note that the estimate of the coherent signal from hard alpha also depends on uncertain material properties; however, computational methods for this problem are in relatively good shape compared to the backscatter problem. Hence, our effort has been focused on the development of a quantitative theory of backscatter.

Most structural materials are polycrystalline aggregates, that is, they consist of many small single crystals bonded together. The velocity of sound in each microscopic single crystal is anisotropic. Sound waves propagating in such aggregates scatter energy out of the main beam due to variations in the velocity of sound from crystallite to crystallite. Such scattering has a number of important consequences. First, the main beam is attenuated. Second, the scattering from the crystallites is diffuse and generally incoherent, and tends to mask signals from discrete defects such as cracks, voids and inclusions. Finally, the strength and frequency-dependence of the backscattering depend on the material properties of the aggregate, e.g. the size of the crystallites and the amount of texture. A quantitative theory will allow us to determine the degree to which such material properties may be inferred from the backscattered signal.

At the beginning of the project, no quantitative theory existed for the prediction of ultrasonic backscatter given the microstructure of the solid. However, a fair amount of work has been done on the characterization of structural materials and biological tissues using ultrasonic backscatter. Notably, Goebels [3] in a substantial series of work has used the temporal decay of the backscattered signal to estimate the grain size of metals. This work culminated in a device that predicts the grain size from the backscatter. The backscatter signal has also been investigated for the characterization of composite materials and for porosity in cast metals. Ultrasonic backscatter has also been investigated extensively as a means for determining the health of biological tissue. [4] These works have provided a substantial experimental and theoretical base for the development of a quantitative theory of backscatter.

Other work has been of two kinds. Several authors (e.g. Stanke and Kino, [5] and Hirsekorn) [6] have developed theories for the attenuation and velocity shift of the main beam in macroscopically isotropic single-phase aggregates. These theories include the effects of scattering only insofar as they effect the propagation of the main beam. Explicit expressions for the backscattered signal were not given. Margetan et al. [7] developed expressions for the signal due to the backscatter of ultrasound from polycrystalline media as part of the Air Force program.

B. Project

The first year's work, FY90, had two major components. First, we made a brief survey of possible probes for hard alpha detection. Second, we developed a rigorous and calculable theory for the backscatter of ultrasound from the microstructure.

Two probes were identified as useful for the detection of hard alpha: neutron activation and ultrasound. We will discuss the progress on neutron activation first since this material is briefer. Neutron activation works by irradiating and converting part of the metal to unstable radio nucleides. These radio nucleides decay and emit gamma rays, which can be detected. The composition of the metal can be inferred by examining the characteristic energies of the gamma ray. In particular, it appears that the method may be sufficiently sensitive to detect the trace amounts of nitrogen that are present in hard alpha inclusions.

Two actions resulted from the identification of neutrons as a possible probe of hard alpha. First, in 1990, J. H. Rose of the CNDE and J. Bartko of Westinghouse submitted a patent disclosure with the Ames Laboratory and Iowa State University concerning a device that uses neutron activation as the starting point for positron emission tomography. As of January 3, 1992, the laboratory has not proceeded with this disclosure. However, we have been assured that a decision to proceed or not will be made soon. Second, Gray initiated experiments at the Center for NDE and Iowa State University to test the feasibility of using neutron activation to detect hard alpha inclusions under separate CNDE funding. His work focuses on detecting contaminants in the sponge that the titanium alloy is refined from, and on detecting hard alpha in either billets or manufactured parts. Dr. Gray indicates that experiments at the small ISU research reactor demonstrate the possible feasibility of inspection by neutron inspection.

The focus of the project's first year effort was the development for the first time of a quantitative theory for the backscatter of ultrasound from the microstructure of metals. Previous work on the subject had been empirical and based on various guesses for the probe-flaw interaction. The current work removes these guesses and establishes the theory on a systematic basis. The major conceptual advance was to formulate the problem of backscattering in the time-domain, where most of current experiment is carried out, rather than the frequency domain, which has been used up to now. The frequency-domain presents certain technical problems in the development of the theory, the leading order term in the standard series expansion for the backscattered energy of a plane wave is *infinite* and thus nonsensical. Various authors have introduced *ad hoc* methods for avoiding this difficulty. The infinite response in the frequency-domain approximation can be traced to the scattering that in the model occurs for very great depths in the solid and hence at very late times. The reformulation of the calculation in the time domain allows us to study the backscattering as a function of time and to limit ourselves to scattering at early times where the theory can be put on a rigorous and systematic basis. The two major outcomes of the first-year effort on ultrasound were: (1) a systematic and calculable theory for acoustic backscatter, and (2) preliminary development of a method for estimating the material properties of a metal from the backscatter signal. [8]

Objective and Scope

The overall practical objectives will be described first. Then we will describe the scientific objectives that need to be met in order to achieve the practical objectives. The primary practical objective is related to the ultrasonic inspection of jet engine materials. Explicitly, the objectives are:

- To develop the theoretical base needed for the ultrasonic inspection of jet engine materials.
- To find a means of detecting hard alpha inclusions.

These practical objectives are supported by the following scientific objectives:

- To develop a quantitative theory for the backscatter of ultrasound from titanium alloys.
- To develop methods for inferring the properties of the microstructure from backscattered ultrasound.

The scope of this year's work is as follows. The theory of ultrasonic backscatter was reduced to a calculable form for single phase materials, and tested against experiment. Second, the theory was extended with the intention that one could eventually compute the ultrasonic backscatter from complicated alloys such as titanium jet engine alloys. In this task, the emphasis was on the multiphase nature and texturing of the alloy. Third, the signal-to-noise ratio for hard alpha inclusions was estimated. Finally, the basic theory was used to establish the reliability of previously used approximations for backscatter, such as the independent scattering approximation of Thompson et al. [7]

Approach

The basic scientific approach is to develop a theory that describes the backscatter of ultrasound from the microstructure of titanium alloys. This impacts the inspection of jet engine alloys in two ways. First, in order to estimate the signal from hard alpha, we need to understand ultrasonic backscatter, since the microstructure of these inclusions have been altered from the nominal alloy. Second, the noise that will be encountered in the inspection depends on the backscatter from the surrounding region of normal alloy. Hence the theory of ultrasonic backscatter determines both the signal and the relevant noise for the detection of hard alpha. The signal-to-noise ratio for hard alpha inclusions can easily be modeled once the theoretical development is complete and detailed models become available for the microstructure of the alloy and the hard alpha inclusions. The development of a systematic theory for ultrasonic backscatter from metals (polycrystalline aggregates) also has significant implications for the areas of materials evaluation and materials design.

This project interacts strongly with several other projects. First and foremost, the present project is the theoretical part of effort at the Ames Laboratory to develop ultrasonic methods for characterizing the microstructure of solids and detecting hard alpha inclusions. Further, the present project is highly leveraged by other work carried out at the CNDE. These projects, if successful, will significantly complement the efforts of the current project. Other activities (under a variety of funding) include the development of expressions for the ultrasonic backscatter from textured metal (Ahmed, EPRI), and the provision of samples with realistic hard alpha inclusions (Brasche, FAA). Gray is investigating further the feasibility of detecting hard alpha using neutron activation again under CNDE funding for the early sponge stage of titanium metal processing.

The strength of the approach is due to its very general nature and its applicability to a wide range of problems. The theory as presently developed is calculable and detailed results have been obtained and successfully compared to experiment for single phase materials. Further, the theory can be easily generalized (this work in progress) to multiphase media such as titanium alloys. As soon as plausible models of the microstructure of hard alpha inclusions are available, the present theory can be used to predict signal-to-noise ratios for inclusions of arbitrary size and shape in parts with simple geometries. The current approach is unique and novel. Up to the present time, there is no competing, calculable basic theory for acoustic backscatter from the microstructure of metals.

Technical Progress

The technical description of the theory requires a large amount of terminology. These definitions are contained in the paper "Ultrasonic Backscatter from Microstructure" that was presented at the Review of Progress of Quantitative NDE, held in July of 1991. Three new results were presented in this paper and are summarized in the paragraphs that follow. First, we showed that the independent scattering approximation used by Marguetan et. al. [7] can be interpreted as the first term in a systematic expansion for the backscattered signal if the elastic constants are estimated in the Voigt [9] approximation. Second, we gave explicit formulas for the backscattered power from single-phase aggregates of hexagonal or cubic crystallites. Finally, a preliminary comparison was made between theory and experiment.

Backscattering in the Independent Scattering Approximation

The independent scattering approximation is the simplest theory for computing backscatter from metals. The foundations of the approximation have been somewhat suspect, since it prescribes that one should add the powers scattered from each grain (rigorously, it is necessary to add amplitudes not powers). Further, the theory is not entirely defined, and depends on the choice of a particular reference medium. Below, we will show that the independent scattering model is the first term in a systematic expansion of the rigorous theory if the material properties are statistically independent from grain to grain. (The assumption of statistical independence from grain to grain is reasonable for macroscopically isotropic materials. The assumption of statistical independence implies that the isotropy of the material arises due to uncorrelated relative orientations of the crystallites.) This systematic expansion removes the ambiguity mentioned above, and explicitly defines the reference medium. Consequently, the independent scattering approximation may (within these limits) be used to explore more complex situations: e.g. textured and multiphase media.

Single-phase polycrystalline aggregates are considered. The material is assumed to be macroscopically uniform and isotropic; that is, the ensemble average of the material properties are assumed to be spatially uniform and isotropic. The elastic constants vary from crystallite to crystallite and will be characterized by

$$C_{ijkl}(r) = \sum_I c_{ijkl}^I \gamma^I(r). \quad (1)$$

Here, γ^I denotes the characteristic function that is defined to be one inside the I 'th crystallite and zero elsewhere, while the elastic constants of the I 'th crystallite are assumed to be constant and are denoted by c^I . We also define the deviation in the elastic constants

$$\delta C_{ijkl}(r) = \sum_I (c_{ijkl}^I \gamma^I(r) - c_{ijkl}^0). \quad (2)$$

Here, c^0 is an average elastic constant that will be shown to be given by the Voigt [9] average in the approximation used in this paper. The following assumptions are made about the variation in elastic constants. First, we assume that the variation in the elastic constants is weak $|\delta C|/C \ll 1$. Second, we assume that the variation in the elastic constants in different crystallites is statistically independent. Finally, we assume that the variation in the elastic constant of the I 'th crystallite and its characteristic function are statistically independent. A general review of wave propagation and scattering from random media can be found in Ref. 10.

We briefly review the origin of grain scattering. The velocity within each crystallite is anisotropic, and consequently depends on the crystallites orientation. Since, the crystallites are randomly oriented the velocity varies from crystallite to crystallite as does the resulting acoustic impedance. The variation in acoustic impedance gives rise to the backscattering. We assume that all of the scattering is due to the contrast in acoustic velocity. That is, we assume that there is (as expected) no variation in density, ρ , from crystallite to crystallite, and we assume that there is no significant scattering that is specifically due to the grain boundaries and other internal surfaces.

The backscattered signal amplitude, S , is given by the reciprocity theorem as

$$S(\omega) = \frac{1}{4\pi\rho c_l^2} \int d^3y \delta C_{ijkl}(x) u_{i,j}^0 u_{k,l} \quad (3)$$

Here, u^0 denotes the displacement field of the receiver that would have occurred in the absence of the variation in velocity (i.e., for a uniform solid), while u denotes the displacement field in the presence of the velocity variations. We use tensor notation; repeated Roman subscripts indicate summation, while subscripts which follow commas indicate derivatives. Finally, c_l indicates the velocity of propagation of longitudinal sound. The assumption that the elastic constant deviation is small allows us to evaluate the scattered signal in the Born approximation. That is, we replace u by u^0 in Eq.(3). We find

$$S(\omega) = \frac{1}{4\pi\rho c_l^2} \int d^3y \delta C_{ijkl}(x) u_{i,j}^0 u_{k,l}^0 \quad (4)$$

This approximation is expected to be valid for the early time portion of the signal when the main beam has not been significantly attenuated.

Next, we require that the ensemble average backscattered amplitude be zero; $\langle S \rangle = 0$; that is the signal should have zero mean. Taking the ensemble average of (4), we find that $\langle \delta C_{ijkl} \rangle = 0$. This implies (for backscatter evaluated in the Born approximation) that the elastic constants of the uniform reference space are given by the Voigt average

$$c_{ijkl}^0 = \langle c_{ijkl} \rangle \quad (5)$$

It is interesting to note that if the backscattered signal is evaluated using a more sophisticated approximation, then the evaluation of the elastic constants of the uniform reference space becomes more complicated. For example, if the scattering is evaluated to second order in multiple scattering theory, one finds that the elastic constants are given by the theory of Stanke and Kino [5]. In some measurements made by the experimental portion of the project, it has been noted that the role of attenuation in the measurement process is important. In these cases, higher order terms in the backscatter must be incorporated, and the first such correction implies the use of the Stanke-Kino theory for attenuation.

The backscattered power is obtained from the amplitude via

$$P(\omega) = \langle S(\omega) S^*(\omega) \rangle \quad (6)$$

An explicit formula is obtained by substituting Eq.(4) in (6). One finds

$$P(\omega) = \frac{1}{(4\pi\rho c_l^2)^2} \int d^3y \int d^3y' <\delta C_{ijkl}(y)\delta C_{pqrs}(y')> u_{i,j}^o u_{k,l}^o u_{p,q}^o u_{r,s}^o \quad (7)$$

Equation (7) is crucial for the rest of this paper. We will show that it has the following consequences. First, it implies the independent scattering approximation. Second, it leads to an explicit formula for the backscatter for single phase materials of hexagonal or cubic symmetry. Finally, it permits us to make a preliminary comparison of theory and experiment.

We will now show that the independent scattering model is implied by Eq. (8) if the average elastic constants are obtained from the Voigt [9] average. The independent scattering approximation as used by Margetan et al. [7] is defined as follows. First, one calculates the longitudinal to longitudinal scattering amplitude, A , for a single crystallite in an isotropic background medium. The power backscattered from such a single crystallite is equal to $|A|^2$. Within the independent scattering amplitude, the total backscattered power is assumed to be

$$P(\omega) \approx N <|A|^2> \quad (8)$$

Here N denotes the total number of crystallites in the active volume of the transducer. A denotes the L-L scattering amplitude in the Born approximation, which for a particular crystallite is defined to be

$$A = -\frac{\Delta C_{ijkl}}{4\pi\rho c_l^2} \int d^3y \gamma(y) u_{i,j}^o u_{k,l}^o \quad (9)$$

Here, ΔC denotes the difference between the actual elastic constants of the crystallite and some homogeneous and isotropic reference medium; the actual choice of the reference medium is ambiguous within the usual form of the independent scattering approximation. For example, should one determine the elastic constants using the Voigt average [9], the Reuss average [11] or perhaps one of the more sophisticated average such as the Hashin and Shtrikman [12] bounds? As we show below, Eq. (8) can be interpreted as the first term in a systematic expansion if the Voigt approximation is used. If we substitute Eq. (9) in (8), we find that the independent scattering approximation implies

$$P \approx N \frac{<\Delta C_{ijkl}\Delta C_{pqrs}>}{(4\pi\rho c_l)^2} \int d^3y \int d^3y' \gamma(y)\gamma(y') u_{i,j}^o u_{k,l}^o u_{p,q}^o u_{r,s}^o \quad (10)$$

We now show that the general expression for P that was derived from the reciprocity theorem reduces to the independent scattering approximation. We start by considering the elastic constant correlation function that appears in Eq.(7)

$$<\delta C_{ijkl}(r)\delta C_{pqrs}(r')> = \sum_l \sum_j <\delta c_{ijkl}^l \delta c_{pqrs}^l> <\gamma^l(r)\gamma^l(r')> \quad (11)$$

Here, we have used the fact that the elastic constant variation and the characteristic functions are assumed to vary independently. Next, we remember that the deviation in the elastic constants is assumed to vary independently from crystallite to crystallite. This implies that $\langle \delta c^I \delta c^J \rangle = 0$, unless $I = J$. This is the crucial point, the elastic constant variation is assumed to vary independently from crystallite to crystallite, and consequently the double sum reduces to a single sum over I . That is we can calculate the backscattering from each crystallite and then sum. Consequently, the general expression obtained from the reciprocity relation reduces to

$$P \approx N \frac{\langle \delta c_{ijkl} \delta c_{pqrs} \rangle}{(4\pi\rho c_l)^2} \int d^3y \int d^3y' \langle \gamma(y) \gamma(y') \rangle u_{i,l}^o u_{k,l}^o u_{p,q}^o u_{r,s}^o. \quad (12)$$

Here we have used the fact that $\langle \gamma^I \gamma^I \rangle$ and $\langle \delta c^I \delta c^I \rangle$ are the same for all crystallites, since the material is homogeneous on the ensemble average.

The reciprocity formulation, Eq.(12), for the backscattered power is identical with the independent scattering model formulation, Eq.(10), when both are evaluated in the Born approximation and the reference medium is defined by the Voigt average. This equivalence has several important consequences. First, it verifies the use of the independent scattering approximation in the set-up and analysis of experiments. Second, it completes the independent scattering approximation by providing a precise definition of the uniform reference medium. Finally, it provides a systematic method of deriving corrections to the independent scattering approximation.

Explicit Formulas For L-L Backscatter From Hexagonal And Cubic Materials

An explicit formula for L-L backscatter from polycrystalline materials of hexagonal (or cubic) symmetry can be obtained from Eq.(12). First we note that the incident field u^o can be written as

$$u_i^o = e^{ik\delta \cdot x} \hat{e}_i, \quad (13)$$

and that translational invariance implies that the correlation function $\langle \gamma \gamma \rangle$ depends only on the difference in coordinates. After obtaining the appropriate normalization constants, one finds

$$\langle \gamma(r) \gamma(r') \rangle = \frac{\langle vol^2 \rangle}{\Omega} p(r - r'). \quad (14)$$

Here, vol denotes the volume of a grain, while Ω denotes the volume of the sample. Further, p is the probability per unit volume that the line segment defined by $r - r'$ lies in a single crystallite; i.e. that the points r and r' lie in the same crystallite. Using Eqs. (13) and (14) in (12) yields

$$P(\omega) = \frac{\langle \delta c_{ijkl} \hat{e}_i \hat{e}_j \hat{e}_k \hat{e}_l \delta c_{pqrs} \hat{e}_p \hat{e}_q \hat{e}_r \hat{e}_s \rangle}{(4\pi\rho c_l^2)^2} k^4 \frac{\langle vol^2 \rangle}{\langle vol \rangle} \int d^3u p(u) e^{2ik\delta \cdot u}. \quad (15)$$

The ensemble average over the elastic constants can be carried out explicitly, and one obtains [13]

$$P(\omega) = \frac{Q}{(4\pi\rho c_l^2)^2} k^4 \frac{\langle vol^2 \rangle}{\langle vol \rangle} \int d^3u p(u) e^{2ik \cdot u}, \quad (16)$$

where

$$Q = (192C_{11}^2 - 128C_{11}C_{13} + 48C_{13}^2 - 256C_{11}C_{33} + 32C_{13}C_{33} + 112C_{33}^2 - 256C_{11}C_{44} + 192C_{13}C_{44} + 64C_{33}C_{44} + 192C_{44}^2) / 1575. \quad (17)$$

Here, C_{11} , C_{12} , etc. are the standard contracted notation for the elastic constants. Aggregates of cubic crystallites can be obtained by setting $C_{13} = C_{12}$ and $C_{33} = C_{11}$.

The frequency dependence of the backscattered signal is also of considerable interest. Generally, the backscatter power, P , depends on the particular form chosen for the probability function, p . Preliminary experimental work indicates that the probability function for polycrystalline aggregates can be well represented by an exponential. In particular, we parameterize the probability function as

$$p(u) = \frac{1}{8\pi a^3} \exp(-u/a). \quad (18)$$

Here, a is a length scale that is on the size of the average crystallite radius. The expression for the backscatter power that results from substituting Eq.(18) in (16) is given by

$$P(\omega) = \frac{Q}{(4\pi\rho c_l^2)^2} \frac{\langle vol^2 \rangle}{\langle vol \rangle} \frac{k^4}{(1 + (2ka)^2)^2} \quad (19)$$

Note that the backscatter tends to saturate for $ka > 1$.

At low frequency the signal rises as a k^4 , and can be written asymptotically as

$$P(\omega) \approx \frac{Q}{(4\pi\rho c_l^2)^2} k^4 \frac{\langle vol^2 \rangle}{\langle vol \rangle} \quad (20)$$

At high frequency, the backscatter becomes independent of frequency (and decreases as one over a length characteristic of the grain size). Explicitly,

$$P(\omega) \approx \frac{1}{16} \frac{Q}{(4\pi\rho c_l^2)^2} \frac{\langle vol^2 \rangle}{\langle vol \rangle} \frac{1}{a^4}. \quad (21)$$

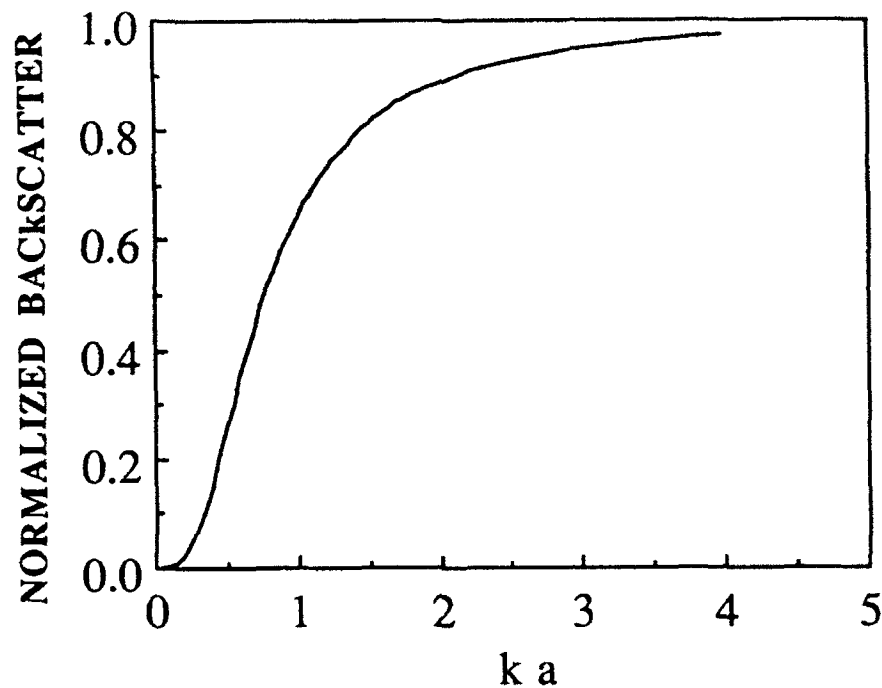


Figure 1 Shows the normalized backscatter as a function of frequency as calculated from an exponential correlation function.

Preliminary Comparison With Experiment

Experimental measurements of the backscattered power from single phase polycrystalline aggregates of pure alpha-phase titanium, stainless steel and copper have been made by Thompson et al. [14] They quantified the backscatter in terms of a quantity they called the figure-of-merit. They estimated the average radius and the figure of merit. We estimated the long wave length limit of the figure-of-merit using Eq.(20), the known elastic constants, and the radius estimates of Thompson et al. (the relevant quantities are tabulated in Ref.12). Theory and experiment are compared in Table (1).

Table I. Compares Theoretical And Experimental Values Of The Figure-Of-Merit (in $\text{cm}^{-1/2}$)

	THEORY	EXPERIMENT
Alpha Titanium (15 MHz)	0.021-0.048	0.035-0.042
Copper (5 MHz)	0.044-0.124	0.060-0.080
Stainless Steel (5 MHz)	0.021	0.032-0.038

It should be remarked that these signals are 40 or 50 dB smaller than the signal that would be generated by reflecting the incident beam off a steel plate in water. Consequently, the most important job of the theory is to correctly predict this order of magnitude for the signal strength. As we see, reasonable estimates for the size of the crystallites leads to agreement within several dB's. More detailed comparisons will require detailed studies of the statistics of $\langle \gamma \gamma \rangle$. Such studies are underway.

Finally, we remark that the backscattered power depends on the third power of the radius of the crystallites. Most of the uncertainty in the theoretical calculation result from the difficulty in measuring the average grain radius from micrographs. Small variations in the estimated grain size, 20%, lead to factor of two uncertainties in the predicted backscattered power. However, the same factor works in our favor if we are attempting to predict grain sizes from backscatter. Namely, factor of two uncertainties in the measured backscatter leads to errors of only 20% in the estimated grain size.

Summary

A first principles theory for the power backscattered from polycrystalline aggregates has been proposed and has been evaluated in the Born approximation. In this approximation the power varies as frequency to the fourth power and as the crystallite radius to the third power for wavelengths that are much larger than the crystallite size. For shorter wavelengths (comparable to the size of the crystallites or shorter) the backscattered power saturates, and becomes independent of frequency. For these shorter wavelengths the power varies inversely with the average grain size.

Calculable expressions were given for the backscatter from materials with hexagonal and cubic symmetry. These expressions were evaluated in the long wavelength limit for samples of copper, stainless steel and alpha titanium. Theory and experiment agree to within 3 dB; we consider this agreement to be rather good since the predicted change in signal is on the order of -50 dB. The variations in the theoretical answers arise due to uncertainties in the distribution of the radii of the crystallites. In order to remove these remaining uncertainties we are proceeding as follows. The backscatter is determined by certain statistical information concerning the sample. For macroscopically isotropic, polycrystalline aggregates we require both $\langle \text{vol}^2 \rangle / \langle \text{vol} \rangle$ and $p(r-r')$, the probability distribution that the line segment defined by $r-r'$ falls in a single crystallite. We are currently in the process of evaluating these statistical measures from microphotographs of the experimental samples measured above. Once available they will allow us to make a precise quantitative comparison of experiment and the theory presented.

The independent scattering approximation was shown to be the first term in a systematic expansion for the backscatter when the uniform reference medium was defined by the Voigt average of the elastic constants. This result is important for two reasons. First, it justifies the experimental data analysis method of Margetan et al. Second, it provides a simple method for analyzing more complicated solids, such as textured materials or multiphase alloys.

Finally, the theory developed in this work will be useful in determining if regions of altered microstructure (such as hard alpha inclusions in Ti) occur in a sample. First, it will allow us to understand the grain scattering from normal titanium. The detection of hard alpha implies that we can discriminate it from this background. Second, the presence of hard alpha inclusions would cause changes in the incoherent backscattered signal. If the backscatter from hard alpha is significantly larger than from the host material, it might

provide a method for the detection of hard alpha. Finally, and more generally, the results presented in this paper can be used as the basis of a method for inferring the average grain size as well as the average strength of the acoustic impedance variation.

Other aspects of the work have been published in two references. These papers examine the role of multiple scattering [15] and relation of the microstructure to the backscattered noise. [16]

Results in addition to those stated above are as follows. First, the backscatter coefficients (see e.g. Eqs. 16 and 17) were determined for single phase materials of arbitrary crystal symmetry (orthorhombic or higher). Second, the backscatter coefficients were calculated for pitch-catch geometries (again to the same level of detail as Eqs. 16 and 17). Third a general formulation of the theory was achieved for multiphase alloys with general texture. We note that Dr. Ahmed, in collaboration with R. B. Thompson under EPRI funding, is developing computable equations for backscatter from textured media (intended in this case to model austenitic steels). Substantial insights have been developed that connect ultrasonic backscatter with the attenuation of the ultrasonic wave by the material. These insights will provide the key to incorporating the attenuation into the estimate of the backscatter coefficient. Finally, Margetan and Thompson have presented model results for the signal-to-noise ratio of hard alpha inclusions. A number of technical challenges remain in order to estimate the backscatter given the microstructure. These challenges will be discussed immediately below.

Plans for Next Year

The understanding and quantification of the ultrasonic noise generated by the backscatter of ultrasound from the microstructure of metals, such as titanium, will continue to be our principle scientific goals. As this understanding is attained, we will integrate it with our primary engineering goal: the engineering design of a system for the ultrasonic inspection of commercial engine alloys. We will also continue to monitor the experiments of Gray and others that are designed to show the feasibility of using techniques other than ultrasound to detect the presence of nitrogen contamination in the sponge material from which the titanium is refined, and hard alpha inclusions in finished titanium parts.

The primary technical challenges that remain in the prediction of backscatter noise are as follows. First, we will develop a method for determining the microscopic acoustic properties of a given crystallite from measurements of the microstructure. Second, we will develop computable expressions for ultrasonic backscatter from multiphase materials (such as jet engine materials). Third, the effects of texture and preferential grain orientation will be studied since they appear to be crucial for understanding titanium alloys. Fourth, the effects of prior grain structure and the consequent correlation of grain properties will be studied; again, because of their importance for titanium alloys. Finally, we will establish the reliability of the current theory, which is based on a single scattering approximation, by estimating the second order terms.

At all stages the theory will be compared with the results of measurements as they become available. In particular, any experimental ultrasonic measurements of hard alpha inclusions will be the focal point of the theoretical effort. At present, an effort is being made at the CNDE to construct samples with hard alpha inclusions. The theoretical effort will be focused on these samples as they become available; we will focus on these samples until ultrasonic measurements made on them are quantified and understood.

We will also seek to establish the general qualitative ways that the backscatter noise depends on complex microstructures, such as those that occur in titanium alloys. The thrust of this work is to provide that basic work that is needed to connect the design of materials with acoustic properties.

Finally, we will seek to establish the reliability of our theory for the prediction of ultrasonic backscatter. This will have two parts. First, we will continue to compare our results with measurement. An important element in this process will be learning better how to calculate the required input data from microphotographs (and possible other microstructural studies). In particular, we have to learn how to better extract the relevant elastic constant correlation functions from such data. Second, we will extend the theory to include second order scattering terms. The relative size of these terms will indicate the range of validity of the current single scattering theory.

References

1. Proceedings of the Second Workshop on Nondestructive Evaluation (NDE) of Titanium Alloys, Eds. N.K. Batra, H.M. Chaskelis and O.P. Arora, (Office of Naval Research, Arlington Va, 1984).
2. R. B. Thompson, F. J. Margetan, J. H. Rose and N. K. Batra, "Effects of Interstitial Oxygen on the Ultrasonic Properties of Titanium Alloys", in Review of Progress in Quantitative Nondestructive Evaluation, Vol. 11 (in press).
3. K. Goebels, "Structure Analysis by Scattered Ultrasonic Radiation", in Research Techniques in Nondestructive Evaluation, Ed. R. S. Sharpe (Academic Press, New York, 1980), Vol. IV pp. 87-157.
4. B. Barzali, Z. Vered, G.A. Mohr, K.A. Wear, M. Courtois, B.E. Sobel, J.G. Miller and J. E. Perez, "Myocardial Ultrasonic Backscatter for Characterization of Ischemia and Reperfusion: Relationship to Wall Motion" Ultrasound in Medicine and Biology (In press).
5. F. E. Stanke and G. S. Kino, J. Acoust. Soc. Am., **75**, 665 (1984).
6. S. Hirsekorn, J. Acoust. Soc. Am. **79**, 1269 (1986).
7. F. J. Margetan, T. A. Gray and R. B. Thompson, Review of Progress in Quantitative Nondestructive Evaluation, Eds. D.O. Thompson and D.E. Chimenti (Plenum, NY) **10**, 1721 (1991).
8. J. H. Rose, "Ultrasonic Backscattering From Polycrystalline Aggregates Using Time-Domain Linear response Theory", Review of Progress in Quantitative Nondestructive Evaluation, Eds. D.O. Thompson and D.E. Chimenti (Plenum, NY) **10**, 1715 (1991).
9. W. Voigt, Lehrbuch der Krystallphysik, 962 pp, (B. G. Teubner, Leipzig) (1928).
10. A. Ishimaru, Wave Propagation and Scattering in Random Media, Academic Press, 1978.
11. A. Reuss, Z. Angew. Math. Mech., **9**, 49 (1929).
12. Z. Hashin and S. Shtrikman, J. Mech. and Phys. Solids, **10**, 343 (1962b).
13. J. H. Rose, "Ultrasonic Backscatter from Microstructure", Review of Progress in Quantitative Nondestructive Evaluation, Vol. 11 (in press).
14. R. B. Thompson, F. J. Margetan, Y. H. K. Han and C. E. Shamblen, "Relationship of Microstructure to Backscattered Ultrasonic Noise", Review of Progress in Quantitative Nondestructive Evaluation, Vol. 11 (in press).
15. R. B. Thompson, J. H. Rose and S. Ahmed, "Effects of Multiple Scattering on Ultrasonic Velocity, Attenuation and Backscatter in Polycrystals" to appear in Application of Multiple Scattering Theory to Material Science, Eds. R. L. Weaver, W. H. Butler, P. H. Dederichs and A. Gonis (Materials Research Society, Pittsburg, in press).

16. R. B. Thompson, F. J. Margetan, J. H. Rose and K. Y. Han, "Influence of Microstructure on Ultrasonic Backscatter Noise in Titanium Alloys", Nondestructive Testing and Evaluation (in press).

ULTRASONIC DETECTABILITY OF SMALL FLAWS IN ADVANCED ENGINE ALLOYS

R. B. Thompson and F. J. Margetan
Center for NDE
Iowa State University

Executive Summary

This project is concerned with the development of an engineering methodology to predict the ultrasonic detectability of small flaws in advanced engine alloys. The research effort is focussed on the particular problem of detecting hard-alpha inclusions in titanium aircraft engine alloys. These inclusions result from excess local concentrations of oxygen or nitrogen which occasionally occur during processing. Such impurities tend to occupy interstitial sites and cause excess brittleness. An engineering understanding of their detectability requires three elements: (1) knowledge of the strengths of the ultrasonic signals reflected from the inclusion; (2) knowledge of the strength of the competing backscattered noise signals associated with normal microstructural inhomogeneities such as grain and phase boundaries; and (3) use of this information to predict probabilities of detection. During the past year, major progress has occurred in each of these areas.

To estimate the strength of ultrasonic signals reflected from hard-alpha inclusions, one requires a knowledge of how the elastic moduli and density of the inclusions differ from those of the host alloy in which they reside. Based on reviews of the literature plus additional experiments conducted as needed, the influence of interstitial oxygen and nitrogen on those properties has been determined. It is clear that, at solute concentrations of a few percent, there are sufficient changes in the moduli to produce significant ultrasonic signals from hard-alpha inclusions in single phase microstructures. Some questions remain to be answered regarding the influence on detectability of a related effect, in which the presence of the interstitial contaminants modifies the microstructure of two-phase commercial alloys by converting beta to alpha phase.

During FY 1990, a phenomenological model was derived for the prediction of absolute noise levels in ultrasonic inspections, and some preliminary experimental validations of the model were performed. The model incorporated a figure-of-merit (FOM) for grain noise severity which depended solely on the microstructure of the specimen. However, in FY 1990, no computable expressions were available defining this relationship quantitatively. Other model factors were introduced which described the influence of the measurement system on the observed noise level. During FY 1991, the model was put on a much firmer theoretical foundation by the work of Rose in a companion task, which included the derivation of a formula relating the noise FOM to grain size and single crystal elastic constants. A much more extensive set of validations of the noise model, including this expression for the FOM, were also completed. For single-phased alloys, absolute comparisons between theory and experiment were in agreement to within a factor of 2. This level of agreement is considered to be quite good since the model contains no adjustable parameters and the predicted average noise level is typically 50-60 dB below a measured front-surface "reference" signal. In two-phase alloys, the component of the theory relating the noise FOM to the microstructure is not yet complete. However, a technique has been developed which makes it possible to determine this FOM experimentally. The FOM has been found to vary significantly from sample to sample and with direction within a given sample in a suite of commercial alloys. An approach has been defined which we believe will lead to a quantitative understanding of the origin of these microstructural variabilities.

Given the present level of our understanding of signal levels and noise levels encountered in the detection of hard-alpha inclusions, some illustrative calculations of signal-to-noise ratios have been performed. Among the conclusions reached is the importance of proper beam focussing as a means of enhancing the detection of hard-alpha inclusions.

In summary, during FY91 we have:

- Determined the effects of interstitial oxygen and nitrogen on the elastic constants of alpha titanium.
- Shown how to define a noise figure-of-merit (FOM) which is a material property essential to detectability calculations.
- Developed experimental techniques to measure this FOM.
- Shown that measured FOM values are in good agreement with first-principles theoretical predictions in single phase alloys.
- Studied experimentally the anisotropy and sample-to-sample variability of the FOM in two-phase, commercial alloys.
- Performed illustrative detectability calculations based on the signal-to-noise ratios expected in various inspection situations.

Project Background

A. General

As advanced materials are introduced into aircraft engines, operating under higher temperatures, at greater stresses and for longer lives, the need to detect small, internal defects becomes increasingly important. Ultrasound is often the preferred form of interrogating energy because of its ability to penetrate to the interior of the components. However, energy reflected from microstructural inhomogeneities such as grain boundaries produces a background noise which can inhibit the ability to detect reflections from small internal pores, cracks or inclusions. This project was initiated in response to the general need to better understand the physical factors influencing the detectability of such flaws. Such understanding can be used for such purposes as the development of criteria to predict flaw detectability in alloys with particular microstructures, the design of improved ultrasonic systems for detecting defects and the development of improved material processing procedures which produce "low-noise" microstructures and hence enhance detectability.

Certain key scientific elements are presently missing and must be developed in order to satisfy this need. In general, there is a good understanding of the principles governing the strengths of signals reflected from defects [1], although the inputs to the theories, i.e. material properties, are not always well known for particular cases. However, such is not the case for noise signals. Certain general features have been known for a long time, e.g. the fact that at low frequencies the noise will increase as the square of frequency due to Rayleigh scattering. More recently, quantitative attention has been placed on understanding the rate of decay of noise signals and using this information to study attenuation and material properties. Important pioneering work was done by Goebbels, who demonstrated the ability to determine grain size from backscattering measurements in parts in which only single-sided access was possible [2]. Within the Advanced NDE Technology Program, Tittmann and Ahlberg studied the attenuation and backscattering noise in nickel based alloys and demonstrated the important contribution that can be made by microporosity [3]. In the context of developing techniques to measure porosity in cast aluminum, Nagy, Adler and Rypien studied the relationship of the decay of the noise signals to the attenuation that would be observed in a coherent pulse-echo measurement, and demonstrated some fundamental differences between the two [4,5]. However, prior to the present work, there has been little effort devoted towards quantitative study of the absolute level of the noise, as needed to make detectability predictions. One exception is the work of Gray and Thompson [6,7], also conducted in a previous project of the Advanced NDE Technology Program, which serves as the starting point for the work reported here.

B. Project

Failures of rotating components in aircraft engines have demonstrated the difficulty of detecting metallurgical defects in commercial alloys. An important case is the problem of detecting hard-alpha inclusions in titanium alloys. Here, the cause for structural concern is the embrittlement of the alpha phase of commercial titanium alloys by the presence of oxygen or nitrogen impurities in interstitial sites, a condition occasionally introduced during processing. The development of a better understanding of the detectability of such inclusions is the primary focus of research in this project, as well as the companion theoretical project being conducted by J. H. Rose. Development of an understanding of flaw detectability requires two pieces of information; a knowledge of the strength of signals reflected from the metallurgical discontinuities, known as hard-alpha inclusions, and a knowledge of the absolute level of the backscattered noise, as influenced by the microstructure of the material and various parameters of the ultrasonic measurement setup. Work has been undertaken to develop models which quantitatively predict this information.

During FY 1990, efforts were devoted towards demonstrating the feasibility of quantitatively predicting detectability for ultrasonic detection of interior flaws. The fundamental reason that detection of hard-alpha inclusions is difficult is the fact that their density and elastic constants differ only slightly from those of the host medium and hence they scatter elastic waves only weakly. From the perspective of predicting signal strengths, this weak scattering has the advantage that the Born approximation [8] to scattering theory becomes an accurate, computationally simple, approximation. In order to make predictions of the signal strengths, one need only know the elastic moduli and density as functions of position within the inclusion. The Born approximation can then be used to predict the scattering amplitude, a fundamental quantity defining the strength of the scattered ultrasonic signal, in terms of integrals whose integrands depend on the deviations of the moduli and density of the inclusions from the values of the host. For spheroidally shaped inclusions, simple analytical expressions can be obtained. For more complex shapes, the results can be expressed in terms of the spatial Fourier transform of the shape of the inclusion. Using such scattering amplitudes as inputs to the ultrasonic measurement model, developed previously in the Advanced NDE Technology Program [9], one can compute the actual signal that would be observed in a particular experimental situation.

When applying this methodology to hard-alpha inclusions, one finds that the major cause of scattering is the change in the elastic moduli of the alpha phase of the titanium associated with the oxygen and nitrogen interstitials. In FY 1990, preliminary experiments were performed to assess the magnitude of these moduli changes since these values are needed as inputs to scattering calculations. It was observed that the ultrasonic wave velocities in the inclusions could vary from those of the host medium by several percent. Based on that finding, estimates of backscattered signal strengths were made for ultrasonic inspections of hypothesized hard-alpha inclusions of various sizes. These studies revealed a number of other factors which could also influence the wave velocities and hence signal strengths for the hard-alpha inclusions. *Studies of those effects were continued in FY 1991 as discussed in the Technical Progress section.*

The ability to detect these weak flaw signals is limited by the presence of microstructurally related noise. Numerous studies of ultrasonic backscattered noise had been made in the past. However, these had concentrated on such factors as the rate of decay of the noise signals rather than on their absolute amplitudes [2-5]. Since it is those absolute amplitudes that are needed to predict flaw detectability, additional work was required. During FY 1990, a phenomenological model was developed to predict that noise level for tone burst measurements [10]. This independent scattering model (ISM) assumed that the power scattered from individual grains could be added to determine the total backscattered power, i.e. the scattering was assumed to be incoherent. The measurement model of Thompson and Gray [9] was utilized to quantify the relative contributions of the parameters of the measurement system and of the microstructure. The most important aspect of the measurement system was found to be the beam pattern radiated by the transducer, which was predicted using the Gauss-Hermite beam model [11-12]. The microstructure was found to be characterized by a figure-of-merit (FOM) given, for a single-phased microstructure, by the quantity $n^{1/2} |\bar{A}|$, where n is the number density of grains and $|\bar{A}|$ is the rms scattering amplitude of a grain embedded in an effective medium. An experimental procedure was developed to measure the rms backscattered noise in an immersion configuration by illuminating the sample at normal incidence, translating the probe to obtain backscattered signals at multiple positions, averaging these signals to obtain their mean, and computing the rms value of the difference between the individual signals and this mean. It was found that the ISM did a good job of predicting various aspects of the experimental output. In particular, the time histories of the rms noise were found to be peaked at the focal position of both experimental and theoretical plots, the shapes of these

matched well, and they showed similar dependences upon such parameters as pulse length and frequency. It was thus concluded that the ISM provided a good first order description of the backscattered noise.

Objective and Scope

The overall objective of the project is to develop a capability to quantitatively predict the detectability of small interior flaws in advanced aircraft engine alloys using ultrasonic techniques, with primary emphasis being placed on the case of hard-alpha inclusions in titanium alloys. The specific objectives for FY 1991 are concerned with [1] validating and extending various aspects of the signal and noise models whose feasibility were demonstrated in FY 1990, and [2] demonstrating the use of these models in the analysis of flaw detectability. Primary emphasis is to be placed on quantifying the magnitude of the oxygen and nitrogen induced changes in elastic moduli of alpha titanium, as needed to predict the strength of signals reflected from hard-alpha inclusions, and on validating the noise model's ability to predict absolute signal levels.

Approach

Predictions of the detectability of hard-alpha inclusions are based on independent predictions of the strengths of the ultrasonic signals from the inclusions and of the absolute level of the microstructurally induced noise. Our approach, therefore, is to develop models which quantitatively predict each of these quantities, following procedures which have been discussed in some detail in the Project Background.

The Born approximation [8] combined with the ultrasonic measurement model [9] is used to predict the signals from the inclusions. Inputs required are the elastic moduli and densities of the inclusion with respect to those of the host. From the Born approximation, one can compute the scattering amplitude which, when used as an input to the measurement model, leads to a prediction of the absolute signal level that will be observed in a particular measurement system. All of these theoretical tools are in hand from work conducted previously in the Advanced NDE Technology Program. One component of the FY 1991 effort is aimed at obtaining estimates of the input parameters (moduli and density) from the literature and from direct experiments on laboratory samples. In the above discussion, it can be seen that, as a starting point, we are viewing the inclusion as an isotropic scatterer in an isotropic host of slightly different elastic properties. Other aspects of the project are concerned with defining the effects of crystallographic texture, variation of second phase content, and other metallurgical variables.

For the case of the metallurgical noise, no comparable model was available at the beginning of the project. As discussed in the Project Background, a major effort in this program is the development of such a model. Two tightly coupled approaches are being pursued. In this project, a phenomenological model is being formulated which places major emphasis on defining the influence of the parameters of the measurement system. The effects of the material's microstructure are contained in a parameter, designated the figure-of-merit (FOM). In a companion project, Rose has been studying the backscattering problem from a more fundamental point of view which leads to a rigorous definition of the effects of the microstructure but does not as conveniently introduce the effects of the measurement system. By comparing the predictions of the two theories in various limits, it appears possible to develop a fairly comprehensive model of the backscattered noise. For example, as will be discussed below, Rose's analysis has led to an explicit expression for the FOM of randomly oriented, equiaxed microstructures in terms of the single crystal elastic constants of the material.

Given well validated models for the signal strength and noise levels, it will be possible to predict signal-to-noise ratios in various experimental situations. Such a capability can be employed in a wide range of applications, including: the prediction of statistical performance measures, for flaw detectability, such as POD curves; the design of optimum detection configurations; and the specification of microstructures which will have lower noise and hence enhanced detectability.

Technical Progress

Strengths of Hard Alpha Signals

Prediction of the strengths of signals reflected from hard-alpha inclusions depends on a knowledge of the elastic moduli and density of the inclusions with respect to those of the host medium. This can be most easily motivated by recalling that the reflection coefficient R for a planar interface is given by

$$R = \frac{\rho_1 v_1 - \rho_0 v_0}{\rho_1 v_1 + \rho_0 v_0} \quad (1)$$

where ρ is density, v is ultrasonic wave speed and the subscripts 0 and 1 denote the material on either side of the interface. These densities and velocities also determine the reflection from a localized inhomogeneity such as an inclusion, although the exact mathematical equation is somewhat more complicated. When the properties are constant within the inclusion and are similar in value to those of the host medium, the Born approximation [8] provides an excellent estimate, with the scattering amplitude A predicted to be

$$A = \frac{k^2}{4\pi} \left[\frac{\delta\rho}{\rho} \cos\theta - \frac{\delta\lambda + 2\delta\mu \cos^2\theta}{\lambda + 2\mu} \right] S(k, \theta, \phi). \quad (2)$$

Here k is the propagation wave number, λ and μ are the Lamé elastic moduli for isotropic materials, θ and ϕ are scattering angles, and S is a shape factor. S is related to the spatial Fourier transform of the object shape and can be evaluated analytically for spheroidal shapes.

In hard alpha inclusions, the primary reason for the change in properties (denoted by $\delta\rho$, $\delta\lambda$ and $\delta\mu$ in Eq. (2)) is the presence of interstitial oxygen or nitrogen which occasionally enters the material during its processing. The primary data needed to predict the scattered ultrasonic signals are the values of these property changes as functions of impurity concentration. A review of the literature conducted during this year showed that there was considerable information available on the effects of oxygen interstitials on the properties of pure alpha titanium, the hexagonal phase that is stable at room temperature [13,14]. By examining the published data in those papers, and assuming the variation in properties at low concentrations to be linear, it was concluded that the moduli, density and velocities have the following fractional derivatives [15]:

$$\frac{1}{V_L} \frac{\partial V_L}{\partial x_0} \cong 3\% / \text{wt.}\% \quad (3a)$$

$$\frac{1}{V_T} \frac{\partial V_T}{\partial x_0} \cong 5\% / \text{wt.}\% \quad (3b)$$

$$\frac{1}{\rho} \frac{\partial \rho}{\partial x_0} \cong 1\% / \text{wt.}\% \quad (3c)$$

where V_L is the longitudinal wavespeed, V_T is the transverse wave speed, ρ is the density and x_o is the weight percent of interstitial oxygen. These results can be re-expressed in terms of the Lamé moduli λ and μ as

$$\frac{1}{(\lambda + 2\mu)} \frac{\partial(\lambda + 2\mu)}{\partial x_o} \cong 7\% / \text{wt.}\% \quad (3d)$$

$$\frac{1}{\mu} \frac{\partial\mu}{\partial x_o} \cong 11\% / \text{wt.}\% \quad (3e)$$

It can be seen that the effects of the interstitials on the moduli appears to be considerably more important than their effects on the density, and the effect on shearing deformations is somewhat greater than that on compressional deformations.

Similar information was not located for the effects of nitrogen, so new experiments had to be performed. Two sets of synthetic samples were obtained through the courtesy of L. Brasche of the Center for Aircraft Safety and Reliability, sponsored by the FAA [16]. One set was fabricated at CNDE by powder metallurgy techniques and contained nitrogen impurities in the tenths of percent range. The other set was provided by the FAA, as fabricated at a major aircraft engine manufacturer, and had somewhat greater concentrations. Measurements of the interstitially induced shifts in the longitudinal velocities in these specimens were quite close to those obtained on the specimens with oxygen impurities, being about 3% shift in velocity per weight percent nitrogen impurity [17].

By inserting these evaluations of interstitially induced property shifts into Eq (2), it would be possible to predict the scattering from a hard-alpha inclusion in a pure titanium matrix. However, the practical situation is different because commercial alloys have two-phase structures. Hence one should also consider the shift in the moduli of these two-phase alloys with oxygen or nitrogen interstitials. Here the situation has been found to be more complex. We have measured the shift in the speed of a surface wave propagating on a Ti-6% Al-4% V alloy before and after the growth of an oxygen induced alpha case, also using a sample provided by L. Brasche of the Center for Aircraft Safety and Reliability [16]. It was found that the velocity increased by about 7.5% when the alpha case contained 17 wt% oxygen. Although a substantial increase in velocity was observed, the fractional change per wt% impurity was only about 1/7 of that observed in the pure alpha titanium. Published data in the literature from another alloy, Ti-6% Al-2% Nb-1% Ta-1% Mo deviates even further from the single phase behavior, indicating a decrease in the moduli with the addition of oxygen [18].

An interpretation of this apparently inconsistent set of observations has recently been suggested by the investigators [15]. It is proposed that one must not only be concerned with the interstitial induced changes in the moduli of each phase, but one must also consider the changes in the phase content induced by the interstitials. Specifically, it has been proposed that the differences between the single-phase and two-phase behavior described above are a result of the conversion of beta to alpha phase by the alpha-stabilizing oxygen interstitials. This suggestion requires that the elastic stiffness of the beta phase be greater than that of the alpha phase, and arguments are presented in Ref. [15] in support of that position. This interpretation must be considered as quite preliminary. However, it is believed that the possibility of competing effects between the solute dependences of single crystal moduli and phase conversion on polycrystal moduli has great potential implications on the detectability

of hard alpha inclusions and requires a more exhaustive, systematic study. Also included in such studies should be the effects of crystallographic orientation, which can have significant influence on the differences in ultrasonic velocities of the host and inclusions.

Absolute Level of Backscattered Grain Noise

During FY 1990, the ISM model was derived as described in the Project Background. The result was the following relationship for the backscattered noise seen at time t in a pulse/echo tone-burst immersion experiment [10,19]:

$$N(t) = \sqrt{n} |\bar{A}| \frac{\sqrt{2} T_{o1}^2 \rho_1 v_1 e^{-2\alpha_o(Z_{os}-Z_{or})}}{R_{oo} \alpha^2 \rho_o v_o D k_1} \left[\iiint |C^4| \left| \frac{E(t-t_o)}{E_{max}} \right|^2 e^{-4\alpha_1 z} dx dy dz \right]^{1/2} \quad (4)$$

$N(t)$ is the rms backscattered noise (averaged over transducer location above the specimen), normalized by the amplitude of a front surface reference signal. Here n is the number of grains per cubic centimeter and $|\bar{A}|$ is the rms average scattering amplitude for backscatter from a single grain at the inspection frequency. ρ , v , α and k are respectively density, velocity, attenuation, and wave number, with subscript "o" referring to water and "1" referring to solid; T_{o1} and R_{oo} are liquid-solid transmission and reflection coefficients, respectively, a is the transducer radius, D is a diffraction (beamspread) correction factor in the reference experiment, and $C(x, y, z)$ is a normalized beam displacement amplitude. For the front-surface reference signal, $E(t)$ is the envelope of the tone burst, and has maximum amplitude E_{max} . Z_{or} and Z_{os} are the water path lengths in the reference and noise experiments, respectively. The integration is performed over the volume of the solid. Here t_o is a function of depth within the solid (z), and represents the time delay between the reference signal and the noise signal scattered from a grain at depth z .

Examination of this equation shows that it has the attractive feature that the effects of the measurement system have been separated from the microstructurally sensitive factor $\sqrt{n} |\bar{A}|$. Here, the latter has been defined as a material figure-of-merit (FOM). During FY 1990, various aspects of the predictions of this equation were verified, as discussed previously. These were all concerned with the variation of the predictions of the model as various physical parameters were changed rather than the absolute values of those predictions.

During FY 1991, significant effort was devoted to the validation of the absolute predictions [20]. Since the dependence of the model predictions on a variety of parameters had been previously demonstrated, the major remaining issue was whether the absolute level of the signals was properly set by the FOM. To test this it was necessary to develop signal processing procedures to infer the FOM from experimental noise measurements, to prepare a set of specimens with controlled microstructures, to quantitatively characterize those microstructures by metallographic methods, and to compare the values of the FOM inferred from the ultrasonic and metallographic techniques.

Examination of the ISM, Eq. (4) shows that the backscattered noise can be expressed as the product of the FOM and a series of factors determined by the details of the measurement system plus some material properties, including the attenuation. These latter factors were shown in FY 1990 to reproduce a number of key features in the noise data, including:

- (1) The dependence of the observed noise on the duration of the tone-burst.
- (2) The time dependence (or, equivalently, depth dependence) of the observed noise, and the manner in which this time dependence varies with frequency.
- (3) The strong noise peak that is observed when focussed transducers are used. (The peak is centered near the time required for the ultrasonic wave to propagate from the face of the transducer to its focal plane and back.)

The ability of the model to predict absolute noise levels for fine-grained specimens [19] is demonstrated in Figure 1. In the top portion of that figure, we display five rms noise functions observed in a single Ti-6% Al-2% Sn-4% Zn-6% Mo specimen. Five experimental trials were conducted, each using a different transducer excited with a 1- μ sec duration 15-MHz tone-burst. Three of the transducers were focussed and two were planar. In the bottom portion of Figure 1 we display the rms noise functions predicted by the ISM for five experimental trials. (The model results assume a value of 0.06 cm^{-1/2} for the specimen's FOM at 15 MHz.) The overall level of agreement between the measured and predicted noise levels in Figure 1 is striking.

For a given specimen, the FOM can be deduced from an experimental $N(t)$ curve by dividing the observed noise by model values of those factors which lie to the right of $\sqrt{n} | \bar{A} |$ in Eq. (4). Since the FOM depends only upon the microstructure of the specimen, the quotient should be independent of time, and independent of the particulars of the measurement system. In Figure 2, we display the FOM values for the Ti-6246 specimen, deduced from the measured noise data of Figure 1. The scatter in the deduced FOM values is seen to be dramatically less than the variations in the raw noise curves, suggesting that, to first order, the ISM is correct and the FOM is a material property. It should be noted, however, that in strongly attenuating samples, the fit is not as good, presumably due to multiple scattering effects. Further work is required to complete our understanding of such cases.

Given this direct measurement of the FOM, the next step in model validation is to compare the ultrasonically determined values to values obtained independently. For this comparison, we have chosen to make measurements on samples of randomly oriented, single-phased, equiaxed microstructures. These samples include a specimen of alpha-titanium, provided by L. Brasche using powder metallurgical techniques [16], a sample of 304 cast stainless steel, and a sample of commercially pure copper, available from other programs. For each of these samples, the average grain size was determined by standard metallographic analysis to provide an independent value for the grain volume V which appears in the theory to be discussed below. The measured grain diameters are listed in Table I.

To close the loop between the ultrasonic and the metallographic results, formulas are required which relate the FOM to the microstructure. For single-phased, equiaxed microstructures, these have been provided by J. H. Rose based on his work in a companion task [21]. By conducting a more formally rigorous analysis of the backscattering problem, Rose confirmed the validity of Eq. (4) for early times, before diffuse (multiple) scattering effects become important. Based on this analysis, he defines the properties of the proper effective medium to use in these calculations and computes the FOM for equiaxed distributions of cubic and hexagonal crystallites. It is assumed that the wavelength is much larger than the grain size, and that the scatterers are relatively weak. Under these conditions, one obtains, for single phase aggregates of hexagonal crystallites,

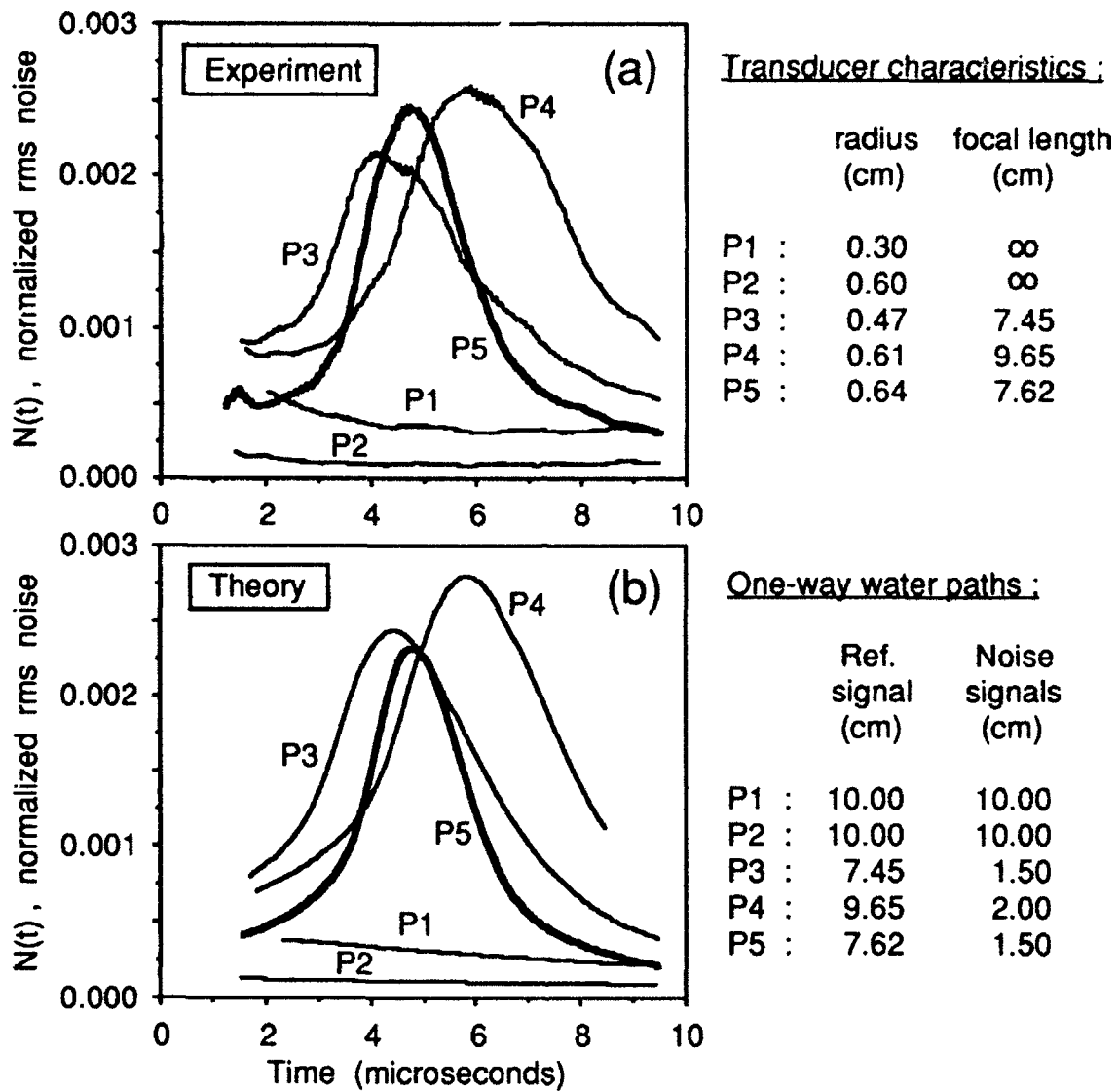


Figure 1 Measured (a) and predicted (b) normalized rms grain noise curves for one Ti-6246 specimen. Five experimental trials were performed using five different transducers.

$$(F.O.M.) = \frac{2\pi^{3/2}f^2}{\sqrt{3}v_1^2(\lambda_o + 2\mu_o)} \sqrt{\frac{\langle V^2 \rangle}{\langle V \rangle}} F_1, \quad (5)$$

where

$$F_1 = (192c_{11}^2 - 128c_{11}c_{13} + 48c_{13}^2 - 256c_{11}c_{33} + 32c_{13}c_{33} + 112c_{33}^2 - 256c_{11}c_{44} + 192c_{13}c_{44} + 64c_{33}c_{44} + 192c_{44}^2)/1575$$

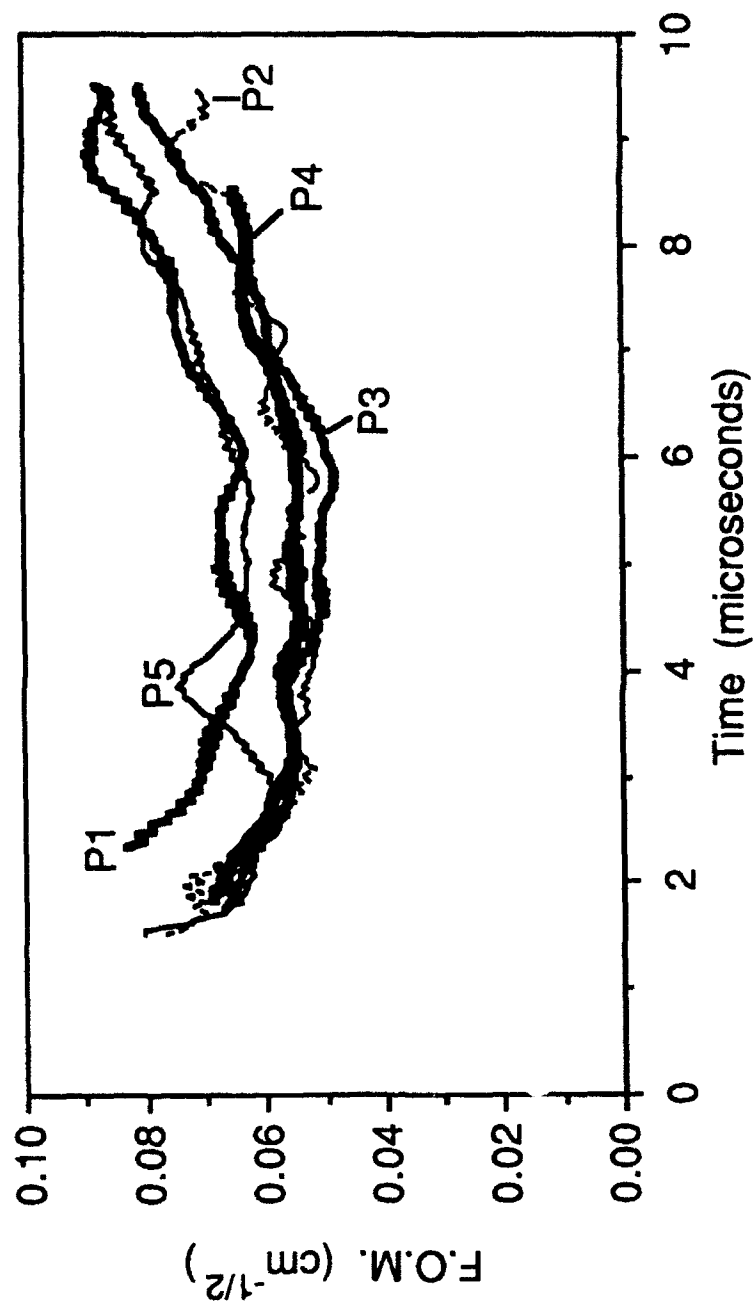


Figure 2 FOM at 15 MHz for the Ti-6246 specimen of Figure 1. The FOM has been inferred from the noise data by using the ISM (Eq. 4) to remove the influence of the measurement apparatus.

The same expression holds for the case of cubic symmetry, with $c_{13} = c_{12}$, and $c_{33} = c_{11}$. Above, V denotes the volume of a scatterer, $\langle \dots \rangle$ denotes the ensemble average, and the c_{ij} 's denote the single crystal elastic constants. The frequency is denoted by f , while ν_1 , λ_0 , and μ_0 are the longitudinal velocity and the Lamé parameters of the effective medium that is obtained from (the density and) the Voigt average of the elastic constants. It is thus possible to directly predict the FOM given the metallographic determination of the grain size as discussed above and the knowledge of the single crystal elastic constants of the material, which can often be found in the literature.

Table I presents the results of a comparison of the FOM values determined by ultrasonic noise measurements and by metallographic analysis [20]. The fourth column gives the FOM as predicted from Eq. (5) while the fifth column presents the value inferred from the ultrasonic experiments. Where a range of values is indicated for the metallographic FOM, this range is a result of uncertainties in the grain size distribution inferred from micrographs. The range of values for the ultrasonically determined FOM arises from the fact that, in practice, the deduced FOM is weakly dependent on the time (or depth) at which the rms noise data is analyzed. Given these variabilities, the agreement in Table I is believed to be quite good, particularly in light of the fact that there are no adjustable parameters involved.

Although requiring more extensive validation, these results indicate that it is possible to predict the FOM for simple microstructures from first principles.

The next step is to consider the two-phased alloys that are used in actual engines. The theory is not presently available to predict those FOM's from first principles. However, some experimental measurements of these parameters have been performed for commercial alloys with very interesting results. The particular set of samples studied in detail were fabricated from Ti-6%Al-2%Sn-4%Zr-6%Mo as part of an Air Force manufacturing technology program [22]. The starting point was VAR melted material, processed to an equiaxed alpha-beta microstructure at 6-inch diameter billet. Further heat treatment utilized to modify the microstructure is summarized in Table II. Note that the beta transus for this alloy is 1775 °F, so that the first 3 samples were annealed below the beta transus while the fourth was annealed above the beta transus.

Table I. Comparison of FOM Values Obtained from Ultrasonic Experiment and Metallographic Analysis.

Material	Frequency (MHZ)	Grain Diameter (Microns)	Metallographic FOM ($\text{cm}^{-1/2}$)	Ultrasonic FOM ($\text{cm}^{-1/2}$)
α -Titanium	15	64-112	0.021-0.048	0.035-0.042
304-Stainless	5	~ 100	~ 0.021	0.032-0.038
Copper	5	150-300	0.044-0.124	0.06-0.08

Table II. Further Heat Treatment of Ti-6246 Specimens.

Specimen	Anneal Temp.	Anneal Time	Cooling Method
A1	1670°F	1 Hr.	Air Cool
A2	1745°F	1 Hr.	Air Cool
B2	1745°F	8 Hr.	Water Quench
C1	1795°F	1 Hr.	Air Cool

(Beta transus = 1775°F)

Backscattered grain noise measurements at 15 MHz were made through three orthogonal faces of each specimen, and the noise data for each propagation direction was analyzed to extract the ultrasonic FOM [19]. The results are summarized in Figure 3. It is interesting to note that the sample processed above the beta transus had similar FOM values in each direction, while those processed below the beta transus exhibited considerable anisotropy, with the lowest values being obtained when the ultrasonic waves propagated along the axis of the billet. The origin of this anisotropy has not yet been fully identified, since micrographs indicate that the microstructure in the three orthogonal directions are quite similar, as shown in Figure 4. We believe that properties not revealed by these micrographs, such as preferred grain orientation and/or macrostructure are determining the absolute noise levels. Isolation of those factors is an important objective for the future.

During FY1991, a number of improvements were also incorporated in the model. In addition to the introduction of expressions relating the FOM to the single crystal elastic constants based on the work of Rose and as discussed above, extensions which generalize Eq. (4) to the case of oblique angle and pitch-catch measurements were introduced. For the case of oblique incidence, the changes are relatively superficial and simply introduce the idea that the beam pattern changes with angle of incidence. Rather than the single longitudinal sound beam which exists in the metal at normal incidence, there are generally both longitudinal and shear wave beams in the metal at oblique incidence. Both beams contribute to the total backscattered noise, and each is governed by a separate FOM. For equiaxial materials, the longitudinal FOM can be determined from backscattered noise levels at normal incidence using the method described in this report. The shear wave FOM can be determined in a similar manner by choosing the angle of incidence in water to be greater than the longitudinal critical angle. Then, only a shear wave beam exists in the metal, and Eq. (4) may be used to deduce the FOM for backscattered shear waves. For the case of pitch-catch measurements, the extension introduces a FOM which depends on the direction of scattering, with the previous results corresponding to the limit of backscattering. These extensions can be important for inspection of near net shape components, when normal incidence inspection is impractical or non-optimal.

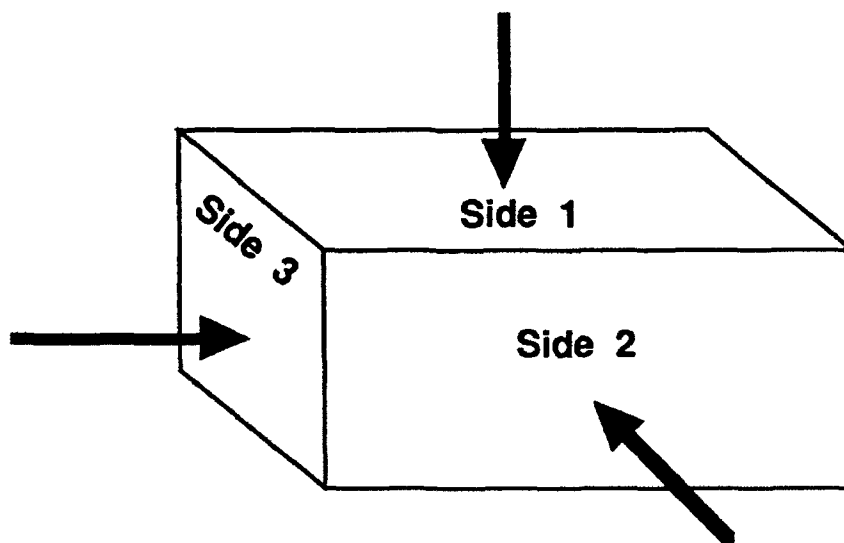
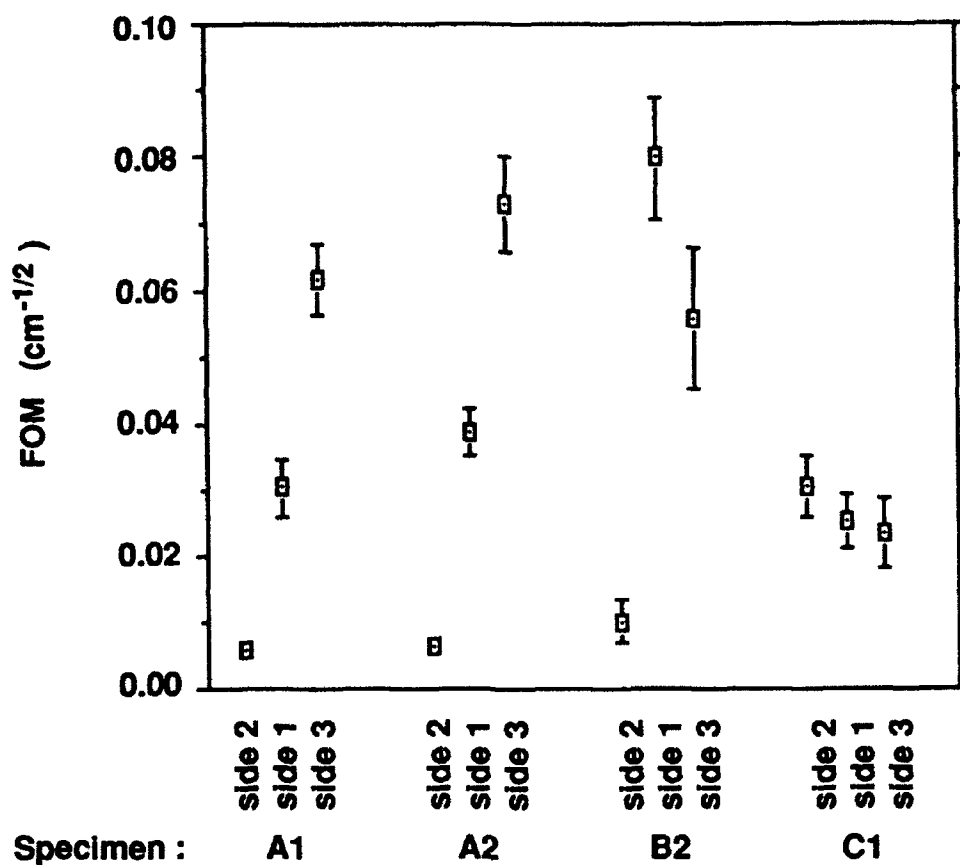


Figure 3 Figure-of-Merit for Grain Noise Severity. Values at 15 MHz for Four Ti-6246 specimens.

METALLOGRAPHY OF Ti-6-2-4-6

Specimen A2

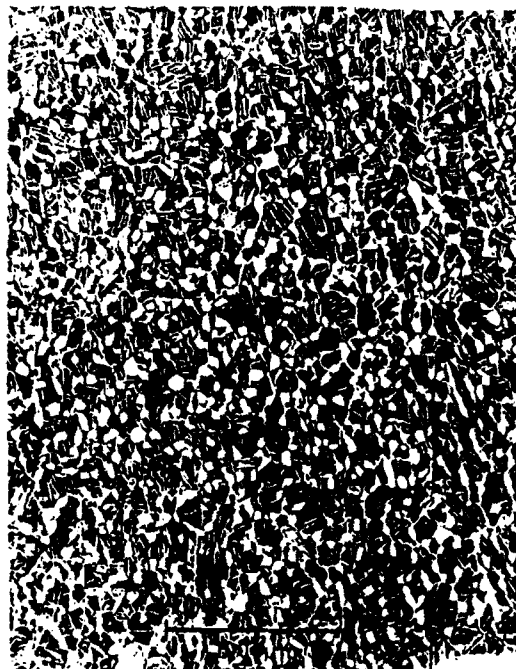
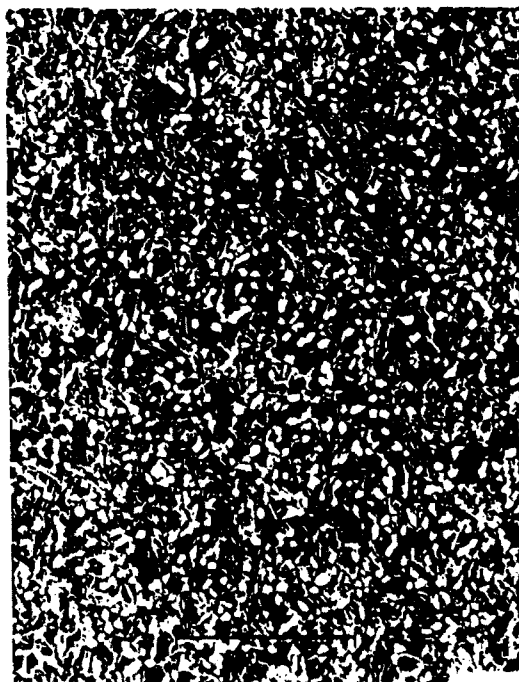
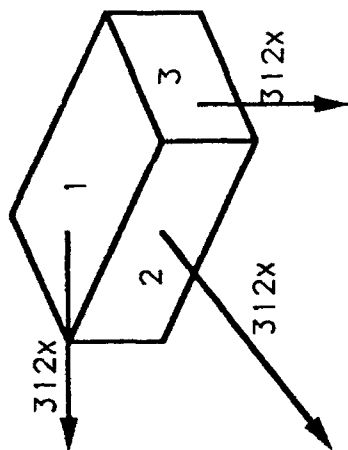
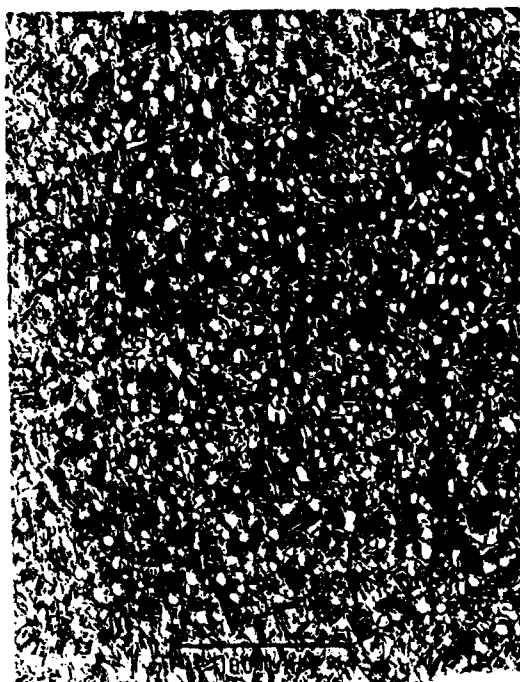


Figure 4 Micrographs of 3 orthogonal faces of Ti-6246 specimen' 12.

Signal-to-Noise Levels

With techniques in place to predict the absolute values of the defect signals and the rms noise, it becomes possible to make quantitative predictions of the signal-to-noise ratios, an important step towards the development of a fully engineered detection capability. To illustrate this possibility, a series of calculations has been made [19]. In these simulations, three types of reflectors were compared; a flat crack oriented perpendicular to the beam, a spherical void, and a spherical hard-alpha inclusion. The latter was assumed to have ultrasonic wave speeds that were 8% greater than those of the titanium-alloy matrix and a density that was 1% less. Thus, this might be thought of as the response of an inclusion containing a few weight percent oxygen or nitrogen interstitials (recognizing the qualifications that were previously stated concerning the uncertain role of beta to alpha phase conversion). Predictions were made for two materials. One had a FOM of $0.080 \text{ cm}^{-1/2}$ at 15 MHz, and the other had a FOM of $0.008 \text{ cm}^{-1/2}$. These values were chosen to correspond to the extremes of the FOM values observed in the four Ti-6246 specimens. Some pertinent assumptions of the inspection simulations are summarized in Figure 5. In Figure 6, the performances that would be expected using the focussed probe and the unfocussed probe are compared. The 20 dB improvement offered by focussing for this particular case is clearly evident. Note, however, that the beam has been assumed to be focussed on the flaw rather than on the surface of the part, in contrast to a common industrial practice. Figure 7 compares the reflectivity of the three flaw types at 15 MHz. The crack and the pore are seen to produce backscattered signals of comparable amplitude, with the signal from the hypothesized hard-alpha inclusion being lower by about 40 dB. Finally, Figure 8 compares the detectability of the hypothesized hard-alpha inclusion in the two materials with differing noise levels when the focussed probe is used. The FOM's chosen correspond approximately to the maximum and minimum of those shown in Fig. 3. Whereas a 10dB signal-to-noise ratio is reached at a radius of 0.3 mm in the low-noise alloy, it has not been reached for radii as large as 1 cm in the high-noise alloy. Such calculations provide a means of quantitatively predicting the effects of microstructure on flaw detectability.

Summary

To assess the detectability of hard-alpha inclusions in titanium alloys, one requires: (1) knowledge of the ultrasonic properties of the inclusions relative to those of the host alloys; and (2) an understanding of backscattered noise levels in the hosts. In FY 1991, substantial progress was made on both fronts. For alpha-phase titanium we have determined the dependences of elastic moduli and density on the interstitial contaminants (oxygen and nitrogen) which lead to hard-alpha embrittlement. These property changes allow one to infer the strengths of ultrasonic signals backscattered from inclusions of various sizes and locations. In our investigation of backscattered noise, we have defined a figure-of-merit (FOM) for inherent noise severity, and shown how this material property may be extracted from measured noise data. For single-phase metal specimens, including alpha-titanium, we have demonstrated that the extracted FOM is in good agreement with the value expected from a first-principals model calculation. We have also demonstrated that the rms noise level observed in a given inspection scenario can be accurately predicted if the specimen's FOM is known. Finally, we have carried out illustrative calculations of signal-to-noise ratios for hypothesized hard-alpha inclusions in titanium specimens. A number of issues remain to be addressed and clarified before a proper assessment of inclusion detectability in commercial alloys can be made. These include: the conversion of beta phase to alpha phase by contaminants, and the influence of this conversion on elastic moduli; the origin of the noise anisotropy which has been observed in commercial alloys; and the relationship between rms noise and peak noise levels. These topics for future study are more fully discussed in the following section.

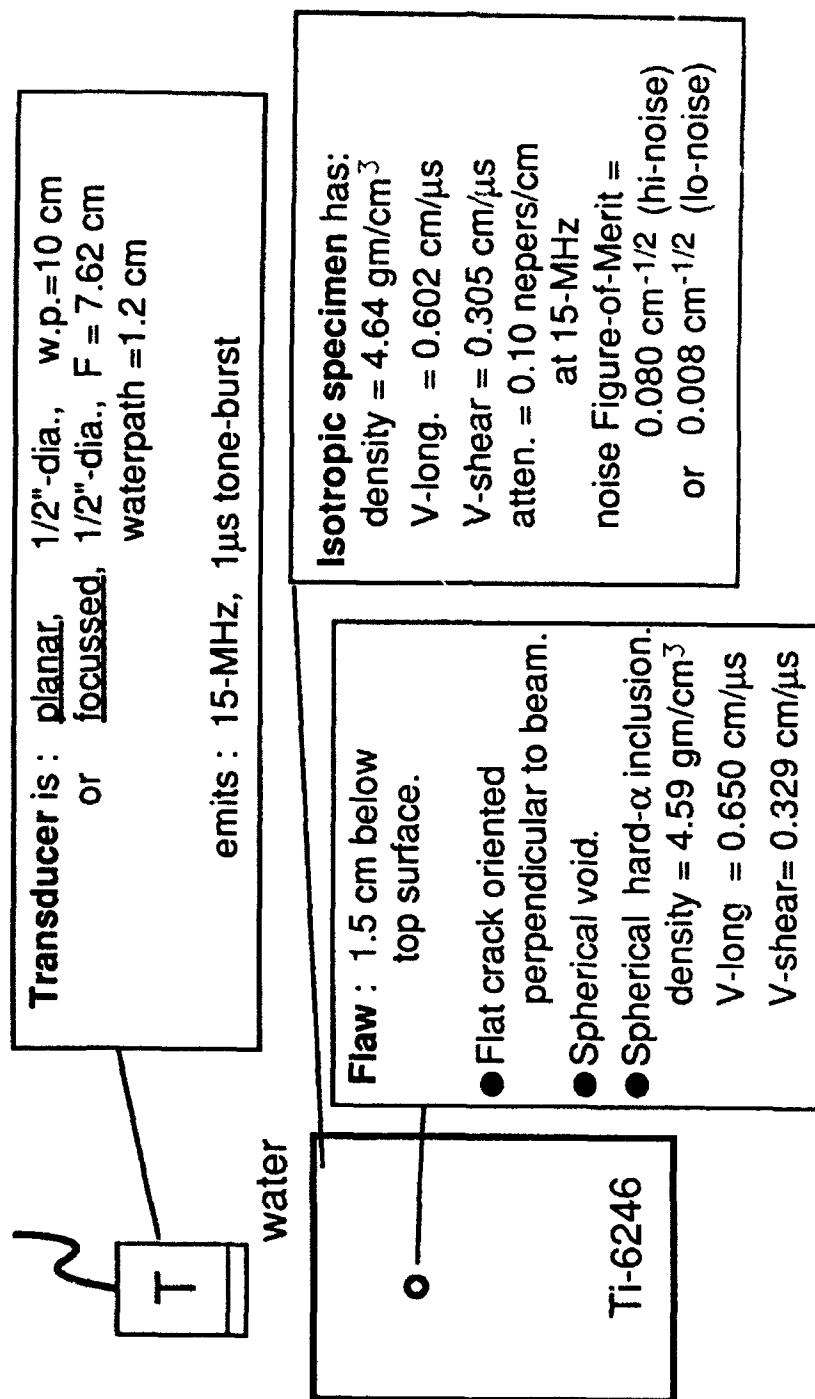


Figure 5 Measurement system, defect, and material parameters assumed in model predictions of signal/noise ratios.

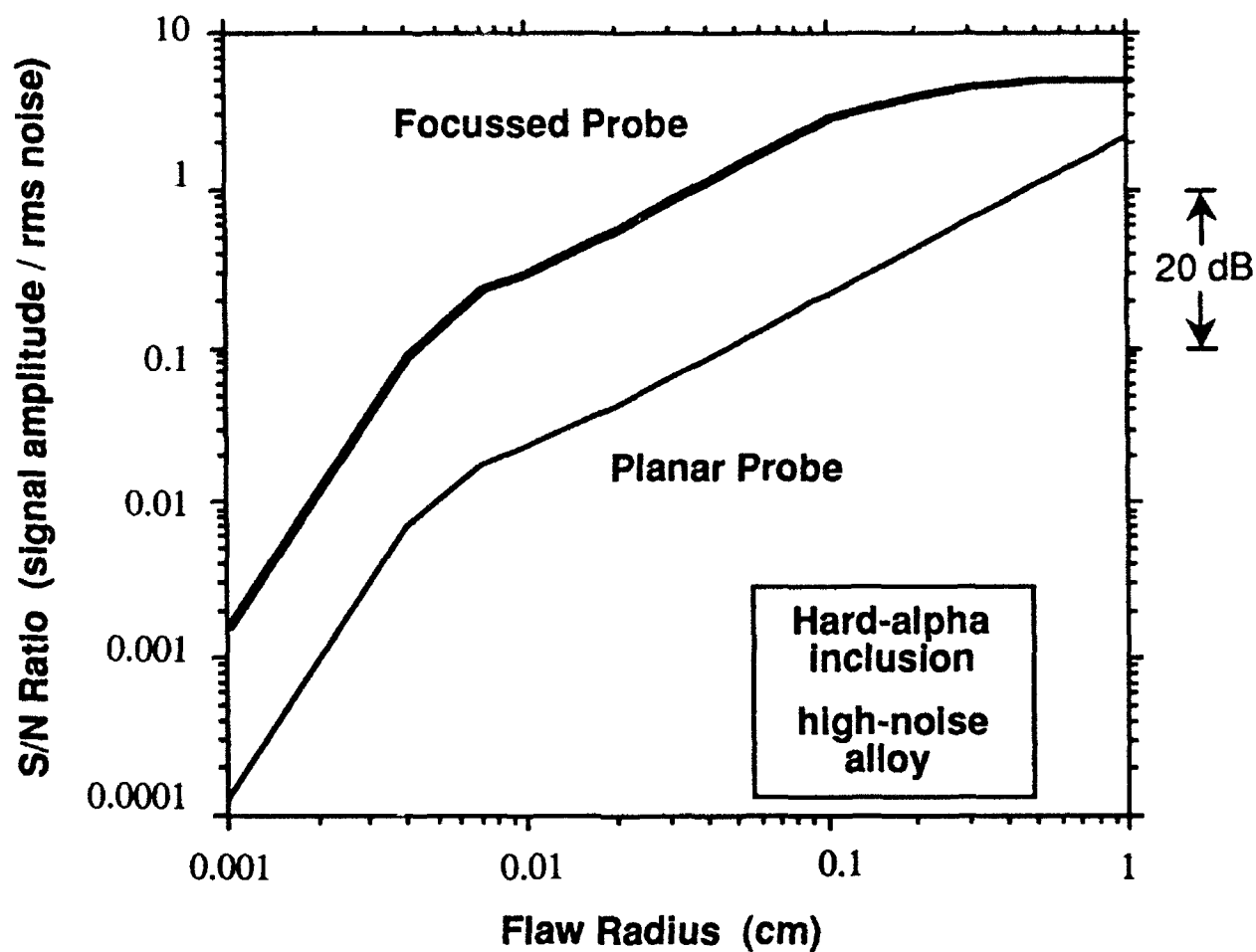


Figure 6 Comparison of detection of hypothetical hard-alpha inclusion using focussed and planar probes in high-noise, Ti-6246 alloy (15 MHz, 1- μ second toneburst).

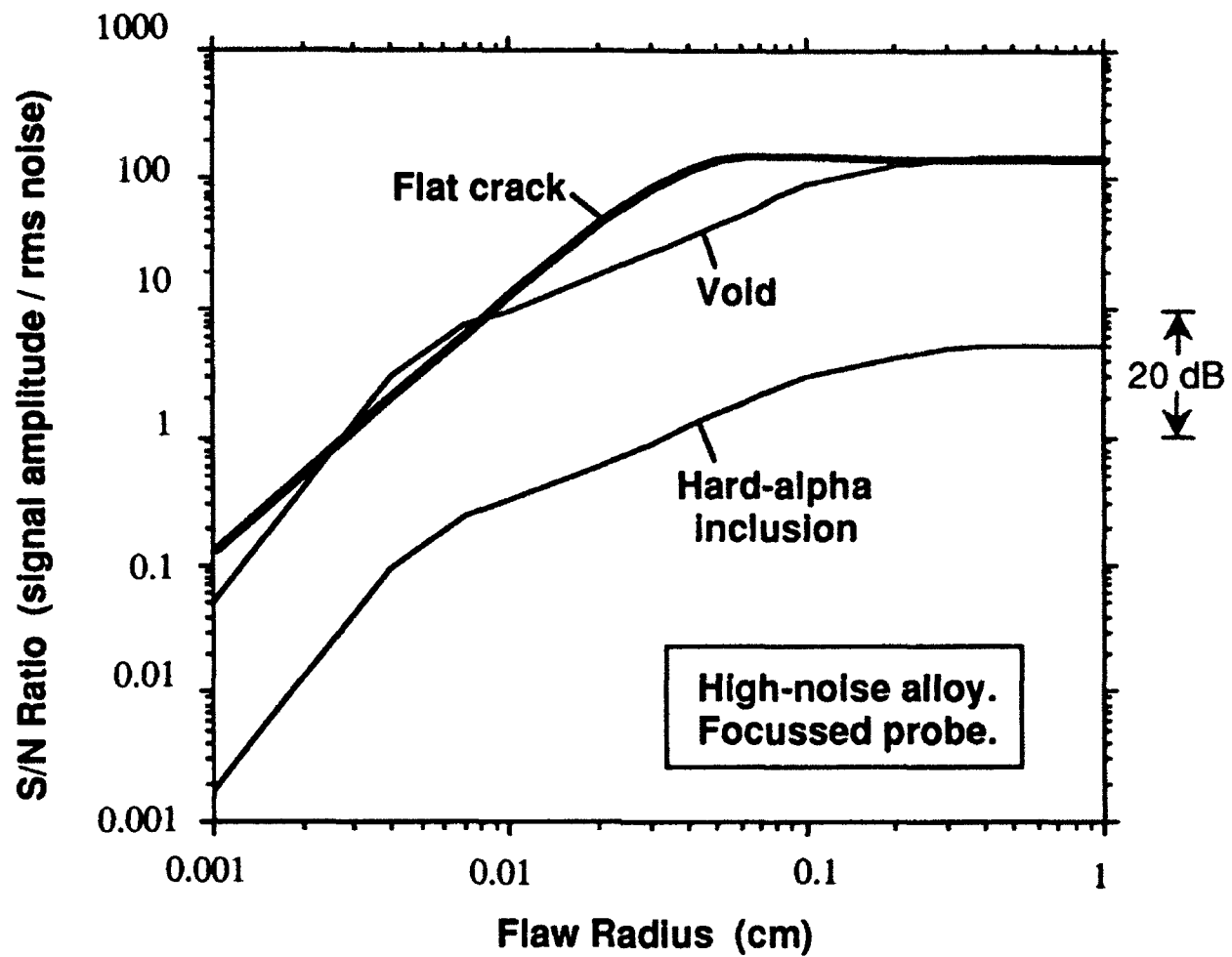


Figure 7 Comparison of the detection of three classes of inclusions with a focussed probe (15 MHz, 1-μsecond toneburst).

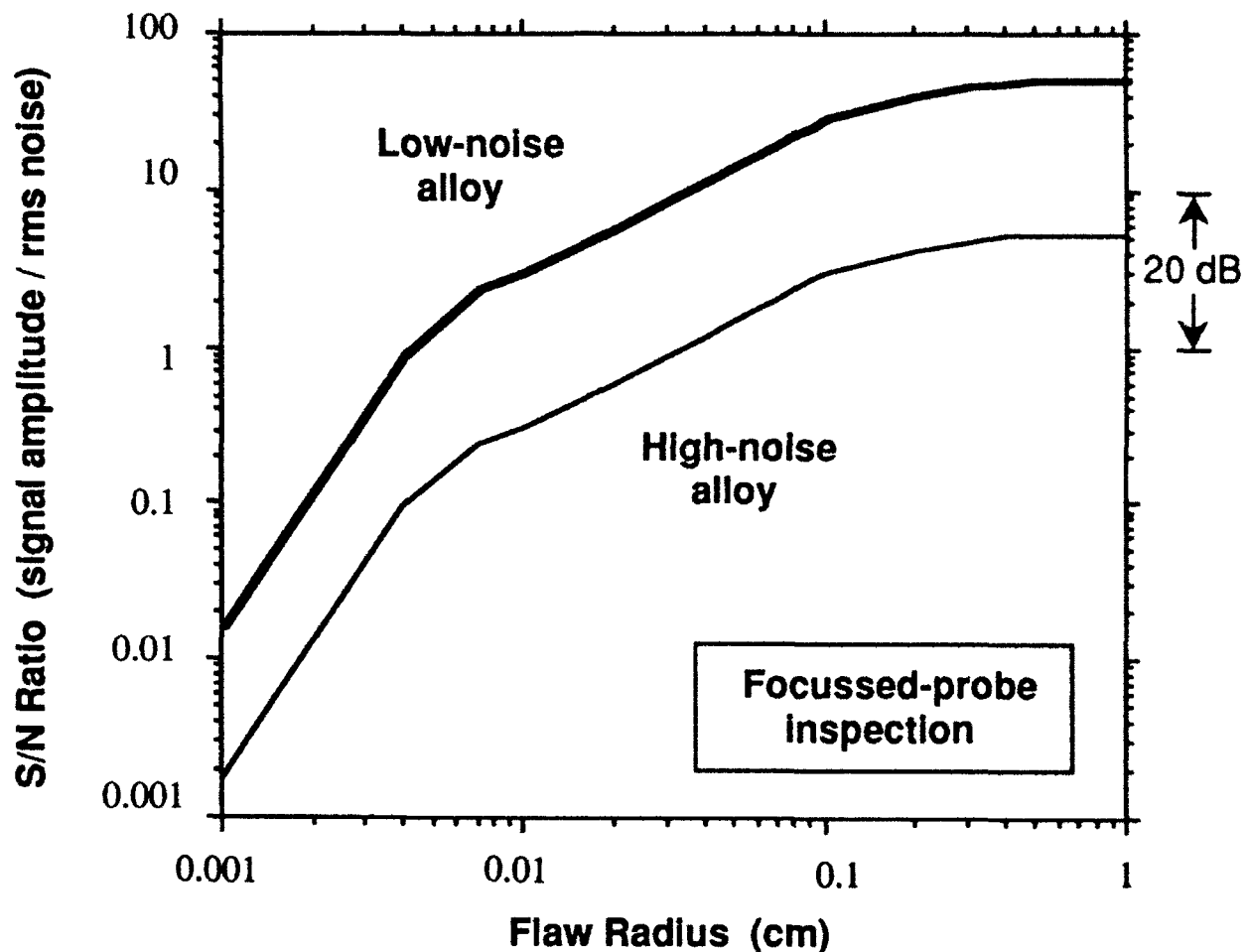


Figure 8 Comparison of the detectability of a hypothetical hard-alpha inclusion in two alloys with differing levels of microstructural noise (15 MHz, 1- μ second toneburst).

Plans for Next Year

The objective for FY 1992 is to clarify a number of unresolved issues which arose in 1991 and whose answers are required for establishing an engineering basis for understanding the detectability of hard-alpha inclusions in advanced titanium alloys. These are concerned with the effects of changes in phase content on the reflectivity of hard-alpha inclusions, the relationship of noise levels to microstructure in two-phase alloys, understanding the distributions of noise about its rms value, and identifying more fully the role of multiple scattering. A summary of the work expected in each of these areas follows.

In FY 1991, it was found that interstitial oxygen or nitrogen strongly influences the wave speeds in single-phase, alpha titanium. However, in alpha-beta alloys, the effect is considerably less. In fact, the data in the literature is somewhat ambiguous, in some cases suggesting that velocity increases and in others suggesting that velocity decreases as interstitials are added. An important factor appears to be the conversion of beta to alpha phase by the alpha stabilizing interstitials. If the wave speeds in the beta phase are higher

than those in the alpha phase, the weaker effect in the two-phase alloys would be explained. During FY 1992, we plan to examine this question in greater detail. Included in the methodology will be measurements on samples produced by powder metallurgical techniques in which oxygen and nitrogen are added in a controlled fashion to alloy powders. Our initial plans call for the preparation of 2 groups of 3 specimens. In each group the level of nitrogen content will be varied. Heat treatment will be changed between the groups to modify the underlying microstructure. We will carefully measure the changes in both ultrasonic properties and microstructure as functions of interstitial content and heat treatment. Results will be interpreted in terms of theories of wave propagation in polycrystalline aggregates.

In 1991, a quantitative understanding of the mechanisms of noise generation in single phase alloys was gained. Central to this was an expression relating a material FOM to the single-crystal elastic constants of the phase. However, in two-phase alloys, two new phenomena were encountered. Our simple formulae were not applicable to the complex microstructures so we could not predict absolute noise levels. Moreover, some large anisotropies in the noise were observed which had no apparent correlation with microstructural features. In FY 1992, we plan to uncover the mechanism of this noise anisotropy in two-phase microstructures and, in collaboration with J. H. Rose, to develop a quantitative model for the absolute value of the noise. It is our hypothesis that the absolute value of the noise and its anisotropy is controlled by macrostructural features which are not visible in the micrographs, and the first portion of our experiments will be aimed at identifying those features using such techniques as macroetching. We will then try to quantify the controlling microstructure features. We believe that this will require both macroscopic texture analysis using x-ray diffraction and microscopic texture analysis based on x-ray channeling patterns in an SEM. Further information may be obtained by interpreting the $V(z)$ response of high-frequency, scanning acoustic micrographs to obtain local elastic constant information. This information will be coupled with microscopic models for noise in two-phase alloys, developed in collaboration with J. H. Rose, to predict the absolute noise levels and their anisotropies.

The third major thrust of the effort will be directed towards developing a better understanding of the distribution of the signal strengths about their mean. It is intuitively clear that the reliability of detection depends not only on the rms noise level (as presently predicted by our models) but on the likelihood of fluctuations of the noise about that rms value. It is these fluctuations that can cause "spikes" in the noise which might be mistaken for defect signals. It is also clear that these fluctuations will be larger near a focal spot, since a smaller number of grains will be contributing to the backscattered signal and hence the distribution of signals about the rms mean will be broader. We plan to investigate this question through an experimental study of the distribution of noise about its mean value, combined with modeling studies, involving Monte Carlo calculations. In these calculations, we will select members from an ensemble of samples having a specified distribution of grain sizes. Using the measurement model of Thompson and Gray, we will predict the time dependence of the backscattered signal for each ensemble member. Such a model will allow us to answer a number of important practical questions, including the dependence of the noise on grain size, ultrasonic pulse width, and preferred orientation. Outputs will include rms signals (obtained by analysis of the response of several ensemble members), deviations from that mean, spectral features of the noise, etc. We believe that this model can also be readily extended to two phase media and will provide an important predictive tool.

Attention will also be given to multiple scattering effects. Both the models of Rose and ourselves have been based on the assumption of single scattering, which is rigorously valid for early times. We have found that, in many samples, this is a valid description for the range of times of practical interest. However, in strongly scattering cases, we observe breakdowns which we tentatively attribute to multiple scattering effects. We plan to undertake further study of this effect in collaboration with J. H. Rose.

References

1. R. B. Thompson and H. N. G. Wadley, "The Use of Elastic Wave - Material Structure Interaction Theories in NDE Modeling, CRC Critical Reviews in Solid State and Material Sciences," 16, 37-89 (1989).
2. K. Goebbels, "Structure Analysis by Scattered Ultrasonic Radiation," Research Techniques in Nondestructive Testing, R. S. Sharpe, Ed. (Academic Press, N.Y., 1980), pp. 87-157.
3. B. R. Tittmann and L. Ahlberg, "Attenuation and Grain Noise Parameters in Ni-Base Alloys," Review of Progress in Quantitative NDE, Vol. 2A, D. O. Thompson and D. E. Chimenti, Eds. (Plenum Press, NY, 1983) pp. 129-145.
4. P. B. Nagy, D. V. Rypien and L. Adler, "Ultrasonic Attenuation Measurement by Backscattering Analysis, *ibid*, Vol. 6B, pp. 1411-1417 (1987).
5. P. B. Nagy and L. Adler, "Scattering Induced Attenuation of Ultrasonic Backscattering," *ibid*, Vol. 7B, pp. 1263-1271 (1988).
6. T. A. Gray and R. B. Thompson, "Ultrasonic Detection of Cracks in Web Geometries," *ibid*, Vol. 3A, pp. 47-56 (1984).
7. T. A. Gray and R. B. Thompson, "Use of NDE Models to Predict Ultrasonic NDE Reliability," *ibid*, Vol. 5A, pp. 911-918 (1986).
8. J. E. Gubernatis, E. Domany, J. A. Krumhanst and Huberman, "The Born Approximation in the Theory of the Scattering of Elastic Waves by Flaws," *J. Appl. Phys.* 48, 2812 (1977).
9. R. B. Thompson and T. A. Gray, "A model Relating Ultrasonic Scattering Measurements Through Liquid-Solid Interfaces to Unbounded Medium Scattering Amplitudes," *J. Acoust. Soc. Am.* 74, 1279 (1983).
10. F. J. Margetan, T. A. Gray and R. B. Thompson, "A Technique for Quantitatively Measuring Microstructurally Induced Ultrasonic Noise," Review of Progress in Quantitative Nondestructive Evaluation, Vol. 10B, D. O. Thompson and D. E. Chimenti, Eds. (Plenum Press, N.Y., 1991), pp. 1721-1728.
11. R. B. Thompson and E. F. Lopes, "A model for the Effects of Aberrations on Retracted Ultrasonic Fields," *ibid* Vol. 5A, pp. 117-125 (1986).
12. B. P. Newberry and R. B. Thompson, "A Paraxial Theory for the Propagation of Ultrasonic Beams in Anisotropic Solids," *J. Acoust. Soc. Am.*, 85, 2290-2300 (1989).
13. N. Hsu and H. Conrad, "Ultrasonic Wave Velocity Measurements on Titanium-Oxygen Alloys," *Scripta Met.* 5, 905-908 (1971).
14. J. N. Pratt, W. J. Bratina, B. Chalmers, "Internal Friction in Titanium and Titanium-Oxygen Alloys," *Acta Met.* 2, 203-708 (1954).
15. R. B. Thompson, F. J. Margetan, J. H. Rose and N. K. Batra, "Effects of Interstitial Oxygen on the Ultrasonic Properties of Titanium Alloys," Review of Progress in Quantitative Nondestructive Evaluation, D. O. Thompson and D. E. Chimenti, Eds., (Plenum, New York, in press).
16. L. J. Brasche, F. J. Margetan and R. B. Thompson, "Sample Preparation Techniques and Material Property Measurements of Hard Alpha Titanium Samples," *ibid*.
17. F. J. Margetan and C. P. Chiou (unpublished results)
18. Proceeding of the Second Workshop on Nondestructive Evaluation (NDE) of Titanium Alloys, N. K. Batra, H. M. Chaskelis and V. P. Arora, Eds. (Office of Naval Research, Arlington, VA., 1984).

19. F. J. Margetan and R. B. Thompson, "Microstructural Noise in Titanium Alloys and its Influence on the Detectability of Hard-Alpha Inclusions", Review of Progress in Quantitative Nondestructive Evaluation, D. O. Thompson and D. E. Chimenti, Eds. (Plenum Press, New York, in press).
20. R. B. Thompson, F. J. Margetan and K. Han, "Relationship of Microstructure to Backscattered Ultrasonic Noise," *ibid.*
21. J. H. Rose, "Ultrasonic Backscatter from Microstructure", *ibid.*
22. Manufacturing Technology for Premium Quality Titanium Alloys for Gas Turbine Engine Rotating Components, Interim Technical Report No. 4, W. H. Buttrill, G. B. Hunter, E. L. Raymond and C. E. Shamblen, Report R91AEB160, General Electric Aircraft Engines, Engineering Materials Technology Laboratory, 1991.

SPECTROSCOPIC EVALUATION OF ADHESIVE BONDS: LINEAR AND NONLINEAR ANALYSIS

J. D. Achenbach
Northwestern University
Evanston, IL 60208

Executive Summary

The feasibility of obtaining residual adhesive bond strength from ultrasonic test results has been investigated. An analysis has been carried out based on the postulate that adhesive bond deterioration due to cyclic loads and/or infiltration of moisture is localized in thin boundary layers at the adherend - adhesive interfaces. A simple nonlinear mechanical model relating load and deformation parameters has been proposed for the adhesive bond. This model allows an extrapolation to the failure point, and hence a prediction of the residual strength from pre-failure ultrasonic test results.

This year's accomplishments are:

- Characterization of the adhesive bond's nonlinear relation between load and deformation parameters from the higher harmonics of reflected ultrasonic signals.
- Comparison with results obtained from a finite element analysis.
- Analysis for an adhesive layer in a beam configuration that is being used for experimental work.
- Investigation of viscous phenomena in pre-stressed adhesive bonds, and their effects on experimental results.

Background

A. General

It is well known that the strength of an adhesive bond can be seriously deteriorated under in-service conditions. Such deterioration can be a consequence of adverse environmental conditions such as the infiltration of moisture, or of thermal and/or cyclic loading conditions. The as yet largely unanswered challenge to nondestructive ultrasonic methods is to obtain information on the deterioration of adhesive bond strength from ultrasonic test results. A single parameter or a set of parameters should be defined which determine the quality of the adhesive bond, and which can be measured by an ultrasonic technique.

The development of techniques for NDE of adhesive bonded structures is a problem of long-standing importance. A case for a fundamental approach was made at a workshop held at Rockwell International Science Center, Thousand Oaks, CA., in January 1979. This workshop resulted in a program plan to address the needs in NDE in this area, which was subsequently reported by Kelley, Knauss, and Kaelble [1]. The objectives of this plan were to develop a program rationale and strategy, and to determine the existence of reasonable approaches. The plan encompassed the basic elements of an accept/reject methodology based on fracture mechanics, expected developments of valid flaw growth models, stress analysis and nondestructive measurement techniques.

In the years since the 1979 Workshop some progress has been made. Research in the area has concentrated on detecting and characterizing the onset of three failure modes: (1) adhesive failure, (2) cohesive failure and (3) failure due to the presence of a distribution of discrete flaws. Success has been slow, and most success has been achieved in categories (2) and (3). It has proven to be very difficult to obtain information on the adhesive bond strength from ultrasonic (and other) test results.

A fairly comprehensive state-of-the-art review of nondestructive evaluation of adhesive bond quality has been presented by Light and Kwun [2]. A substantial amount of work has been carried out using such ultrasonic techniques as amplitude domain reflection/transmission [3]-[5], spectral domain reflection/transmission [6]-[9], low frequency testing [10], interface waves [11]-[13], Lamb waves [14], the stress-wave factor method [15], horizontally polarized transverse waves [16] and obliquely incident ultrasound [17]-[18]. In these papers it was attempted to correlate the ultrasonic results with the adhesive strength of the bond, where the latter was obtained by a destructive testing method. To the present authors' knowledge it has, however, so far not been possible to define a fundamental adhesive bond parameter that can be measured by an ultrasonic technique. This is not surprising because ultrasonic methods generally yield stiffness and dimensional parameters. In some cases low stiffness and/or a thin bond happen to coincide with low strength, and hence ultrasonic results can be correlated with strength. This is, however, not a generally valid result, and exceptions have been found.

B. Project

In work on this project it has been postulated that failure of an adhesive bond is preceded by nonlinear behavior in thin boundary layers at the interfaces of the adhesive and the adherends. The nonlinear adhesive bond behavior has been represented by a relation between tractions and gross displacement increments across the adhesive layer. Inertia of the adhesive layer was taken into account, and the effect of a nonlinear adhesive response on the reflection and transmission of longitudinal waves was investigated for the case of

normal incidence. A procedure was presented to obtain the nonlinear relation from reflected wave results. As an alternative to a completely nonlinear analysis, the case of prestressing the adhesive layer in the nonlinear range and superimposing a small ultrasonic disturbance has been considered, but the inertia of the adhesive has been neglected for this case. For this case, the propagation of interface waves and horizontally polarized plate waves has been discussed. Finally, for the nonlinear case the generation of higher harmonics has been investigated, and it has been shown that certain nonlinear parameters can be obtained from the spectrum of higher harmonics.

Much of the previous work carried out on this project has been summarized in a number of recently published papers, [19]-[21].

The results as obtained by Sept. 1991 may be summarized as follows:

- Comparison of the results for the Spring Model and the Spring-Mass Model indicates that the effect of inertia cannot be ignored when the mass density of the adhesive is comparable to that of the adherends.
- For normal incidence of a longitudinal or transverse signal, the nonlinear relation between tractions and gross displacement increments can be obtained from the reflected signals.
- For a pre-stressed bond, interface waves and antiplane transverse waves provide a useful method to determine the slopes of the nonlinear $Q(\Delta)$ relation between interface stresses and displacement discontinuities. By varying the pre-stress, the load at which the slope becomes zero can be obtained by extrapolation.
- A nonlinear bond generates higher harmonics in the reflected signal, which yield the linear and nonlinear parameters of the $Q(\Delta)$ curve.

Objective and Scope

The objective of this work is to explore the feasibility of a nondestructive technique to assess the adhesive bond strength of adhesive layers by analyzing the nonlinear behavior that accompanies adhesive deterioration in thin boundary layers at the adherend-adhesive interfaces. The work on this project is analytical in nature. The analytical studies are, however, related to experimental studies that are carried out by L. Adler and S. I. Rokhlin, both of Ohio State University.

In earlier work on this project new ideas on adhesive failure have been developed, which take account of the nonlinear behavior that are thought to accompany deterioration of an adhesive bond. A set of simple nonlinear relations has been derived which relates tractions and gross displacement increments across an adhesive layer. Efforts to bring out this nonlinear behavior in an unambiguous manner are in progress. The sources of the nonlinear behavior are also being investigated.

The strength of the approach is its direct relation to residual strength of an adhesive bond. The major difficulty so far has been that nonlinear effects are very difficult to measure when they are expected to be generated by externally applied load. Recent experimental work has, however, indicated that deterioration due to cyclic loading (Adler) or due to environmental effects (Rokhlin) produces the same general kind of bond-stiffness

decay that is associated with our theoretical work, and that these effects are quite easy to observe. Hence, applications are becoming realistic as the experimental work of Adler and Rokhlin reaches the point of technology transfer.

Approach

The uniqueness of the approach of this work is its focus on detection and characterization of residual adhesive strength. It is recognized that the deterioration of adhesive strength depends on what happens in thin layers at the interfaces of adherends and adhesives. In this work adhesive-bond damage mechanisms are modeled and their relations to reflection and transmission of ultrasonic signals are analyzed.

A typical thickness of an adhesive layer is 100 μm . Since the dominant wavelength of a pulse of ultrasonic wave motion can be chosen sufficiently larger than 100 μm , it may be assumed that the strains in the adhesive layer are homogeneous. The mechanical behavior of the adhesive can then effectively be modeled by one-dimensional elements (non-linear springs) which relate the tractions on the faces of the adherends to the displacement discontinuities across the thickness of the adhesive. Here we consider a spring model, as discussed in Ref. [20], but we do not neglect the effect of inertia of the adhesive layer.

Let us consider the one-dimensional configuration of two semi-infinite linear elastic solids joined by a thin nonlinear adhesive material, as shown in Figure 1. An ultrasonic pulse of longitudinal wave motion propagating in the y-direction is transmitted and reflected by the adhesive layer. For the spring-mass model that is being considered here, the thickness of the layer is shrunk to a surface at $y = 0$, across which the following conditions apply [22]

$$\sigma_y|_{y=0^+} - \sigma_y|_{y=0^-} = \frac{1}{2}\rho h[\ddot{v}|_{y=0^+} + \ddot{v}|_{y=0^-}] \quad (1)$$

$$\sigma_y^0 = \frac{1}{2}[\sigma_y|_{y=0^+} + \sigma_y|_{y=0^-}] \quad (2)$$

$$\Delta = v|_{y=0^+} - v|_{y=0^-} \quad (3)$$

where ρ is the mass density of the adhesive layer, h is the actual thickness of the layer, σ_y is the normal stress and v is the displacement in the y-direction. To account for the separate contributions from the boundary layers and the interior of the adhesive layer, we write

$$\Delta = 2\Delta^{\text{BL}} + \Delta^{\text{IL}}, \quad (4)$$

where $2\Delta^{\text{BL}}$ are the contributions from the boundary layers and Δ^{IL} is the contributions from the interior of the adhesive layer. We may then assume general relations between Δ^{BL} and σ_y^0 and Δ^{IL} and σ_y^0 of the forms:

$$\Delta^{\text{BL}} = \Delta^{\text{BL}}(\sigma_y^0) \quad \text{and} \quad \Delta^{\text{IL}} = \Delta^{\text{IL}}(\sigma_y^0) \quad (5a, b)$$

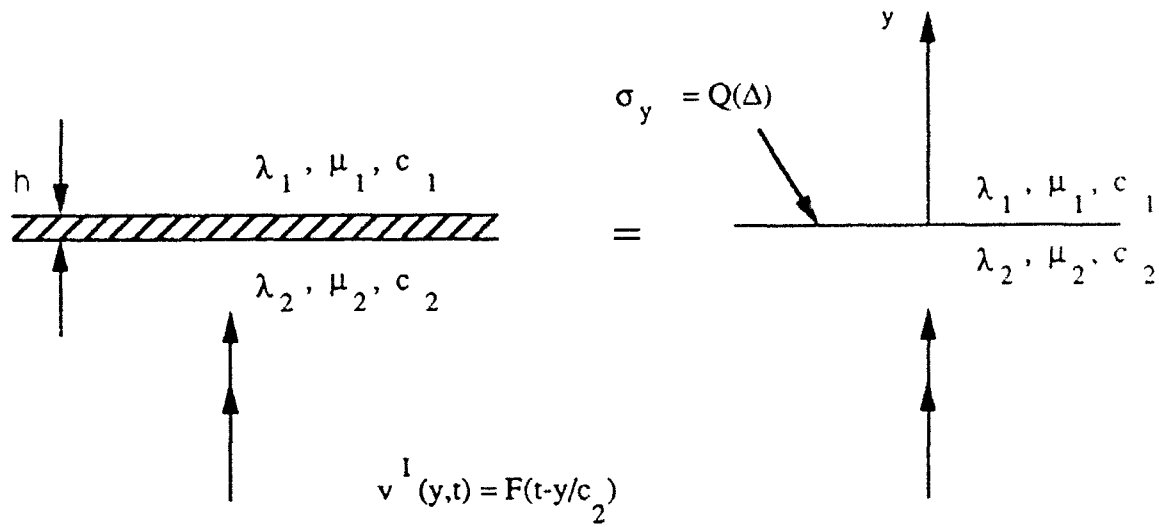


Figure 1 Pulse of longitudinal wave motion incident on adhesive bond.

It follows that

$$\Delta = 2\Delta^{BL}(\sigma_y^o) + \Delta^{IL}(\sigma_y^o) \quad (6)$$

Both functions $\Delta^{BL}(\sigma_y^o)$ and $\Delta^{IL}(\sigma_y^o)$ may be nonlinear. It is, however, assumed that the mechanical behavior of the bulk adhesive is known, i.e., $\Delta^{IL}(\sigma_y^o)$ is a known function.

Equation (6) can be inverted, to yield

$$\sigma_y^o = Q(\Delta) \quad (7)$$

The adhesive layer function $Q(\Delta)$ describes a nonlinear elastic relation between σ_y^o and Δ . Since Eq. (7) is an elastic relation, it will not be valid for a viscoelastic adhesive. The general behavior of $Q(\Delta)$ is shown in Figure 2. Clearly there is a critical value of Δ beyond which the average stress in the adhesive layer decreases with increasing Δ . The values of $Q(\Delta_{cr})$ and Δ_{cr} define the failure point of the adhesive. We are interested in obtaining these critical values of the adhesive bond from the ultrasonic wave reflection and transmission data.

Since the resistance to tension is generally smaller than to compression, we consider $Q(\Delta)$ of the form

$$Q(\Delta) = a\Delta e^{-b\Delta}, \quad (8)$$

For the numerical solution, it is convenient to introduce the following dimensionless variables

$$\bar{\Delta} = \frac{\Delta}{h}, \bar{t} = \frac{t}{(h/c_1)}, \bar{F} = \frac{F}{h}, \quad (9)$$

where h is the actual thickness of the adhesive layer. The adhesive is characterized by

$$\bar{a} = \frac{ah}{\rho_1 c_1^2}, \quad \bar{b} = bh \quad (10)$$

For $\bar{a} = 1.0$ and $\bar{b} = 1.5$ the dimensionless form of $Q(\Delta)$, defined by Eq. (8), is shown in Figure 2.

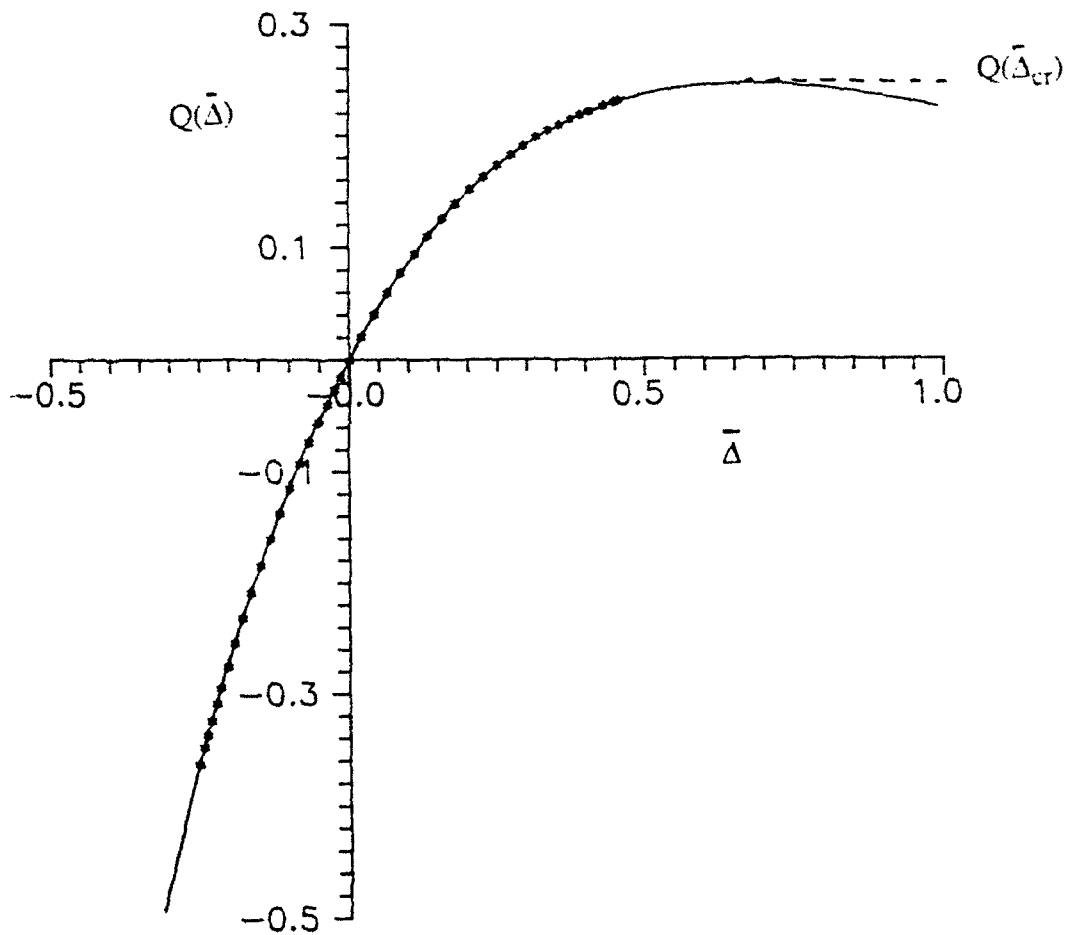


Figure 2 Relation between tractions across the adhesive layer and displacement discontinuity.

Particular attention has also been devoted to the case that the adhesive layer is prestressed in the nonlinear range and a small ultrasonic disturbance is superimposed. The resulting problem statement is a linear one, but with parameters that depend on the state of prestress. For this case the propagation of interface waves and horizontally polarized plate waves has been discussed. Also for the nonlinear case the generation of higher harmonics has been investigated, and it has been shown that certain nonlinear parameters can be obtained from the spectrum of higher harmonics [21].

Technical Progress

The usefulness of harmonic generation to study nonlinear mechanical properties of solids is well recognized [23]. In work on this project it has been shown that analyzing the reflected wave in the frequency domain, by taking the Fourier transform of the reflected wave and separating out the various harmonics, is a good approach to determine the parameters of the $Q(\Delta)$ vs. Δ curve.

For the configuration shown in Figure 1, consider as an example, an incident wave of the form

$$F(t) = \frac{1}{2} A [1 - \cos(2\pi t/t_0)], 0 \leq t \leq T_0. \quad (11)$$

The ratio of the mechanical impedances of the adherends is taken as $\rho_2 c_2 / \rho_1 c_1 = 1.5$, and the mass density of the adhesive as $\rho = 0.5 \rho_1$. Also $\bar{a} = 1.0$ and $\bar{b} = 1.5$.

The incident wave is defined by the dimensionless constants

$$\frac{A}{h} = 0.5, \quad \frac{t_0}{(h/c_1)} = 10.0, \quad \frac{T_0}{(h/c_1)} = 500.0 \quad (12)$$

Figure 3 shows the normalized reflected wave \bar{G} , which was obtained by using the analysis of Ref. [21], versus the dimensionless time \bar{t} . Figure 4 shows the discrete spectrum decomposition of the reflected wave of Figure 3 into the fundamental frequency and the higher harmonics [24]. The decomposition was obtained using the Fast Fourier Transform (FFT). It can be seen that the amplitude of the second harmonic is quite significant.

In work during the past completed period, a study of the effect of nonlinear viscoelastic behavior of adhesive layers has been completed. The adhesive bond was assumed to display the simplest nonlinearly viscoelastic behavior in shear, which is of the form

$$\sigma_{yx} = f(\epsilon_{yx}) + \kappa \dot{\epsilon}_{yx} \quad (13)$$

where $f(\epsilon_{yx})$ is some nonlinear function of ϵ_{yx} . An analysis has been carried out related to the measurement of $f(\epsilon_{yx})$ and κ by an ultrasonic technique. The configuration consists of two metal strips which are adhered to each other by a thin layer of adhesive material. The approach that has been explored involves pre-loading the adhesive layer into the nonlinear range by a low-frequency excitation and then superimposing a small amplitude

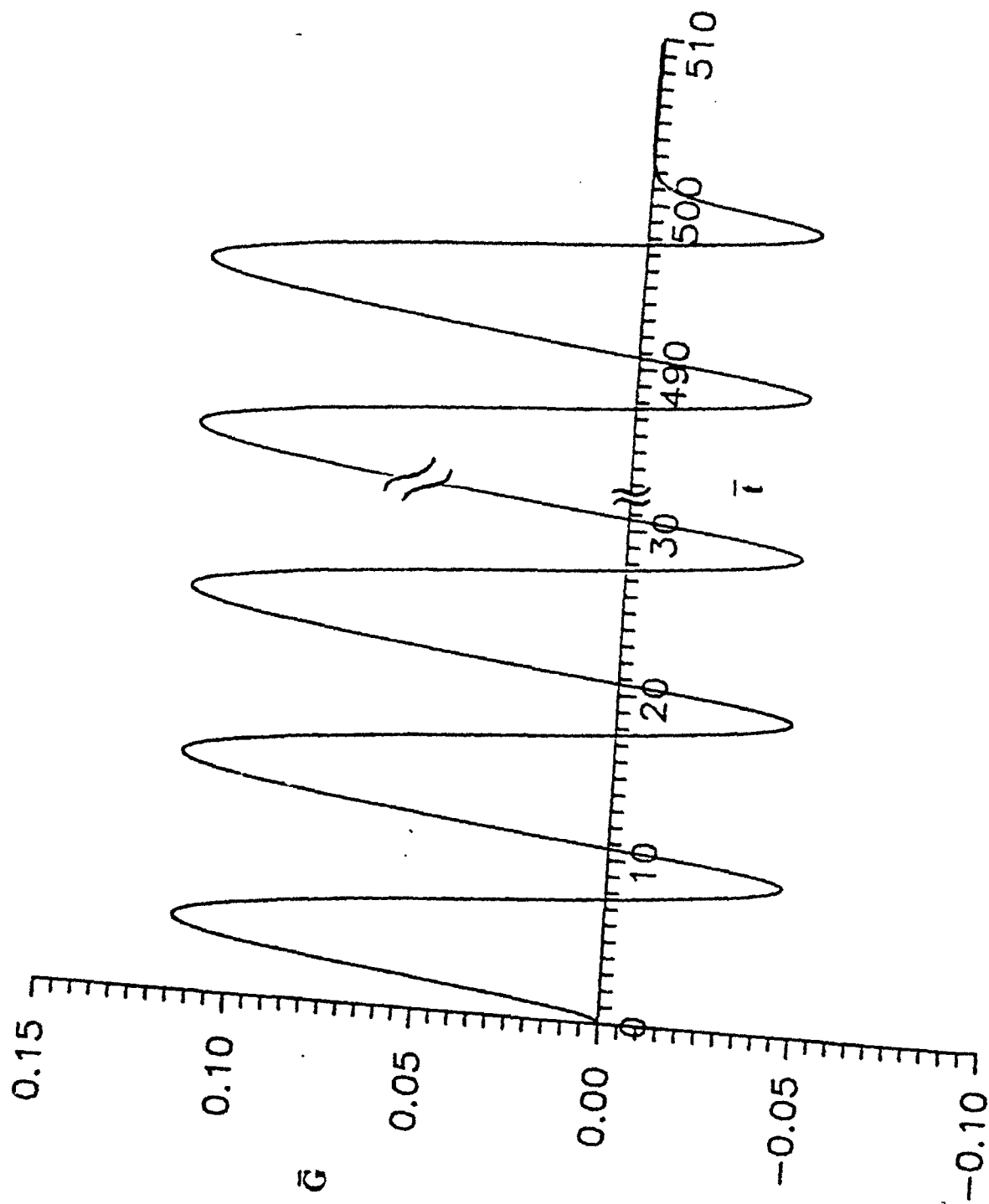


Figure 3 Normalized reflected wave versus dimensionless time for $\rho / \rho_1 = 0.5$.

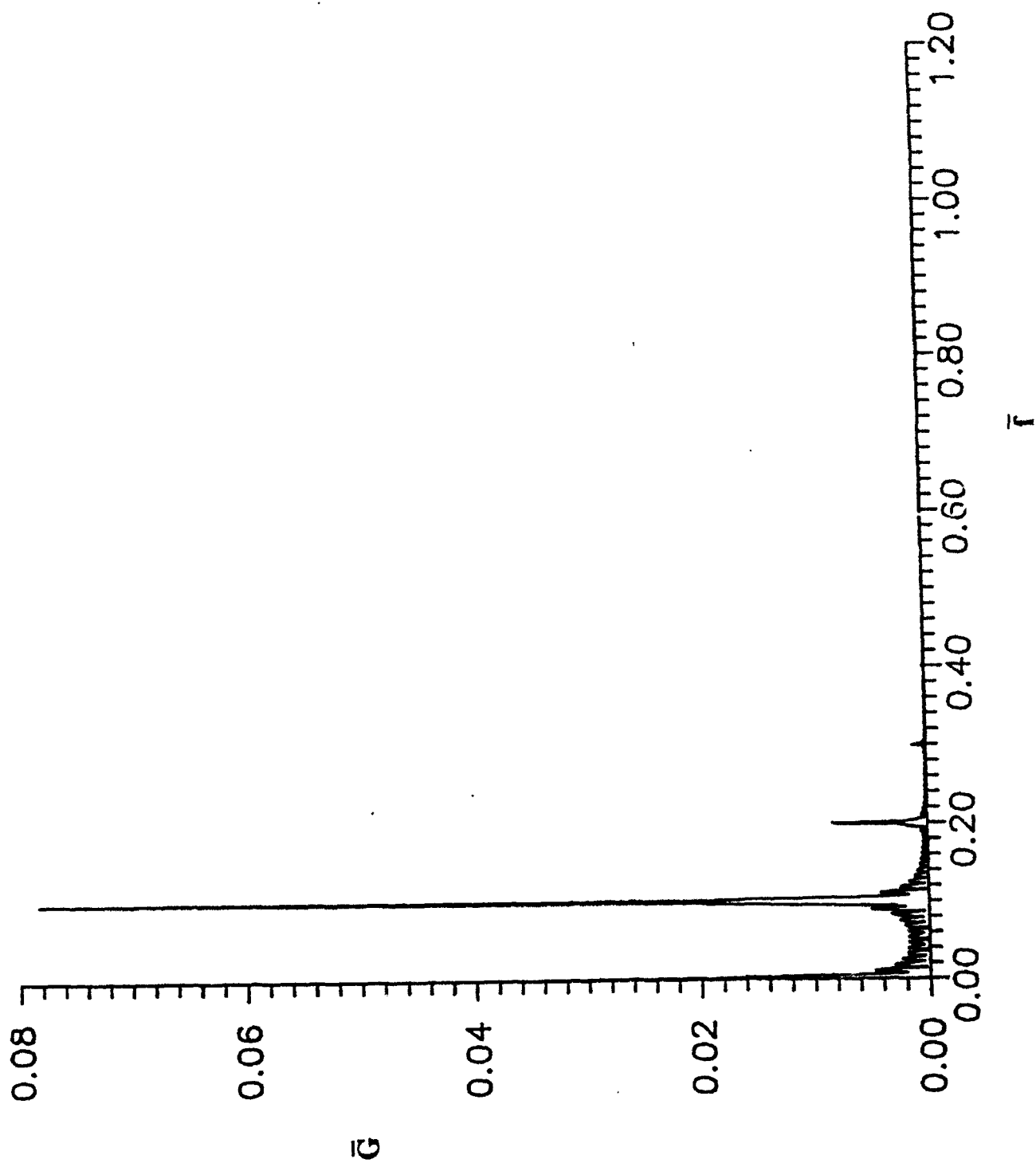


Figure 4 Normalized amplitude of the fundamental frequency and the harmonics of the reflected wave.

ultrasonic disturbance to probe the nonlinear behavior near specified strain levels. Ultrasonic reflection and transmission from the adhesive layer have been analyzed. The resonance separation and resonance depth have been computed for specific cases. A method has been investigated to reconstruct the nonlinear stress-strain behavior from the ultrasonic data.

As an example we have considered

$$f(\epsilon_{yx}) = \alpha \epsilon_{yx} - \beta \epsilon_{yx}^3 \quad (14)$$

The form of the relation between σ_{yx} and ϵ_{yx} given by Eqs. (1) and (2) has been numerically tested by considering a stress of the form

$$\sigma_{yx} = \sigma_0 \sin\left(\frac{2\pi t}{t_0}\right) \quad (15)$$

Substitution of Eqs. (14) and (15) in Eq. (13), gives a first order nonlinear ordinary differential equation for ϵ_{yx} . Solving for ϵ_{yx} and plotting σ_{yx} vs. ϵ_{yx} , shows that for a low frequency large amplitude loading, the viscoelastic effect governed by $\kappa \dot{\epsilon}_{yx}$ can be ignored. On the other hand the results also show that a high frequency small amplitude loading, the viscoelastic behavior can not be ignored, but now the adhesive is being pulled only a linear range and consequently the nonlinearity governed by $\beta \epsilon_{yx}^3$ can be ignored. From the above results we conclude that for the low frequency prestressing, the adhesive layer behavior is of the form

$$\sigma_{yx} = f(\epsilon_{yx}) = \alpha \epsilon_{yx} - \beta \epsilon_{yx}^3 \quad (16)$$

while for a small superimposed deformation we have

$$\sigma_{yx} = S_1 \epsilon_{yx} + \kappa \dot{\epsilon}_{yx} \quad (17)$$

where

$$S_1 = [df(\epsilon_{yx})/d\epsilon_{yx}]_p = \alpha - 3\beta(\epsilon_{yx})_p^2 \quad (18)$$

In Eq. (18), $(\epsilon_{yx})_p$ is the low-frequency pre-strain.

For the small ultrasonic signal superimposed on the pre-strained bond the mechanical behavior in the adhesive layer is thus governed by Eq. (17). For such an adhesive layer the reflection coefficient has been calculated. The reflection coefficient vs. the frequency is an oscillatory curve with a decaying amplitude. The spacing of the minima is not much affected by the viscosity coefficient κ , and can be used to obtain the wave speed and hence $df/d\epsilon_{yx}$ as a function of the pre-stress in the nonlinear range. The viscosity parameter κ is obtained from the change of the resonance depth (a quantity originally defined in a paper by Alers et al. [4]).

Once

$$S_1 = \frac{df}{d\epsilon_{yx}} \quad (19)$$

is known at a number of points (i.e., at a number of values of the prestrain), the function $f(\epsilon_{yx})$ can be obtained by numerical integration.

The results were presented in Ref. [25]. Figure 5 shows the reflection coefficient R vs. the dimensionless frequency $\bar{\omega}$ for three different values of the dimensionless viscoelastic parameter \bar{K}_m , where $K_m = \kappa$. As shown in the figure the positions of frequency minima $\bar{\omega}_{FM}$ are not influenced much by \bar{K}_m . They can be related to the dimensionless local slope $\bar{\alpha}'$, where $\alpha' = S_1$, using the relation

$$\bar{\omega}_{FM} = n\pi(\bar{\alpha}'/\bar{\rho})^{1/2} \quad (20)$$

Here $n = 1$ defines the first minimum, $n = 2$ the second minimum and so on. On the other hand, as shown in Figure 5, the resonance depth which was originally defined by Alers et al. [4] depends on both the elastic and the viscoelastic parameters. For a fixed value of $\bar{\alpha}'$, Figure 6 shows the resonance depth as a function of the viscoelastic parameter \bar{K}_m . Thus, analysis of the reflected signal yields the local slope of the elastic part as well as the viscoelastic parameter. By repeating this procedure for various values of prestress or induced damage, and using numerical integration, the stress-strain behavior of the adhesive layer can be reconstructed, as discussed in some detail in Ref. [25].

Summary

In summary, considerable progress has been achieved in our understanding of how nonlinear behavior in thin boundary layers of an adhesive bond can be observed in ultrasonic tests. The work of Rokhlin and Adler (this report) appears to show that deterioration due to moisture infiltration or fatigue processes is quite pronounced. It is, however, not yet completely clear how information on nonlinear effects can be employed to draw conclusions on the residual strength of adhesive bonds. To determine residual strength further study on the origins of nonlinear effects will be required, particularly with regards to the development of small disbonds, due to moisture infiltration or cyclic loading. A suitable model which relates stress and deformation in an adhesive bond containing disbonds in the adhesive/adherend interfaces should remove this limitation. It is expected that significant progress in that direction will be achieved during the next project period.

Plans for Next Year

The first question that will require further investigation is the origin of the nonlinear behavior. In earlier work it has been assumed that nonlinearity is inherent in adhesive bonding. It has, however, been suggested that a major source may be the development of small disbonds.

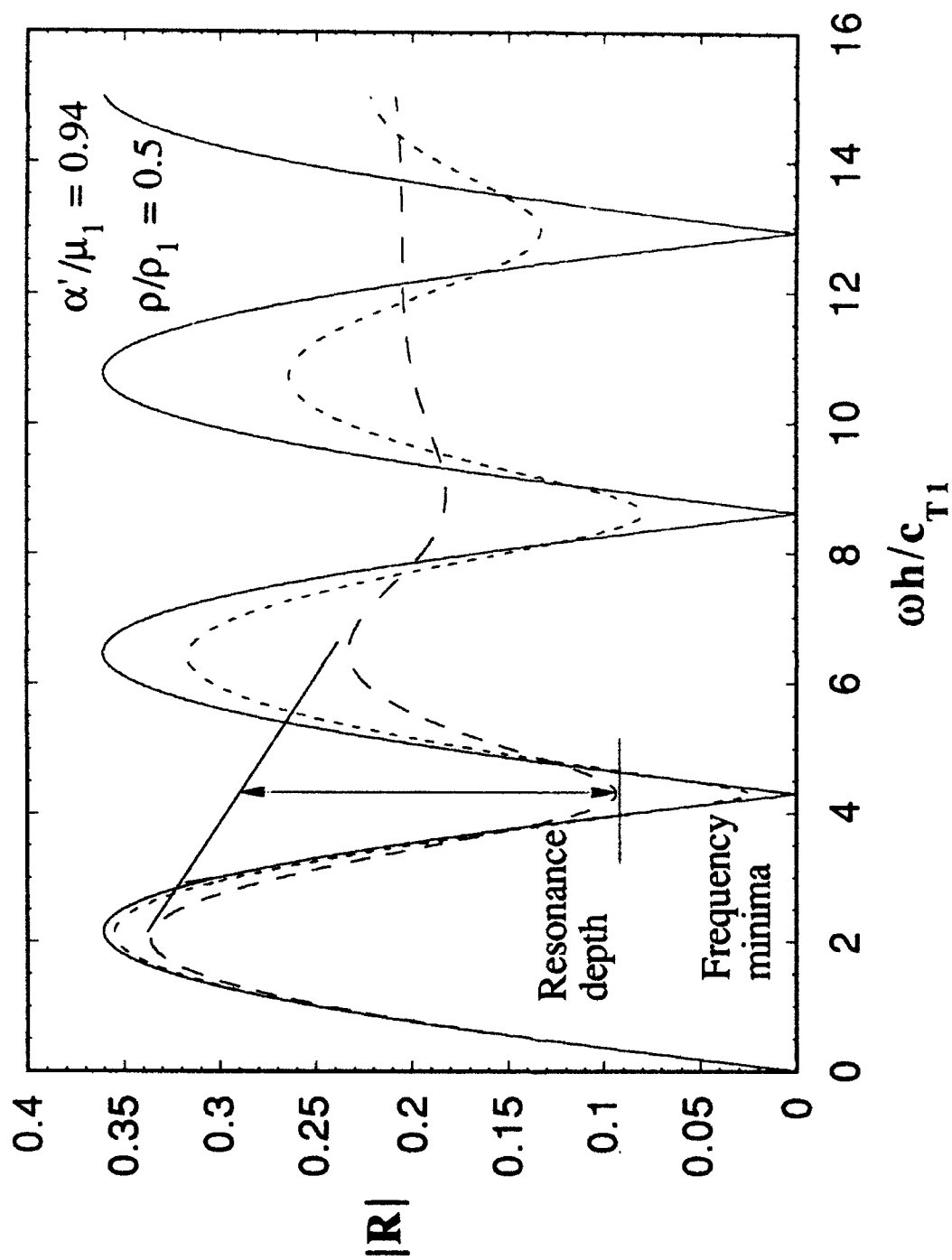


Figure 5 Reflection coefficient as a function of frequency.

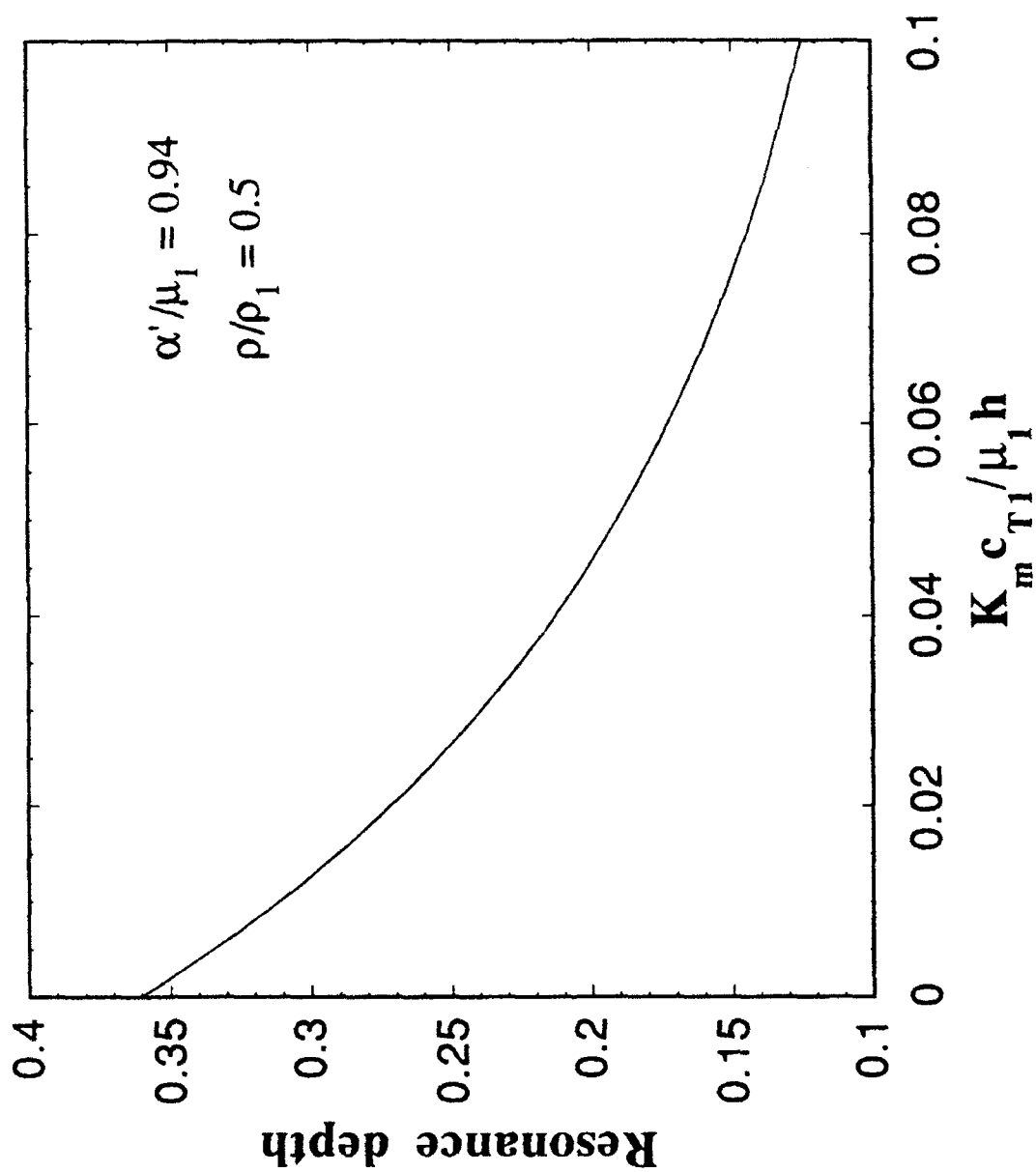


Figure 6 Resonance depth as a function of the viscoelastic parameter.

Recent results obtained by Rokhlin (this report) show that deterioration of an adhesive bond due to microcrack formation caused by moisture infiltration can be characterized by measurements of the reflection coefficient. During the first stage of moisture infiltration the amplitude of the reflected waves decays, but the frequency minima do not shift. However, during the subsequent process of bond deterioration not only does the amplitude decay further, but the minima also show considerable and easily measurable shifts.

It is very interesting that this behavior observed by Rokhlin is consistent with the nonlinear model that was studied on the present project, as discussed in Section 6, see Eqs. (13) and (14), but where the function $f(\epsilon_{yx})$ now also depends on a parameter, say γ , which represents the density of microcracks. The frequency shift is consistent with the variation of α with γ and with the presence of the nonlinear term in Eq. (14), while the amplitude decay is consistent with the viscous term in Eq. (13). An intuitive explanation is as follows. As more and more microcracks are formed due to moisture infiltration, α decreases. These microcracks may retain some frictional contact, which is however overcome as the stress increases, hence the appearance of both the nonlinear term and the viscous term.

It is proposed to consider a bond represented by the spring layer model. At discrete locations the springs will be replaced by frictional contacts simulating the development of microcracks. It is possible to introduce statistical concepts in the size distribution of these microcracks. An averaging procedure will yield the effective stress-strain behavior, and hence the parameters for the deterioration adhesive bond. The experimental results of Stan Rokhlin will provide guidance for this modeling effort, which is basically a reinterpretation of previous results.

References

1. F. N. Kelley, W. G. Knauss and D. H. Kaelble, in Proceedings of the DARPA/AFML Review of Progress in Quantitative NDE, Rockwell, Int. Science Center, 1980.
2. G. M. Light and H. Kwun, Nondestructive Evaluation of Adhesive Bond Quality, Nondestructive Testing Information Analysis Center, Southwest Research Institute, San Antonio, Texas, (1989).
3. P. A. Meyer and J. L. Rose, Journal of Adhesion, **8**, 145-153 (1976).
4. G. Alers, P. L. Flynn and J. J. Buckley, Materials Evaluation, **35**, No. 4, 77-84 (1977).
5. J. L. Rose, M. J. Avioli and R. Bilgram, British Journal of Nondestructive Testing, 67-71 (1983).
6. F. H. Chang, J. C. Couchman, J. R. Bell and D. E. Gordon in: Proceedings of the 10th Symposium on NDE, San Antonio, (1975).
7. J. W. Raisch and J. L. Rose, Materials Evaluation, **37**, No. 6, 55-64 (1979).
8. G. A. Alers and R. K. Elsley, in: 1977 Ultrasonics Symposium Proceedings, IEEE Catalogue No. 77CH1264-ISU, New York, (1977).
9. G. H. Thomas and J. L. Rose, Journal of Adhesion, **10**, 293-316 (1980).
10. D. O. Thompson, R. B. Thompson and G. A. Alers, Materials Evaluation, **32**, No. 4, 81-85 (1974).
11. S. Rokhlin, Journal of Acoustical Society of America, **67**, No. 4, 1157-1165 (1980).
12. A. Pilarski, Materials Evaluation, **43**, 765-770 (1985).
13. S. I. Rokhlin, M. Hefets and M. Rosen, Journal of Applied Physics, **52**, No. 4, 2847-2851 (1981).
14. S. I. Rokhlin, M. Hefets and M. Rosen, Journal of Applied Physics, **51**, No. 7, 3579-3582 (1980).

15. H.L.M. D. Rois, L. A. Bergman and J. H. Bucksbee, Journal of Nondestructive Testing, 357-358 (1986).
16. C. H. Yew, Journal of Acoustical Society of America, 76, No. 2, 525-531, (1984).
17. S. I. Rokhlin and D. Marom, Journal of Acoustical Society of America, 80, No. 2, 585-590 (1986).
18. A. Pilarski and J. L. Rose, Journal of Applied Physics, 63, No. 2, 300-307 (1988).
19. J. D. Achenbach, O. K. Parikh and Y. C. Lu, in: Annual Review of Quantitative Nondestructive Evaluation, Vol. 9B, 1693-1700, Plenum Press, New York (1990).
20. P. B. Nagy and L. Adler, in: Elastic Waves and Ultrasonic Nondestructive Evaluation, North-Holland Publ. Co., 229-239 (1990).
21. J. D. Achenbach and O. K. Parikh, J. Adhesion Sc. Technol., 5, No. 8, 601-618 (1991).
22. J. M. Baik and R. B. Thompson, Journal of Nondestructive Evaluation, 4, Nos. 3/4, 177-196 (1984).
23. M. A. Breazeale and D. O. Thompson, in: Applied Physics Letters, 3, 77 (1963).
24. R. B. Randall, Frequency Analysis, Bruel and Kjaer Publishers, Denmark, (1987).
25. O. K. Parikh and J. D. Achenbach, in Annual Review of Quantitative Nondestructive Evaluation, 11, in press.

SPECTROSCOPIC EVALUATION OF ADHESIVE BONDS: LINEAR AND NONLINEAR METHODS

Laszlo Adler
The Ohio State University

Executive Summary

The objective of this work is to demonstrate feasibility of nondestructive evaluation of joint quality in adhesively bonded structures. The approach is to introduce new ultrasonic techniques to measure strength related parameters in the adhesive joint. Since previous results indicate that problems such as gross defects, porosity, excessive adhesive thickness, improper solidification are detectable by either bulk waves or Lamb waves, we concentrated our strength evaluation on (apparently) flawless adhesive joints. This year's accomplishments are summarized below.

- Developed a new ultrasonic technique to detect intimate mechanical contact between the adhesive and adherend, which occur without actual bond. Such apparently flawless, but defective "kissing" bonds are dangerous because they remain hidden from conventional ultrasonic inspection. Our new technique is called "microscopic" guided wave technique, which uses high frequency focused probe and improved the detectability of such "kissing" bonds significantly.
- Demonstrated that nonlinear ultrasonic measurements can be used to detect failure in a flawless adhesive joint when strength degradation takes place. Specifically, the measured nonlinearity of the adhesive joint is a much more sensitive measure of strength degradation than linear ultrasonic measurements. Our new nonlinear ultrasonic inspection methods have been further developed to study feasibility of direct strength assessment from ultrasonic measurements. Correlation of ultrasonic strength measurements to mechanical strength measurements is in progress.

Background

A. General

Ultrasonic methods have been extensively used for evaluation of the quality of adhesive bonds and were identified as one of the most challenging problems of nondestructive evaluation. A detailed summary of the Air Force-DARPA sponsored research (between 1974-1980) on adhesive bonds is given in a recent review article [1]. The main problem lies in the lack of understanding of the correlation between mechanical parameters, e.g. adhesive thickness, elastic moduli, which are measurable ultrasonically, and overall joint quality characterized by tensile, shear or peel strength, fracture toughness, creeping, etc. The overwhelming complexity of the relationship between these quantities must be simplified by appropriate models in order to establish a workable procedure for bond quality assessment. Prior to this work, most models developed for bond assessment were linear elastic ones [2,3,4] but it was questionable whether certain joint qualities, like strength, could be approached this way at all. Strength is a nonlinear parameter related to behavior of the material in the region where it produces unproportional effects additional loading. As for the feasibility of the linear approach there was a great abundance of supportive and contradicting evidence as well [2,3,4]. All that evidence indicated that linear elastic measurement should be inherent but not an exclusive part of ultrasonic bond assessment of adhesive joints. In order to obtain correlation between ultrasonic data and strength assessment of the adhesive joint nonlinear ultrasonic measurements are needed to be introduced.

B. Project

In the past year we have progressed in several areas in the development of new ultrasonic spectroscopic methods, both linear and nonlinear to evaluate the quality of adhesive bonds. To follow up on our main objective we have concentrated our research efforts on the crucial problem of apparently "flawless" adhesive joints with reduced interfacial strength. The category of so called "flawless" joints may include 1) defective joints with hidden flaws and 2) actually flawless joints. The boundary between these two subclasses of flawless joints is not well defined and greatly depends on the inspection technique used to find possible defects. For example, certain types of defects may be undetectable with bulk waves, but easily detected by interface waves: porosity, uneven adhesive layer etc.

For a linear ultrasonic method, we have developed a flexible imaging technique suitable for either leaky Lamb waves [5] or for our new novel technique of leaky guided interface waves in order to detect most types of defects, such as porosity, lack of adhesion, excessive bond line, etc. Leaky guided interface waves in the adhesive layer were studied the first time by both theoretical and experimental means. We determined the ultrasonic transmission coefficients of both longitudinal and transverse waves as function of frequency at oblique incidence and identified the spectral maximum as guided interface modes at a given phase velocity. We determined the dispersive properties of the lowest order modes over a wide phase velocity range above the phase velocity of the substrate by changing the angle of incidence. These leaky guided interface waves are useful in nondestructive evaluation of adhesive joints. We showed that such waves can be excited and detected by the same single technique used for leaky Lamb wave transmission with the addition of time gating. We also showed that leaky Lamb wave inspection of the adhesive joint is mainly sensitive to the property of the adherend plates and much less to those of the adhesive layer and the interface between them. Due to the usually rather weak acoustical coupling through the adhesive layer only the amplitudes of certain Lamb modes and not their frequencies are really affected by bond defects. Leaky guided interface waves are more sensitive to both adhesive and cohesive type of defects and the results are easier to evaluate. In addition to

leaky guided interface waves, we have developed both experimental and theoretical work for true guided interface waves. These interface waves are directly generated in the adhesive layer by a shear transducer with either vertical or horizontal polarization relative to the adhesive layer.

We have introduced for the first time a measurement technique for acoustical nonlinearities in adhesively bonded structures in order to study feasibility of strength related ultrasonic measurements [6,7]. Before this work, nonlinear ultrasonic measurements were developed only to obtain third order elastic constants from harmonic generation of finite amplitude waves and/or from acousto-elastic technique for bulk materials only. A new nonlinear inspection technique was introduced based on the dynamic acousto-elastic effect and was shown to be sensitive enough to measure both first order and second order nonlinearities at load levels of less than 3% of the ultimate strength. Possible strength related components of the measured nonlinearity were identified (second order) and separated from the other much stronger effects by polarization and or by harmonic (frequency) analysis. Comparison of destructive (joint) and nondestructive bond strength assessment must take into account the uneven stress distribution in the adhesive sample to obtain reasonable agreement.

Objective and Scope

The main objective of this investigation is to use linear and nonlinear ultrasonic techniques to assess bond quality in adhesive joints and to detect hidden flaws in adhesive joints. This will be achieved by establishing a relationship between measured nonlinearity parameters in the adhesive joints and mechanical strength. Since conventional bulk and Lamb wave techniques have proven to be capable of detecting gross cohesive and adhesive defects, we were focusing our efforts on the crucial problem of apparently flawless joints of reduced strength. This category includes defective joints with hidden flaws, e.g. "kissing" bonds, as well as actually flawless ones. "Kissing" bonds are mechanical contacts between adhesive and adherend without the presence of an actual bond. These joints appear to be flawless for most conventional ultrasonic techniques. Our goal is to develop techniques which can detect them. For the second subclass which includes actually flawless or perfect joints our objective is to correlate the measured ultrasonic parameters (linear and nonlinear) to strength degradation due to fatigue damage and to mechanical strength measurements. The scope of this work is to develop ultrasonic measurements to assess interfacial strength in an adhesive joint of metallic plates. The techniques could also be applied to measure strength in a large variety of materials and joints e.g. composites, thermoplastic joints.

Approach

In this program we are developing a multistep ultrasonic technique for nondestructive evaluation of adhesive joints. First, we introduce linear spectroscopic techniques using various types of guided waves to detect hidden flaws in the adhesive joints. As a second step, nonlinear elastic measurements are introduced to find better correlation between ultrasonic data and strength reduction of apparently flawless joints. In the first category this year, we have addressed the problem of detecting the so called "kissing" bonds, which are intimate mechanical contacts between adhesive and adherend without actual bonds. We have developed a microscopic guided wave technique using a high frequency (50 MHz) focused probes to interrogate a single adhesive-adherend interface without sending the ultrasonic wave through the highly absorbing inhomogeneous adhesive layer. This technique proved to be very sensitive in the detection of very weak "kissing" bond defects in lapjoints, which were not detectable otherwise. The acoustic nonlinearity in a perfectly

bonded adhesive joint is measured by our recently developed dynamic-acoustoelastic technique. The specimens are cyclically loaded in shear-tension or bending configuration and measurements of the nonlinearity parameter, velocity, and attenuation are carried out under various external stresses from 1-2% of the ultimate strength up to failure. New nonlinear elastic models are developed in cooperation with Professor Jan Achenbach in order to correlate experimental data to bond strength. According to this model, the measured nonlinearity parameters allow an extrapolation of the stress-strain curve to the points to adhesive failure. The samples used in this study are Al 2024 plates, which were bonded by FM 300, AF 191, FM-355 and epoxy adhesive of 150 μ thick layer prepared by Northrop Corporation. We are also using adhesive plates in our measurements provided us by Professor Stan Rokhlin at Ohio State University. These samples are prepared for assessment of environmental degradation.

The same computer controlled system, which we developed for ultrasonic measurement it utilized to measure mechanical strength in the standard shear lap adhesive joint sample.

Technical Progress

To follow up our main objective, we have concentrated our research efforts on the crucial problem of apparently flawless adhesive joints of reduced strength. The category of so called "flawless" joints may include 1) defective joints with hidden flaws, and 2) actually flawless joints. For example, certain types of defects may be undetectable with leaky Lamb waves, but are easily detected by leaky interface waves as we have shown earlier. [5] Mechanical contact between adhesive and adherend can easily take place without actual bond. In this effort we have introduced a high frequency guided wave technique, the so called "microscopic" leaky guided waves to improve detectability of such hidden flaws. For adhesive strength assessment of actually flawless joints, we have developed a computer controlled ultrasonic system to measure nonlinearity parameter in the adhesive joint as a function of strength degradation. The same automated system is used to monitor linear ultrasonic parameters, e.g., velocity and attenuation, as well as static moduli and mechanical strength.

Microscopic Guided Wave Technique

In our earlier work we have introduced a technique based on the so called leaky guided interface waves, which are generated in the adhesive layer. [5] We showed that they are much more sensitive to the properties of the adhesive layer than the leaky Lamb waves excited in the sandwich like structure of the adhesive-adherend structure. These guided interface waves are trapped in the regions where all defects are expected to occur; on the other hand Lamb waves are trapped in the whole joint. With all of their advantages however, with guided interface waves hidden adhesive type defects like "kissing" bonds are difficult to detect. These "kissing" bonds occur as a result of plastic contact between smooth or slightly rough surfaces. It is a typical interfacial defect between adhesive and adherend and the cohesive properties of the adhesive material are not affected. To detect these defects, we have introduced a new guided wave technique which generates waves not in the adhesive layer but at the interface of the adhesive-adherend. We call these waves "microscopic" guided waves because of the high frequency focused [frequency range is from 25 MHz to 75 MHz] transducer used to generate these waves on the interface.

A schematic diagram of microscopic guided wave inspection technique is shown in Figure 1. A 50 MHz transducer is focused to the adhesive-adherend interface. Due to the fact that a very high frequency and viewing angle are used to inspect the interface, this technique is limited to one side access because of the inherently high attenuation of the adherend. Six specimens were prepared to test the sensitivity of the suggested microscopic

guided wave technique. The 150mmX150mm, 6mm thick Al 2024 plates were bonded by FM 300K epoxy adhesive applied as a 150 μ thick layer. The adherend surfaces were treated by BR-127 primer according to the specifications (America Cyanamid Co.). Localized "kissing" bonds were generated by five circular spots of 25 mm diameter which were painted with a release agent. Figure 2b shows typical images obtained from the defective side and from the other side of the adhesive bond. There are clear indications of increased reflection at each of the five kissing bonded spots.

Acoustic Nonlinearity Measurements in Adhesive Joints

In order to enhance our ability to inspect the integrity and assess the strength of adhesively bonded structures, we have introduced new techniques to measure the linear and nonlinear behavior of these structures. We have developed a dynamic acousto-elastic technique where the specimen was loaded in shear-tensile configuration as shown in Figure 3. A broadband shear transducer in the MHz region is used to interrogate the bond line at normal incidence. A fatigue machine operating at 10 Hz is used to load the sample. The spectrum analyzer is used as a selective receiver tuned to f_1 and f_2 , frequencies below and above the resonance minimum. The amplitude modulation at these frequencies was

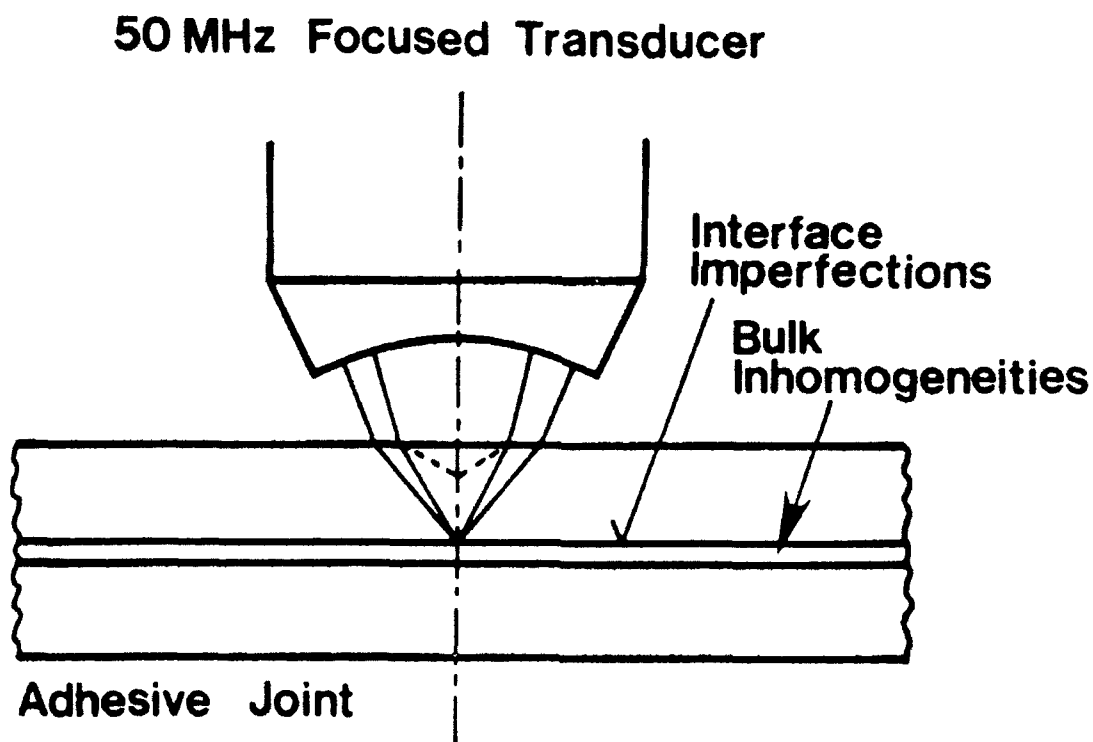
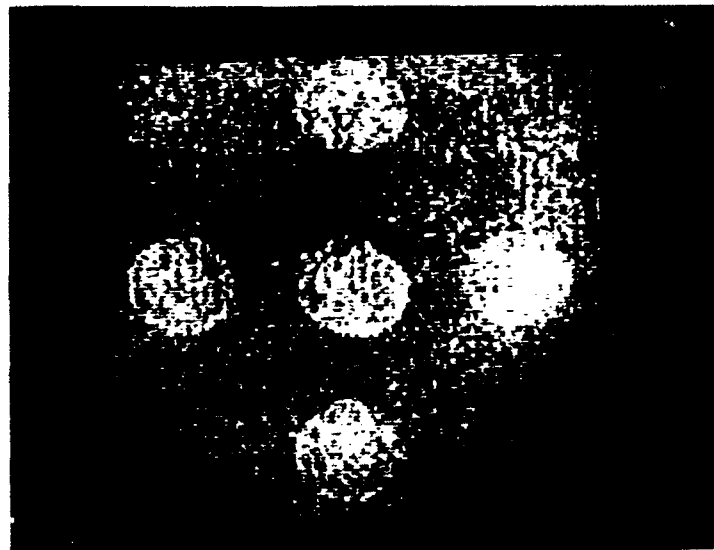


Figure 1 Schematic diagram of the microscopic guided wave inspection technique.

**KISSING BONDS DETECTED BY HIGH-ANGLE
INSPECTION AT 50 MHz
FREKOTED SIDE**



DEFECT-FREE SIDE

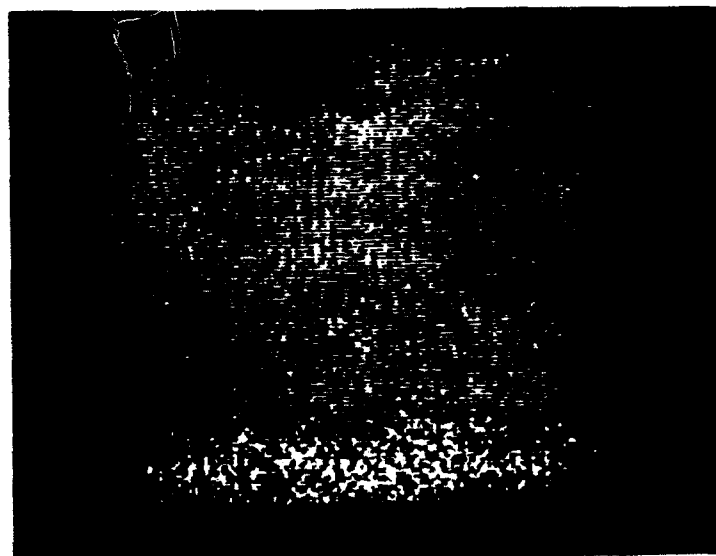


Figure 2 Ultrasonic images from a) the frecoated side and b) the defect free side.

measured by a lock-in-amplifier to the fatigue machine. Both first and second order nonlinearity parameters were obtained from the change of velocity as a function of the first and second harmonic of the external load respectively. We have shown that the second order nonlinearity can be measured at low (less than 3% of the ultimate strength) external load. The question still remains whether this nonlinearity parameter is more strength related than its linear counterparts, e.g. ultrasonic velocity and attenuation? In order to address this question, first, we have developed a control experiment. In Figure 4, a schematic diagram of the experimental arrangement is shown. A viscoelastic bar, which models the adhesive, is rigidly held at one end while the other end is moved by a computer controlled linear scanner in discrete steps. The resulting bending deformation produces an uneven stress distribution in the sample with a strong stress concentration at the rigidly held end where an ultrasonic transducer is used to monitor both linear and nonlinear parameters as a function of reduced strength due to excessive fatigue loading. The measured nonlinearity seems to be much more sensitive to the degradation of strength due to long-term fatigue loads than linear parameters.

One adhesive failure model assumes that the failure in an adhesive joint takes place in a very thin layer near the adhesive adherend interface. This layer, which is typically of the order of a micron or less, is known as Weak Boundary Layer (WBL). We have demonstrated the advantage of using a nonlinearity measurement to detect a region of reduced strength in the WBL. An A polymer bar was cyclically loaded up to several hundreds of cycle, with frequency of 0.1Hz. The second order nonlinearity parameter, as well as linear parameters, e.g. sound velocity, attenuation and static modulus, were measured using the experimental system shown in Figure 5. To obtain the WBL in the polymer, the sample was cut and bonded together with an acrylic cement. On Figure 5 the second order nonlinearity parameter variation is shown as a function of fatigue loading, at 30% of the ultimate, for a weakened and for two solid samples. Notice that both the initial value, as well as the growth rate for the sample with the weak boundary layer is an order of magnitude larger than the solid ones. No significant change of the measured velocity, attenuation, or the static modulus was observed comparing these samples before or after fatigue loading.

The same phenomena is also demonstrated in an actual adhesive lapjoint using an AF 191 adhesive with aluminum plates as the adherend. On Figure 6, the behavior of the normalized second order nonlinearity parameter and the normalized velocity are plotted at 0.8 KSI external load vs. the number of fatigue cycles up to failure. The factor of 10 increase in the nonlinearity parameter vs. the less than 1% variation in the sound velocity clearly demonstrates the superior sensitivity of the former for strength assessment. Correlation between ultrasonic and mechanical strength measurements of the adhesive joint is in progress. Initial data indicates reasonable good agreement between destructive and nondestructive results when the uneven stress distribution in the joint is properly considered.

Summary

In summary we have addressed the problem of ultrasonic strength assessment of an apparently flawless adhesive joint. We have developed a new technique, a so-called microscopic guided wave technique, which is capable of detecting hidden adhesive type flaws, such as a "kissing" bond. These bonds have zero strength. We have further developed our capabilities to measure nonlinear behavior of the adhesive joint under external shear-tensile and bending stresses. We have shown that second order nonlinearity measurements are much more sensitive in the detection of Weak Boundary Layers and strength degradation due to fatiguing than are linear parameters. The feasibility of direct

Dynamic Measurement

$$F = F_0 \sin \Omega t$$

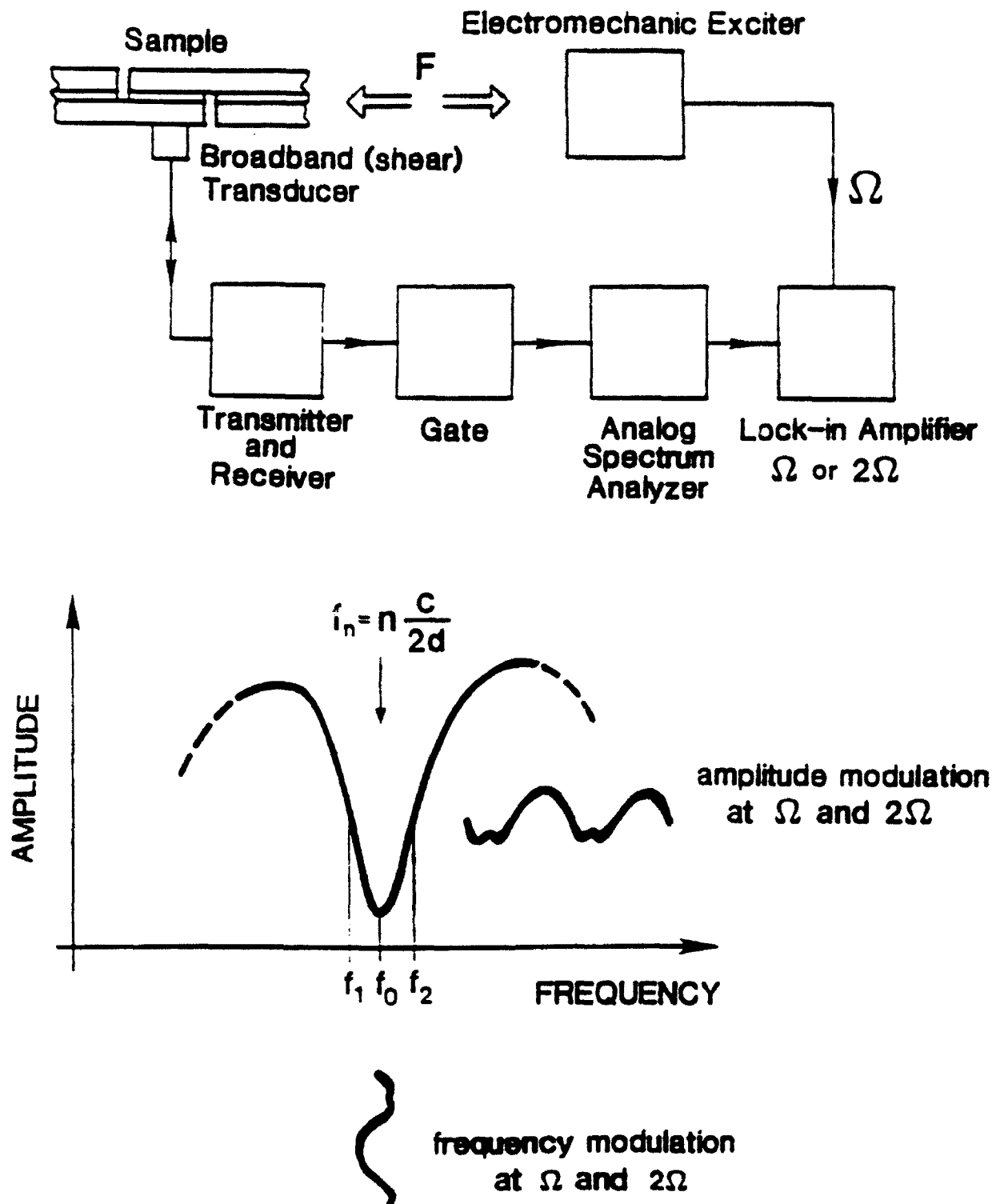


Figure 3 Schematic diagram of dynamic acousto-elastic measurement system.

Experimental Arrangement

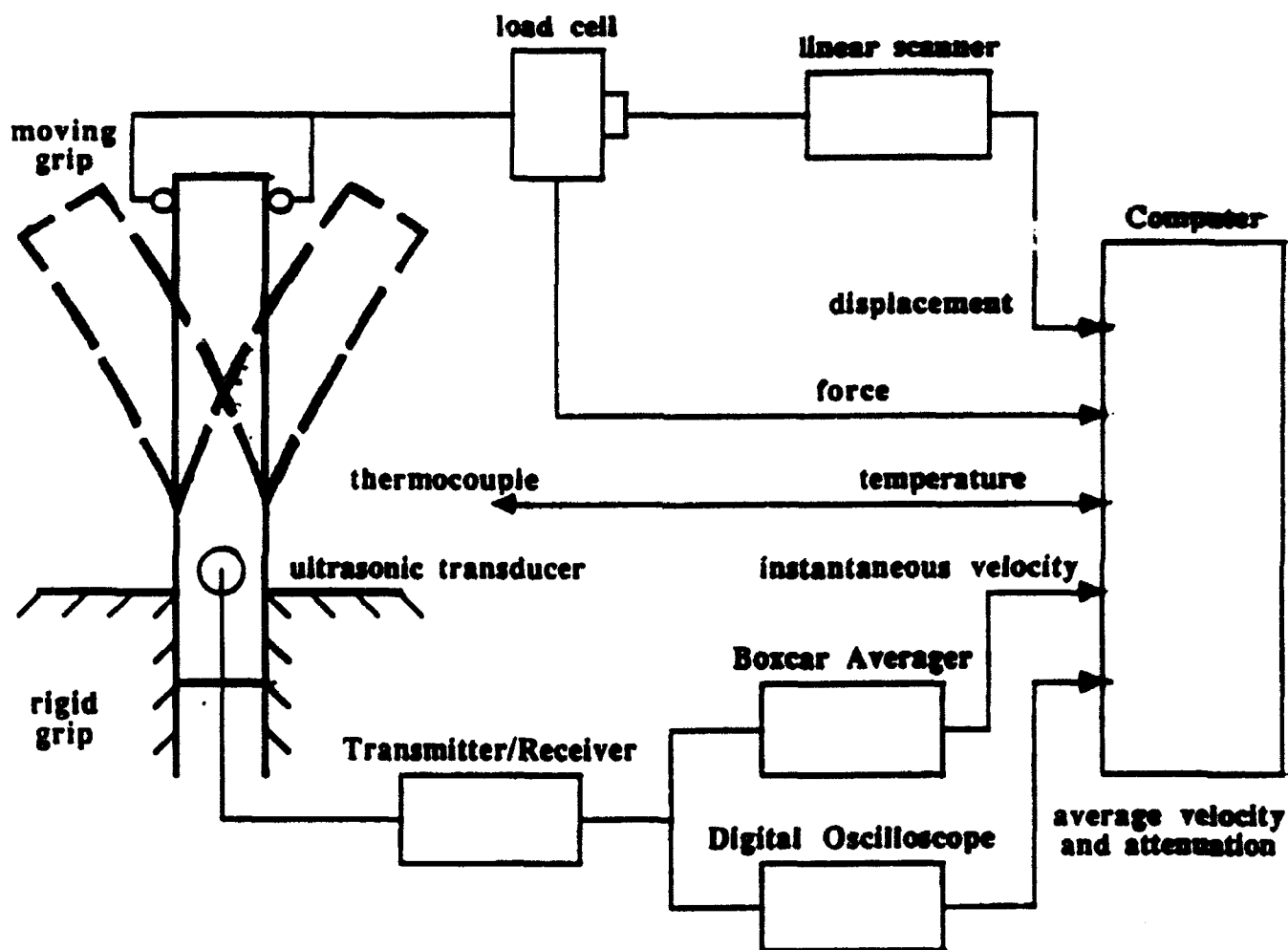


Figure 4 Experimental system to measure linear and nonlinear parameters of materials.

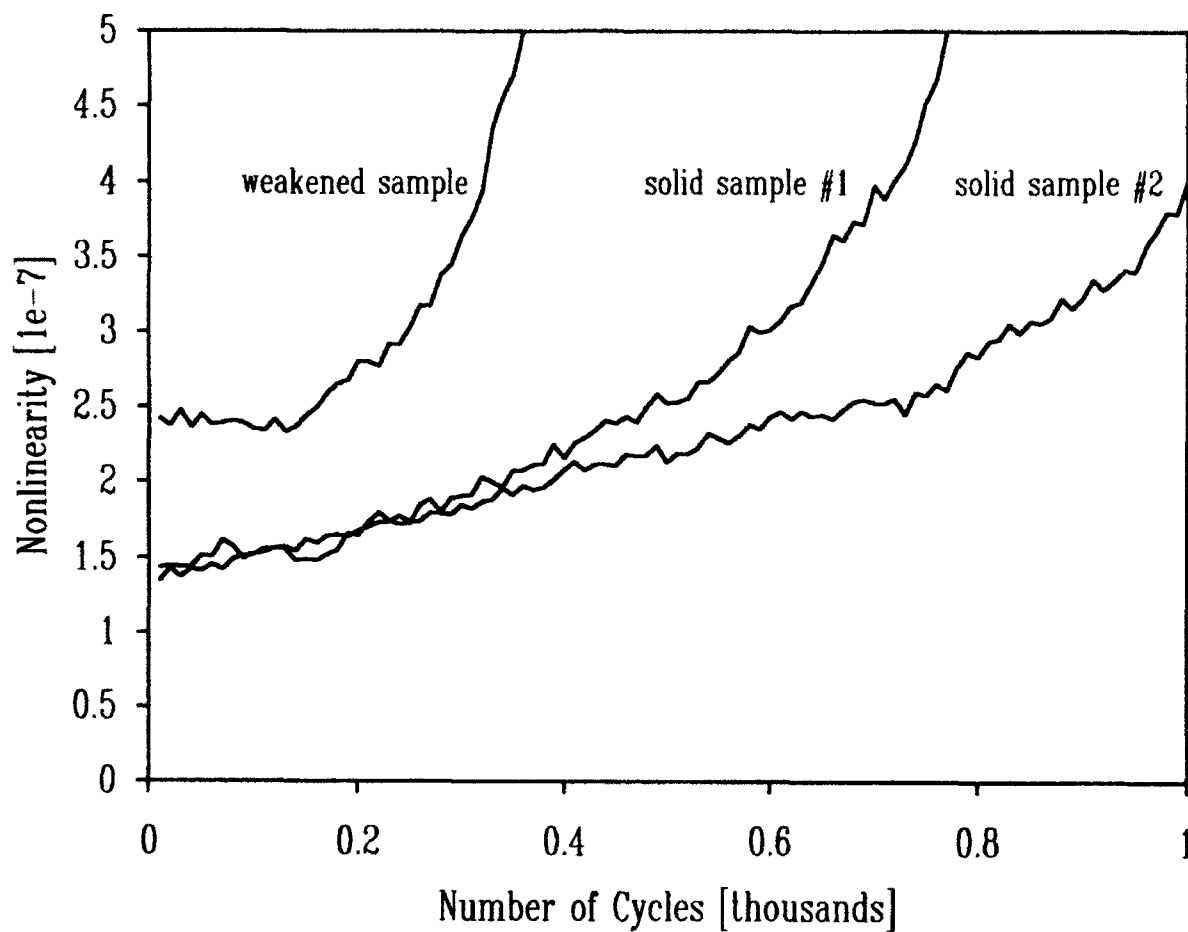


Figure 5 Variation of the second order nonlinearity parameter as function of fatigue cycles up to failure for polymer samples both solid and with WBL.

FATIGUE OF AF-191 ADHESIVE

NORMALIZED PARAMETERS VS CYCLES

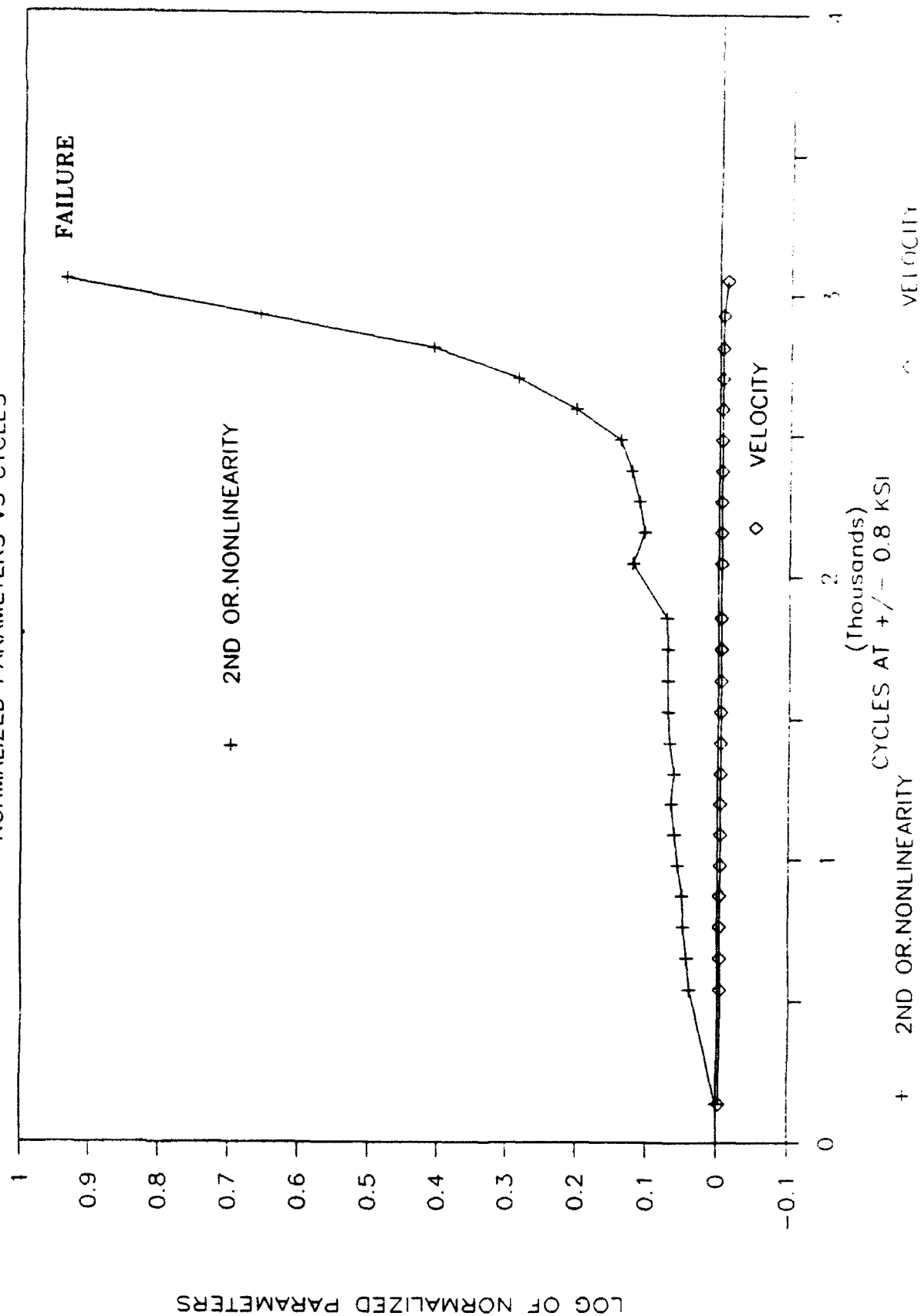


Figure 6 Variation of 2nd order nonlinearity parameter and velocity in adhesive joint as function of fatigue cycles.

ultrasonic strength assessment of the adhesive joint from nonlinearity measurement has been addressed and correlation between ultrasonic data and mechanical strength is in progress. One of the remaining unanswered questions is whether a single measurement, e.g. the measurement of a nonlinearly parameter is sufficient to describe the interfacial strength. Another problem that has to be considered is the strength degradation in a joint due to microvoids in the adhesive layer and at the interface.

Plans for Next Year

Our previous results showed that the relatively high acoustic nonlinearity observed in adhesive joints is mainly due to distributed defects in the adhesive, as well as the adhesive-adherend interface. This effect is directly related to strength reduction caused by microscopic degradation of material integrity. In addition, the adhesive material itself is highly nonlinear and this intrinsic nonlinearity can be used to assess certain material properties (such as the degree of hardening) more sensitively than from conventional linear acoustic measurements.

In order to separate these two different types of nonlinearities in our results, we are going to study the effects of various key parameters on the acoustic nonlinearity.

The acoustic nonlinearity will be measured by our recently developed dynamic acousto-elastic technique. The specimens will be loaded in shear-tensile or shear-torsion configuration up to approximately 30% of their ultimate strength. At these levels, the acousto-elastic effect produces a readily measurable 0.01% change in the ultrasonic velocity. It is well known that in adhesive joints the measured strength might be significantly different for different strain rates and temperatures. Therefore, the effect of these two parameters will be separately investigated by changing the operating frequency and temperature between 10^{-3} and 1 Hz and 30°F and 80°F, respectively. In all other experiments, these two parameters will be kept constant at 0.1 Hz and 70°F. It is expected that these experiments will verify that acoustic nonlinearity is a better indication of adhesive bond quality than any linear parameters such as sound velocity or attenuation.

We have previously demonstrated in different plastic specimens that strength degradation due to cyclic fatigue loading can be best assessed by monitoring the acoustic nonlinearity of the materials. We are going to use the same approach to detect fatigue damage in adhesive joints.

Previously, a propagation delay of the second interface echo was measured as a function of the load to obtain the overall nonlinearity parameter related to the overall integrity of the adhesive layer. We are going to measure the amplitude of the first interface echo as a function of the load to assess a more localized nonlinearity parameter related to the "adhesive" integrity of the adhesive-adherend interface. Although fatigue loading was found to be uniquely well suited to control material strength without affecting other parameters, other processes such as heat damage, exposure to humidity, and imperfect polymerization will be also considered.

Conventional destructive measurements will also be conducted on the adhesive bonds to establish their actual strength. We are going to compare the acoustic nonlinearity parameter to the measured degradation of the bond strength. New models will be developed in collaboration with Prof. Jan Achenbach to correlate experimental data to bond strength. Adhesive samples developed by Prof. Stan Rokhlin will be also used to evaluate the different ultrasonic techniques to measure strength degradation.

References

1. R. B. Thompson and D. O. Thompson, "Past Experiences in the Development of Tests for Adhesive Bond Strength", *J. Adhesion Sci. Technol.*, Vol. 5, 1991.
2. G. F. Curtis, "Nondestructive Testing of Adhesively Bonded Structures with Acoustic Methods", *Ultrasonic Testing*, ed. F. Szilard (John Wiley and Sons, Ltd.), 1982.
3. E. Segal and J. L. Rose, "Nondestructive Testing of Adhesive Bond Joints", *Research Techniques in Nondestructive Testing*, Vol. IV, ed. R. S. Sharpe, (Academic Press, London), 1980.
4. G. M. Light and H. Kwun, "Nondestructive Evaluation of Adhesive Bond Quality", *Nondestructive Testing Information Center*, (Southwest Research Institute, San Antonio, Texas), 1989.
5. Peter B. Nagy and L. Adler, "Adhesive Joints Characterization by Leaky Guided Interface Waves", in *Review of Progress in QNDE*, Vol. 8B (Plenum Publishing Co., New York), 1988.
6. Peter B. Nagy, P. McGowan, and L. Adler, "Acoustic Nonlinearities in Adhesive Joints", in *Review of Progress in QNDE*, Vol. 9B (Plenum Publishing Co., New York) 1990.
7. L. Adler and P. B. Nagy, "Second Order Nonlinearities and Their Application in NDE", in *Review of Progress in QNDE*, Vol. 10B (Plenum Publishing Co., New York) 1991.

NONDESTRUCTIVE EVALUATION METHOD FOR ASSESSMENT OF ENVIRONMENTAL DEGRADATION OF ADHESIVE JOINTS

S. I. Rokhlin
The Ohio State University

Executive Summary

One of the critical issues in the wide application of adhesives for structural joints is the integrity and reliability of the joint in service. It has been known in practice for a long time that sometimes adhesive joints fail catastrophically, especially in humid environments. Usually such failure happens at the adhesive-adherent interface and is called the "interfacial" or "adhesion" mode of failure. The causes of such failure are currently not completely understood, although it is known that surface preparation prior to bonding and environmental conditions in service are the most important factors in joint reliability.

While the extreme importance of environmental attack in relation to adhesive joint integrity has been understood, there has been no prior development of nondestructive methods to assess the integrity of adhesive joints in humid environments. The first development of this type is undertaken in this work.

The main objective of this project is to develop a nondestructive evaluation method for assessment of the environmental degradation of the structural integrity of the adhesive joints. We aim to assess the life expectancy and strength reduction of adhesive joints in the environment, including effects of moisture, temperature and structural load.

Our accomplishments can be briefly summarized as:

- Found experimental conditions such as temperature and load for accelerated environmental degradation of adhesive joints.
- Observed that adhesive joints under these conditions failed in the interfacial mode.
- Found that the ultrasonic signature carries information on the state of the interface and may be used for joint life expectancy assessment.
- Showed that the shift of frequency of the reflection minima starts to occur at approximately 70% of the joint life time and increases with time.

Background

A. General

The use of adhesive joints in aircraft structures has been addressed in the Primary Adhesive Bonded Structure Technology (PABST) Program [1] which was initiated by the Air Force in the seventies. The program focused on surface pretreatment of the metal adherents to guarantee initial bond strength and long term durability [2]. This program established that the major disadvantages of adhesive joints are unpredictable failure in service, especially in humid environments, and poor inspectability. Lack of nondestructive inspectability of the interphasial properties of adhesive joints is one of the factors limiting applicability of adhesive bonding technology. With this understanding a plan was developed according to the DARPA/AF initiative [3], "to set forth a program plan to address the needs in NDE for adhesive bonded structures". The plan identified major directions for research on mechanisms of adhesive joint failure and joint evaluation. In particular it has been recognized that joint strength needs to be directly related to micro-defect properties and to the intrinsic distribution of these properties. The importance of understanding the effect of environmental attack and interphase property measurements has been emphasized. However, the plan was not implemented at that time [4] and has only been partially addressed in the current Air Force NDE Program.

Currently available ultrasonic nondestructive techniques can detect delaminations in adhesive joints. There are also available methods to measure the adhesive elastic modulus and the porosity content of the joint. The correlation between the elastic properties and the cohesive strength of the adhesive has been established [4]. However, these techniques fail in evaluation of the integrity of the interfacial adhesion between adhesive and adherents. Efforts to evaluate adhesive joint interfaces have recently begun to show promise. It has been established [5] that an ultrasonic wave that produces shear stress on the interphase is sensitive to interphase properties in adhesive joints. Such stresses can be produced using interface waves [5,6], guided waves in the bonded plates [7,8,9], or ultrasonic waves obliquely incident from the substrate onto the interface [10,11,12].

The major problem of adhesive joint usage in aircraft applications is catastrophic environmental failure, which has interfacial character. It was proposed [2] that an aluminum-adhesive interphase fails environmentally through degradation of the Al_2O_3 interphase layer. Proper penetration of the primer into the pores prevents (or hinders) transport of water along the interphase leading to degradation. A second mechanism of environmental degradation of an adhesive joint is the weakening of the thin layer of adhesive on the interphase between adhesive and adherent and disruption of inter-molecular bonds on the oxide-adherent interface.

While the extreme importance of the effect of humid environments on adhesive joint integrity has been established in the past, there has been no prior development of nondestructive methods to assess the integrity of adhesive joints in humid environments. The first development of this type is undertaken in this work.

Previous to this project we developed an ultrasonic method for evaluation of thin interphasial layers in adhesive joints. A special ultrasonic goniometer for adhesive bond evaluation has been designed. We have also developed a theoretical model of ultrasonic wave interaction with adhesive joints of aluminum.

B. Project

During the first stage of this project we developed an ultrasonic method sensitive to interfacial properties in adhesive joints. This method utilizes frequency analysis of the reflection coefficient of a transverse wave obliquely incident on the joint interface. The experimental system, which implements a novel type of ultrasonic goniometer, has been developed. This goniometer simplifies measurements by requiring only one ultrasonic transducer for reflection coefficient measurements of obliquely incident waves.

During the second stage of this project we performed an experimental study on adhesive joints prepared with controllable interface properties. This was done by introducing very thin layers of epoxy resin, with different amounts of curing agent, on the interface between adherent and polymer. We have demonstrated that the elastic properties of these interfacial layers were measurable using the experimental technique we have developed. We have also developed a theoretical model which relates the ultrasonic signatures to the interfacial properties, including the properties of the porous anodized aluminum oxide and weak boundary interfacial layers. Using this model we were able to measure the properties of the interfacial layers we made and to show that they were close to the properties of the bulk epoxy.

In the last year, which is the period here reported, we have begun to develop a method for assessment of environmental degradation of adhesive joints. During this period we have developed facilities for joint preparation and aging in humid environments under stress. Our initial experimental results have demonstrated that the signature of the reflected ultrasonic signal from an adhesive joint interface carries information on moisture diffusion, the state of the adhesive-adherent interface, and whether the dominant mode of failure is interface or cohesive. A preliminary relation between ultrasonic signature, environmental degradation and life expectancy has been established.

Objective and Scope

The goal of this project is to develop an ultrasonic nondestructive evaluation method for assessment of the environmental degradation of the structural integrity of the adhesive joints. We aim to assess the life expectancy of adhesive joints in the environment, including effects of moisture, temperature, and structural load.

The past year was the first year of our work in this direction. Our specific objectives were:

- To define the experimental conditions (temperature and load) for preparation of environmentally degraded samples.
- To develop and apply the damaged samples.
- To relate ultrasonic and mechanical data and thus determine the potential applicability of the technique for joint integrity assessment.

Here we must stress that mechanical properties of the material; such as strength, cannot be determined nondestructively. One should note that under load the stress in the adhesive joint is distributed nonhomogeneously with a high level of stress concentration at the joint edge. The failure load of the joint (which is its operational characteristic), called the "joint strength", depends on stress concentration level and microdefect population in the adhesive, i.e. the "material strength" (we suppose absence of macrodefects in the joints which can be detected by conventional NDT techniques). When microstructural changes and microstructural defects occur in a material, they lead to mechanical property changes (strength reduction). The intrinsic microstructural and chemical parameters (for example, degree of cross-linking of the adhesive, nature and density of bonds at the adhesive-adherent interface, interface morphology, and microdefects) will affect not only

strength but also elastic and inelastic properties of the material which can be measured ultrasonically. This provides a basis to correlate the mechanical strength and the viscoelastic properties of the adhesive and interfacial regions. When moisture attacks the interface it produces changes even on the molecular level. Highly polarized molecules of water and salt ions may alter van der Waals bonds on the adhesive-adherent interface. When such interfacial degradation progresses, it changes microscopic conditions (stress transfer) through the interface thus affecting the reflected ultrasonic signal. The same effects lead to strength reduction of the adhesive and joint failure under load.

Approach

We evaluated environmentally degraded adhesive joints exposed to hot water under strain. The samples were degraded in fresh and salt water at different temperatures under different loads. Ultrasonic measurements were made using the angle-beam ultrasonic reflection technique. As will be shown below, several parameters of the reflected ultrasonic signal in the frequency domain can be used as indicators of joint degradation. The ultrasonic data will be related to the lap shear joint strength determined by static tests.

To attain the required sensitivity to the properties of the interface between adhesive and adherents, we need to induce shear stresses on the interface. This can be done using obliquely incident longitudinal or transverse waves at a selected angle. In order to make such an approach practical, a novel ultrasonic goniometer was built which focuses an obliquely-incident ultrasonic wave at different incident angles on the same area of the interface. An illustration of the concept of the design of the goniometer is shown in Figure 1. A transducer is positioned on the arc of a cylindrical reflector. The latter, which acts as a focusing lens, reflects the ray from the interface of interest to the transducer. The goniometer therefore has the ability to measure interface signals at various incident angles with only one transducer and scan the joint.

To analyze the effects of changes of the properties of these interfacial layers on ultrasonic signals and to consider the inverse problem we developed a theoretical model. The model incorporates adherents, anisotropic porous oxide, and viscoelastic layers of primer, adhesive, and WBL (weak boundary layer). The adherents are considered as solid semispaces; this is appropriate when short ultrasonic pulses are used. (This approach has the advantage that interference of ultrasonic waves in the adherent is excluded.)

Using theoretical analysis we have selected the optimum experimental conditions for ultrasonic assessment of interfacial properties. We have performed ultrasonic measurements on samples which have different times of exposure to the humid environment, temperature, and mechanical load. We have found shifts in the frequency of the minima of the reflected ultrasonic signals when the interface is attacked by moisture and becomes partially degraded. We have related this phenomenon to the transition of the cohesive mode of failure for good samples to the interfacial mode of failure for samples with degraded interfaces. This corresponds to the beginning of significant reduction in the joint strength, finally leading to joint failure under the operational load in the environment. Our preliminary results indicate that this occurs at approximately 70 percent of the joint lifetime, thus suggesting a method for predicting joint life expectancy.

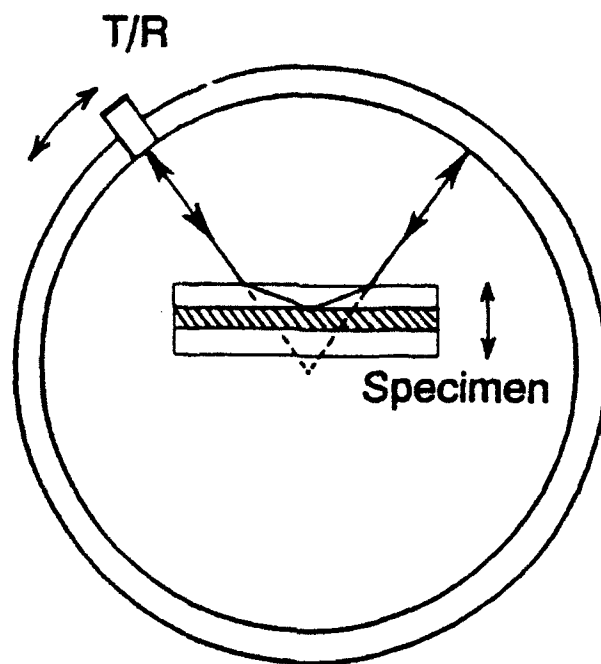


Figure 1 Arrangement for ultrasonic measurements: schematic of an ultrasonic goniometer.

Technical Progress

The single lap shear joints were prepared using 1.60 mm thick Alclad 2024-T3 alloy, FM-73 adhesive film, and BR-127 primer. Alclad 2024-T3 was selected because it is representative of those used in the aircraft industry, and because it is the standard alloy used for testing of bonded joints in the ASTM D1002-72 code. The adhesive prepreg FM-73, manufactured by American Cyanamid, is a modified epoxy adhesive film supplied with a polyester knit fabric. The corrosion inhibiting primer BR-127, from the same manufacturer, is a modified epoxy phenolic resin used as a general purpose aerospace primer.

The aluminum adherent surfaces were prepared prior to bonding to phosphoric acid anodization (PAA) following standard Boeing procedure. A thin layer of BR-127 primer was sprayed on the aluminum coupons after air drying. After 40 minutes air drying and 30 minutes curing at $120^{\circ}\text{C} \pm 6^{\circ}\text{C}$, the aluminum coupons were ready for bonding.

The standard curing cycle was employed for bonding with FM-73 adhesive film. The joints were heated in 30 minutes to 120°C , then held for 60 minutes at 40 ± 5 psi and $120^{\circ}\text{C} \pm 3^{\circ}\text{C}$, carefully calibrated by thermocouple. After pressure release the specimens slowly cooled to room temperature. The thickness of the adhesive layer was measured by micrometer and was usually between 100 and $140\text{ }\mu\text{m}$.

Single lap shear joint samples were used in the experiments. Some of the joints were dimensioned as described in ASTM D1002-72 with 0.5 in^2 overlap areas (1.0 in. wide); the others, in order to increase the stress level in the joint, had 0.375 in^2 overlap areas ($3/4$ in. wide). The environmental degradation was performed on different sets of samples for different loads, temperatures, and exposure mediums. The joined samples were found to be

initially all of approximately the same strength. Thus, the joint properties after environmental treatment performed on samples from the same set can be compared to each other.

The service environment always includes the effects of stress, temperature and humidity. Ideally, evaluation of environmental degradation of adhesive joints should be done in the natural environment. However, we selected accelerated aging, requiring the joints to be broken in 1-3 weeks. The temperature, the load, and the exposure medium were selected for experiment to satisfy this time requirement.

In this work, an Alcoa aluminum stressing fixture was used to apply the load on a single lap adhesive joint in an environmental degradation experiment. The fixture is an aluminum ring which keeps the adhesive joint samples under tension. The applied load was measured as deflection of the ring by a dial indicator, and then the deflection value was converted to a load value by using a stressing fixture calibration curve. Loaded samples were then immersed for different times in fresh or saturated salt water at different temperatures (60°C, 68°C, 70°C, and 80°C) in order to find the proper temperature, load, and exposure medium. From these experiments it is found that in saturated salt water at 68°C under 800 lb. load (for 3/4 in. wide samples) or 1000 lb. load (for 1 in. wide samples), the joints would be broken within one to several weeks. These conditions were selected for further experiments.

A set of experiments was done for samples (1 in. wide) aged at 70°C. Figure 2 shows a summary of the sample lifetimes under these conditions. One sample was found broken immediately after it was put into salt water; the other three samples were broken in 18, 24, and 48 hours; the remaining ten samples were broken between 48 to 96 hours. This shows that the lifetime is affected greatly by load, temperature and exposure medium and varies greatly between samples while, as noted above, different samples had the same strength before degradation. From the experimental data one can see that the adhesive joint lifetime is poorly predictable and varies over a wide range despite the fact that the initial strength of the different joints is the same. This shows the necessity of nondestructive assessment of the state of the joints during service.

Ultrasonic measurements were performed before and after environmental degradation using the ultrasonic goniometer. The complete experimental system is shown in Figure 3. A computer-controlled DC motor was used for simultaneous control of the transducer rotation and sample translation. Angle and translation accuracies are 0.01 ° C and 0.01 mm, respectively. At each angle of rotation the signals received were automatically digitized and averaged by a computer controlled LeCroy 9400 125 MHz digital oscilloscope and fed to a computer through an IEEE interface. The signals were then Fourier-transformed to the frequency domain and deconvolved with the reflected spectra from an air-backed aluminum plate. The water tank was temperature-stabilized at 29.8 ± 0.05 ° C.

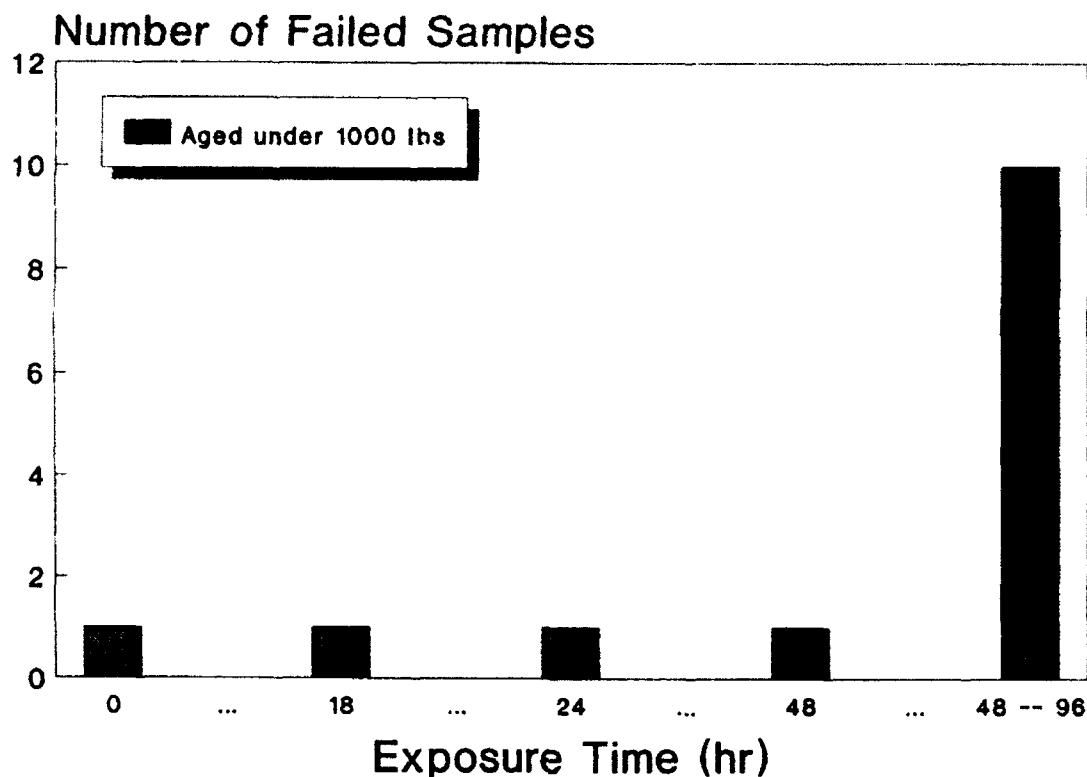


Figure 2 Lifetime of single lap shear adhesive joints aged in saturated salt water under 1000 lb. load at 70°C. The axis of ordinates represents the number of broken samples at the indicated times.

Properly prepared adhesive joints failed cohesively inside the adhesive as a result of lap shear tensile tests. The failure mode of an adhesive joint becomes interfacial after severe environmental degradation. The interfacial mode of failure in environmentally affected samples is due to accumulation of a critical concentration of water in the interfacial regions, which is governed by the rate of diffusion of water through the bulk adhesive and is accelerated by temperature and applied load. Loss of integrity of the interfacial regions occurs due to rupture of interfacial bonds and hydration in the oxide layers [13]. Brewis et al. [14] suggested that water may penetrate either by transport through the bulk adhesive, or by transport along the adhesive-adherent interface. Water accumulates at hydrophilic centers in the boundary layer, and interferes with adhesive/adhesive and metal oxide/adhesive hydrogen bonds, thus weakening the boundary layer. This is followed by stress-hydrolysis of covalent bonds in the interfacial layer as well as hydration of metal oxide.

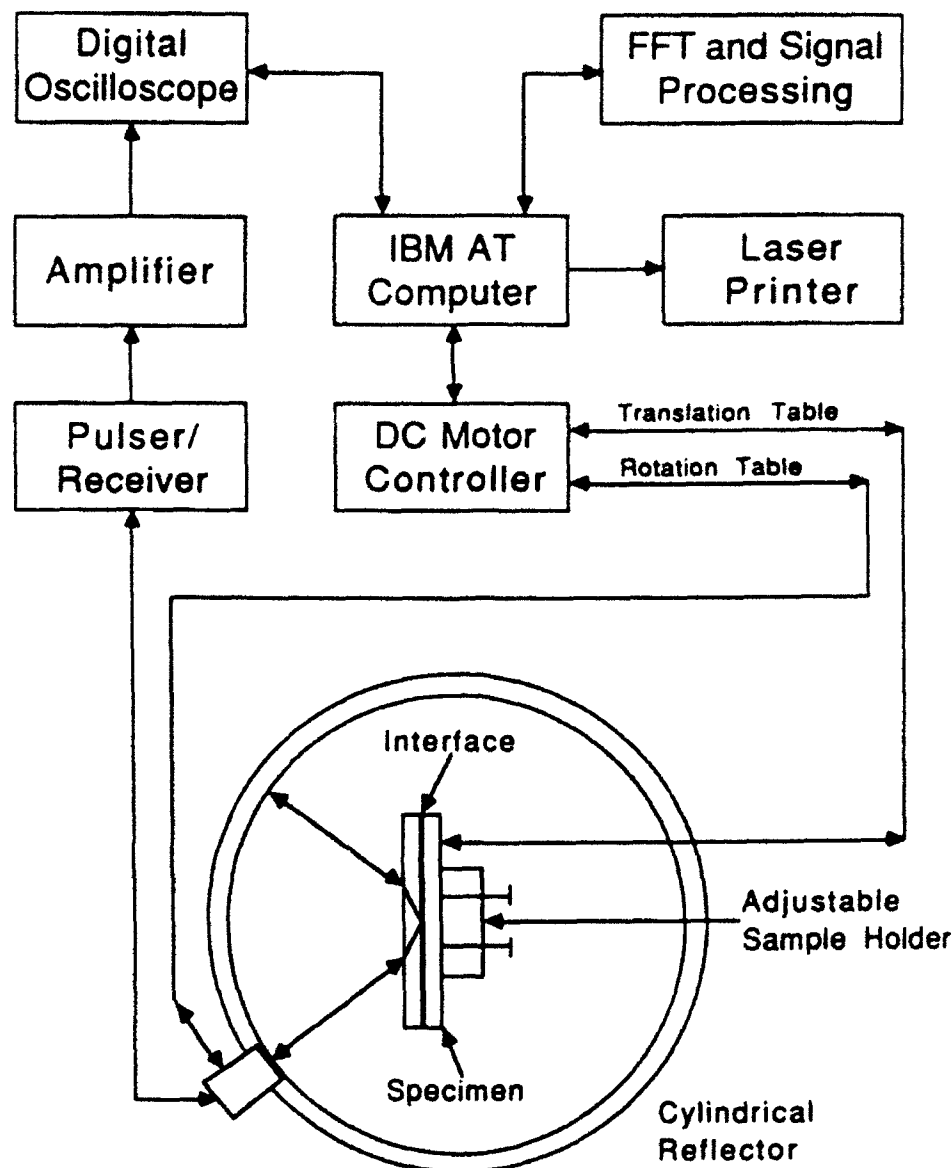


Figure 3 Ultrasonic experimental system.

Hydration of aluminum oxide on the adhesive/adherent interface may play an important role in joint failure. Venables [15] found that pseudo-Boehmite may be created by the reaction $Al_2O_3 + H_2O \rightarrow AlOOH$. Secondly, the aluminum metal comes into contact with water and gas evolution occurs which is governed by the reaction $2Al + 4H_2O \rightarrow 2AlOOH + H_2 \uparrow$. Thus the conversion of aluminum oxide to a hydroxide may even cause corrosion of aluminum adherents. This phenomenon is also observed in the photograph shown in Figure 5; the corrosion area is located at the lap joint edge which has the highest stress concentration and is the first region attacked by water. We performed a special study of the hydration of thin porous aluminum oxide membranes [16]. It was found that the porous aluminum oxide membranes degraded in either salt or fresh water at

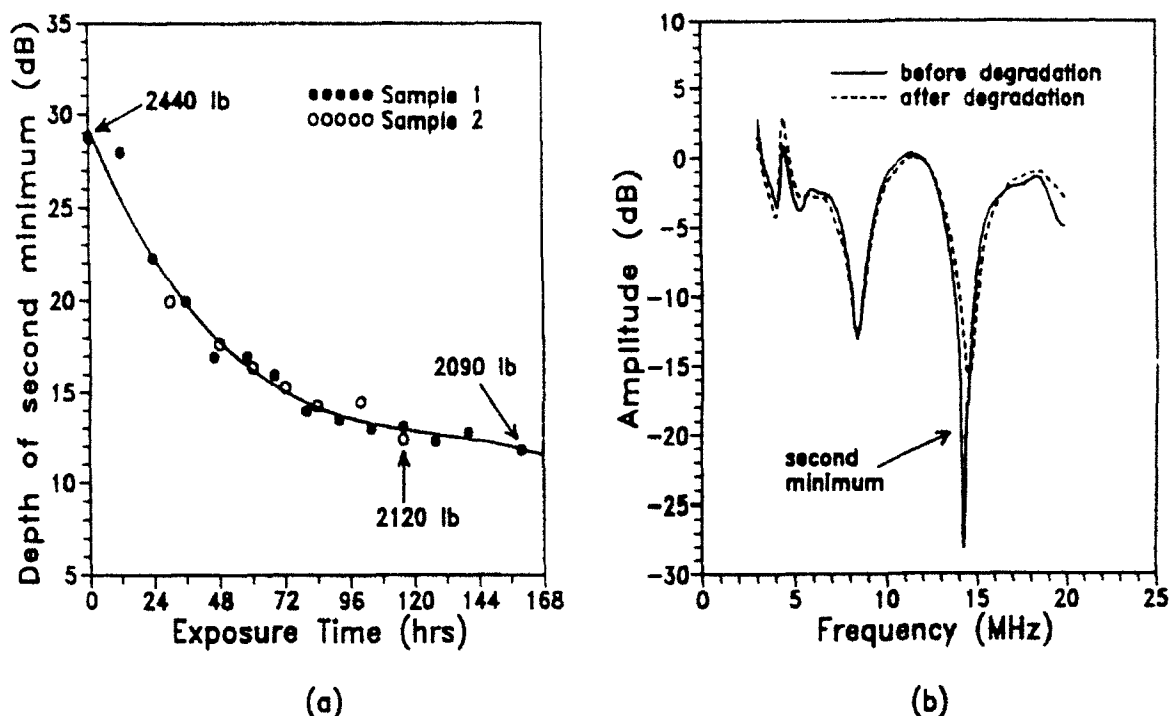


Figure 4 (a.) Depth changes of the second ultrasonic reflection minimum during exposure in salt water under 800 lb. load at 68 °C. Initial failure load and failure load after exposure are shown. (b.) An example of measured reflected spectra from the interface before (solid line) and after (dash line) the degradation.

temperatures below 70 °C which is close to the possible service conditions. As a result of exposure the morphology of Al_2O_3 was changed and cracks developed in the pore walls, thus significantly changing the strength and elastic properties of Al_2O_3 .

To find the relation between ultrasonic parameters and joint exposure time we made ultrasonic measurements on samples loaded in the fixture for different time intervals. The samples were held in salt water under 800 lb. load at 68 °C. The results for two samples measured with a 15 MHz transducer are shown in Figure 4(a). The depth of the second minimum in the reflected spectrum is shown on the ordinate axis. Examples of reflected spectra for two points are shown in Figure 4(b). Lap shear strength of these samples after exposure is also indicated in Figure 4(a). It is reduced to about 2100 lb. from the initial strength, 2440 lb., which is determined from the average strength value of four randomly selected samples from the same set. In this experiment there was no visible frequency shift of the minima.

One can see from Figure 4(a) that the two samples shown did not fail by themselves in the process of aging. So the actual lifetimes for these samples are unknown (they were broken by mechanical testing). The results of a similar test at a higher load of 1000 lb. and 68°C are shown in Figure 5. The sample failed by itself at 64 hours of exposure time. Since it was under 1000 lb. load this is its failure load (compared with the failure load of 2100 lb.

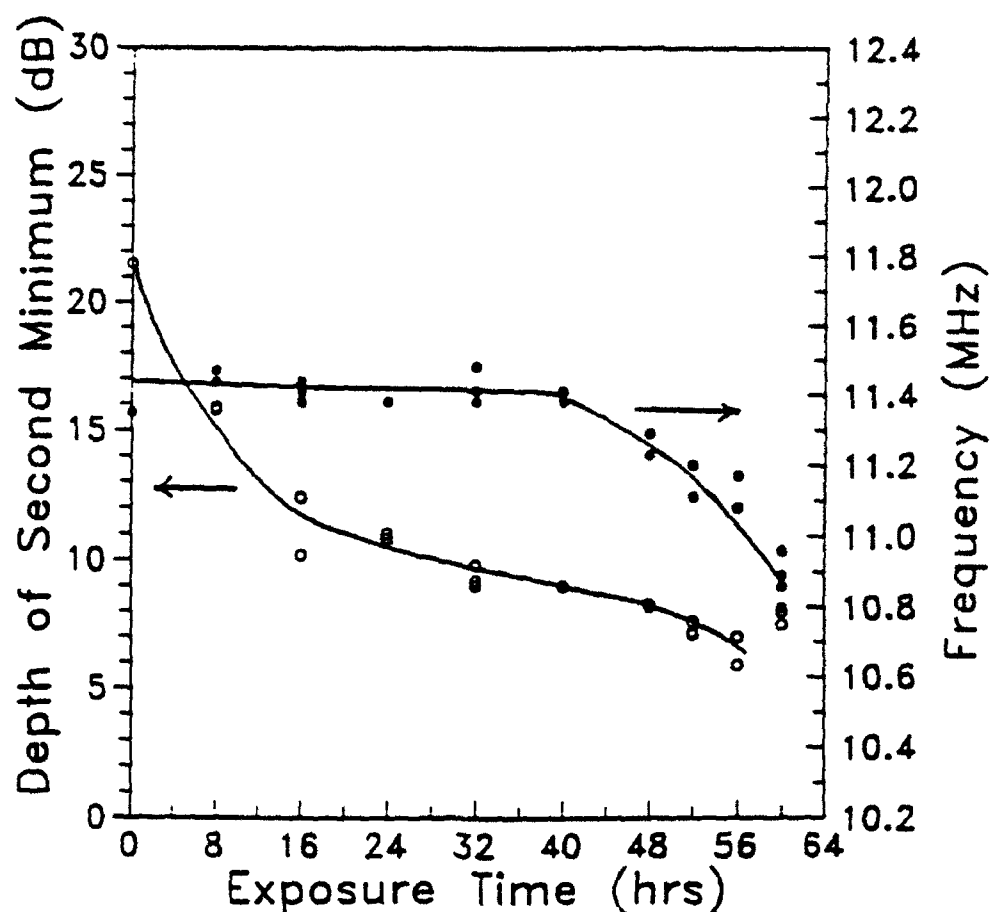


Figure 5 Frequency and depth changes of reflection spectrum minimum due to exposure in salt water under 1000 lb. load at 68°C.

for samples shown in Figure 4(a). The change of the second minimum depth and the frequency shift of this minimum are shown. One can see that the frequency shift of the minimum begins to be significant after 45 hours, roughly after 70% of the lifetime. Fractographic analysis of the failed sample shows that it failed mostly in the interfacial mode with a large area of clean Al_2O_3 surfaces (an Al_2O_3 surface can be clearly recognized by color changes of the light reflected from the sample fracture surface viewed through a polarizing optical filter).

One may suggest the following explanation of the observed phenomenon. Because high corrosion inhibiting primer BR-127 was used in the interfacial regions, the water first diffused through the bulk adhesive, resulting in increase of attenuation there; thus the amplitude of the reflection minimum decreased. At this stage of water accumulation the bulk elastic properties did not change very much; therefore, no frequency shift of the minimum was observed, as shown in Figure 4(a) and Figure 5 for the first 40 hours of exposure. Because of the inhomogeneity of adhesive and primer in the bonding region, some of the interfacial region was affected by the water attack. For this reason and because of the plasticization of bulk adhesive by the absorption of water, the strength of the adhesive joint was reduced but the failure mode was mixed though dominated by cohesive failure.

During the next stage the water attacked the interfacial regions. This was followed by the hydrolysis of interfacial covalent bonds and rupture of interfacial secondary bonds, which caused significant mechanical weakening of the interfacial regions resulting in interfacial failure (after 64 hour exposure). It is important once more to note that a shift of the ultrasonic minimum preceded the failure and thus can be used for failure prediction.

Summary

The results of this year can be summarized as follows. Degradation of adhesive joints of aluminum samples has been performed in fresh or salt water at different load levels and temperatures. The strength of the samples undergoes significant change during such treatment. The lifetime of a joint sample depends on load level and temperature, and varies greatly between samples. Cohesive failure in the adhesive has been observed for non-exposed samples; partial cohesive and partial interfacial failure has been found for samples in an early stage of degradation; and interfacial failure has been found for severely degraded samples. One may speculate that the interface weakening is due to replacement of adhesion bonds by absorbed water and the hydration of porous aluminum oxide.

It was found that ultrasonic data correlated well with strength reduction during degradation. Both the depth and position of minima in the reflected ultrasonic frequency spectra from adhesive joint interfaces are related to mechanical properties of the joints, and can be indicators of joint degradation. Our preliminary results showed that the reflection minima began to shift in frequency at approximately 70% of the joint lifetime. Thus the technique shows promise for predicting service life of adhesive joints under environmental attack.

Plans for Next Year

The objectives for the next year's work and to develop a methodology for NDE of joint integrity degradation and assessment of joint life expectancy.

The work will concentrate on the development of nondestructive methodologies to assess the integrity of adhesive joints in humid environments and their life expectancies under load. We have found that in humid environments, adhesive joints fail in the interfacial mode. We will focus on the relation between ultrasonic signature and the percentage of interfacial failure, depending on time of exposure to the environment. Thus we will establish a microstructural relation between ultrasonic signature and degradation of mechanical properties. Our preliminary results show good correlation between frequency shift of the minima of ultrasonic reflectivity, percentage of interfacial failure and strength of the degraded adhesive joint. We will continue to explore physical models for computer simulation of ultrasonic wave interaction with degraded interfaces during this year. We will consider the weak interfacial layer as a two-phase medium, one phase having properties equal to those of the bulk adhesive and the other having low moduli. To relate the model to the ultrasonic measurement, the face volume fractions will be determined from fractographic measurement of the failed joints which correspond to interfacial failure. The first phase will fail in the bulk and the second in the interface.

Samples and results will be shared with Dr. L. Adler for evaluation using nonlinear techniques. Results and models will also be discussed with Dr. J. Achenbach. We have had an extensive discussion with Dr. Achenbach in December 1991 and such discussions will be continued.

References

1. E. W. Thrall, in *Proc. 10th National SAMPE Tech. Symp.*, Kiamesha Lake, N.Y., Oct. 17-19, P. 73, (1978).

2. J. D. Venable, in Adhesive Joints, Formation, Characteristics, and Testing, K. L. Mittal ed., pp. 453-467, Plenum, N.Y. 1984.
3. F. N. Kelley, W. G. Knauss and D. H. Kaelble, in Proc. of the DARPA/AFML Review of Progress in Quantitative NDE, p. 719, Report AFWAL-TR-80-4078.
4. R. B. Thompson and D. O. Thompson, in J. of Adhesion Sci and Technology, 5, 583-599, 1991.
5. S. I. Rokhlin, M. Hefetz and M. Rosen, J. Appl. Phys. 52, 2847-2851 (1981).
6. S. I. Rokhlin, J. Acoust. Soc. Am. 73, 1619-1623 (1983).
7. G. A. Alers and R. B. Thompson, 1976 Ultras. Symp. Proc. IEEE, 138-142 (1976).
8. S. I. Rokhlin, in Review of Progress in Quantitative NDE, D. O. Thompson and D. E. Chimenti (eds.), Vol. 5B, 1301-1308 (1986).
9. C. M. Teller, K. J. Diercks, Y. Bar-Cohen, and N. N. Shan, in Review of Progress in Quantitative NDE, D. O. Thompson and D. E. Chimenti (eds.), Vol. 7B, 935-942 (1988).
10. S. I. Rokhlin and D. Marom, J. Acoust. Soc. Am. 80, 585-590 (1986).
11. A. Pilarski and J. L. Rose, J. Appl. Phys. 63, 300-307 (1987).
12. P. B. Nagy and L. Adler, in Review of Progress in Quantitative NDE, D. O. Thompson and D. E. Chimenti (eds.), Vol. 8B, 1417-1424 (1989).
13. R. A. Gledhill, A. J. Kinloch, and S. J. Shaw, J. Adhesion, Vol. 11, 3-15 (1980).
14. D. M. Brewis, J. Comyn, and J. L. Tegg, Int. J. Adhesion and Adhesives, Vol. 1, 35-39 (1980).
15. J. D. Venable, J. Mater. Sci. 19, 2431-2453 (1984).
16. M. Hefetz, W. Huang, and S. I. Rokhlin, in Review of Progress in Quantitative NDE, D. O. Thompson and D. E. Chimenti (eds.), 1992.

EDDY CURRENT CHARACTERIZATION OF COMPOSITES

R. E. Beissner
Southwest Research Institute

Executive Summary

Metal matrix composites with excellent strength and thermal properties have been identified as candidate materials for advanced gas turbine engine components. At the present time, applied research in this area is focused on the manufacturing technology needed for the reliable and cost effective fabrication of such components. This work has revealed the need for NDE methods that can efficiently measure fiber volume fraction and layup in multi-ply structures. Accordingly, the research reported here is aimed at developing eddy current technology for the purpose of measuring fiber volume fraction and layup in advanced composites.

The principal impediment to eddy current characterization of composites is that the electrical properties of such materials are anisotropic. This complicates the flow of eddy currents in the material and has a decided influence on the response of an eddy current probe to material characteristics. As a result, conventional methods for interpreting eddy current signals in terms of material properties, all of which were developed for isotropic materials, are not applicable to composites. The general aims of the research are, therefore, to develop a scientific basis for eddy current testing of composites and to develop specific measurement methods for volume fraction and layup in metal matrix composites.

During the first year of work the basic framework of a theory was developed for materials with uniaxial anisotropy and applied to studies of eddy current flow patterns and to measurement methods for determining layup in multi-ply structures. Efforts in the past year were concentrated on an extension of the theory to biaxial conductors, development of a model relating anisotropy characteristics to composite microstructure, experimental verification of the overall method, and preliminary studies of methods for measuring volume fraction. Specific accomplishments covered in this report are the following:

- Completed theory of eddy currents in biaxial conductors
- Developed theory of conductivity tensor for arbitrary arrangements of parallel fibers
- Verified models by comparison with experimental data
- Began investigation of volume fraction measurement methods

With the successful achievement of these goals, the basic theoretical framework needed for interpreting eddy current measurements is complete. Future work will involve applications and experimental testing.

Background

A. General

The general aim of the research program described here is to apply eddy current nondestructive evaluation (NDE) methods to the characterization of the microstructure of continuous fiber metal matrix composites. While other NDE methods might also be used for this purpose, the eddy current method is more easily implemented than other methods in a scanning mode to search for material abnormalities. Thus, potential applications tend to focus on inspection during manufacturing processes, where there is a need for fast, reliable methods to insure the quality of materials and fabricated parts.

The need for better NDE methods was demonstrated in a recent pilot study of the fabrication of a part for a gas turbine engine [1] using a commercially available metal matrix composite. Problems encountered in this study were misalignment of layers in the multilayer structure and the existence of localized regions with abnormal fiber spacing. In particular, it was noted that fiber damage (cracking) tends to occur in regions of high fiber volume fraction, where fibers may form clumps with little or no matrix material between them. A similar conclusion regarding the importance of volume fraction was reached in a separate, independent study [2]. In the first study, an attempt was made to apply ultrasonic and radiographic methods to the inspection of materials and structures, but without much success. It was concluded that more sensitive methods are needed.

NDE methods for metal matrix composites are summarized in the 1988 review by Reynolds [3]. The principal conclusions noted here are that while radiography and high frequency ultrasonics are potentially capable of detecting defects of interest, these methods are time-consuming and expensive, and therefore not well suited to large scale use during manufacturing. Eddy current methods received only cursory attention, though the potential value of such methods in providing rapid inspection was noted.

The material summarized by Reynolds was updated by means of computerized searches of more recent literature, using facilities available at Southwest Research Institute and at the Metal Matrix Composite Information Analysis Center. With a few exceptions, nothing of significance was added to the information provided by Reynolds. Most attempts to use eddy current continue to be cursory, making use of the off-the-shelf equipment and standard analysis methods.

Exceptions are the work of Sabbagh, et al. [4], Bowler, et al. [5], and, more recently, Burke [6]. All of these authors recognized that because composites have anisotropic electric conductivity, standard methods of analysis, which are based on isotropic conductivity models, are not applicable. Their approach, which is followed in the work reported here, is to return to the physics of electromagnetic fields in anisotropic conductors in an effort to understand eddy current behavior in such materials. The basic idea is that in order for eddy current NDE to be successful for composites, it will be necessary to first understand how anisotropic conductivity affects probe response and then design measurement methods specifically for such materials.

B. Project

During the first year of the present project, a probe response model was developed for multilayer structures consisting of uniaxially anisotropic layers. The theory makes use of transverse electric and transverse magnetic Hertz potentials, and is an extension of a previously published theory [5] from the case of a uniform half-space of material to a multilayer configuration. The transmission and reflection properties of each layer are represented by matrices which are calculated individually and then combined to give the

overall response of a multilayer structure. Provisions are made for calculating the response of circular coils with axes either normal or parallel to the surface of the composite, and for a special serpentine coil which tends to produce unidirectional current flow in the material.

Calculations were performed for graphite-epoxy structures because conductivity data for this material are readily available. In addition to coil impedance data, eddy current fields within the material were calculated to show how much fields differ in isotropic and anisotropic materials. The results of one such calculation are plotted in Figure 1. These data show that, unlike isotropic materials where current flow is always parallel to the surface, the current vector in the anisotropic case can have a normal component which could prove advantageous in the detection of delaminations. Additional calculations showed that with proper attention to probe design, delaminations should be detectable and layup is measurable [7].

By the end of the first year it was evident that additional developments were needed to complete the theory and its validation for composites with abnormal fiber arrangements. The first of these was a generalization from uniaxial anisotropy, which applies with the fibers are well-ordered in a regular array, to biaxial anisotropy, which occurs when fibers are more closely spaced in one direction than another. This is an important point because one of the abnormalities one would hope to detect is fiber clumping, which is characterized by a high volume fraction with the fiber spacing being smaller in the direction parallel to the surface

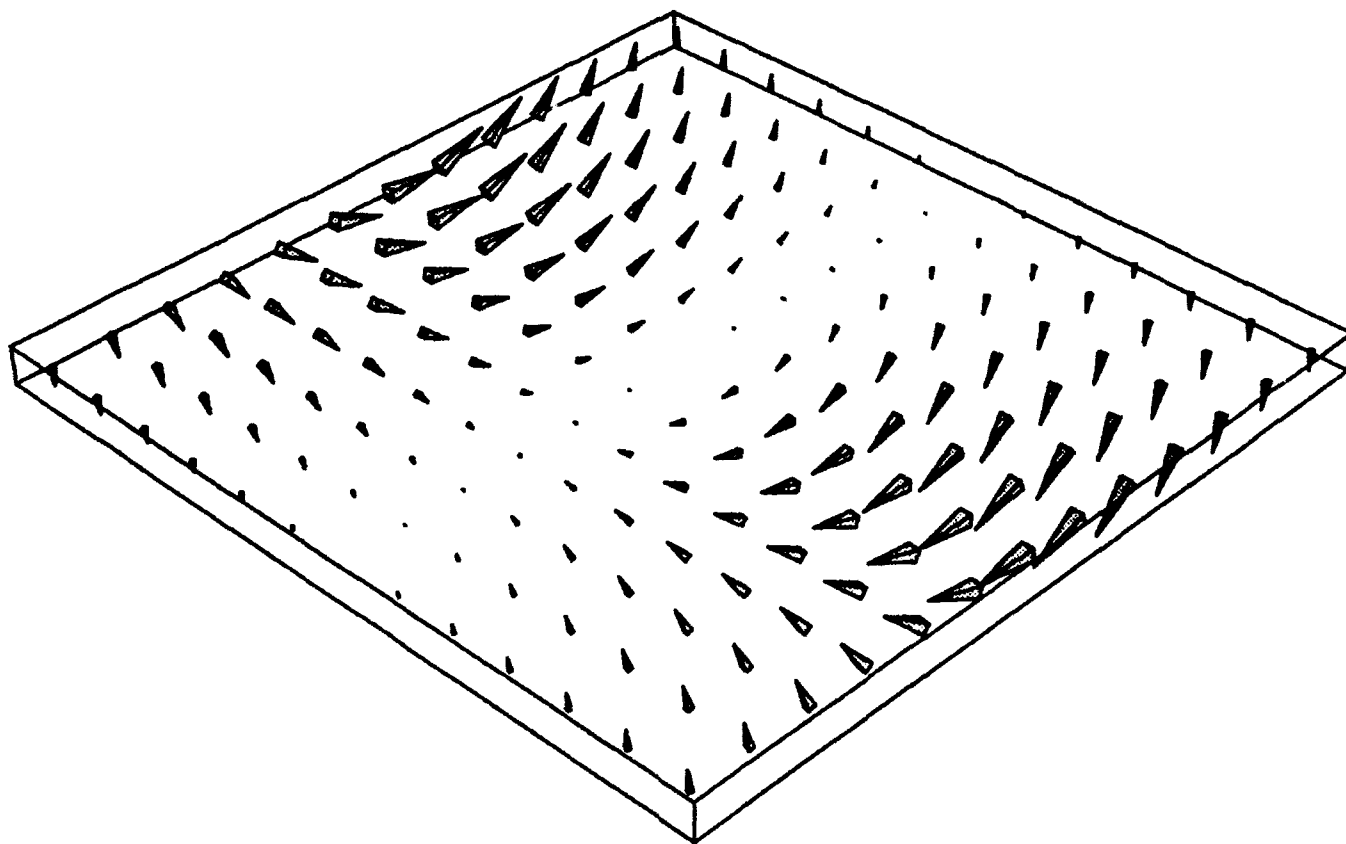


Figure 1 Eddy current pattern below the surface of a graphite-epoxy composite. At sufficient depth current flow is predominantly across the fibers with a significant component normal to the surface, which is the vertical direction in this plot.

than it is in the direction normal to the surface. The second development needed at this point was a model that gives the conductivity tensor for abnormal fiber arrangements, so that probe response can be related to the fiber distribution. The only models available at that time were a theory for square or hexagonal arrays, and various theories for random distributions. Neither of these models is applicable to the case of concern, which is an arbitrary, but fixed arrangement of fibers in a conducting matrix. Finally, and most importantly experiments on controlled samples are needed to confirm and validate the theoretical advances.

Objective and Scope

The overall objective of this project is to develop eddy current technology of characterizing the microstructure of metal matrix composites. Specific objectives for this, the second year of research, are the following:

- Develop a theory of eddy currents in biaxial conductors
- Develop a model of the conductivity tensor for arbitrary arrangements of parallel fibers
- Verify models by comparison with experimental data

In addition, it was intended that models be applied to numerical studies of the measurement of volume fraction under various conditions, i.e., with different fiber arrangements, matrix conductivities, frequencies and different probe configurations. The purpose of this study is to identify the most promising approach to volume fraction characterization.

Although most numerical and experimental work is focused on a specific metal matrix composite, Ti 6Al-4V/SCS-6, it is expected that the methodology developed, and certainly the theory, will be applicable to any material with continuous fiber reinforcement. As exemplified by some of the early results, this includes graphite-epoxy composites as well as several other metal matrix materials. Other types of composites, such as particle-reinforced, are not included, though it should be possible to develop similar techniques and theories for these materials as well.

The principal areas of application are inspection of materials during manufacture and inspection of parts involving composite materials. It is in such applications, where there is a need for rapid screening of large quantities of materials, that eddy current methods offer an important advantage over NDE methods for composite inspection.

Approach

The extension of the eddy current model to biaxial conductors was based on the recent work of Wait [8], who developed a system of coupled partial differential equations for the electric and magnetic fields in a half-space under the influence of an incident plane wave. To apply Wait's theory to the eddy current problem it was necessary to reformulate the calculation in terms of the Fourier components of the incident field from an eddy current probe and then solve the boundary value problem for a plate of finite thickness. Once this was done the probe impedance was calculated from the reciprocity theorem in the usual way.

For reasons cited above, a new approach was needed to calculate the conductivity tensor. The new theory is based on the integral equation for the electrostatic potential in a system consisting of an arbitrary arrangement of parallel fibers in a conducting matrix. The equation is solved by substituting the Fourier expansion of the potential on the surface of each fiber, thus reducing the problem to a system of algebraic equations for the Fourier

coefficients. The resulting system is then numerically solved for applied fields in three orthogonal directions and the results are substituted in integral expressions for the components of the conductivity tensor.

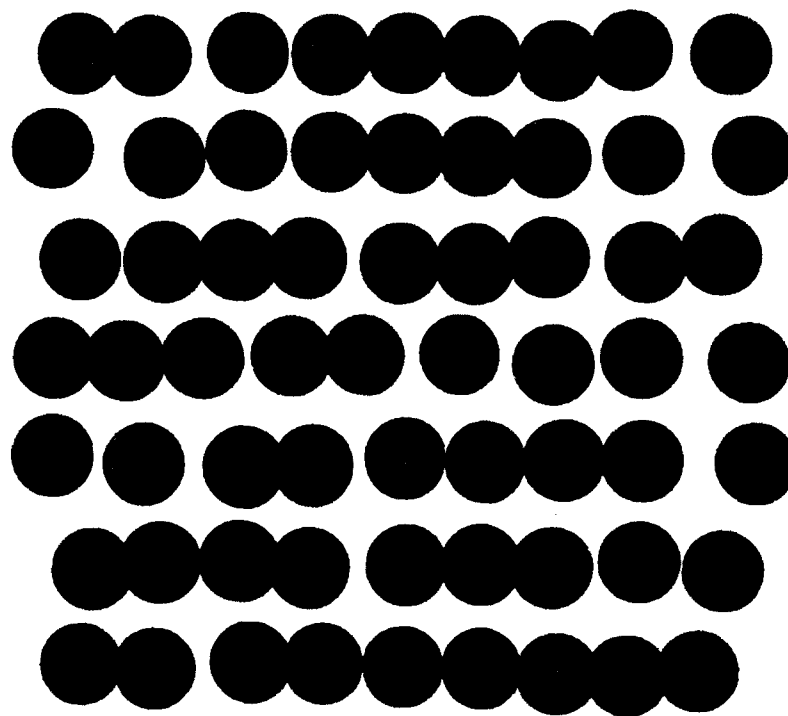
To generate experimental data for verification of the conductivity and probe response models, an attempt was made to fabricate a scaled up model of a metal matrix composite by drilling holes in an aluminum block. This proved to be impractical because of the very large length-to-diameter ratio required for the holes to properly simulate fibers. A second attempt made use of a small specimen of a titanium alloy composite. Although some useful data were obtained, this effort was also largely unsuccessful because available probes exhibited resonances in the frequency range of interest. Finally, experimental data for an Al/B composite were obtained from Steve Burke of ARL Melbourne, and these data were used for verification of the models.

To investigate the measurement of volume fraction and fiber orientation in specimens with regular and irregular fiber distributions, and with variations in the matrix conductivity, the models described above were used to calculate probe response as a function of specimen characteristics, probe configuration and frequency.

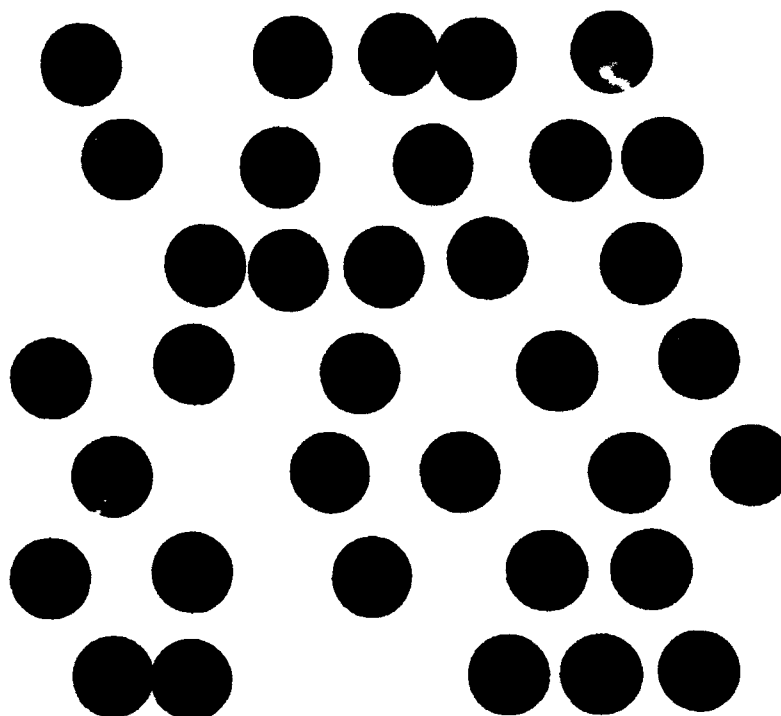
Technical Progress

The major accomplishment of the second year of work was the development of a model of the conductivity tensor for an arbitrary distribution of fibers. The theory bears some resemblance to one developed several years ago for periodic arrays in that the conductivity tensor is calculated in terms of the Fourier coefficients of the electrostatic potential on the surface of a fiber. The main difference is that in the new theory the fibers need not be periodically arranged, and the potential can therefore differ from one fiber to the next. This results in a considerably more complicated problem which has, nevertheless, been solved with an efficient computer algorithm.

To investigate the influence of fiber distribution on the conductivity tensor, calculations were performed for a large number of different distributions ranging from periodic to highly disordered. Figure 2 shows two of the fiber distributions used in this study, one at low volume fraction (0.24) and the other at high volume fraction (0.43). It was found that when fibers tend to pack closely together in rows parallel to the surface, which is often observed in experimental studies of fiber distributions, the conductivity in the normal direction can be significantly lower than in the direction parallel to the rows, resulting in biaxial rather than uniaxial anisotropy. This can be seen in Figure 3, which summarizes the results of the study. At low volume fraction the transverse conductivity components (yy and zz) are approximately equal, but as the volume fraction increases due to closer packing of fibers in rows parallel to the surface, the normal (zz) component decreases more rapidly. This finding, which is contrary to the assumption inherent in all earlier models of current flow in composites, called for a generalization of the probe response model from uniaxial to biaxial anisotropy.



(a)



(b)

Figure 2 Computer simulations of fiber distributions: (a.) high volume fraction, (b.) low volume fraction.

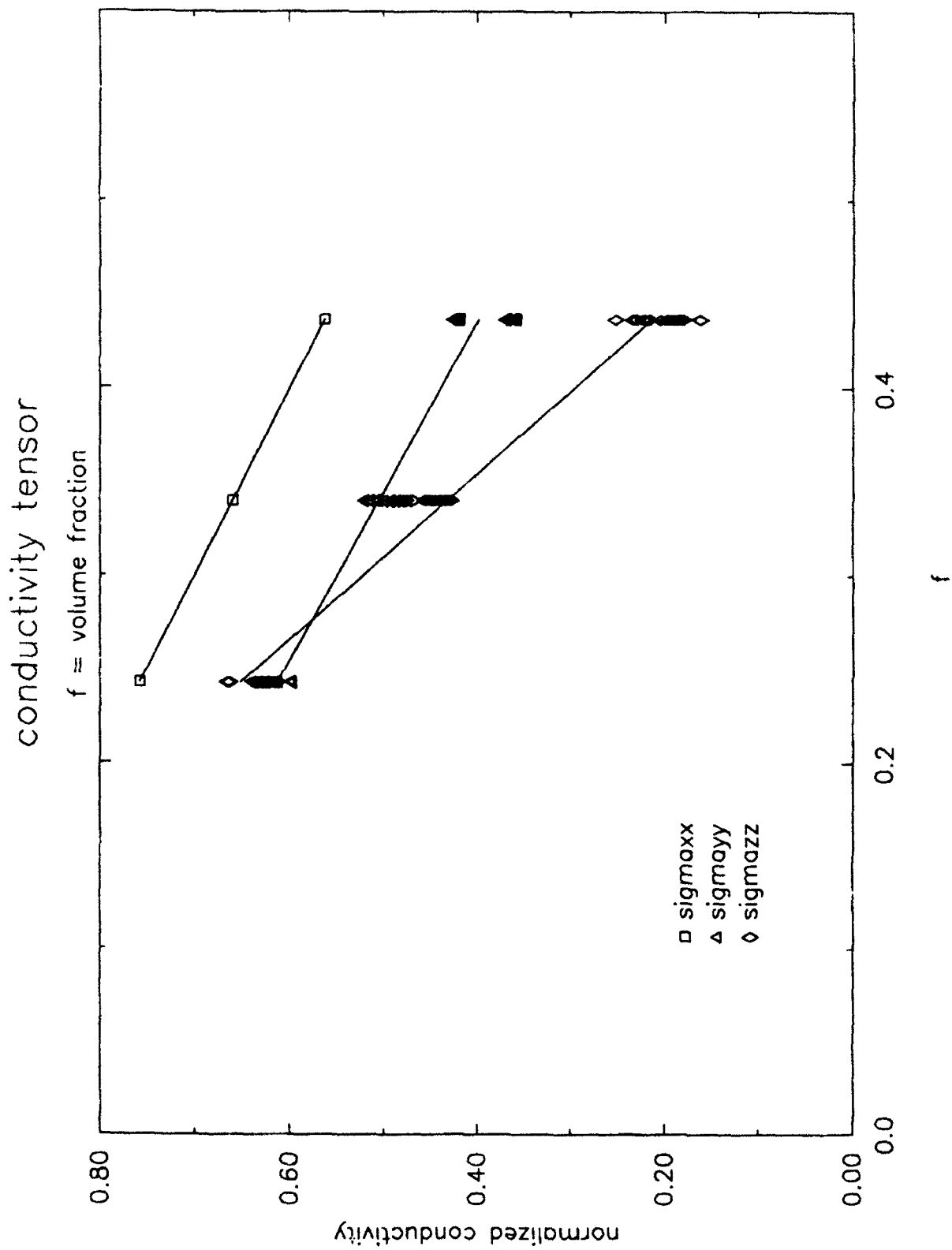


Figure 3 Calculated conductivity tensor normalized to the matrix conductivity. Points with the same label correspond to different fiber arrangements. The straight lines are least squares fits.

The new model of eddy currents in a biaxial anisotropic medium is based on the work of Wait [8]. For the half space $z < 0$ with a diagonal conductivity tensor, Wait's analysis shows that the two-dimensional Fourier transform of the electric field, which is

$$\vec{E}(\vec{k}, z) = \frac{1}{2\pi} \int e^{-i\vec{k} \cdot \vec{\rho}} \vec{E}(\vec{\rho}, z) d^2\rho, \quad (1)$$

has components of the form

$$e_x(\vec{k}, z) = a e^{\lambda z} + b e^{\chi z}, \quad (2)$$

where $\vec{\rho}$ is a vector in the xy plane and a and b are constants to be determined by the boundary conditions; similar expressions exist for the components of the transform of \vec{H} , the magnetic field. The propagation parameters λ and χ are complicated functions of the components of the conductivity tensor and the wave vector \vec{k} [8]. If two of the conductivity components are equal, the material is uniaxially anisotropic, and Wait shows that the analysis simplifies to a form equivalent to the TE/TM modal theory of Bowler, et al. [5].

Wait's theory was extended to the solution of the boundary value problem for a half space with an arbitrary current source in the space $z > 0$. Then, given the expressions for the tangential components of the transforms of \vec{E} and \vec{H} , substitution in the reciprocity expression for the probe impedance led to the form

$$\Delta Z = \frac{2i\omega}{\mu_0 I^2} \int \Gamma(\vec{k}) \hat{z} \cdot \vec{k} \times \vec{a}_s(\vec{k}) \hat{z} \cdot \vec{k} \times \vec{a}_s(-\vec{k}) \frac{d^2 k}{k}, \quad (3)$$

where $\vec{a}_s(\vec{k})$ is the transform of the vector potential associated with the current source in free space, evaluated at $z = 0$. The reflection function Γ depends on the components of the conductivity tensor, as well as \vec{k} , but is independent of $\vec{a}_s(\vec{k})$.

After developing a generalized theory of probe response, numerical studies were conducted to simulate the measurement of fiber volume fraction and layup. It was shown that variations in the spatial distribution of fibers causes no difficulties in the measurement of volume fraction or the determination of layup direction provided that the probe is properly designed. However, variations in the conductivity of the matrix have the same effect on probe response as variations in volume fraction, and this seemed to pose a problem in the unambiguous determination of these properties.

Recently, however, Burke [9] suggested an approach that may provide a simple way to determine both volume fraction and matrix conductivity from two eddy current measurements. His calculation is based on two assumptions, the first being that one can design an eddy current probe to measure the resistivities parallel to the fiber direction (ρ_x) and transverse to the fiber direction (ρ_y). The second assumption is that the transverse resistivity is of the form

$$\rho_y = \rho_m / g(f), \quad (4)$$

where ρ_m is the matrix resistivity and $g(f)$ is some known function of the volume fraction f . Then, from the exact relation

$$\rho_x = \rho_m / (1 - f), \quad (5)$$

and the definitions

$$\Delta\rho = \rho_y - \rho_x, \quad (6)$$

and

$$\rho = (\rho_y + \rho_x) / 2, \quad (7)$$

one finds

$$\frac{\Delta\rho}{\rho} = 2 \frac{1 - f - g(f)}{1 - f + g(f)}. \quad (8)$$

If ρ_y and ρ_x can be measured, then the quantity on the left side of Eq. (8) can be experimentally determined, and the equation can presumably be solved for f . Once f is known it can be substituted in Eq. (4) or (5) to find the matrix conductivity.

Numerical calculations based on known resistivities for square and hexagonal arrays of fibers, for which $g(f)$ is a simple function of f , show that this method works very well for all volume fractions of interest. However, two questions remain. The first is whether an eddy current measurement can provide ρ_y and ρ_x with sufficient accuracy; the second is whether Eq. (4) holds for nonuniform arrays of fibers. The models developed here can provide answers to both of these questions and will be used for this purpose in next year's work.

Finally, in the first experimental tests of the models, eddy current data for a 2 mm thick plate of an aluminum-boron fiber composite were obtained from Burke [6,9]. According to Burke, photomicrographs of the fiber arrangement indicated an almost regular hexagonal array with fiber spacing slightly closer in rows parallel to the surface. It was expected, therefore, that the uniaxial model would suffice in this case. From volume fraction data supplied by Burke and published conductivity data for the aluminum alloy, the conductivity model was used to calculate the conductivity tensor for the composite. The results are in excellent agreement with conductivity measurements supplied by Burke. The calculated conductivity tensor was then used to predict the impedance of Burke's probe as a function of frequency from 100 Hz to 100 kHz. The results of reactance calculations are shown in Figure 4, which was supplied by Burke [9]. Actually, there are three calculated results shown here. The curve labeled SKB Uniaxial is Burke's calculation based on his uniaxial model, RB Square is our result for a square array of fibers and RB Rectangle is our result for a rectangular array with closer fiber spacing in rows parallel to the surface. Again, in all cases agreement between theory and experiment is excellent, thus verifying both the conductivity model and the generalized probe response model.

Summary

By the end of the year all objectives for the year were realized, and all of the theory and software needed for the study of measurement methods was in place. In the final year emphasis will shift to the development of techniques for experimentally characterizing metal matrix composites in terms of volume fraction, matrix conductivity and layout.

Normalized Reactance

Al/B composite - C3 Pancake Coil

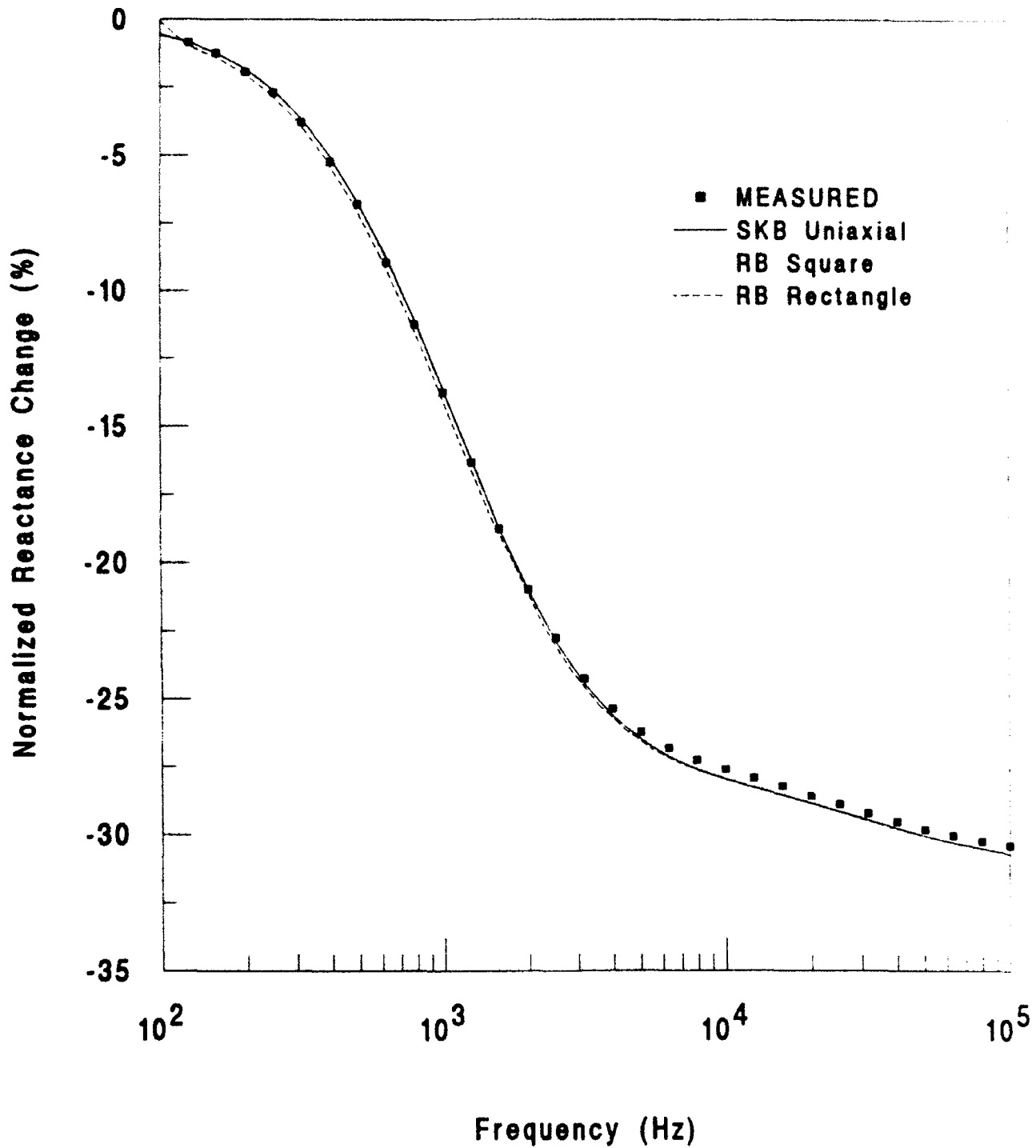


Figure 4 Measured and calculated reactance for an aluminum-boron composite. SKB and RB refer to calculations performed by S. K. Burke and the present author, respectively. Figure supplied by Burke [9].

Plans for Next Year

The first task for next year is to answer the questions posed above concerning Burke's approach to measuring volume fraction and matrix conductivity. This will be done by an application of existing models to a thorough parametric study of probe response as a function of volume fraction and matrix conductivity, with the parameters being fiber distribution, exciter and receiver coil size, shape and orientation, frequency and liftoff distance. The aim of the initial task is to determine the most promising method or combination of methods for measuring volume fraction in situations where the matrix conductivity is uncertain. Once this is done, the next step will be to optimize the measurement strategy and develop a plan for experimental testing of the procedure. The final task will be an experimental demonstration of the measurement method, making use of specimens with known volume fractions and matrix conductivities. In this connection it should be noted that the acquisition of well-characterized specimens may pose a problem. For this reason, attempts to locate a source of specimens will begin early in the project. If a suitable source cannot be located, methods for fabricating artificial mockups will be developed.

To prepare for transition of the work from research to the development of specific applications, steps will be taken with program personnel to identify inspection problems in metal matrix materials. An example might include the manufacturing preparations for high temperature.

References

1. E. M. Sterling and J. E. Bell, U. S. Army Aviation Research and Technology Activity Report, USAAVSCOM TR 90-D-5, 1990.
2. R. A. MacKay, Scripta Met. 24, 167 (1990).
3. W. N. Reynolds, Harwell Laboratory Report AERE-R 13040, 1988.
4. T. M. Roberts, H. A. Sabbagh, L. D. Sabbagh, IEEE Trans. Mag. MAG-24, 3193 (1988).
5. J. R. Bowler, H. A. Sabbagh, and L. D. Sabbagh, in Review of Progress in Quantitative NDE, Volume 7, edited by D. O. Thompson and D. E. Chimenti (Plenum Press, New York, 1988), p. 1021.
6. S. K. Burke, J. Appl. Phys. 68, 3080 (1990).
7. R. E. Beissner, in Review of Progress in Quantitative NDE, Volume 10, edited by D. O. Thompson and D. E. Chimenti (Plenum Press, New York, 1991), p. 333.
8. J. R. Wait, J. Phys. D: Appl. Phys. 24, 487 (1991).
9. S. K. Burke, ARL Melbourne, private communication (1991).

ADVANCED TECHNOLOGY PROGRAM-PROPERTIES AND MATERIALS CHARACTERIZATION

**Ward D. Rummel
Martin Marietta
Littleton, CO 80125**

Executive Summary

Advanced NDE technology planning, development, peer validation and implementation must be tempered by: current and anticipated needs; by boundary conditions and constraints inherent to application; and by mechanisms for technology transfer to potential users. Innovation and creativity are known to be critical elements in discovery and advancements in basic sciences. Support of innovation and creativity is inherently tied to transfer of the discovered "truths" to both peers and to society. Technology transfer is therefore an essential consideration in the discovery, evaluation, validation and maturation of most modern research and development tasks. Technology transfer is, however, one of the most difficult elements in a successful research product and often depends on a facilitator to match mature work with on-going needs.

This report documents an independent view of the concepts, progress, and windows of opportunity for technology transfer and use of advanced NDE technology being developed under the overall Air Force Advanced Technology Program. The mode of operation is to bring awareness and knowledge of near-term and anticipated problems within the Air Force/Aeronautics and Astronautics communities that could potentially benefit from independent research and development to aid in the selection of promising ideas and research/development tasks to aid in technology transfer by communications, development of beta site testing opportunities, skill development, and performance assessments.

Background

A. General

Problem selection and design of experiment are based on experience, "corporate memory", and community review. Project and community peer view are accomplished by team review sessions at the Center for NDE and by community review at the annual "Review of Progress in Quantitative Nondestructive Evaluation" and many public seminars presented by program researchers. The community peer review is archived in the "QNDE Proceedings" as well as the usual peer reviewed literature. Project progress and accomplishments are documented in progress and final reports. Care is taken to report and document unexpected results as valuable contributions to both the science base and the engineering technology base.

Technology implementation requires "transfer of ownership" from the research/development laboratory to the production line, maintenance line, flight line, etc. (collectively termed "production"). Rigid discipline in validation and qualification on a production line are required to assure minimum variance in critical characteristics of the product. Small improvements that reduce variance and increase yield may be as important as a major, first principles scientific breakthrough. Technology improvement problems are therefore encouraged in candidate research tasks. Experience, knowledge, communications, and impatience hallmark the role of the "facilitator" in the implementation process. This is a primary role in this project consultation/support task. The results of task review, progress assessment, analysis, integration of related experience and cognizance of the changing and projected needs of government and industry are reported herein.

B. Project

This project has taken on a new focus this year as a facilitator in the definition of timely problems in need of research and development and in the identification of technology transfer opportunities for ongoing work.

Objective and Scope

The objective of the project is to provide expert information on a wide range of NDE issues from field inspection techniques, materials, processes, and transitions of new technology from research to NDE field inspection practice.

Technical consultation/support is provided as an independent assessment of the application potential, the methods and boundary conditions of the NDE theory, the engineering models, and the technical application procedures being developed.

Approach

NDE engineering consultation/support services were provided by review and participation in program planning, project reviews and semi-annual technical reviews as identified by the program manager. During 1991, this included a review at the Center for NDE, the Review of Progress in Quantitative NDE Conference in Brunswick, Maine, incremental reviews in unrelated meetings and facilities visits, and a status/planning meeting review at the Wright Aeronautical Laboratories.

Consultation/support was provided in the form of:

1. Clarification of technical issues and opportunities for implementation;
2. Aid in data/information dissemination and technology transfer;
3. Aid in test specimen preparation and use; and
4. Aid in design of experiment and data analyses.

Commentary on various tasks in this report is summarized below.

Technical Summaries

Application of Time-Resolved Infrared Radiometry (TRIR) to Identify Damage in Composite Materials (J. C. Murphy, Johns Hopkins University)

Problem

Fiber reinforced composite materials are subject to impact damage that is not visible at the surface. The impact damage may result in fiber breakage, delamination and exposure of reinforcing fibers to the environment. The combined engineering effects are a potential loss of structural integrity, a reduction of fatigue life, and initiation of composite stress corrosion. X-radiographic, ultrasonic and thermal methods have been demonstrated to be effective in identifying, locating and quantifying the level of impact damage in composites. Improvements in detection and quantification are needed in the form of faster, better, and cheaper operation.

Application

Composites are widely used in commerce, and have special engineering applications in commercial and Air Force Aircraft structures. As such, broad area scanning is required to increase confidence in composite structure life-cycle management and to increase efficiency in composite structures applications.

Objective

To assess the visibility of defects in composite materials created by impact using thermal techniques in combination with IR detection; and to understand the physical basis of defect visibility using heat flow models of composites.

Technology Transfer/Implementation

This was primarily an exploratory task and direct implementation is not anticipated. The results will be published and distributed in an Air Force report and will be used by other investigators to build on the information/knowledge developed. It is recommended that the thermal model be made available to other investigators in documented and validated magnetic media.

Limited Data Computed Tomography (CT) Using A Priori Data (R. Roberts, Ames Laboratory and the Center for NDE)

Problem

The development and application of computed x-ray tomography in industry has provided an assessment capability that was not previously available. The capability to provide a three-dimensional image and information on the interior of complex engineering structures accounts for the interest in CT application. Inherent characteristics limitations of the method are special equipment required, artifacts in the imaging process and the time required to acquire data and present the three-dimensional image. Methods of decreasing the time for test object characterization are not only desirable, but are necessary for broad application of the technology.

Application

Reduction of data acquisition/imaging times would find application in most industrial applications and would provide potential benefit to medical applications.

Objective

Develop computed tomography algorithms for reconstruction of incomplete projection data sets using a priori component geometry and material information.

Suggested Task Enrichment

Suggested problems for test and validation of the methods being developed include braze joints and solid rocket motor components. Both problems involve examination of test objects of symmetry. Production data sets are required to test the capabilities. I will aid in acquiring data files from the San Antonio ALC facility on brazed components and from the Ogden ALC on solid rocket motor components. This will provide a real data test set to test both the concepts and the practicality to perform faster, cheaper, and better.

Technology Transfer/Implementation

If the methods developed are significant improvements, initial application at the ALC facilities will be expected.

Laser Based Ultrasonics (R. C. Addison, Rockwell Science Center)

Problem

Ultrasonics is widely used in industrial applications and is an essential tool for life-cycle management of Air Force aircraft. The requirement to use a fluid couplant in ultrasonic applications, limits the applicability and desirability of application to many problems. The development of methods for ultrasonic application without need for a fluid couplant is both desirable and has economic impact.

Application

Application of the procedure could initially be an aid in the examination of aircraft surfaces at unusual attitudes and at increased examination speed. The laser based technology offers potential for faster, better, and cheaper application of ultrasonic inspection methods to a variety of problems.

Objective

The objective of this program will be to demonstrate the feasibility of a research prototype system employing a practical, eventually field usable, concept of source-detector integration for laser based ultrasonics. The system will be designed with the intent of eventually applying the concept to the inspection of large-area composite airframe structures. The concept resulting from this work will need to be insensitive to environmental disturbances typically found in the case of industrial inspection. Disturbances of particular concern include mechanical vibration, temperature variations and suspended particles along the optical path. The concept must have sufficient sensitivity to detect flaws of interest without causing surface damage to the part under test.

Technology Transfer/Implementation

Technology transfer to the Air Force program is suggested by awareness and transfer of ownership to field personnel. The first step in transfer is that of awareness and data transfer. Presentation of the method, results and requirements for application at the annual Air Force Wide NDI meeting in San Antonio is suggested. This may be arranged through the Air Force NDI program office.

Detection of Hard Alpha Inclusions in Titanium Jet Engine Components (J. H. Rose, Ames Laboratory and the Center for NDE)

Problem

Titanium alloys have high strength at elevated temperatures and are thus candidates for applications that need a high strength to weight ratio, such as fan components in gas turbine (jet) engines. Titanium and titanium alloys are characterized by an affinity for carbon, hydrogen, nitrogen, and oxygen, when heated to high temperatures. Carbon, hydrogen, nitrogen, and oxygen are interstitial elements that stabilize and second (alpha) phase in an otherwise, homogeneous alloy. The alpha inclusions are brittle, are susceptible to cracking, and provide for crack initiation in the bulk matrix. Titanium component production processes are designed to prevent the formation of the alpha inclusions and titanium processing development has focused on methods of preventing and eliminating inclusion formation. Titanium production processing includes the use of various inspection methods to detect and eliminate inclusions in production products. Advanced methods for detection and/or increasing the capability for detection are needed.

Application

Improved detection methods have application to gas turbine engine components and to a wide variety of titanium alloy engineering components.

Objective

To find an NDE probe that will allow detection of hard alpha inclusions and to develop the theory needed to implement that probe. Develop the quantitative theory needed to: (1.) determine the ultrasonic backscatter from titanium alloys, and (2.) to infer microstructural properties from the backscatter signal.

Implementation

This is an exploratory task and knowledge gained will be utilized in development and application of improved production ultrasonic methods.

Ultrasonic Detectability of Small Flaws in Advanced Engine Alloys (R. B. Thompson and F. J. Margetan, Ames Laboratory and the Center for NDE)

Problem and Application

As discussed in previous task.

Objective

The objective of our work for this year is to complete a predictive model describing the limits of ultrasonic detectability of hard-alpha inclusions in advanced titanium alloys, as influenced by the microstructure of those alloys.

Implementation

The results of the theory and validation data will be incorporated into engineering design and into production processes for both new engine components and the maintenance of engines in the field.

Spectroscopic Evaluation of Adhesive Bonds: Linear and Non-Linear Analysis (J. Achenbach, Northwestern University, and L. Adler, Ohio State University)

Problem

Measurement of bond strength in adhesive bonded joints has been a long continuing challenge to nondestructive measurement science. Quantification of bond strength would add a new dimension to NDE measurement science and would enable both increased confidence in the structural integrity of adhesive bonded structures and greater efficiencies in adhesive bond joint design.

Application

Adhesive bonding is used extensively in engineering applications and greater use would be enabled by increased confidence in the structure integrity of joints produced and confidence in continuing joint serviceability. A general theory and measurement method would be applicable to a wide variety of adhesive bond, structural integrity problems. If specifically successful, the methodology might be developed and applied to additional adhesive bonding systems to provide an NDE engineering basis for bond strength characterization and quantifications.

Objective

The objective of the work is to devise a nondestructive technique to assess the adhesive bond strength of adhesive layers. This is done by analyzing the nonlinear behavior that precedes adhesive bond failure in thin boundary layers at the adherend-adhesive interfaces. The first part of the work involves the development of a theory for nonlinear joint response. The second part is to demonstrate the feasibility of linear and nonlinear ultrasonic measurement techniques to evaluate adhesive bond quality.

Implementation

This is an exploratory task to provide proof of principle. Extensive development of instrumentation and measurement procedures will be required to production/field implementation.

Nondestructive Evaluation Method for Assessment of Environmental Degradation of Adhesive Joints (S. I. Rokhlin, Ohio State University)

Problem and Implementation

As discussed in the task above.

Objective

The main objectives of the work for this year are: (1.) to apply the technique developed to evaluate and study environmentally degraded adhesive joints, (2.) to develop a model of the degraded interface in adhesive joints, (3.) To relate nondestructive predictions to strength reduction of degraded joints.

Implementation

Technology transfer and validation should be sought for a single, well characterized adhesive bond application. Work was initiated on Northrup specimens. Further validation, evaluation of the effects of other parameters and quantification of measurement threshold and precision are suggested.

Eddy Current Characterization of Composites (R. Beissner, Southwest Research Institute)

Problem

The structural properties of metal matrix composites depend, in part, on the fiber matrix ratio and on the uniformity of fiber spacing and orientation. Optimization of the production process depends, in part, on the ability of measure and control the fiber distribution. Eddy current methods have been shown to be sensitive to both fiber density and fiber orientation in resin matrix composite materials. Exploratory work to investigate the feasibility of applying eddy current methods to metal matrix composites is logical.

Application

If successful, the work would be applicable to material characterization and to production process control.

Objective

This year's objective is to provide a theoretical model that relates to microstructure of a metal matrix composite to its response to an eddy current probe. Initial studies will focus on continuous fibers in titanium alloy matrix.

Implementation

This is exploratory work and implementation depends on the development and validation of a successful model that may be used in process control. The outcome is uncertain at this time.

Additional Areas of Need/Interest and Opportunity (Ward D. Rummel, Technical Advisor)

The following areas are suggested as needs and opportunities for new work, and for extension of efforts to new problem areas:

- Corrosion detection and quantification;
- Bonded structure POD using available amplitude/phase relationships (Models and experimental data);
- Visual inspection measurements;
- Ion implant/wear; coating measurements and characterization;
- Ceramics; and
- Eddy current measurements (POD) on irregular geometries such as the chamfer on the edge of a "deburred, tumble polished, etc." transition in geometry such as a hole, dovetail slot, etc.